The Role of Fe(III) Oxyhydroxides in Shaping Microbial Communities Capable of Fe(III) Reduction

THE ROLE OF FE(III) OXYHYDROXIDES IN SHAPING MICROBIAL COMMUNITIES CAPABLE OF FE(III) REDUCTION

A dissertation presented

by

Christopher James Lentini

to

The School of Engineering and Applied Sciences

in partial fulfillment of the requirements

for the degree of

Doctor of Philosophy

in the subject of

Environmental Science and Engineering

Harvard University

Cambridge, Massachusetts

May 2013

Dissertation Advisor: Professor Colleen M. Hansel Christopher J. Lentini

THE ROLE OF FE(III) OXYHYDROXIDES IN SHAPING
MICROBIAL COMMUNITIES CAPABLE OF FE(III) REDUCTION

Abstract

Iron oxyhrdroxide exist in a range of crystallinities and subsequent bioavailabilities with the poorly crystalline Fe oxyhrdroxide, ferrihydrite, considered the most bioavailable. Yet, as a result of the instability ferrihydrite it quickly ripens and/or transforms to more thermodynamically stable end-members bringing into question its importance in supporting long-term Fe(III)-reducing microbial communities. Furthermore, while a wide phylogenetic diversity of microorganisms capable of reducing ferrihydrite have been isolated, these organisms show diminished abilities to reduce more stable and dominant crystalline Fe phases. Therefore to address the questions of which microorganisms and what microbial processes are responsible for controlling the reduction of diverse Fe(III) minerals phases, cultivation based approaches using both batch and column-type reactors were employed. Using geochemical and phylogenetic analysis it was revealed that the Fe oxide substrate was important in dictating the mechanisms of Fe(III) reduction, and the structure of the microbial communities. While model dissimilartory Fe reducing microorganisms were capable of reducing ferrihydrite when acetate was provided as a carbon source these organisms did not enrich and were incapable of reducing crystalline Fe(III) oxides. Instead, in enrichments where crystalline Fe(III) oxides were reduced, organisms associated with fermentation and sulfate respiration dominated, this despite using freshwater media low in sulfate (less than 200 μM). In addition, these non-model Fe reducers dominated in ferrihydrite enrichments when carbon compounds other than acetate were given. Interestingly, a

strong negative correlation between Fe(III) and sulfate respiration was observed with the canonical thermodynamic view that ferrihydrite should precede sulfate as a terminal electron acceptor being challenged. Further experiments with pure cultures of *Desulfovibrio putealis* indicated that a catalytic sulfur cycle may be responsible for greater than expected Fe(II) values under low sulfur conditions. These findings, have broad implications in predicting microbially mediated electron flow to oxidized substrates which will dictate the pathways and degree of carbon mineralization and subsequent carbon sequestration within sediments and soils. Further, given the importance of Fe(III)-reducing communities and Fe(II) in the sequestration of both inorganic and organic contaminants, these findings will have direct bearing on contaminant mitigation and remediation.

TABLE OF CONTENTS

Appendix

LIST OF TABLES

LIST OF FIGURES

Acknowledgments

There are many people who deserve a thank you and/or acknowledgment for contributing to my success as a graduate student; I hope I remember to thank them all. I would like to first thank my advisor and friend, Colleen Hansel. I am not sure I would have ever stumbled upon that amazing world of biogechemistry if it were not for you and your guidance. I can only imagine I would be somewhere thinking about how I could ignore microbiology and focus on chemistry, I am glad I am not. Colleen continually encouraged me to explore new and exciting ways to address my scientific problems. Your graduate courses were always a joy for me to take and your vigor for the subject always reminded me how interesting sciences really is. Outside of academia, Colleen, Scott, the girls, and O'Malley became my family on the east coast. While it was sometimes a struggle for me to be so far away from family, I always knew that I had a group of people who were interesting in seeing me succeed and more importantly my well being. I thank you for that.

I would also like to thank my committee members for meeting with me in addition to taking the time to learn about my research and provide insightful feedback.

I should also thank all of the members of the Hansel group throughout the years. Many who provided scientific guidance and/or friendship. At the very least you dealt with looking at my messy lab bench and sometimes my testy lab personality. You all made it a joy to come to work over the past 6 years and I owe you many thanks. In addition to my lab mates, I also thank my friends and roommates while at Harvard (Ben, Katy, Tom and Pete), for keeping me sane and making sure I had fun outside of the lab.

There were also many people we helped me develop as a student of science that also deserve recognition and praise. First, the faculty and staff at Orange Coast Community College for giving me such an amazing foundation from which this was all built. Without you, this would not have been possible. I also owe many thanks to the chemistry faculty at Chapman University. I have never seen a group of faculty who truly cared about their students as they did. I enjoyed getting to know them personally and scientifically over the years and I hope I can share this achievement with them soon. A special thank you to Chris Kim who became my mentor as an undergrad and has continued to be my friend. Chris was one of the first people to believe that undergraduates could work and collect high quality data at synchrotrons and I feel extremely fortunate to be among his first group of students. I am sure that I will lean on Chris for professional/personal advise in the years to come.

Portions of this research were carried out at the Stanford Synchrotron Radiation Lightsource, a national user facility operated by Stanford University on behalf of the U.S. Department of Energy, Office of Basic Energy Sciences. Many thanks to the staff at SSRL for assistance at the beam and for making sure such a great resource available to the scientific community. In addition, much of this work was supported by a National Science Foundation Graduate Research Fellowship under grant no. DGE-0946799 and DGE-1144152.

Lastly, and most importantly, I owe all my happiness and success to my family. First the Beaver family (Nana, Robert, Peggy, Bobby, Jeff and Kaitlin), thank you for all of the love and support you have shown Kristin and I over the last few years. Special thanks to Robert, Peggy and Mojo for providing me a home, delicious food, and much

joy during those long runs at SSRL. Kathy and Guy, you have both served as an inspiration to me and have taught me what can be achieved with hard work. Guy, I am especially grateful to you for treating me as your son. I am so lucky to have such an amazing father and I know that I owe much of my success as a person to you. Danny and Mandy, thank you for all the support and putting up with my shenanigans.

Kristin, what can I say other than thank you for being my wife. I am inspired daily by your hard work and compassion for people. While working absurd hours and taking care of all you patients you still found time to take care of me and ensure that I was happy. Even though we worked way too much and didn't get to know the city as we had hoped, I will always look back at our years in Boston fondly and remember it as the city where we started our lives together. I thank you for being part of my life and look forward to seeing where life takes us.

CHAPTER 1

MINERALOGICAL CONTROLS ON MICROBIAL REDUCTION OF FE(III) (HYDR)OXIDES

Published as: Hansel, C.M., and Lentini, C.J. (2011). "Mineralogical Controls on Microbial Reduction of Fe(III) (Hydr)oxides," in *Microbial Metal and Metalloid Metabolism: Advances and Applications,* eds. J.F. Stolz & R.S. Oremland. (Washington, DC: ASM Press), 93-115.

1.1 Introduction

Iron oxides, oxyhydroxides, and hydroxides (hereinafter referred to collectively as (hydr)oxides) are ubiquitous in the environment with contents ranging from one to several hundred g kg^{-1} in aerobic soils (Cornell and Schwertmann, 2003). The reduction of Fe(III) (hydr)oxide phases regulates the degradation of carbon, the flow of electrons within subsurface sediments and soils, and the fate and transport of nutrients and contaminants. In particular, Fe (hydr)oxides are considered one of the most important sinks for (in)organic contaminants and nutrients within soils, sediments, and waters. As a consequence of their high surface area and density of reactive surface sites, Fe(III) (hydr)oxides may sorb numerous organics (e.g. pesticides, PAHs), nutrients (e.g. phosphate), and metals (e.g. Pb, As, U) (Cornell and Schwertmann, 2003). Consequently, the dissolution of metal-laden Fe(III) (hydr)oxide phases poses a potential threat to water quality should anaerobiosis occur. In contrast, the reduction of Fe(III) (hydr)oxides may also be coupled to the degradation and/or sequestration of contaminants within natural and engineered systems. In fact, stimulated *in situ* microbial Fe(III) reduction has received considerable attention as a promising means of environmental remediation of a myriad of (in)organic contaminants. Targeted stimulation of dissimilatory metal-reducing bacteria (DMRB) poses a particularly attractive and flexible means of environmental *in situ* remediation (Lovley, 2001). Through both direct enzymatic and indirect metabolic reactions, DMRB can degrade, immobilize, and transform contaminants ranging from benzene to uranium (Anderson and Lovley, 2000;Lovley, 2001). These processes include hydrocarbon oxidation coupled to Fe(III) reduction, sequestration of soluble contaminants (e.g., As) within Fe secondary phases (e.g., magnetite), and/or immobilization of redox-active contaminants (e.g., Cr) by reaction with

the reactive metabolite Fe(II). Thus, central to many proposed remedial approaches are Fe(III)-bearing minerals.

In studies in which treatment progression is dependent on reduction of Fe(III) phases, mineral phase reactivity and longevity currently represents a key limitation. Previous studies have revealed that microbial reduction of various Fe(III) (hydr)oxides is transient, having a diminished reductive capacity over time (Benner et al., 2002;Hansel et al., 2003a;Hansel et al., 2004). Iron (hydr)oxides are mineralogically diverse, with the most studied, and most utilized, phase being ferrihydrite. While ferrihydrite is considered the most 'bioavailable' Fe(III) (hydr)oxide for microbial reduction (Lovley and Phillips, 1986), under some conditions, more recalcitrant phases, such as goethite, can be more reactive (Hansel, unpublished data). Furthermore, ferrihydrite reactivity has been shown to rapidly decline over time (Hansel et al., 2003a). Differences in rates of reaction both between mineral phases and over time are significant, yet an understanding of the controlling factors on reduction rates is incomplete. Our lack of knowledge on what controls the short- and long-term reduction capacity of Fe(III) minerals currently limits our ability to convert this promising biogeochemical process into a successful remediation strategy. In this chapter, we will discuss the current state of knowledge regarding the geochemical controls on the initial and sustained reduction of Fe(III) minerals. We will introduce the major controlling factors for microbial Fe(III) reduction; yet, it is important to note that the properties of Fe minerals are not mutually exclusive and thus defining the individual role of these properties is difficult, if not impossible.

1.2 Physicochemical Properties of Fe Minerals

The Fe(III)-Fe(II) redox couple is an important electron-transfer mediator for many reactions of significance to biogeochemical cycles, especially in soils and sediments. In the reduced state, Fe(II) exists as a hydrated ion in solution, adsorbs onto solid-phases, or precipitates as reactive Fe(II) phases (e.g., siderite, vivianite). The oxidized Fe(III) species can exist as a number of primary and secondary minerals, including Fe-containing phyllosilicates and (hydr)oxides (including oxides, oxyhydroxides, and hydroxides). Above acidic pH values (pH> 4), low solubility Fe(III) (hydr)oxides are the predominant form of Fe(III) in most soils and sediment (Cornell and Schwertmann, 2003). Fe(III) (hydr)oxides consist of an array of Fe^{3+} and O^{2-} or OH^- ions, and differ in how their basic structural units, $Fe(O/OH)_6$ or FeO_6, are arranged in space (Figure 1.1). The term ferrihydrite encompasses a group of oxyhydroxide minerals that lack long-range order and have varying degrees of crystallinity. The two end-members in the crystallinity continuum are referred to as 2-line and 6-line ferrihydrite, based on the presence of either 2 or 6-8 reflections in X-ray diffraction patterns (Cornell and Schwertmann, 2003). Frequently, these phases are erroneously referred to as "amorphous" despite the presence of distinct short-range order. The local structure of ferrihydrite resembles those of well crystalline phases, including hematite, akageneite, or goethite depending on growth conditions (Manceau and Drits, 1993). Interconversion of Fe (hydr)oxides also occurs whereby thermodynamically less stable phases (e.g. ferrihydrite, lepidocrocite) transform to more stable phases (e.g. goethite, hematite). This 'ripening' of Fe(III) (hydr)oxides is catalyzed by reductants, including cysteine and Fe(II) (Fischer, 1972;Cornell et al., 1991;Zachara et al., 2002;Fredrickson et al., 2003;Jang et al., 2003;Hansel et al., 2005).

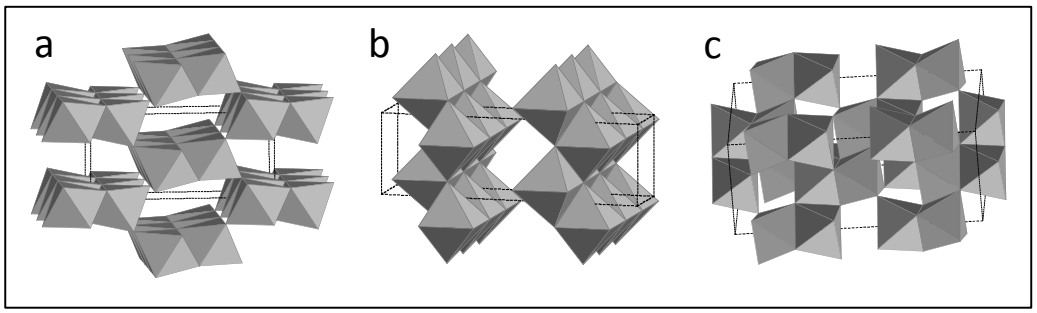

Figure 1.1. Structures of Fe(III) (hydr)oxides commonly used in microbial reduction experiments. (a) Goethite structure composed of octahedral double chains linked through corners. H atoms not shown. (b) Lepidocrocite structure composed of octahedral double chains in corrugated layers. The layers are cross-linked through edges. H atoms not shown. (c) Hematite structure composed of octahedra linked through edge- and corner-sharing as well as face-sharing along the *c*-axis. Unit cell outlined in dashed black line.

Iron(III) (hydr)oxides exist in a spectrum of crystallinities and subsequent bioavailabilities; ranging from ferrihydrite (poorly crystalline/least thermodynamically stable) to hematite (well crystalline/most thermodynamically stable) (Cornell and Schwertmann, 2003). The thermodynamic stability of Fe (hydr)oxides is a function of crystal structure and particle size, which ultimately controls the solubility of the phases. Because solubility is a function of several properties (ionic strength, temperature, particle size, crystal defects) there is a considerable amount of uncertainty with the solubility product values obtained in the pH ranges of most environmental conditions. This has lead to large discrepancies in the literature between calculated solubility products by different authors (Cornell and Schwertmann, 2003). However, the solubility of common, pure Fe(III) (hydr)oxides generally progresses in the order 2-line ferrihydrite > 6-line ferrihydrite > lepidocrocite > goethite > hematite at circumneutral pH (Langmuir, 1969;Baes and Mesmer, 1976;Cornell and Schwertmann, 2003). The physicochemical properties of Fe(III) (hydr)oxides vary widely, including morphology, crystal size, crystal structure, surface area, density, magnetism, conductivity, solubility, and free energy of formation (Table 1.1) (Cornell and Schwertmann, 2003).

Table 1.1. Physiochemical properties of Fe(III) (hydr)oxides commonly used in bioreduction experiments

	Ferrihydrite	**Lepidocrocite**	**Goethite**	**Hematite**
Formula	$Fe_5HO_8*4H_2O$	γ-FeOOH	α-FeOOH	α-Fe_2O_3
Crystal system	Hexagonal	Orthorhombic	Orthorhombic	Hexagonal
Dominant morphology	Spheres	Laths	Acicular	Plates
Range of surface area (m^2/g)	100-700	15-260	8-200	5-200
Standard Free Energy (kJ/mol)	-699	-477.7	-488.6	-742.7
Solubility Product (25ºC) (log K_{so})	-39	-39.5	-40.7	-42.75

*exact formula for ferrihydrite is not established, others include $Fe(OH)_3$, $Fe(OH)_3*nH_2O$, $5Fe_2O_3*9H_2O$

Trivalent and divalent metal cations may isomorphously substitute into Fe(III) (hydr)oxide structures. Within the environment, natural Fe (hydr)oxides always contain co-precipitated ions, frequently containing several mole % of foreign ions (Singh and Gilkes, 1992;Trolard et al., 1995). Aluminum(III) is one of the most prevalent and effective co-precipitates within Fe(III) (hydr)oxides, with substitution reaching 33 mole % in goethite for example (Cornell and Schwertmann, 2003). A number of trace metals may also substitute into Fe(III) (hydr)oxides, including Cd(II), Co(III), Cr(III), Cu(II), Mn(III), Ni(II), V(III) and Zn(II). While Mn(III) can occupy a significant fraction (e.g., ca. 47% in goethite) of Fe(III) sites within Fe(III) (hydr)oxides, the remaining trace metals typically substitute to levels below 10%. Substitution of Fe(III) within (hydr)oxide phases impacts crystallite size, morphology, surface area, solubility, surface chemistry, and rates of acid and reductive dissolution (Cornell and

Schwertmann, 2003). For the most part, metal substitution reduces the solubility and interconversion of Fe (hydr)oxides relative to pure phases (Cornell and Schwertmann, 2003).

The reduction potential (Eh) of Fe is a function of the phase or complex (Figure 1.2). The Eh for Fe(III/II) redox couples varies over 700 mV, while that of Fe(III) (hydr)oxide phases span over 300 mV (Thamdrup et al., 2000;Favre et al., 2006). Remarkably, when corrected for typical environmental conditions, the Eh of more crystalline (stable) Fe(III) (hydr)oxides (e.g., goethite, hematite) falls below the potential for sulfate reduction. Based on a partial equilibrium model, the existence of overlapping Fe(III)- and sulfate-reducing zones within various sedimentary environments can be explained by this large range in Fe (hydr)oxide reduction potentials (Postma and Jakobsen, 1996;Jakobsen and Postma, 1999). Thus, it is predicted that the distribution and proximity of Fe(III)- and sulfate-reducing zones will vary depending on the composition and stability of the Fe(III) phases (Postma and Jakobsen, 1996).

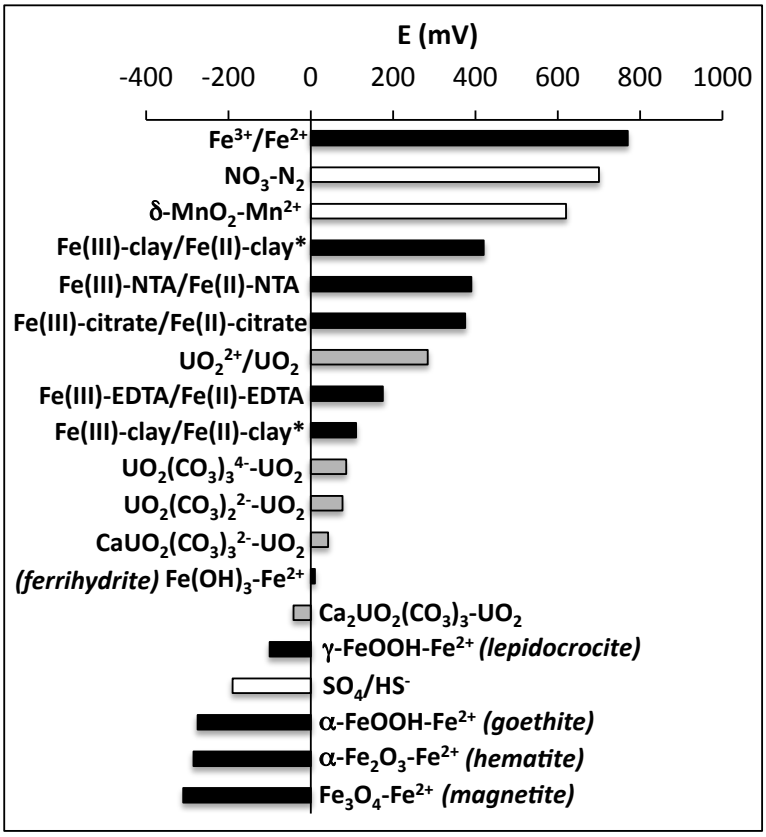

Figure 1.2. Redox potentials of various Fe couples compared to other couples of relevance in groundwater and contaminated systems (modified from (Thamdrup et al., 2000;Brooks et al., 2003)). A variety of U species are included to illustrate the role of complexation on reduction potential of soluble complexes. Temperature 25°C, pH = 7, $[Fe^{2+}]=[Mn^{2+}]=[NO_3^-]$ = 10 μM, [U(VI)] = 50 μM, $[Ca^{2+}]$ = 5 mM, $[HCO_3^-]$ = 28.1-28.7 mM, $[SO_4^{2-}]$ = 10 mM, $[HS^-]$ = 1 μM, P_{N2} = 1 atm. Fe(III)-clay potentials presented for SWa-1 with $[Na^+]$ = 100 μM and either m_{re1} = 0.02 (Eh = 420 mV) or m_{re1} = 0.70 (E = 110 mV) (Favre et al., 2006).

1.3 Microbial Fe(III) Reduction

The importance of microorganisms in the biogeochemical cycling of Fe has long been recognized (Starkey and Halvorson, 1927). The microbial reduction of Fe(III) may be a result of Fe uptake or incorporation into cellular components (assimilatory), or respiration whereby Fe(III) serves as a terminal electron acceptor (dissimilatory). Historically, geochemical and redox gradients within sediments hinted at the presence of microorganisms that link the

oxidation of organic carbon to the reduction of Fe(III) (Froelich et al., 1979;Reeburgh, 1983). Yet, sedimentary Fe(III)-reducing zones were primarily attributed to fermentative bacteria (Jones et al., 1984), which are thought to reduce Fe(III) as a supplementary terminal electron acceptor (Bromfield, 1954b;a;Lovley, 1987). The recent discovery and isolation of bacteria that couple growth to the reduction of Fe(III) (Lovley and Phillips, 1988;Myers and Nealson, 1988) prompted countless studies that unveiled the widespread importance of microbial respiration in the cycling of Fe(III). Fe(III)-reducing microbes are found in a wide range of environmental conditions (e.g, T, pH) and include various members of the domains *Bacteria* and *Archaea*, facultative and obligate anaerobes, and heterotrophs and autotrophs (Lovley, 2000;Lovley et al., 2004;Weber et al., 2006;Ehrlich and Newman, 2009). Due to the ubiquity, abundance, phylogenetic diversity, and metabolic versatility of Fe(III)-reducing microorganisms (Lovley, 1991;Lovley et al., 1991b;Nealson and Saffarini, 1994), it is proposed that metal-reducing bacteria catalyze most of the Fe(III) reduction occurring under non-sulfidogenic, anaerobic conditions (Lovley et al., 1991b). Furthermore, the metabolic versatility of these organisms includes the reduction of a number of metal(loid)s (e.g., Cr, As) and radionuclides (e.g., U, Tc) (Lovley et al., 1991a;Caccavo et al., 1992;Fredrickson et al., 2000;Lloyd et al., 2000;Lloyd et al., 2002;Saltikov and Newman, 2003) highlighting their potential for environmental remediation and biotechnology. Yet, it is becoming increasingly apparent that fermentative bacteria are also important players in Fe(III) reduction within pristine and contaminated sediments (Petrie et al., 2003;Hansel et al., 2008) and, some fermenting organisms, may in fact conserve energy through Fe(III) reduction (Dobbin et al., 1999).

Unlike other metabolisms where the terminal electron acceptor may diffuse into the cell, DMRB respire solid Fe minerals presumably making cytoplasmic-bound terminal reductases

inaccessible. Mechanisms by which bacteria may access Fe(III) from sparingly soluble Fe (hydr)oxides include (i) use of exogenous (*e.g.* humics) or endogenous soluble electron shuttles (*e.g.* phenazines) (Lovley et al., 1996;Hernandez et al., 2004), (ii) use of exogenous or endogenous Fe(III)-chelating compounds (*e.g.* siderophores) (Nevin and Lovley, 2002), and (iii) direct electron transfer through enzymes either embedded on the bacterial outer membrane (Myers and Myers, 1998; 2001;DiChristina et al., 2005) or on extracellular appendages (e.g., nanowires, pili) (Gorby et al., 2006;El-Naggar et al., 2008) (for reviews see (DiChristina et al., 2005;Kappler and Straub, 2005;Gralnick and Newman, 2007)). It has been proposed that the mechanism of electron transfer may vary among microbial species (Nevin and Lovley, 2002). In particular, the need for direct microbial contact with the mineral surface is still ambiguous and may in fact vary among microbial species and environmental conditions (Nevin and Lovley, 2000; 2002;Lies et al., 2005). In fact, multiple electron transfer pathways may be operative within single species biofilms (Hernandez and Newman, 2001). The operative reduction pathway may be a consequence of the distribution and orientation of the microbe within redox and chemical gradients at the Fe(III) (hydr)oxide surface. For instance, within 3-dimensonal biofilm structures on Fe(III) (hydr)oxide surfaces, organisms proximal to the mineral surface may preferentially reduce Fe(III) using extracellular membrane-bound enzymes, while those embedded within the biofilm matrix may employ shuttles or electrically conductive cellular appendages to transfer electrons. Interestingly, it has recently been demonstrated that the DMRB *Shewanella putrefaciens* strain 200 and *S. oneidensis* MR-1 produce soluble organic Fe(III) complexes during anaerobic respiration of various Fe(III) (hydr)oxides (Taillefert et al., 2007). The Fe(III)-solubilizing organic ligands, however, are not siderophores and mutants impaired in their ability to produce soluble organic-Fe(III) and reduce Fe(III) retained wild-type siderophore

production capability (Fennessey et al., 2010;Jones et al., 2010). Furthermore, increasing evidence indicates that a number of species may reduce Fe(III) (hydr)oxides indirectly via soluble electron shuttles (e.g., AQDS) (Kappler and Straub, 2005) or via sulfide production (Straub and Schink, 2004;Haveman et al., 2008). Low sulfide levels favor sulfur cycle-mediated Fe(III) reduction by microbes and this metabolism supports growth in pure culture of species such as *Sulfurospirillum deleyianum*. Interestingly, in the presence of ferrihydrite, only catalytic amounts of thiosulfate (50 μM) are required to maintain growth and sulfur was cycled up to 60 times in these cultures (Straub and Schink, 2004). Thus, direct enzymatic reduction may not be required for electron transfer to solid Fe(III) substrates and, in fact, DMRB incapable of effectively transferring electrons to more crystalline Fe(III) phases may attempt to overcome this constraint by producing Fe(III)-solubilizing organic ligands and/or utilizing exogeneous electron shuttles. The binding and reduction efficiency of these inorganic and organic electron shuttles will undoubtedly be a function of the properties of the Fe(III) phases, in particular the phase solubility.

1.4 Mineralogical and Geochemical Controls on Microbial Fe(III) Reduction

At circumneutral pH, Fe(III) (hydr)oxides are sparingly soluble. Despite this, it is clear that microorganisms have evolved the unique metabolic ability to respire on solid substrates including poorly crystalline Fe(III) (hydr)oxides (Phillips et al., 1993) and iron containing clays (Kostka et al., 1996;Kostka et al., 1999;Vorhies and Gaines, 2009). The ability of DMRB to directly transfer electrons to more crystalline forms of Fe(III) (hydr)oxides, however, is not resolved (Lovley et al., 2004). The inability of crystalline Fe(III) (hydr)oxides to serve as effective terminal electron acceptors was initially suspected by findings in natural environments

in which Fe(III) reduction correlated well with poorly crystalline phases (Thamdrup, 2000;Roden and Wetzel, 2002). Nevertheless, the reduction of highly crystalline phases (goethite, hematite, magnetite) has been observed in the laboratory (Roden and Zachara, 1996;Zachara et al., 1998), within column flow experiments (Roden et al., 2000;Hansel et al., 2004) and in natural soils (Stucki et al., 2007). Yet, cultured model DMRB show diminished abilities to reduce these more crystalline phases, only reducing a small fraction of the potentially available Fe(III). Incomplete microbial reduction of Fe(III) (hydr)oxides is pervasive throughout the literature, regardless of nutrient conditions, Fe(III) (hydr)oxide structure, and hydrologic conditions (dynamic versus static). For instance, merely 25% of ferrihydrite, 5% goethite, and 1% hematite were reduced by *Shewanella putrefaciens* strain CN32 in an artificial groundwater medium under flow conditions (Hansel et al., 2004) – a trend consistent with previous experiments conducted in batch systems (Roden and Zachara, 1996;Fredrickson et al., 2003). The cessation of microbial ferrihydrite reduction is easily attributed to the conversion of surface layers to more crystalline phases (e.g., goethite, magnetite) during Fe(II)-induced remineralization processes (Fredrickson et al., 1998;Zachara et al., 2002;Hansel et al., 2003a). In contrast, secondary mineralization does not occur following reduction of goethite and hematite (Hansel et al., 2004). While Fe(II) sorption to bacterial or mineral surface sites has been previously implicated in this loss of reduction capacity (Urrutia et al., 1999;Roden and Urrutia, 2002), mounting evidence reveals that the lifetime of Fe(II) on the surface of Fe(III) (hydr)oxides is extremely short. Instead, it has been shown both empirically and through *ab initio* modeling that following Fe(II) sorption, electrons are injected into the (hydr)oxide structure and either delocalized within the conduction band (Williams and Scherer, 2004;Larese-Casanova and Scherer, 2007) or lost at distal defect sites (Grantham et al., 1997;Rosso et al., 2003b).

Numerous studies have attempted to tease out the underlying geochemical and mineralogical controls on Fe(III) reduction using Fe(III) phases of varying size, crystallinity, structure, composition, and solubility. However, the major factors controlling Fe(III) reduction remain unclear due to the intimate association these properties share. For instance, differences in solubility may arise from variations in specific surface area, crystallinity and impurity content (Cornell and Schwertmann, 2003). In addition, difficulties occur when comparing the same mineral synthesized under different methods and/or different laboratory conditions. These factors have lead to an ambiguous understanding of the factors controlling microbial Fe(III) reduction. The following sections will attempt to summarize our current understanding of the geochemical and mineralogical constraints on microbial Fe(III) (hydr)oxide reduction with the realization that the field is far from a resolution or consensus on what factors ultimately control the transfer of electrons to Fe(III) mineral surfaces.

1.4.1 Surface Area: The seminal paper exploring the relationship between Fe (hydr)oxide properties and microbial Fe(III) reduction identified a link between mineral surface area and reduction rates by *Shewanella alga* strain BrY (Roden and Zachara, 1996). While cell normalized rates for pure ferrihydrite, lepidocrocite, goethite and hematite ranged nearly two orders of magnitude (~$2x10^{-10}$ to $2x10^{-12}$ mmol Fe(II) h^{-1} $cell^{-1}$), a linear correlation was observed between initial rates of Fe(III) reduction and Fe(III) (hydr)oxide surface area. This correlation was less apparent at higher surface areas (Roden, 2003b;Roden, 2006). For instance, given an equivalent particle size and surface area, both chemical (ascorbate, pH 3) and microbial reduction of lepidocrocite exceeded that of goethite. A similar correlation was observed with a spectrum of synthetic Fe(III) (hydr)oxides and different microorganisms (*Geobacter*

sulfurreducens and *S. putrefaciens*) (Roden, 2003b;Roden, 2006). These results suggested that surface area is the major factor controlling the initial rates of microbial Fe(III) (hydr)oxide reduction, independent of the type of Fe(III) (hydr)oxide present (Roden, 2006). In addition to these pure culture studies, acetate-limited enrichment cultures of wetland sediments suggested that Fe(III)-reducing microorganisms respiring crystalline goethite and hematite in fresh water outcompeted methanogens only if the Fe(III) (hydr)oxides were provided in considerably larger amounts (Roden, 2003a). Hence, methanogenesis could be equally impeded by crystalline Fe(III) (hydr)oxides and "amorphous HFO" only when both were available at equivalent surface loadings. The investigators concluded that these results provided further support that surface area is a dominant control on microbial iron reduction.

Recent evidence brings to question the role of surface area in controlling microbial Fe(III) (hydr)oxide reduction rates. For instance, Bonneville et al. (2009) observed that maximum Fe(III) reduction rates (ν_{max}) showed a stronger correlation with solubility (r^2= 0.90 on a log-log scale) than surface area (r^2= 0.54 on a log-log scale). Furthermore, a recent study by Cutting et al. (2009) convincingly demonstrated that initial surface area normalized Fe(III) reduction rates of various Fe(III) (hydr)oxides vary by approximately 2 orders of magnitude (Figure 1.3). These differences were attributed to subtle variations in the crystallinity and morphology of the synthesized Fe(III) phases, which were characterized in detail using a combination of X-ray diffraction (XRD), transmission electron microscopy (TEM), and X-ray photoelectron spectroscopy (XPS). These studies highlighted the need to thoroughly characterize solid-phase Fe(III) substrates using a suite of complimentary spectroscopic and microscopic techniques due to the limitations of using operationally-defined chemical extraction techniques to assess mineral reactivity and reduction and the large variability in (hydr)oxide

properties with synthesis procedures. As is detailed below, a number of other geochemical parameters, including solubility (Bonneville et al., 2004;Bonneville et al., 2009) and crystallinity (Cutting et al., 2009), have been implicated in controlling Fe(III) (hydr)oxide reduction kinetics and have been used to explain deviation from a single surface area normalized initial reduction rate (see below).

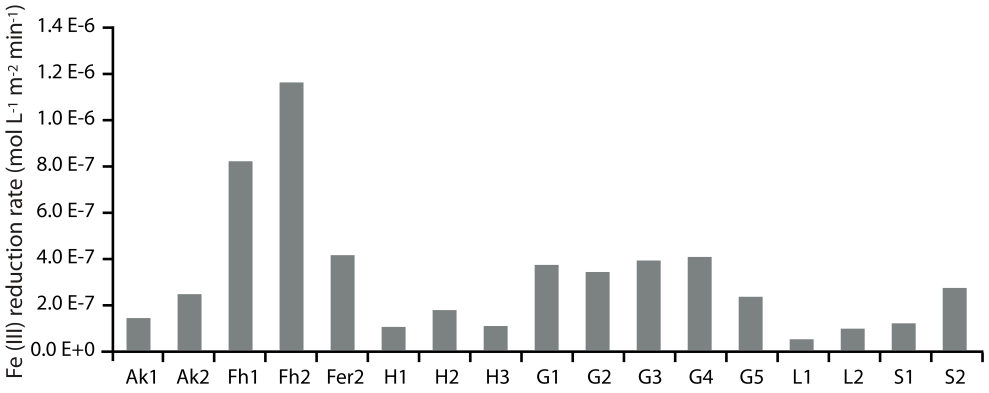

Figure 1.3. Surface area normalized reduction rates (mol L^{-1} m^{-2} min^{-1}) for various Fe(III) (hydr)oxides by *Geobacter sulfurreducens* (Cutting et al., 2009). Hematite (H), goethite (G), lepidocrocite (L), feroxyhyte (F), akaganeite (Ak), Schwertmannite (S), and 2-line ferrihydrite (2Fer) were formed using different synthesis procedures to generate phases varying in size, morphology, surface area, and crystallinity. Reprinted from Cutting et al. (2009) with permission from Elsevier.

1.4.2 Solubility: Recently, microbial Fe(III) reduction of various Fe(III) (hydr)oxide substrates was shown to have a Michaelis-Menten kinetic dependence with respect to the concentration of Fe(III) substrate (Bonneville et al., 2004). The authors implicitly demonstrate that maximum reduction rates per cell (ν_{max}) correlate positively with the solubility of the Fe(III) phase. Given the fact that differences in solubility result from variations in synthesis method, Bonneville *et al.* (2004) determined the solubility of the Fe(III) (hydr)oxides used in their experiment through pε-pH tritrations of Fe(III) phase/Fe^{2+}(*aq*) suspensions (Bonneville et al., 2004). However,

between pH 4 and 7, this method was not suitable with crystalline and low solubility phases. To overcome this issue, Bonneville *et al.* (2009) later employed a dialysis bag pε-pH titration method under acidic conditions (pH 1 – 2.5). Using this improved methodology, the solubility and maximum cell-normalized reduction rates (ν_{max}) for both the crystalline and poorly crystalline Fe(III) (hydr)oxides showed a positive linear relationship (log-log plot) **(**Figure 1.4). Given the correlation between solubility and surface area (r^2= 0.8), the role of surface area in microbial reduction was also considered. However, the correlation between ν_{max} and solubility (r^2= 0.90 on a log-log scale) was far better than for surface area (r^2= 0.54 on a log-log scale) (Bonneville et al., 2009).

The solubility of Fe(III) (hydr)oxides is influenced by endogenous or exogenous organic complexes. As mentioned above, *S. putrefaciens* produces a soluble Fe(III)-organic complex prior to Fe(III) reduction of different Fe(III) phases, ranging from ferric citrate to hematite (Taillefert et al., 2007). Results from this study suggested that the rate of reduction is linearly dependent on the initial rate of production of this soluble Fe(III)-organic complex, suggesting that Fe(III) solubilization is requisite for Fe(III) reduction. Depending on the size of this organic complex (in relation to N_2 and Fe (hydr)oxide pores) the rates of reduction should depend on the amount of reactive surface sites available to complex, which could correlate well with surface area even in aggregates. Assuming that the same organic molecule (metabolite) is produced in the presence of various Fe(III) (hydr)oxides, the solubility of the Fe(III) phase will also exert a large control on the rates and extent of Fe(III) complexation.

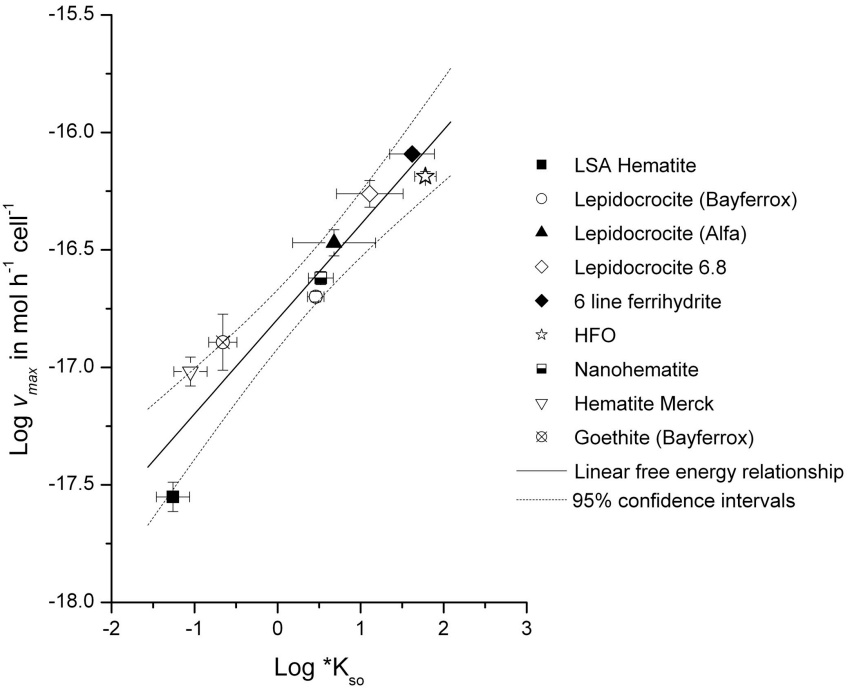

Figure 1.4. Relationship between the solubility product ($^{*}K_{so}$) of various Fe(III) (hydr)oxides and the maximum initial Fe(III) reduction rate per cell (ν_{max}) of *Shewanella putrefaciens* strain 200R (Bonneville et al., 2009). The solubility products were measured for each phase using a dialysis bag technique under acidic conditions (pH 1 to 2.5) at 25°C and defined as $^{*}K_{so} = a_{Fe3+} \bullet a_{H+}^{-n}$. Reprinted from Bonneville et al. (2009) with permission from Elsevier.

1.4.3 Structural Environment: The role of Fe(III) (hydr)oxide crystallinity has recently been implicated in the rate of Fe(III) (hydr)oxide reduction (Cutting et al., 2009). Using a variety of methods, a number of Fe(III) (hydr)oxide minerals were synthesized having inter- and intra-mineral variations in crystallinity, morphology, surface area, and crystallite size. When normalized to surface area, the rates of microbial Fe(III) reduction varied significantly and instead the rates of reduction correlated well with crystallinity, with the poorly crystalline minerals showing higher rates of reduction when compared to their crystalline counterparts (Cutting et al., 2009) (Figure 1.3). This trend was observed both within and among mineral types. This is particularly evident for the feroxyhyte samples, which have similar surface area,

however the poorly crystalline sample (Fh2) was reduced more readily than the relatively crystalline sample (Fh1). These findings implicated crystallinity as the major controlling factor in microbial Fe(III) reduction.

In an attempt to measure the intrinsic susceptibility of Fe(III) (hydr)oxides to microbial reduction, Neal *et al.* accounted for surface area and crystallinity effects by employing three single crystal Fe(III) oxide surfaces (Neal et al., 2003). Cell accumulation of *S. oneidensis* strain MR-1, which was used as a proxy for cell activity, showed significant differences on the surfaces of the three oxides, with accumulation being greatest on the hematite (001) face compared to the magnetite (111) and (100) faces. Calculations employing Marcus and *ab initio* density functional theory were used to model electron transfer rates from the outer-membrane cytochrome to the mineral surface, which showed direct positive correlation between electron transfer rates and the amount of cell accumulation seen in the experiment (Neal et al., 2003).

Constraints on electron transfer to different Fe(III) (hydr)oxides may arise at the protein level. For instance, recent findings indicated that the putative Fe(III) reductase OmcA can bind with high affinity and transfer electrons directly to hematite but not to goethite (Xiong et al., 2006). Adhesion forces have been used to characterize the interactions and affinity between cells or proteins and different mineral surfaces or crystal faces. Lower et al. (2001) used biological force microscopy to measure the adhesion force between *S. oneidensis* MR-1 cells and the (010) surface of the isostructural minerals goethite (α-FeOOH) and diaspore (α-AlOOH). The regulation of a 150-kD putative Fe(III) reductase to the outer membrane suggested that this protein may be specific for goethite reduction and implied molecular recognition of the Fe(III) (hydr)oxide surface relative to the Al substrate (Lower et al., 2001). Using a similar approach, Neal et al. investigated the fine scale effects of surface structures on cell adhesion by *S.*

oneidensis to the hematite (001) and magnetite (111) and (100) crystal faces (Neal et al., 2005). Adhesive forces differed significantly for the three crystal faces, with the hematite (001) face showing statistically significant greater adhesion than both of the magnetite faces (Neal et al., 2005) (Figure 1.5). Furthermore, two of the cell attached cantilevers showed statistical differences between the (111) and (100) magnetite faces. These findings correlated well with the observed pH point of zero charge of the bulk minerals (considering a negative charge for the outer membrane of *Shewanella*) and also with the density of ferric sites. In summary, these findings suggest that microbes as well as proteins can discriminate between different mineral types and even crystal faces.

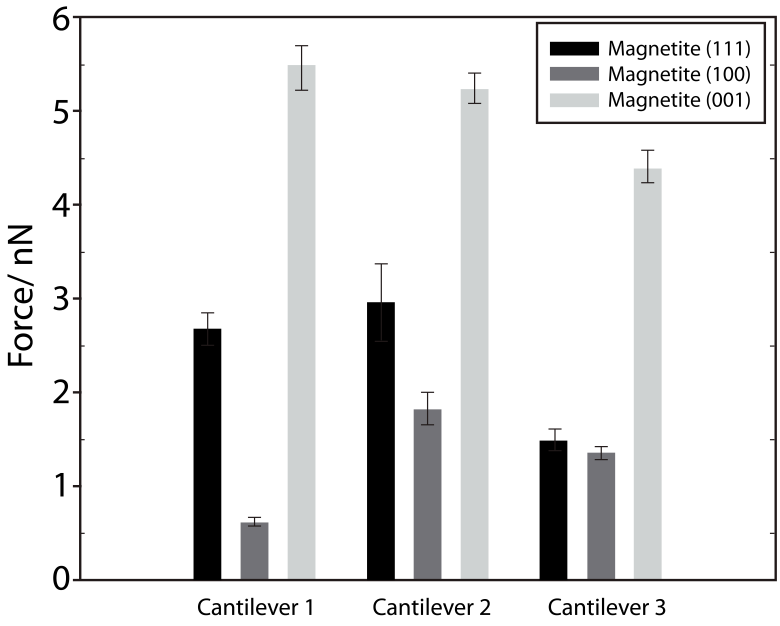

Figure 1.5. Mean force adhesion upon retraction of *Shewella oneidensis* MR-1 embedded on cantilevers and Fe(III) oxide single crystal faces (Neal et al., 2005). Pairwise comparisons between the means across the three cantilevers indicated significant differences between the two magnetite faces and between the magnetite and hematite faces. Figure reprinted from Neal et al. (2005) under the open access license agreement.

Defects in mineral surfaces can lead to an increase in highly reactive sites when compared to mineral terraces. Defects (screw step, edge dislocation, kink, etc…) have long been

considered important in both surface and bulk chemical reactions (Brown et al., 1999). The importance of defects on bacterial reduction of hematite crystals was investigated with *S. putrefaciens* strain CN32 (Rosso et al., 2003b). Reduction of hematite did not happen at the point of contact of the cell/mineral interface but rather "beyond the footprint of the organism." This was initially attributed to the production of quinone-like electron shuttling compounds that attacked high-energy surface defects at a distance from the microbe-mineral interface. Ensuing calculations showed that electron conduction away from the initial site of electron transfer within the hematite crystal to surface defects was a (more) likely explanation (Rosso et al., 2003a;Kerisit and Rosso, 2006).

The limited ability of cultured DMRB to respire crystalline Fe(III) (hydr)oxides (Hansel et al., 2004) may be a consequence of ferrihydrite impurities or regions of enhanced disorder within the mineral structures. Upon consumption of these higher-energy (disordered) sites, reduction may cease leading to only minor amounts of Fe(III) reduction. Using changes in ascorbate-catalyzed reductive dissolution rates, it was estimated that hematite, goethite, and high surface area goethite contained 0.04, 0.10, and 0.32% "ferrihydrite-like" impurities (Roden, 2006). The residual disorder, however, had little impact on the Fe(III) reduction rates since the amount of Fe(III) reduction by *G. sulfurreducens* was 5- to 95-fold higher than the estimated abundance of the ferrihydrite impurities within the (hydr)oxide phases. Recently, we observed that synthesized Fe(III) (hydr)oxides contained a substantial initial degree of disorder, which can approach 25 mole % Fe, depending on the synthesis and washing procedures (Hansel, unpublished data). These values are predicted based on the fractional abundance of a ferrihydrite spectral component required to reconstruct the Fe(III) (hydr)oxide extended X-ray absorption fine-structure (EXAFS) spectra using linear combination fitting. We found that the amount of

Fe(III) reduced within goethite and hematite by *S. putrefaciens* strain CN32 within flow-through columns is in fact a function of the initial degree of disorder within these more stable phases suggesting that the more crystalline component of the (hydr)oxides is not bioavailable for microbial reduction (Hansel et al., 2004). These contrasting findings further highlight the uncertainty of crystalline (hydr)oxide availability for microbial reduction, at least for presently cultured model DMRB. Observations of microbial reduction of more crystalline (e.g., goethite) Fe(III) (hydr)oxides within natural sediments (Stucki et al., 2007) raises the possibility that presently unrecognized groups of microbes are responsible for reducing more recalcitrant Fe phases within the environment (Lin et al., 2007;Lehours et al., 2009;Hori et al., 2010).

1.4.4 Size: Crystal size reflects the growth conditions under which the Fe(III) (hydr)oxide was formed and determines its surface area (Cornell and Schwertmann, 2003). As a result, teasing out which property is controlling microbial reduction is difficult. For instance, due to a log-log relationship between surface area and average particle size, surface area and particle size both correlate strongly with the microbial reduction rates of Fe(III) (hydr)oxides (Roden and Zachara, 1996).

Using empirically derived evidence from nanohematite sorption onto *S. putrefaciens,* Bonneville *et al.* (2006) constructed a model that emphasized the role of microbe-mineral adhesion in the reduction of Fe(III) (hydr)oxide phases. The rate of reduction correlated well with the amount of Fe(III) (hydr)oxide surface coverage of the cell. Based on their model, the apparent half saturation constant increased with particle size, likely due to a decrease in microbe-mineral interaction. This suggested that at similar Fe(III) concentrations, cell surface coverage for larger particles will be smaller resulting in lower rates of reduction when compared to their

smaller counterparts. When applied to previously collected data (Bonneville et al., 2004), the model was able to reproduce initial reduction rates for five Fe(III) (hydr)oxides of varying sizes (Bonneville et al., 2006).

Two studies, which explored the role of particle size on hematite nanoparticle reduction, found contrasting trends depending on the normalization parameter. Using a novel aerosol synthesis method that accurately controlled surface area, the reduction rates for three nanohematite (10, 30, and 50 nm) particles revealed a trend with mass normalized rates decreasing with increasing particle size (Yan et al., 2008). Yet, when normalized to surface area, this trend was reversed. Similarly, surface-area normalized reduction rates of nanohematite ranging in size from 11-99 nm in diameter by *S. oneidensis* MR-1 were an order of magnitude higher for larger (99 nm) particles compared to the smallest particle (11 nm) (Bose et al., 2009). These discrepancies are likely attributed to the dependence of Fe(III) reduction rates on the aggregation state and subsequent microbial accessibility of reactive surface sites (see below).

1.4.5 Mineral Aggregation: Iron(III) (hydr)oxide nano- and micro-meter sized particles are metastable in the environment but due to their high surface energy they tend to aggregate and/or ripen with increased aging (Waychunas et al., 2005). The timeframe with which this happens is still poorly understood, however, a number of investigations have implicated aggregation of Fe(III) (hydr)oxides as a control on microbial Fe(III) reduction.

One noted exception to the linear trend between surface area of synthetic Fe(III) (hydr)oxides and microbial reduction rates was attributed to mineral aggregation. Aggregation resulted in 2-line ferrihydrite and feroxyhyte having lower reduction rates even though they possessed larger surface areas when compared to the other Fe(III) (hydr)oxides. These

aggregated Fe (hydr)oxides deviated far from the linear trend line and could not be used in the regression analysis for this data (Roden and Zachara, 1996;Roden, 2003a). Since BET surface area is measured through N_2 adsorption, it does not necessarily correlate well with reactive site density with respect to microbial accessibility. This data highlights the potential complexity of trying to relate total surface area, measured through BET, with microbial reduction rates. As has been noted, microbial reduction solely based on surface area may be an oversimplification, due to specific limitations of microbial accessibility within aggregated minerals, which is not accounted for in chemical adsorption experiments (Zachara et al., 1998).

Attempts to tease out the role of particle size on microbial reduction using nanometer sized Fe(III) (hydr)oxides have proved problematic due to particle aggregation. As mentioned above, reduction rates for nanohematite particles showed an expected trend with rates decreasing with increasing particle size. However, when normalized for surface area and cell density, reduction rates were greatest for the large particles (30 and 99 nm) and lowest for small particles (10 and 11 nm) (Yan et al., 2008;Bose et al., 2009). A decrease in "effective" surface area for the small particles was likely due to aggregation and resulted in the relative decrease in surface area and cell-normalized reduction rates. The authors argue that aggregated particles correlated better with the area of cell-particle contact rather than total surface area because direct contact was required for reduction (Yan et al., 2008;Bose et al., 2009). Alternatively, Bose et al. (2009) argue that differences in the aggregation state of the Fe(III) (hydr)oxides may induce different microbial Fe(III) reduction mechanisms (i.e., indirect versus direct).

1.4.6 Surface Sorbates and Coprecipitates: Due to their ubiquity and reactive surface chemistry, Fe(III) (hydr)oxides serve as important sorbents and repositories for many nutrients

(*e.g.* phosphate) and metals (*e.g.* Al, Pb) (Cornell and Schwertmann, 2003). Sorbed ions may impact surface site reactivity and/or accessibility for reductive dissolution. Furthermore, isomorphic substitution or coprecipitation of metal cations within Fe(III) (hydr)oxides impacts the physicochemical properties of the phase, particularly solubility. Correspondingly, high concentrations of surface sorbed or substituted ions may diminish the 'bioavailability' of these phases for microbial reduction. In fact, the extent of microbial reduction showed an inverse linear correlation with phosphate loading on 2-line ferrihydrite within batch incubations (Borch et al., 2006). At full surface coverage, the production of Fe(II) decreased nearly 5 fold compared to pure 2-line ferrihydrite. Similarly, arsenate sorption on the surface of ferrihydrite resulted in a decreased extent of microbial Fe(III) reduction (Kocar et al., 2006) compared to that observed previously for pure ferrihydrite (Hansel et al., 2003a) under equivalent flow-through column conditions. More recently, the impact of arsenic sorption on Fe(III) (hydr)oxide reduction was found to be a function of the arsenate concentration (Chow and Taillefert, 2009). Interestingly, the presence of low As(V) concentrations ($\leq$ 1μM) stimulated Fe(III) reduction, while higher As(V) levels (> 1μM) inhibited Fe(III) (hydr)oxide reduction and instead arsenate reduction to arsenite prevailed.

The impact of cation substitution on microbial Fe(III) oxide reduction, however, is not as straightforward as that for surface sorbates. For instance, cation substitution within goethite (Al, Co, Mn, Cr) and ferrihydrite (Ni, Pb) decreased the microbial reduction of the Fe(III) phases (Bousserrhine et al., 1999;Fredrickson et al., 2001;Parmar et al., 2001;Sturm et al., 2008), yet Ni substitution within goethite did not impact the susceptibility of goethite to bioreduction (Zachara et al., 2001). Furthermore, microbial reduction of Si substituted (1 and 5 mole %) ferrihydrite by *S. putrefaciens* CN32 had little effect on the rate and extent of Fe(III) reduction and

biomineralization (Kukkadapu et al., 2004). The presence of merely 5% structural Al within goethite dramatically decreased the rate and extent of bacterial Fe(III) reduction by the anaerobic fermenter *Clostridium butyricum* (Bousserrhine et al., 1999). Furthermore, both abiotic reductive and acid dissolution of Al-containing goethite decreased with increasing substitution (Schwertmann, 1984;Torrent et al., 1987;Bousserrhine et al., 1998; 1999). Yet, reduction of natural Al-substituted goethite by the common DMRB *Shewanella putrefaciens* strain CN32 was found to be comparable to pure, synthetic goethite (Kukkadapu et al., 2001), which was attributed to enhanced disorder or microheterogeneities counteracting the stabilizing-effect of Al within Fe(III) (hydr)oxides (Zachara et al., 1998;Kukkadapu et al., 2001). Thus, the impact of substituted ions on Fe(III) (hydr)oxide reduction is complex, varying with cation type, (hydr)oxide, microbial species, and microbial metabolism (e.g., fermentation versus respiration).

More recently, the impact of Al doping on the rate and extent of Fe(III) reduction by *S. putrefaciens* strain CN32 was shown to vary with Fe(III) (hydr)oxide (Ekstrom et al., in press). In short, Al substitution dramatically decreased the extent and rate of Fe(III) reduction for ferrihydrite but did not significantly impact lepidocrocite and goethite. Interestingly, the extent of Fe(III) reduction consistently declined 1% for every mole % increase in Al substitution in ferrihydrite. As Al substitution increased, the rates of Fe(III) reduction for ferrihydrite began to converge with those for lepidocrocite and goethite. Based on projected rates, at Al molar concentrations above 16%, the rate of ferrihydrite reduction would be less than that of both lepidocrocite and goethite (Figure 1.6). Recent investigations reveal that the dominant Fe(III)-bearing phases utilized by indigenous metal-reducing microbial populations within uranium-contaminated subsurface soils are Al-substituted goethite and Fe-rich phyllosilicates (Stucki et al., 2007). Goethite, in particular, was readily reduced even though the oxides contained a high

degree of Al substitution with mass percentages as high as 35% (Arnseth and Turner, 1988;Phillips et al., 2007;Stucki et al., 2007). This disparity of Al influence on Fe(III) (hydr)oxide bioavailability may explain the persistence of ferrihydrite within sedimentary environments, whereby the capacity for Al-substituted ferrihydrite to serve as a terminal electron acceptor is dramatically diminished making more crystalline phases favorable.

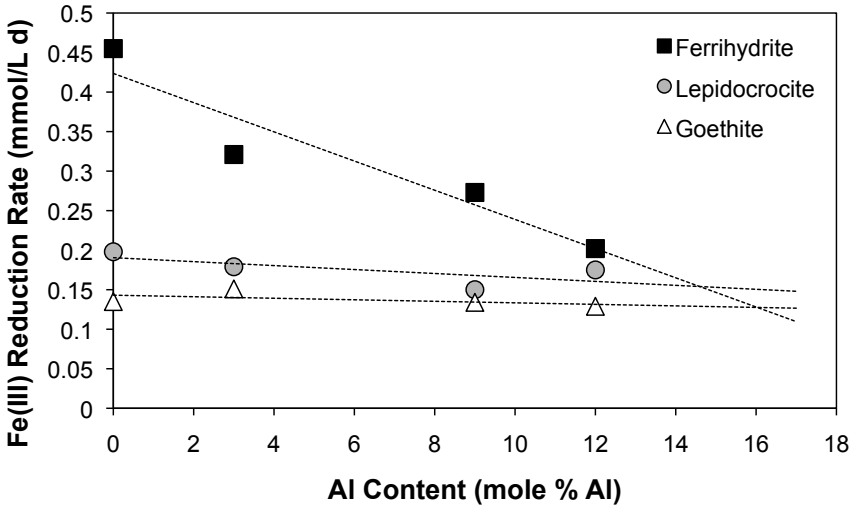

Figure 1.6. Maximum initial Fe(III) reduction rate (mmol L^{-1} d^{-1}) as a function of Al substitution. Trend lines extended to project Fe(III) reduction rates at higher Al levels. Equivalent Fe(III) reduction trends and crossover point were obtained when Fe(III) (hydr)oxides were provided as a slurry or precipitated onto quartz sand. Modified from Ekstrom et al. (Ekstrom et al., 2010)

1.4.7 Reduction Potential: Iron(III) reduction rates were previously shown to be similar over a large range of Fe(III) (hydr)oxide half cell potentials (E_H) (Roden, 2003b;Roden, 2006). Furthermore, reduction of Fe(III) (hydr)oxides within wetland soil incubations proceeded when thermodynamic calculations predicted they were less favorable than methanogenesis (Roden,

2003a). Thus, it was hypothesized that the thermodynamic properties of Fe(III) (hydr)oxides do not affect bacterial enzymatic electron transfer because microbial recognition is the same regardless of crystal structure (Roden, 2003a). In contrast, there is evidence to suggest that the thermodynamic gain of the redox couple may, in fact, affect microbial Fe(III) reduction (Liu et al., 2001), which will vary substantially given the large Eh range for the different Fe(III) (hydr)oxide phases (Figure 1.2).

DMRB display an amazing respiratory versatility, which may be attributed to broad specificity of particular *c*-type cytochromes and/or a large set of cytochromes with widely varying midpoint redox potentials (Dale et al., 2007). For instance, the electron transfer properties of two decaheme cytochromes (OmcA, MtrC) that are considered terminal reductases in *Shewanella* sp. have different properties and mechanisms for binding and transferring electrons to hematite surfaces (Lower et al., 2007;Wigginton et al., 2007). Furthermore, OmcA does not appear to adhere to goethite, likely inhibiting electron transfer (Xiong et al., 2006). Thus, the individual role of the putative terminal reductases in transferring electrons to Fe(III) (hydr)oxides as well as their capacity to interact with phases spanning a large Eh range is unresolved and still under investigation.

Recent investigations have clearly illustrated differential expression of proteins involved in metal respiration (e.g., cytochromes) in the common DMRB *Geobacter* sp. under varying electron acceptor conditions (Ding et al., 2006;Ding et al., 2008). For instance, the physiological status of *G. sulfurreducens* varied in the presence of soluble (i.e., Fe(III)-citrate or fumarate) versus insoluble (i.e., ferrihydrite) electron acceptors with a higher abundance of proteins involved in extracellular electron transfer, such as OmcS. Furthermore, it was recently demonstrated that protein expression of *G. uraniireducens* was significantly different when

grown in a defined culture medium versus subsurface sediments (Holmes et al., 2009). The difference in redox potential of the electron acceptors (e.g., Fe(III)-citrate versus ferrihydrite, ΔE = ~375 mV) will likely have a substantial impact on DMRB physiology; yet, this influence will be masked by the broader signature due to the electron acceptors being difference phases (dissolved versus solid species).

Recently, voltammetric fingerprints of *G. sulfurreducens* adhered to graphite electrodes were found to vary depending on the applied potential on the anode (Busalmen et al., 2008). More energy was produced when higher potentials (600 mV, relative to $Ag/AgCl^-$ electrode with E_{NHE}=197 mV) were applied relative to lower potentials (100 mV), suggesting a greater electron transport capacity at higher Eh. Of particular relevance, however, are recent findings that the succession and composition of anode-hosted bacterial populations differed substantially at different anode potentials (300 versus 600 mV relative to $Ag/AgCl^-$) (White et al., 2009). Microbial fuel cells (MFC) inoculated with seawater contained four dominant bacterial groups, δ-, γ-, and ε-*Proteobacteria* and *Flavobacterium-Cytophaga-Bacteroides* (FCB). While *Geobacter* spp. dominated the bacterial community during peak power production on anodes at 600 mV, FCB phylotypes predominated at lower reduction potentials (300 mV). The reduction potential range for these experiments (corrected for reference to $Ag/AgCl^-$) is approximately -100 to 400 mV spanning Fe(III)-chelates (e.g., Fe(III)-citrate) to lepidocrocite (γ-FeOOH, E=-275 mV) (see Figure 1.2). While these systems did not attempt to mimic the potential of low Eh metal substrates (e.g., goethite), these novel studies revealed that the reduction potential of anodes impacts the phylogeny and physiology of anode-associated communities – findings that can be translated to mineral surfaces. The role of Eh in impacting the structure, activity, and

physiology of Fe(III)-reducing populations remains an unexplored area and one that warrants investigation.

1.5 Impact of Microbial Fe(III) (Hydr)oxide Reduction on the Fate and Transport of Metals and Radionuclides

As a consequence of their high surface area and density of reactive surface sites, Fe(III) (hydr)oxides serve as reactive templates in soils and sediments. They co-precipitate many metals and sorb numerous organics (e.g. pesticides, PAHs), nutrients (e.g. phosphate), and metals (e.g. Pb, As, U). Microbial Fe(III) reduction results in either mineral dissolution or conversion to more stable (e.g., more crystalline) secondary phases having a lower sorptive capacity, such as goethite (Hansel et al., 2005;Tufano and Fendorf, 2008;Tufano et al., 2008). Consequently, the reduction of metal-laden Fe(III) (hydr)oxide phases may release associated contaminants into solution. For instance, the release of sorbed and co-precipiated metals (e.g., As, Ni, Co) and nutrients (e.g., phosphate) during microbial reduction of pure Fe(III) (hydr)oxide phases (Fredrickson et al., 2001;Zachara et al., 2001) and Fe(III)-bearing sediments (Landa et al., 1991;Cummings et al., 1999;Crowe et al., 2007) has been frequently observed. The ultimate fate of the associated ions, however, will be a function of ion speciation, mineral transformations, and the aqueous chemical environment. In fact, the fate of many contaminants will be a function, in large part, of the mineralogy of the initial Fe(III) sorbent and products of microbial Fe(III) reduction.

A number of recent investigations have illustrated that reductive dissolution of Fe(III) (hydr)oxides may actually enhance contaminant attenuation, in particular through sequestration within secondary precipitates. In particular, the formation of secondary magnetite following

microbial reduction of Fe(III) (hydr)oxides in the presence of Zn(II) or Ni(II), results in immobilization of the cations, presumably within the magnetite structure (Cooper et al., 2000;Fredrickson et al., 2001). However, batch experiments examining Fe(III) reduction of synthetic and natural Fe(III) (hydr)oxides in the presence of Zn, illustrate that the immobilization of Zn may be inhibited in the presence of complexing agents, including NTA, clays, and the humic acid analog 9,10-anthraquinone-2,6-disulfonic acid (AQDS) (Coby and Picardal, 2006). Furthermore, lanthanide (Nd, Gd, Tb, Ho, Er) and transition metal (Cr, Mn, Co, Ni, and Zn) substituted magnetites have been formed via microbial Fe(III) reduction of akaganeite (β-FeOOH) (Moon et al., 2007a;Moon et al., 2007b). Recent studies also illustrate that sequestration of arsenic under Fe(III)-reducing conditions may be a function of magnetite formation (Kocar et al., 2006;Tufano and Fendorf, 2008). Microbial reduction of As(V)-sorbed ferrihydrite under advective flow resulted in the enhanced retention of As, as both As(III) and As(V), relative to systems not undergoing magnetite precipitation (Kocar et al., 2006). Similarly, recent studies indicate that As(V) is strongly sorbed (Islam et al., 2005) or is incorporated into the magnetite structure (Coker et al., 2006) following microbial reduction of both ferrihydrite or soluble Fe(III). These findings all contradict the previous assumptions and laboratory observations (Cummings et al., 1999) that microbial reduction of Fe(III) (hydro)oxides, which are strong sorbents of metal(loid)s, would result in the enhanced mobilization of As. Similar behavior has recently been observed for uranium (Neiss et al., 2007). In the presence of Ca, the formation of ternary Ca-UO_2-CO_3 complexes results in the preferential reduction of Fe(III) (Brooks et al., 2003) and subsequent transformation of ferrihydrite to magnetite. The preferential reduction of Fe(III) and mineralization to magnetite results in the preservation and sequestration of the oxidized U(VI) species, which is found adsorbed onto or incorporated into secondary goethite

and magnetite precipitates (Stewart et al., 2009). Thus, the potential for secondary magnetite formation to immobilize contaminants is more extensive than originally thought. While these findings hold promise for introducing additional pathways of contaminant immobilization within reducing environments, the stability of these magnetite complexes is not known and they therefore pose a potential means of contaminant remobilization upon changing environmental conditions. In particular, while microbial reduction of pure magnetite is limited at circumneutral pH (Kostka and Nealson, 1995), distortion of the magnetite structure (Coker et al., 2006) through ion incorporation will likely impact the stability and bioavailability of magnetite for microbial reduction.

Microbial reduction of Fe(III) (hydr)oxides may also result in a cascade of subsequent redox and/or complexation reactions due to the reactivity of the metabolite Fe(II). Microbial Fe(III) reduction provides a strong reductant and complexing ligand (Fe^{II}). The microbial reduction of Fe(III) (hydr)oxides may therefore indirectly result in the immobilization of a number of anion or redox-active contaminants and nutrients. For instance, Fe(II)-stimulated removal of phosphate has received increasing attention as a possible means of attenuating phosphate from septic systems through the formation of the ferrous phosphate mineral vivianite (Robertson, 2000). Furthermore, ferrous Fe is a particularly strong reductant of many contaminants including metals (e.g. Cr) (Fendorf et al., 2000), radionuclides (e.g. U, Tc) (Fredrickson et al., 2004) and organic compounds (e.g. nitroamines) (Hofstetter et al., 1999). Consequently, the rate of contaminant reduction will be a function of Fe(III) reduction rates and the bioavailability of Fe(III) – which will be a function of the geochemical and mineralogical factors discussed above. Interestingly, laboratory simulations indicate that effective reduction of redox-active metals (e.g. Cr) can be sustained on catalytic amounts of Fe(III) (Wielinga et al.,

2001). For instance, biogenic Fe(II) abiotically reacts with Cr(VI) resulting in the formation of mixed Fe(III)-Cr(III) (hydr)oxide phases (Sass and Rai, 1987;Eary and Rai, 1989;Hansel et al., 2003b), resulting in the regeneration of microbially-available Fe(III) (primarily as ferrihydrite) (Hansel et al., 2003b). Theoretically, this continued Fe-Cr redox cycling can result in sustained Cr(VI) reduction, considering minimal Fe loss from the system. In some cases, the rate, extent, and products of Fe(II)-induced contaminant reduction are a function of the bonding environment of the biogenic Fe(II). While aqueous Fe(II) is a potent reductant of chromate (Cr^{VI}), the rates of Tc(VI) and U(VI) reduction are dramatically enhanced via reaction with surface-bound (adsorbed) or co-precipitated Fe(II) (e.g., magnetite) (Lloyd et al., 2000;Fredrickson et al., 2004). For instance, while dissolved concentrations of uranyl (U^{VI}) are unchanged in the presence of aqueous Fe(II) over an 80 h reaction period, Fe(II) adsorbed on hematite results in complete removal of U(VI) via reduction within 60 h (Liger et al., 1999).

1.6 Conclusions

Understanding the geochemical controls on microbial Fe(III) reduction is crucial for defining the reducing capacity of soils and sediments, predicting the fate and transport of (in)organic contaminants, delineating the controls on carbon degradation and cycling, and forecasting electron flow and operative terminal electron accepting processes in subsurface environments. Variations in the rate and extent of microbial reduction of Fe(III) (hydr)oxides has been linked to surface area, solubility, crystallite size, thermodynamics, crystal structure, disorder, aggregation, surface sorbates, and cation substitution. Yet, as a consequence of the intimate association between these physicochemical properties and their evolution with reaction progression, isolating the contribution of various factors on constraining microbial Fe(III)

reduction has proved a challenging task. We contend that to further advance our knowledge, more sophisticated techniques and experimental approaches will need to be employed, including surface sensitive and time resolved spectroscopy to accurately interrogate the molecular environment. We also anticipate that using poised anodes as surrogate minerals holds promise in addressing the role of reduction potential in electron transfer processes. Ultimately, unraveling the enigma of the microbe-mineral interface will require a multi-disciplinary approach requiring an appreciation of the physics and chemistry of mineral surfaces, the enzymatic and non-enzymatic pathways responsible for electron transfer, and the ecology of metal-reducing microbes within a complex mineral framework.

1.7 References Cited

Anderson, R.T., and Lovley, D.R. (2000). Anaerobic bioremedation of benzene under sulfate-reducing conditions in a petroleum-contaminated aquifer. *Environ. Sci. Technol.* 34**,** 2261-2266.

Arnseth, R.W., and Turner, R.S. (1988). Sequential extraction of iron, manganese, aluminum, and silicaon in soils from 2 contrasting watersheds. *Soil Sci. Soc. Am. J.* 52**,** 1801-1807.

Baes, C.F., and Mesmer, R.E. (1976). *The Hydrolysis of Cations.* Malabar, FL: Krieger Publishing Company.

Benner, S.G., Hansel, C.M., Wielinga, B.W., Barber, T.M., and Fendorf, S. (2002). Reductive dissolution and biomineralization of iron hydroxide under dynamic flow conditions. *Environ. Sci. Technol.* 36**,** 1705-1711.

Bonneville, S., Behrends, T., and Van Cappellen, P. (2009). Solubility and dissimilatory reduction kinetics of iron(III) oxyhydroxides: A linear free energy relationship. *Geochimica Et Cosmochimica Acta* 17**,** 5273-5282.

Bonneville, S., Behrends, T., Van Cappellen, P., Hyacinthe, C., and Roling, W.F.M. (2006). Reduction of Fe(III) colloids by Shewanella putrefaciens: A kinetic model. *Geochim. Cosmochim. Acta* 70**,** 5842-5854.

Bonneville, S., Van Cappellen, P., and Behrends, T. (2004). Microbial reduction of iron(III) oxyhydroxides: effects of mineral solubility and availability. *Chemical Geology* 212**,** 255-268.

Borch, T., Masue, Y., Kukkadapu, R.K., and Fendorf, S. (2006). Phosphate imposed limitations on biological reduction and alteration of ferrihydrite. *Environ. Sci. Technol.* 41**,** 166-172.

Bose, S., Hochella Jr., M.F., Gorby, Y.A., Kennedy, D.W., Mccready, D.E., Madden, A.S., and Lower, B.H. (2009). Bioreduction of hematite nanoparticles by the dissimalory iron reducing bacterium *Shewanella oneidensis* MR-1. *Geochim. Cosmochim. Acta* 73**,** 962-976.

Bousserrhine, N., Gasser, U.G., Jeanroy, E., and Berthelin, J. (1998). Effect of aluminum substitution on ferri-reducing bacterial activity and dissolution of goethites. *CR Acad. Sci.* 326**,** 617-624.

Bousserrhine, N., Gasser, U.G., Jeanroy, E., and Berthelin, J. (1999). Bacterial and chemical reductive dissolution of Mn-, Co-, Cr-, and Al-substituted goethites. *Geomicrob. J.* 16**,** 245-258.

Bromfield, S.M. (1954a). Reduction of ferric compounds by soil bacteria. *J. Gen. Microbiol.* 11**,** 1-6.

Bromfield, S.M. (1954b). The reduction of iron oxide by bacteria. *J. Soil. Sci.* 5**,** 129-139.

Brooks, S.C., Fredrickson, J.K., Carroll, S.L., Kennedy, D.W., Zachara, J.M., Plymale, A.E., Kelly, S.D., Kemner, K.M., and Fendorf, S. (2003). Inhibition of bacterial U(VI) reduction by calcium. *Environ. Sci. Technol.* 37**,** 1850-1858.

Brown, G.E., Jr., Henrich, V.E., Casey, W.H., Clark, D.L., Eggleston, C., Felmy, A., Goodman, D.W., Gratzel, M., Maciel, G., Mccarthy, M.I., Nealson, K.H., Sverjensky, D.A., Toney, M.F., and Zachara, J.M. (1999). Metal oxide surfaces and their interactions with aqueous solutions and microbial organisms. *Chemical Reviews* 99**,** 77-174.

Busalmen, J.P., Esteve-Nunez, A., and Feliu, J.M. (2008). Whole cell electrochemistry of electricity-producing microorganisms evidence an adaptation for optimal exocellular electron transport. *Environ. Sci. Technol.* 42**,** 2445-2450.

Caccavo, F., Jr., Blakemore, R.P., and Lovley, D.R. (1992). A hydrogen-oxidizing, Fe(III)-reducing microorganism from the Great Bay Estuary, New Hampshire. *Appl. Environ. Microb.* 58**,** 3211-3216.

Chow, S.S., and Taillefert, M. (2009). Effect of arsenic concentration on microbial iron reduction and arsenic speciation in an iron-rich freshwater sediment. *Geochim. Cosmochim. Acta* 73**,** 6008-6021.

Coby, A.J., and Picardal, F.W. (2006). Influence of sediment components on the immobilization of Zn during microbial Fe-(hydr)oxide reduction. *Environ. Sci. Technol.* 40**,** 3813-3818.

Coker, V.S., Gault, A.G., Pearce, C.I., Van Der Laan, G., Telling, N.D., Charnock, J.M., Polya, D.A., and Llyoyd, J.R. (2006). XAS and XMCD evidence for species-dependent partitioning of arsenic during microbial reduction of ferrihydrite to magnetite. *Environ. Sci. Technol.* 40**,** 7745-7750.

Cooper, D.C., Picardal, F., Rivera, J., and Talbot, C. (2000). Zinc immobilization and magnetite formation via ferric oxide reduction by *Shewanella putrefaciens* 200. *Environ. Sci. Technol.* 34**,** 100-106.

Cornell, R.M., Schneider, W., and Giovanoli, R. (1991). Phase transformations in the ferrihydrite/cysteine system. *Polyhedron* 8**,** 2829-2834.

Cornell, R.M., and Schwertmann, U. (2003). *The Iron Oxides: Structure, Properties, Reactions, Occurrence and Uses.* Weinheim, Germany: VCH.

Crowe, S.A., Roberts, J.A., Weisener, C.G., and Fowle, D.A. (2007). Alteration of iron-rich lacustrine sediments by dissimilatory iron-reducing bacteria. *Geobiol.* 5**,** 63-73.

Cummings, D.E., Caccavo, F., Jr., Fendorf, S., and Rosenzweig, R.F. (1999). Arsenic mobilization by the dissimilatory Fe(III)-reducing bacterium *Shewanella alga* BrY. *Environ. Sci. & Technol.* 33**,** 723-729.

Cutting, R.S., Coker, V.S., Fellowes, J.W., Lloyd, J.R., and Vaughan, D.J. (2009). Mineralogical and morphological constraints on the reduction of Fe(III) minerals by Geobacter sulfurreducens. *Geochimica Et Cosmochimica Acta* 73**,** 4004-4022.

Dale, J.R., Wade Jr., R., and Dichristina, T.J. (2007). A conserved histidine in cytochrome *c* maturation permease CcmB of *Shewanella putrefaciens* is required for anaerobic growth below a threshold standard redox potential. *J. Bacteriol.* 189**,** 1036-1043.

Dichristina, T.J., Fredrickson, J.K., and Zachara, J.M. (2005). Enzymology of electron transport: Energy generation with geochemical consequences. *Rev. Mineral. Geochem.* 59**,** 27-52.

Ding, Y.-H.R., Hixson, K.K., Aklujkar, M.A., Lipton, M.S., Smith, R.D., Lovley, D.R., and Mester, T. (2008). Proteome of *Geobacter sulfurreducens* grown with Fe(III) oxide or Fe(III) citrate as the electron acceptor. *Biochim. Biophys. Acta* 1784**,** 1935-1941.

Ding, Y.-H.R., Hixson, K.K., Giometti, C.S., Stanley, A., Esteve-Nunez, A., Khare, T., Tollaksen, S.L., Zhu, W., Adkins, J.N., Lipton, M.S., Smith, R.D., Mester, T., and Lovley, D.R. (2006). The proteome of dissimilatory metal-reducing microorganism *Geobacter sulfurreducens* under various growth conditions. *Biochim. Biophys. Acta* 1764**,** 1198-1206.

Dobbin, P.S., Carter, J.P., Garcia-Salamanca San Juan, C., Von Hobe, M., Powell, A.K., and Richardson, D.J. (1999). Dissimilatory Fe(III) reduction by *Clostridium beijerinckii* isolated from freshwater sediment using Fe(III) maltol enrichment. *FEMS Microb. Lett.* 176**,** 131-138.

Eary, L.E., and Rai, D. (1989). Kinetics of chromate reduction by ferrous-ions derived from hematite and biotite at 25-degrees-C. *Am. J. Sci.* 289**,** 180-213.

Ehrlich, H.L., and Newman, D.K. (2009). *Geomicrobiology.* Boca Raton, FL: CRC Press.

Ekstrom, E.B., Learman, D.R., Madden, A.S., and Hansel, C.M. (2010). Contrasting effects of Al substitution on microbial reduction of Fe(III) (hydr)oxides. *Geochimica Et Cosmochimica Acta* 74**,** 7086-7099.

Ekstrom, E.B., Learman, D.R., Madden, A.S., and Hansel, C.M. (in press). Contrasting effects of Al substitution on microbial reduction of Fe(III) oxides. *Geochim. Cosmochim. Acta*.

El-Naggar, M.Y., Gorby, Y.A., Xia, W., and Nealson, K.H. (2008). The molecular density of states in bacterial nanowires. *Biophysical J.* 95**,** L10-L12.

Favre, F., Stucki, J.W., and Boivin, P. (2006). Redox properties of structural Fe in ferruginous smectite. A discussion of the standard potential and its environmental implications. *Clays and Clay Miner.* 54**,** 466-472.

Fendorf, S., Wielinga, B.W., and Hansel, C.M. (2000). Chromium transformations in natural environments: The role of biological and abiological processes in chromium(VI) reduction. *Internat. Geol.* 42**,** 691-701.

Fennessey, C.M., Jones, M.E., Taillefert, M., and Dichristina, T.J. (2010). Siderophores are not involved in Fe(III) solubilization during anaerobic Fe(III) respiration by *Shewanella oneidensis* MR-1. *App. Environ. Microb.* 76**,** 2425-2432.

Fischer, W.R. (Year). "Die Wirkung von zweiwertigem Eisen auf Losung und Umwandlung von Eisen(III)-hydroxiden", in: *Pseudogley and gley Trans. Comm. V & VI*, eds. E. Schlichting & U. Schwertmann: Int. Soil Sci. Soc., VCH), 37-44.

Fredrickson, J.K., Kukkadapu, R.K., Liu, C.K., and Zachara, J.M. (2003). Influence of electron donor/acceptor concentrations on hydrous ferric oxide (HFO) bioreduction. *Biodegradation* 14**,** 91-103.

Fredrickson, J.K., Zachara, J.M., Kennedy, D.W., Dong, H., Onstott, T.C., Hinman, N.W., and Li, S.-M. (1998). Biogenic iron mineralization accompanying the dissimilatory reduction of hydrous ferric oxide by a groundwater bacterium. *Geochim. Cosmochim. Acta* 62**,** 3239-3257.

Fredrickson, J.K., Zachara, J.M., Kennedy, D.W., Duff, M.C., Gorby, Y.A., Li, S.-M.W., and Krupka, K.M. (2000). Reduction of U(VI) in goethite (a-FeOOH) suspension by a dissimilatory metal-reducing bacterium. *Geochim. Cosmochim. Acta* 64**,** 3085-3098.

Fredrickson, J.K., Zachara, J.M., Kennedy, D.W., Kukkadapu, R., Mckinley, J.P., Heald, S.M., Liu, C., and Plymale, A.E. (2004). Reduction of TcO4- by sediment-associated biogenic Fe(II). *Geochim. Cosmochim. Acta* 68**,** 3171-3187.

Fredrickson, J.K., Zachara, J.M., Kukkadapu, R.K., Gorby, Y.A., Smith, S.C., and Brown, C.F. (2001). Biotransformation of Ni-substituted hydrous ferric oxide by an Fe(III)-reducing bacterium. *Environ. Sci. Technol.* 35**,** 703-712.

Froelich, P.N., Klinkhammer, G.P., Bender, M.L., Luedtke, N.A., Heath, G.R., Cullen, D., Dauphin, P., Hammond, D., Hartman, B., and Maynard, V. (1979). Early oxidation of organic matter in pelagic sediments of the eastern equatorial Atlantic: Suboxic diagenesis. *Geochim. Cosmochim. Acta* 43**,** 1075-1090.

Gorby, Y.A., Yanina, S., Mclean, J.S., Rosso, K.M., Moyles, D., Dohnalkova, A., Beveridge, T.J., Chang, I.S., Kim, B.-H., Kim, K.S., Culley, D.E., Reed, S.B., Romine, M.F., Saffarini, D., Hill, E.A., Shi, L., Elias, D., Kennedy, D.W., Pinchuk, G., Watanabe, K., Ishii, S.I., Logan, B., Nealson, K.H., and Fredrickson, J.K. (2006). Electrically conductive bacterial nanowires prodiuced by *Shewanella oneidensis* strain MR-1 and other microorganisms. *Proc. Nat. Acad. Sci.* 103**,** 11358-11363.

Gralnick, J.A., and Newman, D.K. (2007). Extracellular respiration. *Mol. Microbiol.* 65**,** 1-11.

Grantham, M.C., Dove, P.M., and Dichristina, T.J. (1997). Microbially catalyzed dissolution of iron and aluminum oxyhydroxide mineral surface coatings. *Geochim. Cosmochim. Acta* 61**,** 4467-4477.

Hansel, C.M., Benner, S.G., and Fendorf, S. (2005). Competing Fe(II)-induced mineralization pathways of ferrihydrite. *Environ. Sci. Technol.* 39**,** 7147-7153.

Hansel, C.M., Benner, S.G., Neiss, J., Dohnalkova, A., Kukkadapu, R.K., and Fendorf, S. (2003a). Secondary mineralization pathways induced by dissimilatory iron reduction of ferrihydrite under advective flow. *Geochim. Cosmochim. Acta* 67**,** 2977-2992.

Hansel, C.M., Benner, S.G., Nico, P., and Fendorf, S. (2004). Structural constraints of ferric (hydr)oxides on dissimilatory iron reduction and the fate of Fe(II). *Geochim. Cosmochim. Acta* 68**,** 3217-3229.

Hansel, C.M., Fendorf, S., Jardine, P.M., and Francis, C.A. (2008). Changes in bacterial and archael community structure and functional diversity along a geochemically variable soil profile. *Appl. Environ. Microb.* 74**,** 1620-1633.

Hansel, C.M., Wielinga, B.W., and Fendorf, S. (2003b). Structural and compositional evolution of Cr/Fe solids after indirect chromate reduction by dissimilatory iron-reducing bacteria. *Geochim. Cosmochim. Acta* 67**,** 401-412.

Haveman, S.A., Didonato, R.J., Villanueva, L., Shelobolina, E.S., Postier, B.L., Xu, B., Liu, A., and Lovley, D.R. (2008). Genome-wide gene expression pattherns and growth requirements suggest that *Pelobacter carbinolicus* reduces Fe(III) indirectly via sulfide production. *App. Environ. Microb.* 74**,** 4277-4284.

Hernandez, M.E., Kappler, A., and Newman, D.K. (2004). Phenazines and other redox active antibiotics promote microbial mineral reduction. *Appl. Environ. Microb.* 70**,** 921-928.

Hernandez, M.E., and Newman, D. (2001). Extracellular electron transfer: Review. *Cell. Mol. Life. Sci.* 58**,** 1562-1571.

Hofstetter, T.B., Heijman, C.G., Haderlein, S.B., Holliger, C., and Schwarzenbach, R.P. (1999). Complete reduction of TNT and other (poly)nitroaromatic compounds under iron-reducing subsurface conditions. *Environ. Sci. Technol.* 33**,** 1479-1487.

Holmes, D.E., O'neil, R.A., Chavan, M.A., N'guessan, L.A., Vrionis, H.A., Perpetua, L.A., Larrahondo, M.J., Didonato, R., Liu, A., and Lovley, D.R. (2009). Transcriptome of *Geobacter uraniireducens* growing in uranium-contaminated subsurface sediments. *ISME J.* 3.

Hori, T., Muller, A., Igarashi, Y., Conrad, R., and Friedrich, M.W. (2010). Identification of iron-reducing microorganisms in anoxic rice paddy soil by 13C-acetate probing. *ISME J.* 4**,** 267-278.

Islam, F.S., Pederick, R.L., Gault, A.G., Adams, L.K., Polya, D.A., Charnock, J.M., and Llyoyd, J.R. (2005). Interactions between the Fe(III)-reducing bacterium Geobacter sulfurreducens and arsenate, and capture of the metalloid by biogenic Fe(II). *Appl. Environ. Microb.* 71**,** 8642-8648.

Jakobsen, R., and Postma, D. (1999). Redox zoning, rates of sulfate reduction and interactions with Fe-reduction and methanogenesis in a shallow sandy aquifer, Romo, Denmark. *Geochim. Cosmochim. Acta* 63**,** 137-151.

Jang, J.-H., Dempsey, B.A., Catchen, G.L., and Burgos, W.D. (2003). Effects of Zn(II), Cu(II), Mn(II), Fe(II), NO_3^-, or SO_4^{2-} at pH 6.5 and 8.5 on transformations of hydrous ferric

oxide (HFO) as evidenced by Mossbauer spectroscopy. *Colloids and Surfaces A:Physicochem. Eng. Aspects* 221**,** 55-68.

Jones, J., Gardener, S., and Simon, B.M. (1984). Reduction of ferric iron by heterotrophic bacteria in lake sediments. *J. Gen. Microbiol.* 130**,** 45-51.

Jones, M.E., Fennessey, C.M., Dichristina, T.J., and Taillefert, M. (2010). Shewanella oneidensis MR-1 mutants selected for their inability to produce soluble organic-Fe(III) complexes are unable to respire Fe(III) as an electron acceptor. *Environ. Microb.* 12**,** 938-950.

Kappler, A., and Straub, K.L. (2005). Geomicrobiological cycling of iron. *Rev. Mineral. Geochem.* 59**,** 85-108.

Kerisit, S., and Rosso, K.M. (2006). Computer simulation of electron transfer at hematite surfaces. *Geochimica Et Cosmochimica Acta* 70**,** 1888-1903.

Kocar, B.D., Herbel, M.J., Tufano, K.J., and Fendorf, S. (2006). Contrasting effects of dissimilatory iron(III) and arsenic(V) reduction on arsenic retention and transport. *Environ. Sci. Technol.* 40**,** 6715-6721.

Kostka, J.E., and Nealson, K.H. (1995). Dissolution and reduction of magnetite by bacteria. *Environ. Sci. Technol.* 29**,** 2535-2540.

Kostka, J.E., Stucki, J.W., Nealson, K.H., and Wu, J. (1996). Reduction of structural Fe(III) in smectite by a pure culture of Shewanella putrefaciens strain MR-1. *Clays and Clay Minerals* 44**,** 522-529.

Kostka, J.E., Wu, J., Nealson, K.H., and Stucki, J.W. (1999). The impact of structural Fe(III) reduction by bacteria on the surface chemistry of smectite clay minerals. *Geochimica Et Cosmochimica Acta* 63**,** 3705-3713.

Kukkadapu, R., Zachara, J.M., Fredrickson, J.K., and Kennedy, D.W. (2004). Biotransformation of two-line silica-ferrihydrite by a dissimilatory Fe(III)-reducing bacterium: formation of carbonate green rust in the presence of phosphate. *Geochim. Cosmochim. Acta* 68**,** 2799-2814.

Kukkadapu, R.K., Zachara, J.M., Smith, S.C., Fredrickson, J.K., and Liu, C. (2001). Dissimilatory bacterial reduction of Al-substituted goethite in subsurface sediments. *Geochim. Cosmochim. Acta* 65**,** 2913-2924.

Landa, E.R., Phillips, E.J.P., and Lovley, D.R. (1991). Release of Ra-226 from uranium mill tailings by microbial Fe(III) reduction. *App. Geochem.* 6**,** 647-652.

Langmuir, D. (1969). The Gibbs free energies of substrates in the system $Fe\text{-}O_2\text{-}H_2O\text{-}CO_2$ at 25C. *U.S. Geol. Surv. Prof. Paper* 650-B**,** B180-B184.

Larese-Casanova, P., and Scherer, M.M. (2007). Fe(II) sorption on hematite: New insights based on spectroscopic measurements. *Environ. Sci. Technol.* 41**,** 471-477.

Lehours, A.-C., Batisson, I., Guedon, A., Mailhot, G., and Fonty, G. (2009). Diversity of culturable bacteria from the anaerobic zone of the meromictic Lake Pavin, able to perform dissimilatory-iron reduction in different in vitro conditions. *Geomicrob. J.* 26**,** 212-223.

Lies, D.P., Hernandez, M.E., Kappler, A., Mielke, R.E., Gralnick, J.A., and Newman, D.K. (2005). Shewanella oneidensis MR-1 uses overlapping pathways for iron reduction at a distance and by direct contact under conditions relevant for biofilms. *App. Environ. Microb.* 71**,** 4414-4426.

Liger, E., Charlet, L., and Van Cappellen, P. (1999). Surface catalysis of uranium(VI) reduction by iron(II). *Geochim. Cosmochim. Acta* 63**,** 2939-2955.

Lin, B., Hyacinthe, C., Bonneville, S., Braster, M., Van Cappellen, P., and Roling, W.F.M. (2007). Phylogenetic and physiological diversity of dissimilatory ferric iron reducers in sediments of the polluted Scheldt estuary, Northwest Europe. *Environ. Microb.* 9**,** 1956-1968.

Liu, C.X., Kota, S., Zachara, J.M., Fredrickson, J.K., and Brinkman, C.K. (2001). Kinetic analysis of the bacterial reduction of goethite. *Environmental Science & Technology* 35**,** 2482-2490.

Lloyd, J.R., Chesnes, J., Glasauer, S., Bunker, D.J., Livens, F.R., and Lovley, D.R. (2002). Reduction of actinides and fission products by Fe(III)-reducing bacteria. *Geomicrob. J.* 19**,** 103-120.

Lloyd, J.R., Sole, V.A., Van Praagh, C.V.G., and Lovley, D.R. (2000). Direct and Fe(II)-mediatd reduction of technetium by Fe(III)-reducing bacteria. *App. Environ. Microb.* 66**,** 3743-3749.

Lovley, D.R. (1987). Organic matter mineralization with the reduction of ferric iron: a review. *Geomicrob. J.* 5**,** 375-399.

Lovley, D.R. (1991). Dissimilatory Fe(III) and Mn(IV) reduction. *Microbiological Reviews* 55**,** 259-287.

Lovley, D.R. (2000). "Fe(III)- and Mn(IV)-reducing prokaryotes," in *The Prokaryotes,* eds. M. Dworkin, S. Falkow, E. Rosenberg, K.-H. Schleifer & E. Stackebrandt. (New York: Springer-Verlag).

Lovley, D.R. (2001). Anaerobes to the Rescue. *Science* 293**,** 1444-1446.

Lovley, D.R., Coates, J.D., Blunt-Harris, E.L., Phillips, E.J.P., and Woodward, J.C. (1996). Humic substances as electron acceptors for microbial respiration. *Nature* 382**,** 445-448.

Lovley, D.R., Holmes, D.E., and Nevin, K.P. (2004). Dissimilatory Fe(III) and Mn(IV) Reduction. *Adv. Microb. Physiol.* 49**,** 219-286.

Lovley, D.R., and Phillips, E.J.P. (1986). Availability of ferric iron for microbial reduction in bottom sediments of the freshwater tidal Potomac River. *Appl. Environ. Microb.* 52**,** 751-757.

Lovley, D.R., and Phillips, E.J.P. (1988). Novel mode of microbial energy metabolism: Organic carbon oxidation coupled to dissimilatory reduction of iron or manganese. *Appl. Environ. Microb.* 54**,** 1472-1480.

Lovley, D.R., Phillips, E.J.P., Gorby, Y.A., and Landa, E.R. (1991a). Microbial reduction of uranium. *Nature* 350**,** 413-416.

Lovley, D.R., Phillips, E.J.P., and Lonergan, D.J. (1991b). Enzymatic versus nonenzymatic mechanisms for Fe(III) reduction in aquatic sediments. *Environ. Sci. Technol.* 25**,** 1062-1067.

Lower, B.H., Shi, L., Yongsunthon, R., Droubay, T., Mccready, D.E., and Lower, S.K. (2007). Specific bonds between iron oxide surface and outer membrane cytochromes MtrC and OmcA from *Shewanella oneidensis* MR-1. *J. Bacteriol.* 189**,** 4844-4952.

Lower, S.K., Hochella, M.F., and Beveridge, T.J. (2001). Bacterial recognition of mineral surfaces: Nanoscale interactions between Shewanella and alpha-FeOOH. *Science* 292**,** 1360-1363.

Manceau, A., and Drits, V.A. (1993). Local structure of ferrihydrite and feroxyhite by EXAFS spectroscopy. *Clay Miner.* 28**,** 165-184.

Moon, J.W., Roy, Y.W., Yeary, L.W., Lauf, R.J., Rawn, C.J., Love, L.J., and Phelps, T.J. (2007a). Microbial formation of lanthanide-substituted magnetites by Thermoanerobacter sp. TOR-39. *Extremophiles* 11**,** 859-867.

Moon, J.W., Yeary, L.W., Rondinone, A.J., Rawn, C.J., Kirkham, M.J., Roh, Y., Love, L.J., and Phelps, T.J. (2007b). Magnetic response of microbially synthesized transition metal- and lanthanide-substituted nano-sized magnetites. *J. Magnetism and Magnetic Materials* 313**,** 283-292.

Myers, C.R., and Nealson, K.H. (1988). Bacterial manganese reduction and growth with manganese oxide as the sole electron acceptor. *Science* 240**,** 1319-1321.

Myers, J.M., and Myers, C.R. (1998). Isolation and sequence of *omcA*, a gene encoding a decaheme outer membrane cytochrome *c* of *Shewanella putrefaciens* MR-1, and detection of *omcA* homologs in other strains of *S. putrefaciens*. *Biochim. Biophys. Acta* 1373**,** 237-251.

Myers, J.M., and Myers, C.R. (2001). Role of outer membrane cyctochromes OmcA and OmcB of *Shewanella putrefaciens* MR-1 in reduction of manganese dioxide. *Appl. Environ. Microb.* 67**,** 260-269.

Neal, A.L., Bank, T.L., Hochella, M.F., and Rosso, K.M. (2005). Cell adhesion of Shewanella oneidensis to iron oxide minerals: Effect of different single crystal faces. *Geochemical Transactions* 6**,** 77-84.

Neal, A.L., Rosso, K.M., Geesey, G.G., Gorby, Y.A., and Little, B.J. (2003). Surface structure effects on direct reduction of iron oxides by Shewanella oneidensis. *Geochimica Et Cosmochimica Acta* 67**,** 4489-4503.

Nealson, K.H., and Saffarini, D. (1994). Iron and manganese in anaerobic respiration: environmental significance, physiology, and regulation. *Annu Rev Microbiol* 48**,** 311-343.

Neiss, J., Stewart, B.D., Nico, P.S., and Fendorf, S. (2007). Speciation-dependent microbial reduction of uranium within iron-coated sands. *Environ. Sci. Technol.* 41**,** 7343-7348.

Nevin, K.P., and Lovley, D.R. (2000). Lack of production of electron-shuttling compounds or solubilization of Fe(III) during reduction of insoluble Fe(III) oxide by *Geobacter metallireducens*. *Appl. Environ. Microb.* 66**,** 2248-2251.

Nevin, K.P., and Lovley, D.R. (2002). Mechanisms of Fe(III) oxide reduction in sedimentary environments. *Geomicrob. J.* 19**,** 141-159.

Parmar, N., Gorby, Y.A., Beveridge, T.J., and Ferris, F.G. (2001). Formation of green rust and immobilization of nickel in response to bacterial reduction of hydrous ferric oxide. *Geomicrob. J.* 18**,** 375-385.

Petrie, L., North, N.N., Dollhopf, S.L., Balkwill, D.L., and Kostka, J.E. (2003). Enumeration and characterization of iron(III)-reducing microbial communities from acidic subsurface sediments contaminated with uranium(VI). *Appl. Environ. Microb.* 69**,** 7467-7479.

Phillips, D.H., Watson, D.B., and Roh, Y. (2007). Uranium deposition in a weathered fractured saprolite/shale. *Environ. Sci. Technol.* 41**,** 7653-7660.

Phillips, E.J.P., Lovley, D.R., and Roden, E.E. (1993). Composition of Non-Microbially Reducible Fe(Iii) in Aquatic Sediments. *Applied and Environmental Microbiology* 59**,** 2727-2729.

Postma, D., and Jakobsen, R. (1996). Redox zonation: Equilibrium constraints on the Fe(III)/SO_4^- reduction interface. *Geochim. Cosmochim. Acta* 60**,** 3169-3175.

Reeburgh, W.S. (1983). Rates of biogeochemical processes in anoxic sediments. *Annu. Rev. Earth Planet. Sci.* 11**,** 269-298.

Robertson, W.D. (2000). Treatment of wastewater phophate by reductive dissolution of iron. *J. Environ. Qual.* 29**,** 1678-1685.

Roden, E.E. (2003a). Diversion of electron flow from methanogenesis to crystalline Fe(III) oxide reduction in carbon-limited cultures of wetland sediment microorganisms. *App. Environ. Microb.* 69**,** 5702-5706.

Roden, E.E. (2003b). Fe(III) oxide reactivity toward biological versus chemical reduction. *Environ. Sci. Technol.* 37**,** 1319-1324.

Roden, E.E. (2006). Geochemicl and microbiological controls on dissimilatory iron reduction. *Comptes Rendus Geosci.* 338**,** 456-467.

Roden, E.E., and Urrutia, M.M. (2002). Influence of biogenic Fe(II) on bacterial crystalline Fe(III) oxide reduction. *Geomicrob. J.* 19**,** 209-251.

Roden, E.E., Urrutia, M.M., and Mann, C.J. (2000). Bacterial reductive dissolution of crystalline Fe(III) oxide in continuous-flow column reactors. *Appl. Environ. Microb.* 66**,** 1062-1065.

Roden, E.E., and Wetzel, R.G. (2002). Kinetics of microbial Fe(III) oxide reduction in freshwater wetland sediments. *Limnology and Oceanography* 41**,** 1733-1748.

Roden, E.E., and Zachara, J.M. (1996). Microbial reduction of crystalline iron(III) oxides: influence of oxide surface area and potential for cell growth. *Environ. Sci. Technol.* 30**,** 1618-1628.

Rosso, K.M., Smith, D.M.A., and Dupuis, M. (2003a). An ab initio model of electron transport in hematite (alpha-Fe2O3) basal planes. *Journal of Chemical Physics* 118**,** 6455-6466.

Rosso, K.M., Zachara, J.M., Fredrickson, J.K., Gorby, Y.A., and Smith, S.C. (2003b). Nonlocal bacterial electron transfer to hematite surfaces. *Geochim. Cosmochim. Acta* 67**,** 1081-1087.

Saltikov, C.W., and Newman, D.K. (2003). Genetic identification of a respiratory arsenate reductase. *Proc. Nat. Acad. Sci.* 100**,** 10983-10988.

Sass, B.M., and Rai, D. (1987). Solubility of amorphous chromium(III)-iron(III) hydroxide solid solutions. *Inorg. Chem.* 26**,** 2228-2232.

Schwertmann, U. (1984). The influence of aluminum on Fe oxides IX. Dissolution of Al-goethites in 6 M HCl. *Clays and Clay Min.* 19**,** 9-19.

Singh, B., and Gilkes, R.J. (1992). Properties and distribution of iron oxides and their association with minor elements in the soils of south-western Australia. *J. Soil Sci.* 43**,** 77-98.

Starkey, R.L., and Halvorson, H.O. (1927). Studies on the transformations of iron in nature. II. Concerning the importance of microorganisms in the solution and precipitation of iron. *Soil Sci.* 24**,** 381-402.

Stewart, B.D., Nico, P.S., and Fendorf, S. (2009). Stability of uranium incorporated into Fe (Hydr)oxides under fluctuating redox conditions. *Environ. Sci. Technol.* 43**,** 4922-4927.

Straub, K.L., and Schink, B. (2004). Ferrihydrite-dependent growth of Sulfurospirillum deleyianum through electran transfer via sulfur cycling. *App. Environ. Microb.* 70**,** 5744-5749.

Stucki, J.W., Lee, K., Goodman, B.A., and Kostka, J.E. (2007). Effects of in situ biostimulation on iron mineral speciation in a sub-surface soil. *Geochim. Cosmochim. Acta* 71**,** 835-843.

Sturm, A., Crowe, S.A., and Fowle, D.A. (2008). Trace lead impacts biomineralization pathways during bacterial iron reduction. *Chem. Geol.* 249**,** 282-293.

Taillefert, M., Beckler, J.S., Carey, E., Burns, J.L., Fennessey, C.M., and Dichristina, T.J. (2007). Shewanella putrefaciens produces an Fe(III)-solubilizing organic ligand during anaerobic respiration on insoluble Fe(III) oxides. *J. Inorg. Biochem.* 101**,** 1760-1767.

Thamdrup, B. (2000). "Bacterial manganese and iron reduction in aquatic sediments," in *Advances in Microbial Ecology, Vol 16,* ed. B. Schink. (New York: Kluwer Academic / Plenum Publ), 41-84.

Thamdrup, B., Rossello-Mora, R., and Amann, R. (2000). Microbial manganese and sulfate reduction in Black Sea shelf sediments. *App. Environ. Microb.* 66**,** 2888-2897.

Torrent, J., Schwertmann, U., and Barron, V. (1987). The reductive dissolution of synthetic goethite and hematite in dithionite. *Clays and Clay Min.* 22**,** 329-337.

Trolard, F., Bourrie, G., Jeanroy, E., Herbillon, A.J., and Martin, H. (1995). Trace elements in natural iron oxides from laterites: A study using selective kinetic extraction. *Geochim. Cosmochim. Acta* 59**,** 1285-1297.

Tufano, K.J., and Fendorf, S. (2008). Confounding impacts of iron reduction on arsenic retention. *Environ. Sci. Technol.* 42**,** 4777-4783.

Tufano, K.J., Reyes, C., Saltikov, C.W., and Fendorf, S. (2008). Reductive processes controlling arsenic retention: Revealing the relative importance of iron and arsenic reduction. *Environ. Sci. Technol.* 42**,** 8283-8289.

Urrutia, M.M., Roden, E.E., and Zachara, J.M. (1999). Influence of aqueous and solid-phase Fe(II) complexants on microbial reduction of crystalline iron(III) oxides. *Environ. Sci. Technol.* 33**,** 4022-4028.

Vorhies, J.S., and Gaines, R.R. (2009). Microbial dissolution of clay minerals as a source of iron and silica in marine sediments. *Nature Geoscience* 2**,** 221-225.

Waychunas, G.A., Kim, C.S., and Banfield, J.F. (2005). Nanoparticulate oxide minerals in soils and sediments: unique properties and contaminant scavenging mechanisms. *Journal of Nanoparticle Research* 7**,** 409-433.

Weber, K.A., Achenbach, L.A., and Coates, J.D. (2006). Microorganisms pumping iron: Anaerobic microbial iron oxidation and reduction. *Nature* 4**,** 752-764.

White, H.K., Reimers, C.E., Cordes, E.E., Dilly, G., and Girguis, P.R. (2009). Quantitative population dynamics of microbial communities in plankton-fed microbial fuel cells. *ISME J.* 3**,** 635-646.

Wielinga, B., Mizuba, M.M., Hansel, C.M., and Fendorf, S. (2001). Iron promoted reduction of chromate by dissimilatory iron-reducing bacteria. *Environ. Sci. Technol.* 35**,** 522-527.

Wigginton, N.S., Rosso, K.M., and Hochella Jr., M.F. (2007). Mechanisms of electron transfer in two decaheme cytochromes from a metal-reducing bacterium. *J. Phys. Chem B* 111**,** 12857-12864.

Williams, A.G.B., and Scherer, M.M. (2004). Spectroscopic evidence for Fe(II)-Fe(III) electron transfer at the iron oxide-water interface. *Environ. Sci. Technol.* 38**,** 4782-4790.

Xiong, Y., Shi, L., Chen, B., Mayer, M.U., Lower, B.H., Londer, Y., Bose, S., Hochella Jr., M.F., Fredrickson, J.K., and Squier, T.C. (2006). High-affinity binding and direct electron transfer to solid metals by the *Shewanella oneidensis* MR-1 outer membrane *c*-type cytochrome OmcA. *JACS* 128**,** 13978-13979.

Yan, B.Z., Wrenn, B.A., Basak, S., Biswas, P., and Giammar, D.E. (2008). Microbial reduction of Fe(III) in hematite nanoparticles by Geobacter sulfurreducens. *Environmental Science & Technology* 42**,** 6526-6531.

Zachara, J.M., Fredrickson, J.K., Li, S.-M., Kennedy, D.W., Smith, S.C., and Gassman, P.L. (1998). Bacterial reduction of crystalline Fe^{3+} oxides in single phase suspensions and subsurface materials. *Amer. Mineral.* 83**,** 1426-1443.

Zachara, J.M., Fredrickson, J.K., Smith, S.C., and Gassman, P.L. (2001). Solubilization of Fe(III) oxide-bound trace metals by a dissimilatory Fe(III) reducing bacterium. *Geochim. Cosmochim. Acta* 65**,** 75-93.

Zachara, J.M., Kukkadapu, R.K., Fredrickson, J.K., Gorby, Y.A., and Smith, S.C. (2002). Biomineralization of poorly crystalline Fe(III) oxides by dissimilatory metal reducing bacteria (DMRB). *Geomicrobiology Journal* 19**,** 179-207.

CHAPTER 2

ENRICHED IRON(III)-REDUCING BACTERIAL COMMUNITIES ARE SHAPED BY CARBON SUBSTRATE AND IRON OXIDE MINERALOGY

Published as: Lentini, C.J., Wankel, S.D., and Hansel, C.M. (2012). Enriched Iron(III)-Reducing Bacterial Communities are Shaped by Carbon Substrate and Iron Oxide Mineralogy. *Frontiers in Microbiology* 3**,** 404.

Abstract

Iron (Fe) oxides exist in a spectrum of structures in the environment, with ferrihydrite widely considered the most bioavailable phase. Yet, ferrihydrite is unstable and rapidly transforms to more crystalline Fe(III) oxides (e.g., goethite and hematite), which are poorly reduced by model dissimilatory Fe(III)-reducing microorganisms. This begs the question, what processes and microbial groups are responsible for reduction of crystalline Fe(III) oxides within sedimentary environments and how do changes in Fe-oxide mineralogy shape oxide-hosted microbial populations? To address these questions, we conducted a large-scale cultivation effort using various Fe(III) oxides (ferrihydrite, goethite, hematite) and carbon substrates (glucose, lactate, acetate) along a dilution gradient to enrich for different microbial populations capable of reducing Fe(III) oxides spanning a wide range of crystallinities and reduction potentials. While carbon source was the most important variable in shaping the microbial community composition within the Fe(III)-reducing enrichments, both Fe oxide type and sediment dilution also had a substantial influence in Fe(III) reduction. With acetate as the carbon source, only ferrihydrite enrichments displayed a significant amount of Fe(III) reduction and the well known dissimilatory metal reducer *Geobacter* sp. was the dominant organism enriched. In contrast, when glucose and lactate were provided, all three Fe oxides were reduced and reduction coincided with the presence of fermentative (e.g. *Enterobacter* spp. and *Firmicutes*) and sulfate-reducing bacteria (e.g. *Desulfovibrio* spp.). Thus, changes in resource availability may shift Fe(III)-reducing communities between dominantly metal respiring to fermenting and/or sulfate-reducing organisms which are capable of reducing more recalcitrant iron phases. These findings highlight the need for further targeted investigations into the composition and activity of speciation-

directed metal-reducing populations and ecology of Fe(III)-reducing populations within natural environments.

2.1 Introduction

Iron (Fe) (hydr)oxide minerals are potent repositories of nutrients (e.g., phosphate) and metal(loid)s (e.g., arsenic). Release of these elements into the aqueous milieu may occur upon dissolution of the Fe (hydr)oxides mediated by a number of abiotic and biotic processes. Under anaerobic conditions, reductive dissolution is primarily attributed to reaction with sulfide in sulfidogenic environments and microbial activity in non-sulfidogenic environments (Lovley et al., 1991). The biotic mechanisms of Fe(III) reduction within soils and sediments are primarily attributed to either an indirect consequence of fermentation or microbial respiration, in which organisms couple the oxidation of carbon or molecular hydrogen to the reduction of Fe(III) for energy conservation (dissimilatory reduction). Given the ubiquity of Fe oxides within soils and sedimentary systems, microbial Fe(III) reduction can have a profound impact on carbon cycling and degradation. In fact, microbial Fe(III) reduction accounts for a up to 50% of carbon oxidation in non-sulfidogenic sediments (Canfield et al., 1993;Thamdrup, 2000).

Most oxidized Fe within soils and sediments (pH > 4) exists as a variety of oxy(hydr)oxides (hereinafter referred to as oxides), where the three most common are ferrihydrite ($Fe_5HO_8 \bullet 4H_2O$), goethite (α-FeOOH), and hematite (α-Fe_2O_3). These Fe(III) phases vary greatly in their physiochemical properties, including solubility, reduction potential, and surface area. Ferrihydrite, the least crystalline and most soluble phase, supports the greatest extent and highest rates of Fe(III) reduction in laboratory incubations with common dissimilatory Fe(III)-reducing microorganisms (DIRMs) (Lovley and Phillips, 1988;Roden, 2003;Hansel et al., 2004). In contrast, under identical conditions, goethite and hematite, phases with higher crystallinities and lower solubilities, support only minimal Fe(III) reduction (e.g., ~1-5% of total Fe; (Hansel et al., 2004)) by these same organisms (Lovley and Phillips, 1988;Roden and

Zachara, 1996;Fredrickson et al., 2003). Based on these laboratory observations, the availability of Fe(III) oxides for microbial respiration is believed to decrease in the order ferrihydrite to goethite to hematite.

Although ferrihydrite is believed to be the most bioavailable Fe(III) oxide, it is a transient phase having a short residence time in sediments where it ripens to more crystalline oxides such as goethite and hematite (Benner et al., 2002;Hansel et al., 2003). Furthermore, as a consequence of the high reactivity of ferrihydrite (Cornell and Schwertmann, 1996), its reduction potential and bioavailability is oftentimes compromised by extensive incorporation of other cations (Ekstrom et al., 2010;Hansel et al., 2011). Thus, the role of ferrihydrite in sustaining long-term DIRM populations and maintaining Fe(II) generation in mature sediments is likely minor (Hansel et al., 2004). In fact, in aged soils and sediments crystalline Fe(III) oxides are 2 to 10 times greater when compared to their less crystalline counterpart (Roden and Urrutia, 2002). Furthermore, it has been shown that crystalline Fe(III) oxides are preferentially reduced and responsible for the oxidation of carbon within some natural sediments (Stucki et al., 2007). Given the limited ability of model DIRM to reduce more crystalline Fe(III) oxides, a link between the reduction of these crystalline phases and microbial Fe(III) respiration (i.e., dissimilatory Fe(III) reduction) within the environment is questionable – or, at least not a consequence of dissimilatory reduction by well-characterized model DIRM (e.g., *Shewanella* spp., *Geobacter* spp.). This begs the question, what processes and microbial groups are responsible for the reduction of crystalline Fe(III) oxides within soil and sedimentary environments? Are there undiscovered dissimilatory Fe(III)-reducing microbes that have a better ability to reduce more crystalline (lower reduction potential) Fe(III) oxides? Or are other microbial processes responsible for Fe(III) reduction in more mature sedimentary systems?

Addressing these questions is complicated by the lack of a universal functional gene for Fe(III) respiration. Thus, here we take a first step at addressing these questions by identifying the microbial communities hosted within sediment enrichments containing Fe(III) oxides spanning a range of crystallinities. To do this, we employ the first large scale cultivation effort using various Fe(III) oxides (ferrihydrite, goethite, hematite) and carbon sources (glucose, lactate, acetate) along a dilution gradient (10^{-1} to 10^{-5}) to provide various ecological niches for Fe(III)-reducing communities. The tested carbon and Fe oxide sources span environments ranging in geochemical maturity and extent of carbon degradation. Further, enrichments along a dilution gradient target organisms occupying different ecological niches, in particular spanning life history traits (e.g., r and K strategies). The results observed here point to microbial groups and processes that are presumed responsible for Fe(III) reduction within contrasting geochemical environments and will therefore aid in the interpretation of Fe dynamics observed in field and natural sediment incubations.

2.2 Material and methods

***2.2.1 Site description and sampling*:** Sediment was collected from Ashumet Pond, Falmouth, MA, in August of 2008. Ashumet Pond is a freshwater kettle-hole pond that receives phosphate-laden groundwater from infiltration beds at a decommissioned wastewater treatment and disposal facility at the adjacent Massachusetts Military Reservation on Cape Cod. In 2004, a permeable reactive barrier containing zero valent Fe (3% Fe(0) by weight) was emplaced subhorizontally on the bottom of the pond (0.6 m deep) to intercept phosphate-laden water that discharges near the shore of Ashumet Pond (McCobb et al., 2009). Three shallow sediment cores were collected within the pond downgradient of the barrier with a water depth of ~0.5 m. Upon sampling, the

cores were stored on ice, transferred back to the laboratory and placed in an anaerobic chamber (94% N_2: 6% H_2). The outer 1 cm of the cores was discarded, the remaining sediment was combined and mixed, and 10 g of the homogenized sediment was placed in anaerobic serum bottles containing sterile HEPES buffer (10 mM). Sediments were thoroughly mixed before ten-fold serial dilutions were carried out in sterile 10 mM HEPES buffer to a final dilution of 10^{-5}. These sediment slurries served as the inocula for the Fe(III) reduction enrichments.

2.2.2 Mineral synthesis: Two-line ferrihydrite, goethite, and hematite were synthesized following the methods of Schwertmann and Cornell (Schwertmann and Cornell, 2007) and characterized in detail previously (Hansel et al., 2003;Hansel et al., 2004). All minerals were washed via repeated centrifugation, dialyzed in Spectra/Pur cellulose membrane tubing (MWCO 12,000 to 14,000) until a steady conductivity was obtained, and maintained as slurries (minimizing alteration). Following dialysis, the pH of mineral slurries was adjusted to 7.5 and stored at 4°C. For anaerobic enrichments, slurries were bubbled with N_2, sealed in anaerobic serum bottles, and sterilized (10 min, 120°C). X-ray diffraction was conducted on samples before and after sterilization (Scintag XDS2000) to confirm Fe oxide identity and purity.

2.2.3 Fe(III)- reducing enrichments: Enrichments were conducted in an anaerobic freshwater medium (Widdel and Bak, 1992), containing (in mM): $MgSO_4$, 0.2; $MgCl_2$, 4; $CaCl_2$, 0.9; KH_2PO_4, 4.4; NH_4Cl, 5.6; $NaHCO_3$, 30, 1 mL L^{-1} trace metal solution and 0.1 mL L^{-1} vitamin stock (pH 7.3). Media was dispensed into anaerobic Balch tubes (BellCo Glass) and the headspace exchanged with 80%N_2/20%CO_2 gas mixture. Prior to inoculation with sediment, media was amended with carbon (acetate, lactate, glucose or a mixture of all three) to a final

concentration of 10 mM and an Fe(III) oxide (ferrihydrite, goethite, or hematite) to a final total Fe concentration of 25 mM. Sediment suspensions along the dilution gradient (10^{-1} to 10^{-5}) were added to a final inoculum of 10%. Enrichments were stored at room temperature in the dark and transferred every three months. Following growth of the 3rd successive transfer, the enrichments were analyzed for Fe(II), organic carbon, and microbial community composition.

2.2.4 Iron chemistry of enrichments: Total Fe(II) (dissolved and solid associated) was measured in acid extracts using the ferrozine assay (Stookey, 1970). Acid extracts were obtained using 1 mL of well-mixed enrichments added to 5 mL of concentrated HCl and shaken for 12 hours to ensure complete dissolution of Fe phases. Total Fe was measured by first reducing all Fe(III) to Fe(II) with hydroxylamine hydrochoride (0.4 M, heated to near boiling).

2.2.5 DNA extraction: DNA from enrichments was extracted from enrichment cultures using a modified protocol for the Ultraclean soil DNA kit (MoBio Laboratories). Enrichment cultures were centrifuged at 5000 x g for 5 minutes. Supernatant was decanted off and the pellet was resuspended in 500 μL of nuclease free water. Prior to adding the bead beating solution, 200 μg of polyadenylic acid was added (Webster et al., 2003;Santelli et al., 2008).

2.2.6 Terminal restriction fragment length polymorphism analysis: Terminal Restriction Fragment Length Polymorphism (T-RFLP) profiles were generated for all enrichment cultures. DNA was amplified with a 5' fluorescently labeled forward primer (8F with 5-hexachlorofluoescein; HEX) and a 5' fluorescently labeled reverse primer (1492R with 6-carboxyfluorescine; FAM). Two independent 50 μL PCRs were combined and purified using

QIAquick nucleotide removal kit (Qiagen). The concentration of combined/purified DNA was determined via nanodrop and concentrated samples were diluted with nuclease free water to ensure proper digestion. Approximately 160 ng of purified DNA was digested in 20 μL reaction with 20 U of *MSPI, HaeIII,* or *HhaI* for 4 hours at 37°C. Duplicate T-RF profiles were prepared for electrophoretic analysis by adding 0.5 μL of digested products to 0.5 μL GeneScan -500 ROX size standard and 9.0 μL of Hi-Di Formamide. The loading mix was heated for 3 minutes at 95°C and immediately chilled on ice before analysis on a 3730xl ABI capillary sequencer.

2.2.7 Cloning, sequencing and phylogenetic analysis: A subset of samples were cloned to assign T-RFLP fragments to bacterial species. Amplification of the 16S rRNA gene was performed using the 8F and 1492R primer set (Lane, 1991) and conditions used previously (Hansel et al., 2008). Sequencing of PCR products were performed using the forward T3 and reverse T7 primers on an ABI 3730xl capillary sequencer. A total of 576 clones were sequenced to assign identity to 53 MspI T-RFLP fragments. Sequencher 4.8 (Gene Codes Corp) was used to trim the cloning vector and poor quality reads from sequences before aligning the contigs and exporting consensus sequences for further analysis. Alignment of sequences was performed in ARB (Ludwig et al., 2004). Upon alignment of sequences, estimation of maximum likelihood phylogenies was performed using the online web interface of PhyML (Guindon et al., 2005). Robustness of clusters were tested with bootstrap resampling (n=1000).

***2.2.8 Nucleotide sequence accession numbers*:** Sequences obtained in this study have been deposited in the GenBank database under accession numbers JX828409 to JX828432 (bacterial 16S rRNA clones).

2.2.9 Statistical analysis: Data was first visually analyzed to ensure quality electropherograms and then aligned and converted into data tables using Genemappers Local Southern method (Applied Biosystems). Peaks from 50 to 550 base pairs were exported for further analysis. The statistical analysis method implemented by Abdo et al. (Abdo et al., 2006) was used to discriminate between signal/noise and to align peaks into appropriate bins. In addition, duplicate digests were performed for each enrichment and peaks not present in both digests were discarded and the peak areas averaged. This method corrects for any potential differences in the amount of DNA injected between digest by relativizing peak area within each digest. T-RFs were then manually assigned to bacterial groups only if 6 out of 6 peaks matched the *in silico* digestion of phylotypes from clone libraries. Bulk phylogenetic groupings were obtained by combining similar organisms, for instance *Desulfovibrio putealis* (454 bp for MspI) and *Desulfovibrio vulgaris* (286 bp for MspI) were combined to produce one *Desulfovibrio* bin. In order to describe the pairwise dissimilarities between enrichments Bray-Curtis index was implemented from the vegdist function in the vegan package (Hothorn et al., 2008) of R (http://www.R-project.org/, 2012). Hierarchical cluster analysis on the set of dissimilarities was performed using the average agglomeration method (hclust function in the stats package of R) and annotated heatmaps were generated using the heat_plus package in R (Ploner, 2011). Finally, the cophenetic correlation was calculated to insure the proper clustering of data when compared to pairwise dissimilarities.

2.3 Results

2.3.1 Fe(III) reduction in enrichment cultures: The amount of Fe(II) produced within sediment incubations varied as a function of carbon source, Fe(III) oxide type, and sediment dilution. Of

the original 120 enrichments (40 for each mineral), 45 enrichments demonstrated reduction greater than 10% of the total Fe provided. The number of enrichments supporting Fe(III) reduction followed the predicted trend of Fe(III) bioavailability within the Fe oxides, with the majority of the Fe(III)-reducing enrichments obtained on ferrihydrite (60%) and goethite (36%) and hematite (4%) representing fewer. The effect of carbon source on these enrichments was also clear, with the most energetic carbon sources, mixed carbon (36%), glucose (33%) and lactate (22%) representing the majority of Fe(III)-reducing enrichments, while those enriched on acetate represented only 9%.

In general, for ferrihydrite, the trend for Fe(III) reduction was similar among all carbon compounds, with the percent of Fe(III) reduced decreasing progressively from the 10^{-1} dilution to 10^{-5} dilution (Figure 2.1). In contrast, within both goethite and hematite enrichments, the amount of Fe(II) produced showed a strong dependence on sediment dilution, with most reduction occurring in the 10^{-3} dilution culture when lactate and glucose were provided as carbon sources (Figure 2.1). Goethite also supported moderate (18-21%) Fe(III) reduction in the 10^{-1} and 10^{-2} dilutions for glucose. In contrast to ferrihydrite, no or minimal Fe(III) reduction was observed within goethite and hematite enrichments when acetate was provided as the carbon source.

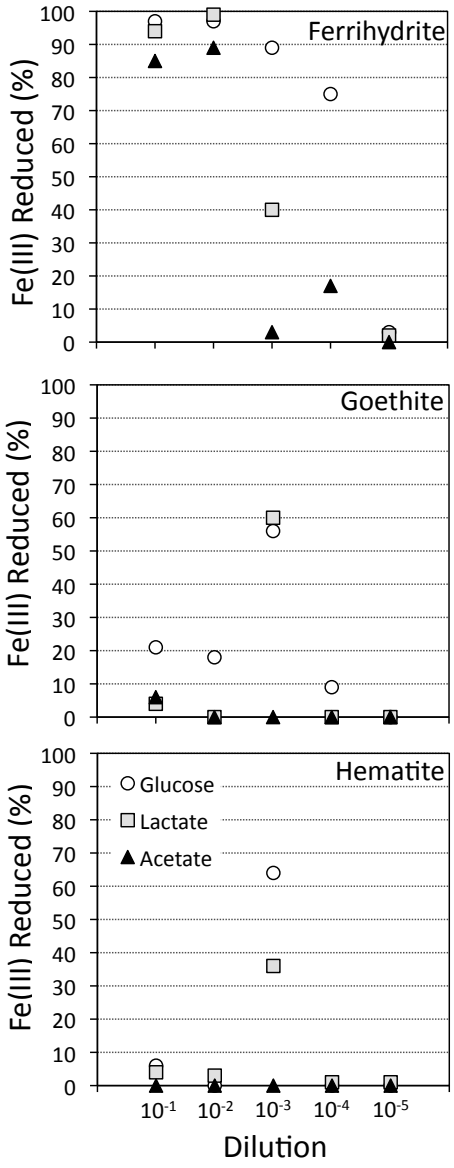

Figure 2.1. Percent of total Fe(III) reduced (Fe^{2+}/Fe_{TOT}) in enrichments supplemented with different Fe oxide (each graph) and carbon sources (▲ = acetate ■ = lactate ● = glucose). Enrichments contained 25 mM Fe_{Tot} and an excess of carbon substrate (10 mM).

***2.3.2 Terminal Restriction Fragment Length Polymorphism (T-RFLP) analysis*:** In order to further understand the microbial communities associated with the reduction of the various Fe(III) phases, only the 45 enrichments in which greater than 10% of the total Fe(III) was reduced were

selected for further analysis. Preliminary T-RFLP analysis revealed low richness within these enrichment cultures (e.g., number of peaks ranging from 2 to 16), which allowed for a large-scale analysis of the 45 enrichments using T-RFLP analysis in combination with cloning for peak identification. The 16S rRNA gene was amplified with fluorescent forward and reverse primers and three separate restriction digests (*MspI, HaeIII, HhaI*) were performed to produce six distinct electrophoretograms for each enrichment culture. In combination with *in silico* digestion of known phylotypes from 16S rRNA gene clone libraries, T-RFs could be identified and matched to peaks in each electrophoretogram (see Table 1.1). In total, the *MspI* enzyme yielded 73 distinct T-RFs in the 45 enrichment cultures, 24 T-RFs (33%) could be assigned to known bacterial groups while 49 (67%) peaks remain unidentified. Of the unidentified fraction, however, 44 were in 2 or less enrichments and consisted of relatively minor peaks, with the median unknown fraction being 7%. Within the 73 distinct T-RFs, a total of 252 peaks were detected with 62% of the peaks represented by known clones. The seven most detected peaks (*Spirochaetes, Actinobacteria, Firmicutes, Aeromonas, Bacteroidetes*, *Desulfovibrio Geobacter*) constituted 51% of the detected peaks and made up 74% of the total peak area. The remaining known peaks constituted another 7% of the total peak area.

***2.3.3 Statistical analysis of TRLP patterns in Fe(III)-reducing enrichments*:** The community composition of the 45 enrichments was analyzed using the Bray-Curtis dissimilarity index (BC_{dis}). Hierarchical clustering analysis was relatively unbiased at reproducing the pairwise Bray-Curtis dissimilarities (cophenetic correlations = 0.82) and revealed a high degree of dissimilarity among all enrichments, with the largest cophenetic dissimilarity (CD) = 0.9059 (Figure 2.2). Further examination of the dendrogram by clustering into three distinct groups

revealed that enrichments grouped based on carbon source utilization. Non-parametric ANOVA (Kruskal-Wallis rank sum test) confirmed that these groupings were indeed different with respect to carbon source ($p < 0.05$).

The first cluster (CD = 0.6996; red grouping), with 5 enrichments, contained all four acetate enrichments and an additional lactate enrichment (Figure 2.2). Within this group, the four acetate samples were more similar to each other (CD = 0.5995) than to the single lactate sample. These enrichments contained between 4 and 7 T-RFs with 2 peaks being present in all samples, corresponding to the phylums *Spirochaetes* and genus *Geobacter*. While *Spirochaetes* were present in all samples, their relative peak area (4 - 15%) was far lower than *Geobacter* (23 - 80%). Within the acetate samples in this cluster, the relative peak area corresponding to *Geobacter* sp. were greatest (66 -80%) in the low dilution (1^{st} and 2^{nd}) samples and decreased (30 - 37%) in higher dilution acetate (4^{th}). The decrease in the relative abundance of *Geobacter* peaks in these higher dilution enrichments corresponded to a concurrent increase in peak area corresponding to the genus *Geothrix* (26% - 49%). A diversity of *Geobacter* species are well known for the ability to couple the oxidization of acetate to the reduction of ferrihydrite and therefore this organism was likely responsible for the reduction of Fe(III) in these enrichments. Interestingly, this cluster contained only ferrihydrite and not the more recalcitrant Fe(III) oxides goethite or hematite. In fact, within the 45 reduced enrichments there was a significant difference ($p < 0.05$) in *Geobacter* sp. abundance based on carbon source and Fe(III) oxide type, with T-RFs from this organism dominating in enrichments containing ferrihydrite and acetate.

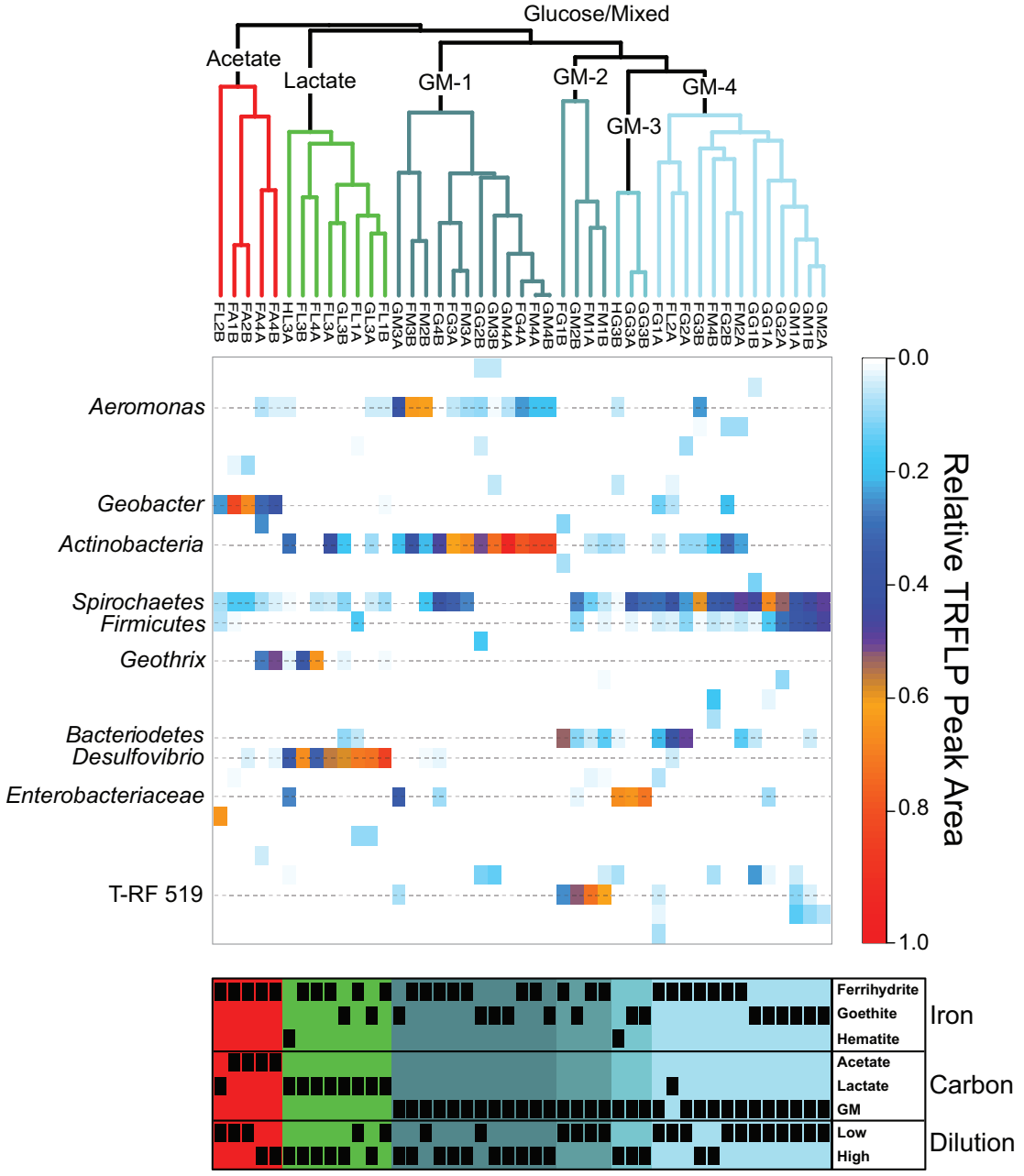

Figure 2.2. Top: Average agglomerative (UPGMA) clustering based on Bray-Curtis dissimilarity of MspI relative abundance T-RFLP profiles. Colors of the clusters indicate groupings based on cutting the dendrogram at BC_{dis}= 0.7. GM is abbreviated for combined glucose and mixed carbon source. Middle: Heatmap depicting the relative abundance of T-RF peak area for each enrichment (column) with identified phylogenetic affiliations (rows) labeled on the left. Bottom: Annotation of enrichments indicating the presence (black box) or absence (blank) of enriched communities within each cluster as a function of Fe oxide, carbon source, and dilution. The dilution variable is presented as either low (1st or 2nd) or high (3rd and 4th) sediment dilution.

The second cluster (CD = 0.5480; green grouping) contained 8 enrichments, all of which contained lactate as the carbon source (Figure 2.2). Within this cluster there were 5 ferrihydrite enrichments, however, unlike the acetate dominated cluster, enrichment cultures capable of reducing the more recalcitrant Fe(III) phases goethite (2 enrichments) and hematite (1 enrichment) were also present. Enrichments within this cluster contained between 2 to 8 T-RFs with 3 phylogenetic groups present in 5 or more samples (*Geothrix*, *Spirochaetes, Desulfovibrio*). Six enrichments contained *Spirochaetes* sp. where they made up 4-11% of the relative peak area. *Geothrix* sp. were present in 5 enrichments and made up 1 – 63% of the relative area. Similar to the acetate cluster, the relative abundance of *Geothrix* sp. was higher (35 and 63%) within higher dilution (3^{rd} and 4^{th}) enrichments. Of the 3 phylogenetic groups present in most enrichments, only *Desulfovibrio* was present in all 8 enrichments, including all three Fe(III) oxides, and represented the largest relative peak area (32 to 82%). Non-parametric ANOVA confirmed that carbon source ($p < 0.05$) but not Fe oxide type was significant in selecting for *Desulfovibrio* species within the enrichments.

The last cluster was the largest and most diverse with 32 enrichments containing all 16 mixed carbon and 15 glucose enrichments with one additional lactate enrichment (Figure 2.2; blue-grey groupings). However, the largest cophenetic dissimilarity for this cluster was high (CD = 0.8471) and was therefore divided further into 4 distinct groups with $BC_{dis} < 0.7$. Analysis of these four clusters showed that they correspond to samples enriched in a diverse set of organisms including *Aeromonas, Actinobacteria*, *Bacteroidetes*, *Firmicutes*, *Spirochaetes*, *Enterobacteriaceae*, and an unknown peak at 519 bp. The first grouping (CD = 0.6130; GM-1) contained 12 enrichment cultures, 7 of which were enriched on ferrihydrite and 5 on goethite. While Fe(III) phase did not seem to play a role in selecting for communities in this cluster,

higher sediment dilutions were clearly selected for – 2 enrichments from the 2nd dilution, 5 from the 3rd dilution, and 5 from the 4th dilution. The 12 enrichments in this group contained 2 to 7 T-RFs with two organisms, *Aeromonas* (0 – 62% peak area) and *Actinobacteria* (19 - 94% peak area) present in 11 and 12 samples, respectively. In the 2nd group (CD = 0.6513; GM-2), 4 enrichment cultures contained 5 to 8 T-RFs and all 4 were enriched in an unknown T-RF at 519 bp (25 - 71% relative peak area) and *Bacteroidetes* (5 – 51% relative peak area). The unknown peak at 519 bp closely matched (5 of 6 T-RF peaks) a *Clostridium* sp. sequence from another enrichment, however, it was left unknown as a direct phylotype accounting for all six peaks was not sequenced. Interestingly, the 3rd group in the GM cluster contained three enrichments on the recalcitrant Fe(III) oxides (2 goethite and 1 hematite) that clustered closely together (CD = 0.3440; GM-3) and showed substantial amounts of reduction (56 to 67%; Figure 2.1). Only two organisms were present in all three enrichments, *Spirochaetes* and *Enterobacteriaceae*, with members of the *Spirochaetes* representing 2 – 35% of the relative peak area, while members of the *Enterobacteriaceae* family represented 63 - 69%. Indeed, non-parametric ANOVA confirmed that Fe(III) oxide phase played a role in selecting for *Enterobacteriaceae* ($p < 0.05$). Only one of the 8 enrichment cultures hosting *Enterobacteriaceae* contained ferrihydrite as the Fe(III) source and *Enterobacteriaceae* sp. were in relatively low abundance. Finally, the last cluster (CD = 0.6038) contained 13 enrichments mostly from low dilution samples (five 1st dilution, six 2nd dilution, one 3rd dilution, one 4th dilution). Two T-RFs corresponding to *Firmicutes* (1 – 46 % relative peak area) and *Spirochaetes* (29 - 67% relative peak area) were present in all 13 enrichments, while *Actinobacteria* (5 - 30%) and *Bacteroidetes* (4 - 49%) were both present within 6 enrichment cultures. Within this cluster Fe mineralogy also seems to play

a role in selecting for community structure as the six goethite samples were more similar to each other than they were to the other seven ferrihydrite samples.

2.3.4 Bacterial community composition as a function of Fe oxide, carbon source and dilution: Select enrichments from the dendrogram (Figure 2.2) are shown in more detail (Figures 3 and 4), in order to more clearly represent the community composition dynamics as a function of carbon source, dilution, and Fe oxides. When glucose was provided as the carbon source for ferrihydrite enrichments, bacterial populations consisted of dominantly 3 members that varied with sediment dilution (Figure 2.3). The enriched bacterial population shifted from dominantly *Bacteroidetes* (29 to 40%) and *Spirochaetes* (39 to 28%) at low dilutions to dominantly *Actinobacteria* (77%) and *Aeromonas* (23%) at higher dilutions (Figure 2.3). This species transition with dilution was seen in the dendrogram as a shift from the low dilution containing, GM-2 and GM-4 groups, to the GM-1 group containing higher dilution enrichments (Figure 2.2). This shift in population corresponded to a moderate decrease (~25% decrease) in observed ferrihydrite reduction (Figure 2.1).

Ferrihydrite-reducing communities enriched on lactate had a greater variability in community composition, evidenced by the fact that they were observed in all 3 major clusters in the dendrogram (Figure 2.2). In comparing the 1st and 2nd dilution where Fe(III) reduction is nearly complete, the communities shifted from dominantly sulfate-reducing *Desulfovibrio* sp. (76%) to the DIRM *Shewanella* (56%) and *Geobacter* spp. (26%) (Figure 2.3). In the 3rd dilution enrichment culture, where Fe(III) reduction was substantially lower (39%), *Desulfovibrio* sp. dominated again but were accompanied by *Geothrix sp.* (43%).

When acetate was provided as the carbon source, *Geobacter sp.* dominated the reduced ferrihydrite enrichments (Figure 2.3) and a substantial amount of Fe(III) reduction (84- 88%) was observed.

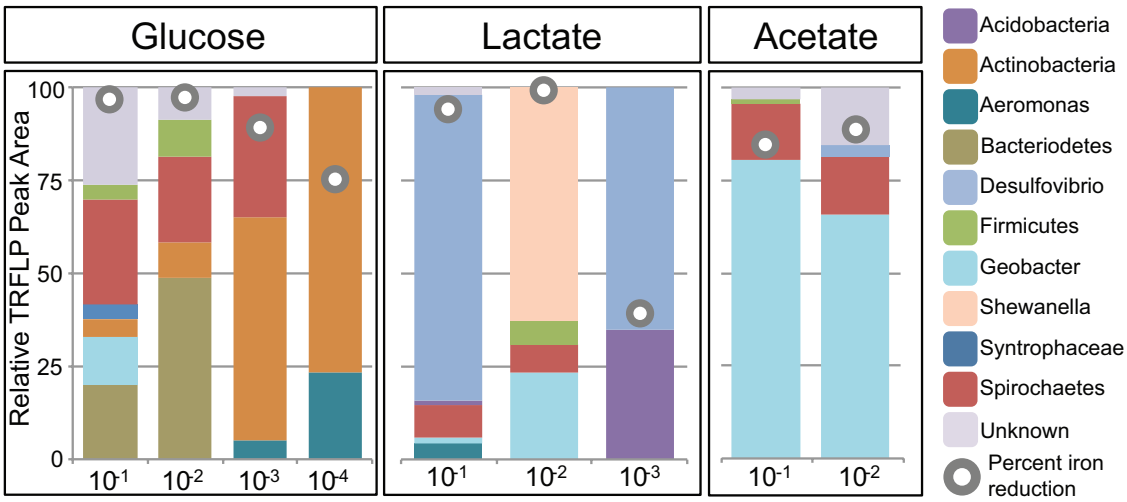

Figure 2.3. Relative peak area (%) of MspI T-RFs for ferrihydrite enrichments as a function of dilution and carbon source. T-RF peak area was used to obtain relative percentages of each phylogenetic group. The gray circles indicate the percent Fe(III) reduced in the enrichment.

Within goethite enrichments containing glucose as the carbon source, peaks corresponding to *Spirochaetes* (35 to 66%), *Firmicutes* (3 to 28%), and *Enterobacteriaceae* (0 to 63%) were observed (Figure 2.4). *Spirochaetes* (51 to 66%) and *Firmicutes* (16 to 28%) dominated the 1st and 2nd dilution enrichments cultures, where 18% - 21% Fe(III) reduction was observed. In the 10^{-3} dilution enrichment, however, where more substantial Fe(III) reduction (56%) was observed (Figure 2.1), *Enterobacteriaceae* was present (63%) alongside *Spirochaetes* (35%). This change in community structure was also seen in the dendrogram as these enrichments move from the low dilution GM-4 group to the GM-3 grouping containing enrichments relatively high in *Enterobacteriaceae* (Figure 2.2). For lactate enrichments

supporting goethite reduction (10^{-3} dilution), the bacterial community was composed of *Desulfovibrio* (70%), *Actinobacteria* (9%), *Aeromonas* (5%), and *Spirochaetes* (5%).

For hematite, substantial Fe(III) reduction was only observed in the 3rd sediment dilution enrichment culture containing either lactate or glucose as the carbon source (Figure 2.1). Within the glucose enrichment, 6 organisms were identified with *Enterobacteriaceae sp*. representing the majority (64%) of the community (Figure 2.4). When lactate was provided as the carbon source, the community within the 3rd dilution enrichment culture was dominated by *Desulfovibrio* (35%), *Actinobacteria* (28%) and *Enterobacteriaceae* (26%).

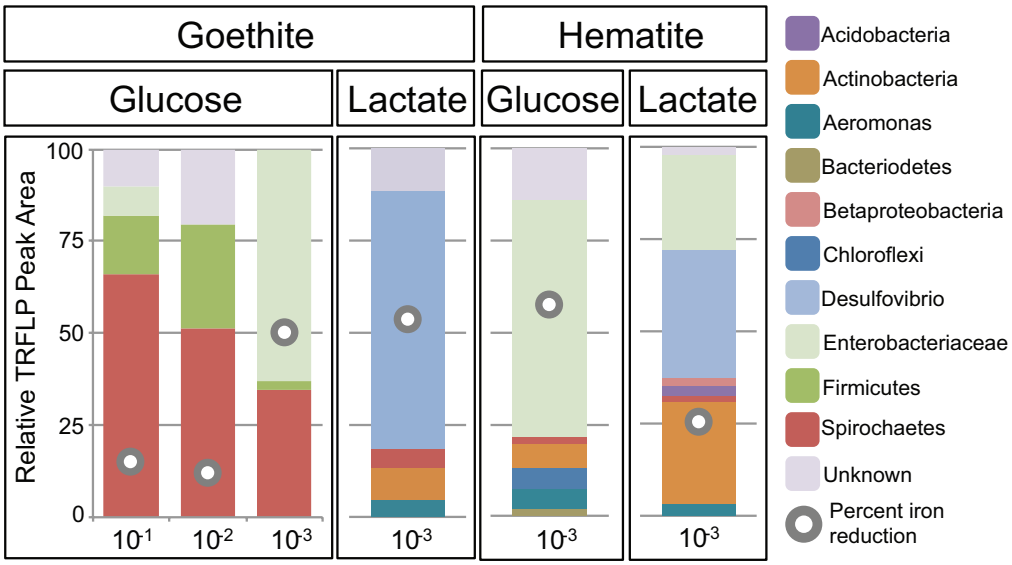

Figure 2.4. Relative peak area (%) of MspI T-RFs for goethite and hematite as a function of dilution and carbon source (glucose or lactate). T-RF peak area weas used to obtain relative percentages of each phylogenetic group. The gray circles indicate the percent Fe(III) reduced in the enrichment.

***2.3.5 Distribution and phylogenetic identity of primary species within enrichment cultures*:** While some microbial groups appeared to proliferate within these enrichments indiscriminately, others appeared to be enriched under select conditions (C, Fe oxide, dilution). For instance, the common Fe(III)-reducer *Geobacter* sp. was obtained within Fe(III)-reducing enrichments

containing primarily acetate and only ferrihydrite. The enriched species shared 97% sequence identity to *Geobacter pelophilus strain Dfr2* (Straub and Buchholz-Cleven, 2001) (Figure 2.5). In contrast, bacteria within the *Enterobacteriaceae* family were predominantly enriched on the more crystalline Fe(III) phases goethite and hematite. Species within the genus *Serratia* were enriched on both goethite and hematite, with 98% sequence identity to *Serratia plymuthica* RVH1 and to *Serratia fonticola* G75. Enriched *Enterobacteriaceae* on hematite supplemented with glucose belonged to a different genus and had 98% sequence identity to *Klebsiella oxytoca*. Thus, in these cases, both carbon and Fe oxide type selected for the putative Fe(III)-reducing organisms within the enrichment cultures.

In some cases, carbon source played a much larger role in selecting for the Fe(III)-reducing community rather than the Fe oxide phase. For instance, the relative abundance of *Desulfovibrio* species were shown to be statistically different based on carbon source, with the majority being enriched on lactate. The dominant *Desulfovibrio* species in these enrichments were similar (99% sequence identity) to the known sulfate-reducing bacterium, *D. putealis* strain B7-43 (Basso et al., 2005) (Figure 2.5). *D. putealis* was enriched on all three Fe(III) oxides, being the only *Desulfovibrio* species enriched on hematite and the closest cultured representative for 2 T-RF enriched on ferrihydrite (the percent sequence identity varied from 96-99%) (Table 1.1). However, in two enrichments amended with lactate, one ferrihydrite and one goethite, the majority (61% and 48%) of the T-RF peak area was most similar to *D. vulgaris* (95% sequence identity) with the remainder of the *Desulfovibrio* relative peak area belonging to *D. putealis.*

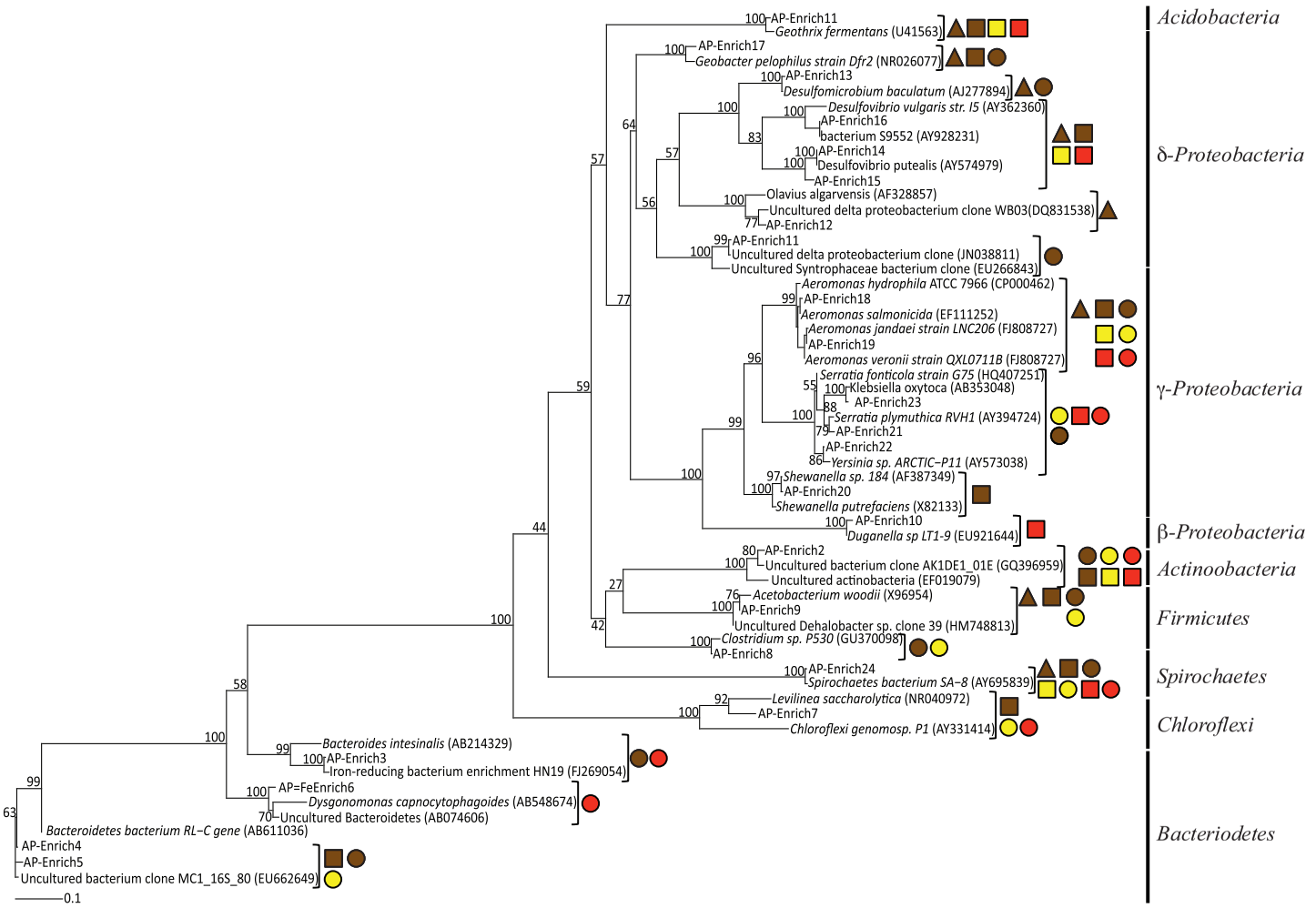

Figure 2.5. Maximum likelihood 16S rRNA phylogenetic tree for Fe(III)-reducing enrichment clones. Shapes indicate carbon sources (▲ = acetate ■ = lactate ● = glucose) and color indicates Fe(III) oxide type (red= hematite, yellow= goethite, brown= ferrihydrite) for which those microorganisms were enriched on. Bootstrap values (n=1000), as percentages, are indicated at nodes.

Some bacterial groups showed a cosmopolitan distribution, seeming to enrich regardless of carbon and Fe oxide provided. Further, these groups in some cases showed little to no species level diversity as a function of Fe(III) oxide or carbon. For instance, despite *Spirochaetes* being present in 34 of the enrichments (76%), including various carbon and Fe(III) oxide substrates, all sequences were 99% similar to the *Spirochaetes* isolate SA-8 (Bonin, 2005) (Figure 2.5). Likewise, *Actinobacteria* sp. were in 25 enrichments (56%) including all 3 Fe(III) oxides and 2 carbon sources (glucose, lactate), yet all species were closely related (~99%) to each other and had no cultured representative with greater than 90% sequence identity (*Olsenella sp. F0004;* 88% similarity). Similarly, 7 enrichments with acetate and lactate as carbon source but varying in Fe(III) oxide contained members of the *Acidobacteria* phylum with all species having 97% sequence identity to *Geothrix fermentans strain H5* (Coates et al., 1999). Lastly, bacteria within the *Aeromonas* genus were present in 18 enrichments including all carbon sources and Fe(III) oxides. The enriched *Aeromonas* bacteria are represented by a wide range of species with ~99% similarity (Figure 2.5 and Table 1.1), with no clear species-level preference for Fe oxide or carbon source.

Table 2.1. Bacterial 16S rRNA phylogeny of sequenced clones with their closest cultured representative (NCBI)

	Forward			Reverse			Accession number	Top BLAST Hit and closest culturable representative (NCBI)		Designation in Tree (Figure 5)
	MspI	***Hha*I**	***Hae*III**	**MspI**	***Hha*I**	***Hae*III**				
ACIDOBACTERIA										
Geothrix										
FA4A, FA4B, FL1B, FL3B, FL4A*, GL3B, HL3A	278	359	201	92	380	125	HM141900	Uncultured bacterium clone MA-9-V94B 16S ribosomal RNA gene	98%	AP-FeEnrich1
							NR_036779	*Geothrix fermentans strain H5* 16S ribosomal RNA, partial sequence	98%	
ACTINOBACTERIA										
Coriobacteriaceae										
FL3A*, FG1A, FG2A, FG2B, FG3A*, FG3B, FG4A*, FG4B, FM1A, FM1B, FM2A, FM2B, FM3A, FM3B, FM4A, FM4B, GL3A*, GL3B, GG2B, GM3A, GM3B, GM4A, GM4B, HG3B, HL3A	172	284	229	128	45	69	GQ396959	Uncultured bacterium clone AK1DE1_01E 16S ribosomal RNA gene	98%	AP-FeEnrich2
							EU592964	*Olsenella* sp. *F0004* 16S ribosomal RNA gene	89%	
BACTEROIDETES										
FG1A*, HG3B	90	94	NC	83	49	116	FJ269054.1	Iron-reducing bacterium enrichment culture clone HN19 16S ribosomal RNA gene	99%	AP-FeEnrich3
							AB214329.1	*Bacteroides intestinalis* gene for 16S rRNA, partial sequence, strain:JCM 13266	92%	
FL1A, FL2A*, FG1B, FG2A*, FM1A, FM1B, FM2A, GG1B	424	86	<50	33	47	112	EU662649	Uncultured bacterium clone MC1_16S_80 16S ribosomal RNA gene	98%	AP-FeEnrich4
							AB611036	*Bacteroidetes bacterium RL-C* gene for 16S rRNA, partial sequence	96%	
FG2A*, FM1A, GL3B, GM1B, GM2B	201	86	<50	33	47	112	AB447707.1	Uncultured bacterium gene 16S rRNA, partial sequence, clone: D242_27F_BAC_042	98%	AP-FeEnrich5
							AB611036.1	Bacteroidetes bacterium RL-C gene for 16S rRNA, partial sequence	96%	
HG3A*	95	100	<50	120	135	116	JQ617816.1	Uncultured Bacteroidetes bacterium clone Rc333 16S ribosomal RNA gene	96%	AP-FeEnrich6
							AB548674.1	*Dysgonomonas capnocytophagoides* gene for 16S ribosomal RNA, strin: JCM 16697	94%	
CHLOROFLEXI										
FL2A, GM3B, HG3B*	159	536	220	76	390	125	JN397974	Uncultured bacterium clone SSB0301-14 16S ribosomal RNA gene, partial sequence	99%	AP-FeEnrich7
							NR_040972	*Levilinea saccharolytica strain KIBI-1* 16S ribosomal RNA, partial sequence	94%	
FIRMICUTES										
Clostridiales										
Clostridiaceae										
Clostridium										
FG1A*, GM1A, GM1B, GM2A	179	193	271	124	403	43	GU370098	*Clostridium* sp. *P530(3)* 16S ribosomal RNA gene, partial sequence	98%	AP-FeEnrich8
Eubacteriaceae										
Acetobacterium										

Table2.1. (Continued)

	Forward			Reverse			Accession number	Top BLAST Hit and closest culturable representative (NCBI)		Designation in Tree (Figure 5)
	MspI	***Hha*I**	***Hae*III**	**MspI**	***Hha*I**	***Hae*III**				
FA1B, FL1A, FL2A, FL2B, FG1A, FG2A, FG2B, FG3B, FM1B, FM2A*, FM4B, GG1A, GG1B, GG2A*, GM1B, GM2A, GM2B	216	371	NC	127	401	NC	JX223412.1	Uncultured bacterium clone EMIRGE_OTU_s5t4a_1110 16S	99%	AP-FeEnrich9
							NR_026326	*Acetobacterium malicum strain DSM 4132* 16S ribosomal RNA > emb|X96957.1|	99%	
β-PROTEOBACTERIA										
Burkholderia										
HL3A*	492	564	200	125	51	255	FJ517671.1	Uncultured Burkholderiales bacterium clone 0-1_46 16S ribosomal RNA gene	99%	AP-FeEnrich10
							EU921644	*Duganella* sp. *LT1-9* 16S ribosomal RNA gene, partial sequence	99%	
δ-PROTEOBACTERIA										
Syntrophaceae										
FG1A*	210	95	197	73	403	125	JN038811	Uncultured *delta proteobacterium* clone P-R23 16S ribosomal RNA gene	99%	AP-FeEnrich11
							CP002629	*Desulfobacca acetoxidans* DSM 11109, complete genome	88%	
Desulfobacter										
FA4A, FA4B	515	95	209	127	405	125	DQ831538	Uncultured *delta proteobacterium* clone WB03 16S ribosomal RNA gene	98%	AP-FeEnrich12
							AF328857	*Olavius algarvensis* sulfate-reducing endosymbiont 16S ribosomal RNA gene	94%	
Desulfomicrobium										
FA4A*, FG1B	161	90.5	71.2	65	46	124	AY604056.1	Uncultured bacterium clone DR9IPCB16SCT4 16S rRNA gene	99%	AP-FeEnrich13
							CP001629.1	*Desulfomicrobium baculatum* DSM 4028, complete genome	99%	
Desulfovibrio										
FA2B, FA4B, FL1A, FL1B, FL2A*, FL3A*, FG4B, FM2B, GL3A*, GL3B, HL3A*	457	95	201	127	142	123	NR_029118	*Desulfovibrio putealis strain B7-43* 16S ribosomal RNA > gb|AY574979.1|	99%	AP-FeEnrich14
FL3B, FL4A*	507	93	201	68	143	122	DQ205193	Uncultured *delta proteobacterium* clone MBNTA-bac1 16S small subunit RNA gene	97%	AP-FeEnrich15
							NR_029118	*Desulfovibrio putealis strain B7-43* 16S ribosomal RNA, > gb|AY574979.1|	97%	
FL1A, GL3A*	289	57	75	74	270	35	AY928231.1	Bacterium S9552 16S ribosomal RNA gene, partial sequence	99%	AP-FeEnrich16
							AY362360	*Desulfovibrio vulgaris strain I5* 16S ribosomal RNA gene, partial sequence	95%	

(Continued)

Table 2.1. (Continued)

	Forward			Reverse			Accession number	Top BLAST Hit and closest culturable representative (NCBI)		Designation in Tree (Figure 5)
	MspI	***Hha*I**	***Hae*III**	**MspI**	***Hha*I**	***Hae*III**				
Geobacter										
FA1B, FA2B, FA4A*, FA4B, FL1B, FL2A, FL2B*, FG1A, FG2B	164	93	217	126	405	124	JN038618	Uncultured *delta proteobacterium* clone MA-R44 16S ribosomal RNA gene	98%	AP-FeEnrich17
							NR_026077	*Geobacter pelophilus* strain Dfr2 16S ribosomal RNA, > gb|U96918.1|	97%	
γ-PROTEOBACTERIA										
Aeromonas										
FA4A*, FA4B, FL1B, FG3A*, FG3B, FG4A*, FM2B, FM3A, FM3B, FM4A,	90	215	<50	123	221	124	AY910844	*Aeromonas salmonicida* subsp. *achromogenes* 16S ribosomal RNA gene	99%	AP-FeEnrich18
GL3A*, GG2B, GM3A, GM3B,	90	215	<50	123	221	124	FJ940821	*Aeromonas jandaei strain LNC206* 16S ribosomal RNA gene	99%	AP-FeEnrich19
GM4A, GM4B, HG3B, HL3A*	90	215	<50	123	221	124	FJ808727	*Aeromonas veronii strain QXL0711B* 16S ribosomal RNA gene	99%	
Shewanella										
FL2B*	496	574	<50	127	49	123	AF387349	*Shewanella* sp. *184* 16S ribosomal RNA gene, partial sequence	99%	AP-FeEnrich20
Enterobacteriaceae										
GG3A*	493	373	206	127	49	123	AY394724	*Serratia plymuthica RVH1* 16S ribosomal RNA gene, complete sequence	98%	AP-FeEnrich21
FG4B, GG1A, GG3B, GM2B, HL3A*	494	371	<50	127	49	123	HQ407251	*Serratia fonticola strain G75* 16S ribosomal RNA gene, partial sequence	98%	AP-FeEnrich22
HG3B*	494	371	<50	127	49	123	DQ068814.1	Uncultured bacterium clone f6h4 16S ribosomal RNA gene, partial sequence	99%	AP-FeEnrich23
							AB353048	*Klebsiella oxytoca* gene for 16S ribosomal RNA, partial sequence, strain: No.8	99%	
GM3A,										
SPIROCHETE										
FA1B, FA2B, FA4A*, FA4B, FL1B, FL2A*, FL2B, FL3A*, FL4A, FG1A*, FG2A*, FG2B, FG3A*, FG3B, FG4B, FM1A, FM1B, FM2A, FM2B, FM3A, FM4B, GL3A*, GL3B, GG1A, GG1B, GG2A*, GG3A*, GG3B, GM1A, GM1B, GM2A, GM2B, HG3A, HL3A*	210	62	210	126	146	125	GU080088	Bacterium enrichment culture clone N47 isolate 2 16S ribosomal RNA gene	99%	AP-FeEnrich24
							AY695839	*Spirochaetes bacterium SA-8* 16S ribosomal RNA gene, partial sequence	99%	

Major peaks in the T-RFLP profiles were assigned to phylogenic groups by conducting in silico digestions of clone sequences. The columns MspI, HhaI, and HaeIII represent the length of in silico T-RF sites for clones. Samples with T-RF sites matching a cloned sequence (*) were placed under the respective bacteria with sample nomenclature as: First letter= Fe(III) oxide, Second Letter= Carbon Source, and Number= Dilution. For example, in the first row under Geothrix FL3 stands for ferrihydrite with lactate in the 3rd dilution. Because clones most closely related to Aeromonas spp. and Serratia fonticola/Klebsiella oxytoca have the same restriction site for the six T-RFs obtained in this study it was no plausible to assign the those sample peaks to either group.

2.4 Discussion

Within soil and sedimentary environments, complex organic matter breaks down into numerous metabolic byproducts fueling fermentation and respiration that may be coupled either directly or indirectly to Fe(III) reduction (Lovley et al., 2006). Despite the obvious significance of microbial activity in the reduction of Fe(III) in non-sulfidogenic environments, the role that carbon source and Fe(III) oxide mineralogy play in controlling community structure and ultimately the reduction of varying Fe(III) phases is still poorly understood. This study represents the first large-scale cultivation effort to identify organisms (and/or communities) responsible for Fe(III) reduction as a function of carbon, Fe(III) oxide structure (hence bioavailability) and sediment dilution. We observed statistically supported clustering of enriched Fe(III)-reducing communities primarily based on the carbon source provided. These findings are consistent with biostimulation experiments in which the choice of electron donor supported diverse and distinct communities capable of metal reduction (Akob et al., 2008;Burkhardt et al., 2009). Secondary to carbon, however, both sediment dilution and Fe(III) oxide shaped Fe(III)-reducing communities and dictated putative Fe(III) reduction pathways (e.g., via sulfate reduction) observed here. In fact, differences in community structure as a function of carbon source and sediment dilution dictated not only the amount of Fe(III) reduced but also whether more recalcitrant Fe phases were available for reduction. Similarly, the crystallinity of Fe oxides has also been shown to affect which organisms assimilate ^{13}C labeled acetate (Hori et al., 2010).

Acetate is considered to be a key product of the breakdown of complex organic matter and one of the primary carbon substrates fueling Fe(III) reduction in reduced soils and sediments (Lovley and Phillips, 1989). Here, when acetate was provided as the electron donor within sediment enrichments, only the reduction of the poorly crystalline Fe oxyhydroxide ferrihydrite

was observed. In these enrichments the well-known DIRM *Geobacter* proliferated and a substantial amount (up to 89%) of Fe(III) reduction occurred (Figures 1-3). Organisms within the *Geobacter* clade are dominant metal-reducing organisms within many sediments (Lovley et al., 2004). While *Geobacter* species have the demonstrated ability to reduce various Fe(III) sources, including ferrihydrite, their ability to reduce more crystalline phases is limited (Lovley and Phillips, 1988). Indeed, although *Geobacter* sp. are present in the sediments here (based on its occurrence in ferrihydrite enrichments), little to no Fe(III) reduction (0-6%) of goethite or hematite was coupled to the oxidation of acetate (Figure 2.1). These findings are in line with previous enrichments of rice paddy soils containing ^{13}C-labeled acetate that showed *Geobacter* sp. assimilated ^{13}C-labeled acetate in both ferrihydrite and goethite enrichments, yet Fe(III) reduction was only measured for ferrihydrite (Hori et al., 2010). Thermodynamic calculations indicate that reduction of goethite coupled to acetate oxidation is, in fact, unfavorable ($\Delta G' = \sim 0$ kJ) under our enrichment conditions (pH 7.3; [acetate]=10 mM; $[Fe^{2+}]$=5 μM; $[HCO_3^-]$=10 mM). Thus, in mature sediments where more stable and hence recalcitrant Fe(III) oxides dominant, acetate oxidation will likely not support substantial Fe(III) reduction.

Geobacter species may also be involved in ferrihydrite reduction when lactate is provided as the electron donor. In the 10^{-2} dilution enrichment containing lactate and ferrihydrite, *Geobacter* and *Shewanella* spp. accounted for greater than 75% of the population (Figure 2.2). *Shewanella* species have a wide metabolic plasticity, including the dissimilatory reduction of various Fe(III) substrates (Myers and Nealson, 1988). Since *Shewanella* species incompletely oxidize lactate to acetate, the presence of both *Shewanella* and *Geobacter* species may, in fact, suggest a syntrophy between the two organisms under these conditions. Under most lactate-oxidizing conditions, however, Fe(III) reduction is not linked to known dissimilatory metal-

reducing organisms and instead appears to be linked to sulfate-reducing and fermenting organisms.

In fact, Fe(III) reduction appears to be correlated to the presence of members of the genus *Desulfovibrio* (Figures 2-4) when lactate is the carbon source. *Desulfovibrio* species are abundant, widespread organisms within the *δ-proteobacteria* known for their ability to couple the oxidation of lactate to the reduction of sulfate to sulfide. The genus, however, is diverse in its ability to use a variety of other electron donors (e.g., lactate, acetate, pyruvate) and acceptors (e.g., Fe(III), NO_3^-) (Bale et al., 1997). Despite sulfate concentrations being similar to the modest levels typical of freshwater environments (200 μM), *Desulfovibrio* spp. were found in 90% of the Fe(III)-reducing enrichments containing lactate, with two species dominating (*D. putealis* and *D. vulgaris*). Fe(III) reduction within these enrichments was likely a consequence, at least in part, to sulfide formation and subsequent reaction between sulfide and Fe(III). In fact, within these enrichment cultures, sulfate is not detected. It has been previously demonstrated that Fe(III) reduction can be sustained on catalytic amounts of sulfur (Straub and Schink, 2004). Given the low S to Fe ratio here (1:125), FeS precipitation could be impeded by scavenging of Fe(II) from solution thus allowing sulfur to remain in the aqueous phases and available for continued Fe-S cycling. Indeed, extensive siderite ($FeCO_3$) precipitation was observed within the goethite enrichments (Supplementary Figure S1). Thus, for a catalytic S cycle to be responsible for the amount of Fe(III) reduction observed here, sulfide would need to: 1) be abiotically re-oxidized by Fe to a S intermediate used by an organism in the consortium, and not elemental sulfur as previously suggested (Pyzik and Sommer, 1981;Poulton et al., 2004) or 2) if oxidized to elemental sulfur, a second organism capable of reducing elemental sulfur or taking it

to a higher oxidation state (i.e. through disproportionation) would need to be present in the enrichment (Thamdrup et al., 1993).

Alternatively, given that there are at least two known *Desulfovibrio* species that can use Fe(III) as an electron acceptor (Lovley et al., 1993;Bale et al., 1997;Park et al., 2008), direct enzymatic Fe(III) reduction within these enrichments could be operative. Yet, based on thermodynamic calculations specific to conditions within these enrichments (pH 7.3; [lactate]=10 mM; [acetate]=1 μM; $[Fe^{2+}]$=5 μM; $[HCO_3^-]$=10 mM; $[SO_4^{2-}]$=200 μM; [HS-]=1 μM), the reduction of SO_4^{2-} coupled to incomplete oxidation of lactate is more favorable ($\Delta G'$ = ~101 kJ) than goethite ($\Delta G'$ = ~86 kJ) even with the modest (200 μM) levels of SO_4^{2-} provided. Indeed, these observations are in line with previous calculations that used a partial equilibrium approach to predict a preference for sulfate reduction within environments dominated by more crystalline (e.g., hematite) Fe oxides (Postma and Jakobsen, 1996) and explain similar field observations in which sulfate reduction happened before or simultaneous with Fe(III) reduction (Jakobsen and Postma, 1999). Further, by profiling mRNA transcripts of putative Fe(III)- and key sulfate-reducing genes, recent research suggested that SRBs play a role in suppressing *Geobacter* sp. activity through competition for acetate even during active Fe(III)-reducing conditions (Akob et al., 2012).

As might be expected, the glucose and the mixed carbon enrichments showed the greatest richness (number of T-RFs) and diversity, as evidenced by the many sub-clusters in the dendrogram (Figure 2.2) as well as the large cophenetic dissimilarity. Interestingly, while the mixed carbon source contained all three carbon compounds (glucose, lactate and acetate), mixed carbon enrichment cultures always clustered closely with the glucose enrichments suggesting that even in the presence of lactate and acetate, the most energetic carbon source, glucose,

selected for the dominate community structure. Glucose and mixed carbon enrichment cultures were dominated by known fermenting organisms, including *Firmicutes* and *Enterobacteriaceae.* Despite the focus on dissimilatory Fe(III) reduction within the last few decades, some studies have agreed with earlier research implicating fermentative bacteria as relevant organisms in environmental Fe(III) reduction (Jones et al., 1984;Petrie et al., 2003;Hansel et al., 2008). It remains unclear if Fe(III) simply provides a sink for excess electrons or is used for energy conservation (Dobbin et al., 1999) by fermenting organisms. Yet, recent evidence supports earlier claims that Gram-positive fermentative organisms are capable of indirect and direct enzymatic electron transfer to Fe(III) oxide surfaces as well as solid phase electrodes (Wrighton et al., 2011a;Wrighton et al., 2011b)

The more complex carbon sources also supported Fe(III) reduction along a wide dilution gradient. The enriched Fe(III)-reducing population varied with sediment dilution, likely reflecting specific environmental niches for the putative Fe(III)-reducing communities. For instance, ferrihydrite enrichment cultures supplemented with glucose showed substantial reduction up to a 10^{-4} sediment dilution (Figure 2.1). At higher dilutions (GM-1 cluster), *Actinobacteria* sp. were the dominant organisms and may have been responsible for ferrihydrite reduction, yet it was present in low abundance at lower dilutions (Figure 2.2). This distribution suggests that *Actinobacteria* species were in high abundance within the natural sediment, yet were slow(er) growing under these conditions and therefore outcompeted for resources by faster growing organisms in low dilutions. *Actinobacteria* sp. are common in sediments where they demonstrate diverse metabolisms ranging from propionic acid fermentation to acetogenesis (Madigan et al., 2002). While metal-reducing capacity by *Actinobacteria* has not been confirmed, they are frequently detected within active metal-reducing communities (Akob et al.,

2007;Lin et al., 2007;Wang et al., 2009) and have also assimilated ^{13}C-labeled ethanol during the metal-reducing phase of sediment incubations (Akob et al., 2011).

Interestingly, members of the *Enterobacteriaceae* family also showed a strong dependence on sediment dilution and were observed primarily (88%) on goethite or hematite enrichments. Members of this family are phylogentically diverse with organisms in the *Serratia* and *Klebsiella* clades being known for mixed acid/butanediol fermentation (Madigan et al., 2002). In fact, fermentation products, including acetate, lactate, succinate, propionate and formate, were abundant within these enrichments (Supplemental Table S1). While the current data cannot directly connect these organisms to Fe(III) reduction observed here, given the low diversity in these enrichments and the correlation between the presence of these species with increased Fe(III) reduction (Figure 2.4), they likely play a role. Indeed, members of *Serratia* have previously been implicated in the reduction of hematite (Ottow, 1970). The observation of goethite and hematite reduction only at one specific dilution (10^{-3}) within these enrichments (Figure 2.1), suggests that these organisms occupy specific environmental niches.

While the dominant putative Fe(III)-reducing organisms in the enrichment cultures appeared to be *Geobacter* sp., *Desulfovibrio* sp., and a number of fermenting organisms (depending on dilution and Fe oxide), various other organisms were present whose role in Fe(III) reduction remains unknown. For instance, while *Geothrix*, *Aeromonas* and *Spirochaetes* spp. have demonstrated abilities to reduce Fe(III), their presence does not seem to correlate with Fe(III) reduction capacity (Figures 3-4) putting into question their role in Fe(III) reduction under these conditions. *Geothrix* sp. are present in 7 enrichments, 6 of which are higher dilutions (10^{-3} to 10^{-4}). Their relative peak area decreases with increasing crystallinity, comprising only a maximum of 3% on hematite and goethite but up to 63% on ferrihydrite. *Geothrix* species have

been shown to couple oxidation of both lactate and acetate to the reduction of poorly crystalline Fe oxides (Coates et al., 1999), where Fe(III) chelation is possibly involved (Nevin and Lovley, 2002). Members of the genus *Aeromonas* and *Spirochaetes* are observed within all Fe oxide and carbon conditions. *Spirochaetes* species have a demonstrated ability to reduce Fe(III) (Vu *et al.*, 2004) and the species enriched here is similar to an isolate (SA-8) obtained from an Fe(III)-reducing enrichment (Bonin, 2005). *Spirochaetes* sp. also have the ability to ferment sugars via the glycolitic pathway, convert H_2 and CO_2 to acetate (acetogens), and fix nitrogen (Leadbetter et al., 1999;Madigan et al., 2002;Vu et al., 2004). Similarly, *Aeromonas* sp. have demonstrated the ability to couple growth to Fe(III) reduction (Knight and Blakemore, 1998;Scala et al., 2006). Yet, our findings support previous research suggesting that the direct reduction of solid-phase Fe(III) by these organisms is minimal (Knight et al., 1996;Knight and Blakemore, 1998). Instead, *Aermonas* have the capacity to grow facultatively by either fermentation or anaerobic respiration with other electrons acceptors (e.g., fumarate) (Knight and Blakemore, 1998).

While these organisms (*Aeromonas* and *Spirochaetes*) were present in high proportions and their direct involvement in Fe(III) reduction is unknown, they may play a supporting role in the Fe(III)-reducing community. For instance, *Aeromonas veronii* stimulated Fe(III) reduction in co-cultures with *Shewanella alga* through the dissimilation of citrate to formate, which *S. alga* used as an electron donor (Knight et al., 1996). Furthermore, a *Spirochaetes* species similar (98% sequence identity) to the enriched species in this paper was a stable member of a hydrocarbon-degrading consortium, where it was predicted that it served a syntrophic role in supporting sulfur cycling (Selesi et al., 2010). While unknown at this time, this type of synergistic interaction may explain the high abundance and widespread distribution of *Aeromonas* and *Spirochaetes* species within the enrichment cultures.

Our findings support previous research concluding that dissimilatory metal-reducing organisms are responsible for the reduction of labile Fe(III) phases, primarily in the presence of acetate. We have shown here however that enrichment cultures supporting substantial goethite or hematite reduction coincided with increased relative abundances of *Firmicutes, Enterobacteriaceae* and *Desulfovibrio* spp. (Figure 2.2-4). These findings suggest that the reduction of more crystalline Fe oxides within natural environments, as observed previously (Stucki et al., 2007), is likely a consequence of fermentation and/or sulfate reduction and not dissimilatory metal reduction. Interestingly, carbon source utilization and resource competition may ultimately dictate active Fe(III)-reducing microbial populations and operative Fe(III) reduction pathways, with increased metal reduction in areas containing more complex (higher) carbon sources (e.g., glucose). In young, dynamic environments where ferrihydrite is likely to exist, the growth and activity of DIRMs would be expected. As ripening and/or dissolution-reprecipitation leads to more stable Fe(III) (hydr)oxide end members, however, we expect a shift to sulfate-reducing and fermenting microbial communities which may be capable of directly or indirectly reducing these more stable Fe(III) phases. In fact, minimal Fe(III) reduction may be possible in aged mature soils and sediments that are dominated by lower carbon sources and stable Fe(III) oxides. Ultimately, these findings have implications for our understanding of the cycling of Fe and degradation of carbon in dynamic Fe(III)-reducing environments.

2.5 References Cited

Abdo, Z., Schuette, U.M., Bent, S.J., Williams, C.J., Forney, L.J., and Joyce, P. (2006). Statistical methods for characterizing diversity of microbial communities by analysis of terminal restriction fragment length polymorphisms of 16S rRNA genes. *Environ Microbiol* 8**,** 929-938.

Akob, D.M., Kerkhof, L., Kusel, K., Watson, D.B., Palumbo, A.V., and Kostka, J.E. (2011). Linking specific heterotrophic bacterial populations to bioreduction of uranium and nitrate in contaminated subsurface sediments by using stable isotope probing. *Appl Environ Microbiol* 77**,** 8197-8200.

Akob, D.M., Lee, S.H., Sheth, M., K¸Sel, K., Watson, D.B., Palumbo, A.V., Kostka, J.E., and Chin, K.-J. (2012). Gene expression correlates with process rates quantified for sulfate- and Fe(III)-reducing bacteria in U(VI)-contaminated sediments. *Frontiers in Microbiology* 3.

Akob, D.M., Mills, H.J., Gihring, T.M., Kerkhof, L., Stucki, J.W., Anastacio, A.S., Chin, K.J., Kusel, K., Palumbo, A.V., Watson, D.B., and Kostka, J.E. (2008). Functional diversity and electron donor dependence of microbial populations capable of U(VI) reduction in radionuclide-contaminated subsurface sediments. *Applied and Environmental Microbiology* 74**,** 3159-3170.

Akob, D.M., Mills, H.J., and Kostka, J.E. (2007). Metabolically active microbial communities in uranium-contaminated subsurface sediments. *Fems Microbiology Ecology* 59**,** 95-107.

Bale, S.J., Goodman, K., Rochelle, P.A., Marchesi, J.R., Fry, J.C., Weightman, A.J., and Parkes, R.J. (1997). Desulfovibrio profundus sp. nov., a novel barophilic sulfate-reducing bacterium from deep sediment layers in the Japan Sea. *Int J Syst Bacteriol* 47**,** 515-521.

Basso, O., Caumette, P., and Magot, M. (2005). Desulfovibrio putealis sp. nov., a novel sulfate-reducing bacterium isolated from a deep subsurface aquifer. *Int J Syst Evol Microbiol* 55**,** 101-104.

Benner, S.G., Hansel, C.M., Wielinga, B.W., Barber, T.M., and Fendorf, S. (2002). Reductive Dissolution and Biomineralization of Iron Hydroxide under Dynamic Flow Conditions. *Environmental Science & Technology* 36**,** 1705-1711.

Bonin, A.S. (2005). *DEEP SUBSURFACE MICROBIOLOGY OF THE SOUTH AFRICAN GOLD MINES.* Ph.D., Portland State University.

Burkhardt, E.-M., Akob, D.M., Bischoff, S., Sitte, J., Kostka, J.E., Banerjee, D., Scheinost, A.C., and Kuãàsel, K. (2009). Impact of Biostimulated Redox Processes on Metal Dynamics in an Iron-Rich Creek Soil of a Former Uranium Mining Area. *Environmental Science & Technology* 44**,** 177-183.

Canfield, D.E., Jorgensen, B.B., Fossing, H., Glud, R., Gundersen, J., Ramsing, N.B., Thamdrup, B., Hansen, J.W., Nielsen, L.P., and Hall, P.O.J. (1993). Pathways of Organic-Carbon Oxidation in 3 Continental-Margin Sediments. *Marine Geology* 113**,** 27-40.

Coates, J.D., Ellis, D.J., Gaw, C.V., and Lovley, D.R. (1999). Geothrix fermentans gen. nov., sp nov., a novel Fe(III)-reducing bacterium from a hydrocarbon-contaminated aquifer. *International Journal of Systematic Bacteriology* 49**,** 1615-1622.

Cornell, R.M., and Schwertmann, U. (1996). "The iron oxides: structure, properties, reactions, occurrence and uses," in *The iron oxides: structure, properties, reactions, occurrence and uses.* (Weinheim: Wiley-VCH), xxxi + 573 pp.

Dobbin, P.S., Carter, J.P., San Juan, C.G.S., Von Hobe, M., Powell, A.K., and Richardson, D.J. (1999). Dissimilatory Fe(III) reduction by Clostridium beijerinckii isolated from freshwater sediment using Fe(III) maltol enrichment. *Fems Microbiology Letters* 176**,** 131-138.

Ekstrom, E.B., Learman, D.R., Madden, A.S., and Hansel, C.M. (2010). Contrasting effects of Al substitution on microbial reduction of Fe(III) (hydr)oxides. *Geochimica Et Cosmochimica Acta* 74**,** 7086-7099.

Fredrickson, J.K., Kota, S., Kukkadapu, R.K., Liu, C., and Zachara, J.M. (2003). Influence of Electron Donor/Acceptor Concentrations on Hydrous Ferric Oxide (HFO) Bioreduction. *Biodegradation* 14**,** 91-103.

Guindon, S., Lethiec, F., Duroux, P., and Gascuel, O. (2005). PHYML Online--a web server for fast maximum likelihood-based phylogenetic inference. *Nucleic Acids Res* 33**,** W557-559.

Hansel, C.M., Benner, S.G., Neiss, J., Dohnalkova, A., Kukkadapu, R.K., and Fendorf, S. (2003). Secondary mineralization pathways induced by dissimilatory iron reduction of ferrihydrite under advective flow *Geochemica et Cosmochimica Acta* 67**,** 2992.

Hansel, C.M., Benner, S.G., Nico, P., and Fendorf, S. (2004). Structural constraints of ferric (hydr)oxides on dissimilatory iron reduction and the fate of Fe(II). *Geochemica et Cosmochimica Acta* 68**,** 3217-3229.

Hansel, C.M., Fendorf, S., Jardine, P.M., and Francis, C.A. (2008). Changes in bacterial and archaeal community structure and functional diversity along a geochemically variable soil profile. *Applied and Environmental Microbiology* 74**,** 1620-1633.

Hansel, C.M., Learman, D.R., Lentini, C.J., and Ekstrom, E.B. (2011). Effect of adsorbed and substituted Al on Fe(II)-induced mineralization pathways of ferrihydrite. *Geochimica Et Cosmochimica Acta* 75**,** 4653-4666.

Hori, T., Muller, A., Igarashi, Y., Conrad, R., and Friedrich, M.W. (2010). Identification of iron-reducing microorganisms in anoxic rice paddy soil by C-13-acetate probing. *Isme Journal* 4**,** 267-278.

Hothorn, T., Hornik, K., Van De Wie, L.M.A., and Zeileis, A. (2008). Implementing a Class of Permutation Tests: The coin Package. *Journal of Statistical Software* 28**,** 1-23.

Http://Www.R-Project.Org/ (2012). *R: A Language and Environment for Statistical Computing* [Online]. Vienna, Austria. Available: http://www.R-project.org/ [Accessed].

Jakobsen, R., and Postma, D. (1999). Redox zoning, rates of sulfate reduction and interactions with Fe-reduction and methanogenesis in a shallow sandy aquifer, Romo, Denmark. *Geochimica Et Cosmochimica Acta* 63**,** 137-151.

Jones, J.G., Gardener, S., and Simon, B.M. (1984). Reduction of Ferric Iron by Heterotrophic Bacteria in Lake Sediments. *Journal of General Microbiology* 130**,** 45-51.

Knight, V., Caccavo, F., Wudyka, S., and Blakemore, R. (1996). Synergistic iron reduction and citrate dissimilation by Shewanella alga and Aeromonas veronii. *Archives of Microbiology* 166**,** 269-274.

Knight, V.V., and Blakemore, R. (1998). Reduction of diverse electron acceptors by aeromonas hydrophila. *Arch Microbiol* 169**,** 239-248.

Lane, D.J. (1991). "16S/23S rRNA sequencing," in *Nucleic Acid Techniques in Bacterial Systematics,* ed. G.M. Stackebrandt E. (Chichester, U.K.: Wiley), 115-175.

Leadbetter, J.R., Schmidt, T.M., Graber, J.R., and Breznak, J.A. (1999). Acetogenesis from H2 Plus CO2 by Spirochetes from Termite Guts. *Science* 283**,** 686-689.

Lin, B., Hyacinthe, C., Bonneville, S., Braster, M., Van Cappellen, P., and Roling, W.F.M. (2007). Phylogenetic and physiological diversity of dissimilatory ferric iron reducers in sediments of the polluted Scheldt estuary, Northwest Europe. *Environmental Microbiology* 9**,** 1956-1968.

Lovley, D., Dworkin, M., Falkow, S., Rosenberg, E., Schleifer, K.-H., and Stackebrandt, E. (2006). "Dissimilatory Fe(III)- and Mn(IV)-Reducing Prokaryotes

The Prokaryotes." Springer New York), 635-658.

Lovley, D.R., Holmes, D.E., and Nevin, K.P. (2004). "Dissimilatory Fe(III) and Mn(IV) reduction," in *Advances in Microbial Physiology, Vol. 49,* ed. R.K. Poole. Academic Press), 219-286.

Lovley, D.R., and Phillips, E.J. (1989). Requirement for a Microbial Consortium To Completely Oxidize Glucose in Fe(III)-Reducing Sediments. *Appl Environ Microbiol* 55**,** 3234-3236.

Lovley, D.R., and Phillips, E.J.P. (1988). Novel Mode of Microbial Energy Metabolism: Organic Carbon Oxidation Coupled to Dissimilatory Reduction of Iron or Manganese *Applied and Environmental Microbiology* 54**,** 1472-1480.

Lovley, D.R., Phillips, E.J.P., and Lonergan, D.J. (1991). Enzymatic versus nonenzymatic mechanisms for Fe(III) reduction in aquatic sediments. *Environmental Science & Technology* 25**,** 1062-1067.

Lovley, D.R., Roden, E.E., Phillips, E.J.P., and Woodward, J.C. (1993). Enzymatic iron and uranium reduction by sulfate-reducing bacteria. *Marine Geology* 113**,** 41-53.

Ludwig, W., Strunk, O., Westram, R., Richter, L., Meier, H., Yadhukumar, Buchner, A., Lai, T., Steppi, S., Jobb, G., Forster, W., Brettske, I., Gerber, S., Ginhart, A.W., Gross, O., Grumann, S., Hermann, S., Jost, R., Konig, A., Liss, T., Lübmann, R., May, M., Nonhoff, B., Reichel, B., Strehlow, R., Stamatakis, A., Stuckmann, N., Vilbig, A., Lenke, M., Ludwig, T., Bode, A., and Schleifer, K.Ä. (2004). ARB: a software environment for sequence data. *Nucleic Acids Research* 32**,** 1363-1371.

Madigan, M.T., Martinko, J.M., Dunlap, P.V., and Clark, D.C. (2002). *Brock Biology of Microorganisms.* Benjamin Cummings.

Mccobb, T.D., Leblanc, D.R., and Massey, A.J. (2009). Monitoring the Removal of Phosphate from Ground Water Discharging through a Pond-Bottom Permeable Reactive Barrier. *Ground Water Monitoring & Remediation* 29**,** 43-55.

Myers, C.R., and Nealson, K.H. (1988). Bacterial manganese reduction and growth with manganese oxide as the sole electron acceptor. *Science* 240**,** 1319-1321.

Nevin, K.P., and Lovley, D.R. (2002). Mechanisms for accessing insoluble Fe(III) oxide during dissimilatory Fe(III) reduction by Geothrix fermentans. *Appl Environ Microbiol* 68**,** 2294-2299.

Ottow, J.C. (1970). Selection, characterization and iron-reducing capacity of nitrate reductaseless (nit-) mutants of iron-reducing bacteria. *Z Allg Mikrobiol* 10**,** 55-62.

Park, H.S., Lin, S., and Voordouw, G. (2008). Ferric iron reduction by Desulfovibrio vulgaris Hildenborough wild type and energy metabolism mutants. *Antonie Van Leeuwenhoek International Journal of General and Molecular Microbiology* 93**,** 79-85.

Petrie, L., North, N.N., Dollhopf, S.L., Balkwill, D.L., and Kostka, J.E. (2003). Enumeration and characterization of iron(III)-reducing microbial communities from acidic subsurface sediments contaminated with uranium(VI). *Applied and Environmental Microbiology* 69**,** 7467-7479.

Ploner, A. (2011). "Heatplus: Heatmaps with row and/or column covariates and colored clusters.", in: *R package.* version 2.2.0 ed.).

Postma, D., and Jakobsen, R. (1996). Redox zonation: Equilibrium constraints on the Fe(III)/SO4-reduction interface. *Geochimica Et Cosmochimica Acta* 60**,** 3169-3175.

Poulton, S.W., Krom, M., and Raiswell, R. (2004). A revised scheme for the reactivity of iron (oxyhydr)oxide minerals towards dissolved sulfide. *Geochim. Cosmochim. Acta* 68**,** 3703-3715.

Pyzik, A., and Sommer, S. (1981). Sedimentary iron monosulfides: kinetics and mechanism of formation. *Geochim. Cosmochim. Acta* 45**,** 687-698.

Roden, E.E. (2003). Diversion of electron flow from methanogenesis to crystalline Fe(III) oxide reduction in carbon-limited cultures of wetland sediment microorganisms. *Appl Environ Microbiol* 69**,** 5702-5706.

Roden, E.E., and Urrutia, M.M. (2002). Influence of biogenic Fe(II) on bacterial crystalline Fe(III) oxide reduction. *Geomicrobiology Journal* 19**,** 209-251.

Roden, E.E., and Zachara, J.M. (1996). Microbial reduction of crystalline iron(III) oxides: Influence of oxide surface area and potential for cell growth. *Environmental Science & Technology* 30**,** 1618-1628.

Santelli, C.M., Orcutt, B.N., Banning, E., Bach, W., Moyer, C.L., Sogin, M.L., Staudigel, H., and Edwards, K.J. (2008). Abundance and diversity of microbial life in ocean crust. *Nature* 453**,** 653-U657.

Scala, D.J., Hacherl, E.L., Cowan, R., Young, L.Y., and Kosson, D.S. (2006). Characterization of Fe(III)-reducing enrichment cultures and isolation of Fe(III)-reducing bacteria from the Savannah River site, South Carolina. *Research in Microbiology* 157**,** 772-783.

Schwertmann, U., and Cornell, R.M. (2007). "Ferrihydrite," in *Iron Oxides in the Laboratory*. Wiley-VCH Verlag GmbH), 103-112.

Selesi, D., Jehmlich, N., Von Bergen, M., Schmidt, F., Rattei, T., Tischler, P., Lueders, T., and Meckenstock, R.U. (2010). Combined Genomic and Proteomic Approaches Identify Gene Clusters Involved in Anaerobic 2-Methylnaphthalene Degradation in the Sulfate-Reducing Enrichment Culture N47. *Journal of Bacteriology* 192**,** 295-306.

Stookey, L.L. (1970). Ferrozine---a new spectrophotometric reagent for iron. *Analytical Chemistry* 42**,** 779-781.

Straub, K.L., and Buchholz-Cleven, B.E.E. (2001). Geobacter bremensis sp. nov. and Geobacter pelophilus sp. nov., two dissimilatory ferric-iron-reducing bacteria. *Int J Syst Evol Microbiol* 51**,** 1805-1808.

Straub, K.L., and Schink, B. (2004). Ferrihydrite-dependent growth of Sulfurospirillum deleyianum through electron transfer via sulfur cycling. *Applied and Environmental Microbiology* 70**,** 5744-5749.

Stucki, J.W., Lee, K., Goodman, B.A., and Kostka, J.E. (2007). Effects of in situ biostimulation on iron mineral speciation in a sub-surface soil. *Geochimica Et Cosmochimica Acta* 71**,** 835-843.

Thamdrup, B. (2000). "Bacterial manganese and iron reduction in aquatic sediments," in *Advances in Microbial Ecology, Vol 16,* ed. B. Schink. (New York: Kluwer Academic / Plenum Publ), 41-84.

Thamdrup, B., Finster, K., Hansen, J.W., and Bak, F. (1993). Bacterial disproportionation of elemental sulfur coupled to chemical reduction of iron or manganese. *Appl Environ Microbiol* 59**,** 101-108.

Vu, A.T., Nguyen, N.C., and Leadbetter, J.R. (2004). Iron reduction in the metal-rich guts of wood-feeding termites. *Geobiology* 2**,** 239-247.

Wang, X.-J., Yang, J., Chen, X.-P., Sun, G.-X., and Zhu, Y.-G. (2009). Phylogenetic diversity of dissimilatory ferric iron reducers in paddy soil of Hunan, South China. *Journal of Soils and Sediments* 9**,** 568-577.

Webster, G., Newberry, C.J., Fry, J.C., and Weightman, A.J. (2003). Assessment of bacterial community structure in the deep sub-seafloor biosphere by 16S rDNA-based techniques: a cautionary tale. *Journal of Microbiological Methods* 55**,** 155-164.

Widdel, F., and Bak, F. (1992). "Gram-Negative Mesophilic Sulfate-Reducing Bacteria," in *The Prokaryotes,* eds. A. Balows, G. Truper, M. Dworkin, W. Harder & K.H. Schleifer. (New York: Springer), 3352-3378.

Wrighton, K.C., Engelbrektson, A.E., Clark, I.C., Melnyk, R.A., and Coates, J.D. (2011a). "Accentuate The Positive: Dissimilatory Iron Reduction by Gram-Positive Bacteria," in *Microbial Metal and Metalloid Metabolism: Advances and Applications,* eds. J.F. Stolz & R.S. Oremland. (Washington, DC: ASM Press), 173-194.

Wrighton, K.C., Thrash, J.C., Melnyk, R.A., Bigi, J.P., Byrne-Bailey, K.G., Remis, J.P., Schichnes, D., Auer, M., Chang, C.J., and Coates, J.D. (2011b). Evidence for direct electron transfer by a gram-positive bacterium isolated from a microbial fuel cell. *Appl Environ Microbiol* 77**,** 7633-7639.

CHAPTER 3

IRON(III)-REDUCING COMMUNITIES UNDER ADVECTIVE FLOW COLUMNS: THE ROLE OF SPATIOTEMPORAL EFFECTS AND FE OXIDE MINERALOGY/ AL-SUBSTITUTION

To be submitted as: Lentini, C.J., Tang, Y., Hansel, C. M., ISME Journal

Abstract

Iron (hydr)oxides are a diverse groups of minerals which exist in a spectrum of crystallinities and subsequent bioavailabilities; ranging from ferrihydrite (poorly crystalline) to hematite (well crystalline). While the organisms responsible for the reduction of the poorly crystalline phase ferrihydrite have been well documented (*Geobacter* and *Shewanella*), these model dissimilatory iron-reducing microorganisms (DIRMs) show diminished abilities to reduce the more crystalline Fe(III) (hydr)oxide phases, goethite and hematite. Yet, ferrihydrite is unstable and it ripens and/or transforms to more thermodynamically stable end-members, which has recently brought into question its importance in supporting long-term Fe(III) respiring microbial communities. Therefore to address the questions of which microorganisms and what microbial processes are responsible for controlling the reduction of diverse Fe(III) minerals phases, experiments were conducted in packed mineral columns amended with the structurally diverse Fe oxides (2-line ferrihydrite, 12 mole % Al ferrihydrite, goethite, and hematite). Artificial ground water solution amended with both lactate and acetate was flowed through the columns to mimic natural groundwater conditions. Analysis using a combined aqueous, geochemical and phylogenetic approach revealed that the initial Fe oxide substrate is key in dictating Fe(III) reduction, the mechanisms of reduction, the subsequent secondary mineral phases, the extent of carbon oxidation, and the structure of the microbial communities. Therefore, model dissimilatory Fe reducing microorganism enriched exclusively on poorly crystalline forms of Fe oxides and were not detected in columns containing goethite or hematite. Furthermore, in all columns, there was a negative correlation between microorganisms known to perform sulfate versus Fe(III) respiration, even in the presence of the poorly crystalline ferrihydrite. While this might be expected, the order in which these microbial processes proceeded was is in contrast to the

canonical view of a energy yield based succession of terminal electron accepting processes within natural systems, which predicts that sulfate reduction would not proceed until ferrihydrite was fully consumed. Thus, sulfate reducing bacteria dominated upgradient near the inlet port at the expense of known Fe(III) reducing organisms. These finding have implications in our understanding of carbon mineralization and how electrons flow from reduced substrates to diverse oxidized products in natural environments.

3.1. Introduction

Iron (Fe), as a consequence of its high redox activity and crustal abundance, is an important element in the geochemical cycling of many nutrients and contaminants. Further, most oxidized Fe within soils and sediments exists as Fe(III) oxides, which serve as potent sorbents of carbon, nutrients and metals (Roden and Edmonds, 1997;Brown and Parks, 2001;Kim et al., 2008). In fact, Fe oxides are receiving increasing attention for their ability to co-precipitate with carbon compounds leading to carbon sequestration and presumable long-term carbon preservation in sediments (Lalonde et al., 2011). The reduction of Fe(III) oxides releases sorbed or co-precipitated nutrients and metals to the aqueous environment (Rozan et al., 2002;Islam et al., 2004;Pedersen et al., 2006;Kocar et al., 2010). A dominant pathway for Fe(III) reduction is via respiration by dissimilatory iron-reducing microorganisms (DIRMs) who couple the oxidation and mineralization of organic compounds to the reduction of solid Fe(III) oxides (Lovley and Phillips, 1988;Thamdrup, 2000;Lovley et al., 2004). In fact, it has been predicted that over half of the carbon oxidation in some sediments is a consequence of microbial Fe(III) respiration (Canfield et al., 1993). Reductive dissolution of Fe(III) oxides leads to the formation of Fe(II), which is a strong reducing agent with the demonstrated capacity to reduce several metal contaminants and radionuclides. Oftentimes, the reduction of these soluble oxidized contaminants (e.g., chromium, uranium) leads to their immobilization within reduced solid-phase products (Cr, U) (Fendorf and Li, 1996;Hansel et al., 2003b;Ginder-Vogel et al., 2006). As a result, *in situ* bioremediation of metal contaminated sites through stimulation of Fe(II) generation either *via* direct or indirect microbial processes has been a topic of much research (Zeng and Giammar;Liger et al., 1999;Wielinga et al., 2001;Scott et al., 2005). Despite the sweeping relevance of Fe in biogeochemistry, our understanding of the processes that control Fe(III)

reduction pathways within the environment is fundamentally incomplete and thus hinders our ability to identify carbon mineralization potentials for global climate models, predict the fate and transport of contaminants, and improve the efficacy of *in situ* bioremediation.

One complicating factor in predicting Fe(III) reduction pathways is the dynamic, evolving nature of Fe oxide minerals in accordance with the Ostwald law of stages. Here, precipitation progresses from small thermodynamically unstable phases (*e.g.*, ferrihydrite) to more stable phases (*e.g.*, goethite, hematite) over time through coarsening and structural evolution (Steefel and Vancappellen, 1990). Indeed, instead of a single thermodynamically stable Fe oxide end member precipitating, a range of Fe oxy-hydroxides, hydroxides, and oxides of varying crystallinities and stabilities form in the environment (hereinafter collectively referred to as Fe oxides). Furthermore, within natural environments, Fe oxides rarely exist as pure phases and instead co-precipitate with organic compounds, nucleate on mineral matrices, and/or incorporate foreign ions such as Al^{3+} into their framework structure (Perret et al., 2000;Wagai and Mayer, 2007;Ekstrom et al., 2010;Hansel et al., 2011). As a result of varying crystal structures and modifying impurities, Fe oxides have a range of electronic and physiochemical properties, including surface area, solubility, crystallinity, and reduction potential. These diverse properties ultimately lead to vastly different rates of Fe oxide reduction and/or solid transformations induced by both microbial and abiotic mechanisms (Postma, 1993;Zachara et al., 1998;Hansel et al., 2003a;Poulton, 2003;Roden, 2003;Hansel et al., 2004;Poulton et al., 2004;Bonneville et al., 2009).

While kinetic limitations may allow for the initial precipitation of poorly crystalline Fe(III) oxide phases, previous research has shown that the biotic and abiotic conversion of these poorly crystalline oxides to more crystalline phases is rapid (Zachara et al., 2002;Hansel et al.,

2003a;Hansel et al., 2005). Thus, in mature environments, more stable crystalline Fe(III) oxide minerals dominant and therefore control the rates and mechanisms of Fe(III) reduction and subsequent Fe-based carbon oxidation in natural systems. In fact, recent studies have shown that even in soils undergoing fluctuating redox oscillations, ferrihydrite is not the dominant phase as would be predicted and instead sustained oxide ripening leads to the dominance of more crystalline phases such as goethite (Thompson et al., 2006). Consequently, the feasibility of poorly crystalline Fe(III) oxides to provide a primary long-term electron acceptor to support Fe(III)-reducing microbial communities is unlikely. Despite this, Fe(III)-reducing microorganisms have historically been enriched, cultivated and investigated using ferrihydrite as the terminal electron acceptor (Zhang et al., 1999;Straub and Buchholz-Cleven, 2001;Lovley et al., 2004;Cummings et al., 2010;Li et al., 2011).

A wide phylogenetic diversity of microorganisms are capable of reducing the poorly crystalline Fe(III) oxide ferrihydrite, including the two most-studied model organisms *Geobacter* and *Shewanella* spp. (Lovley and Phillips, 1988;Roling et al., 2001;Nealson et al., 2002;Nevin and Lovley, 2002;He and Sanford, 2003;Lovley et al., 2004;Lin et al., 2007). A variety of mechanisms by which DIRMs reduce solid substrates has been proposed and remain a topic of much debate. Direct enzymatic contact, Fe(III) chelation, and electron shuttling primarily via organic compounds with quinone-like moieties have been identified as viable mechanisms for promoting Fe(III) reduction (Bucking et al.;Coates et al., 1998;Afkar et al., 2005;Reguera et al., 2005;Gorby et al., 2006;Marsili et al., 2008;Fennessey et al., 2010;Jones et al., 2010;Roden et al., 2010). Yet, the underlying processes that control which mechanisms are operative and how they are regulated by biogeochemical conditions are unknown. In particular, the role that Fe oxide structure and composition play in regulating microbial Fe(III) reduction and the operative

reduction pathway is poorly understood. It is generally accepted that DIRMs preferentially reduce poorly crystalline Fe oxides, yet can only sparingly reduce more crystalline phases (Lovley and Phillips, 1986;Phillips et al., 1993;Lin et al., 2007). In addition, both thermodynamic modeling and experimental observations suggest that under certain conditions sulfate reduction occurs concurrent with or prior to Fe(III) reduction (Postma and Jakobsen, 1996). Sulfide generated upon sulfate reduction is a strong reductant and will therefore compete with DIRMs for the surface sites of the oxidized Fe phase (Yao and Millero, 1996). Therefore, the processes governing Fe(III) reduction within natural systems may not be well-represented by model systems using less environmentally relevant poorly crystalline oxide phases and organisms in isolation of competing organisms and pathways.

We have previously shown that the common Fe(III) respiring microbe *Geobacter* sp. dominated enrichments of Fe-rich sediments when ferrihydrite was the provided terminal electron acceptor and acetate was the carbon source (Lentini et al., 2012). Yet, acetate was unable to support substantial amounts of reduction within either goethite or hematite enrichments. In contrast, when more energetically favorable carbon substrates were used (e.g., glucose, lactate), reduction of goethite and hematite correlated with the presence and activity of the sulfate-reducing bacteria, *Desulfovibrio* sp., despite the use of low sulfate levels to simulate freshwater environments (200 μM). These results point to sulfate reduction as being a dominant pathway for the reduction of more crystalline Fe(III) oxide phases within the environment, in agreement with previous thermodynamic models (Postma and Jakobsen, 1996) and field observations (Jakobsen and Postma, 1999).

Yet, due to the inherent drawbacks of batch cultivations and field-based observations, the exact role of mineral structure in dictating reduction pathways remains unclear. In particular,

within batch studies reaction products accumulate to unnatural levels that no longer mimic the environment, potentially inhibiting reaction progression and forcing microbial communities to irrelevant stable communities. Yet, due to the complexity of the natural environment, testing responses to single variables within field-based investigations is difficult, if not near impossible. As a compromise, column based bioreactors allow for more controlled analysis of biogeochemical variables under a more realistic setting where metabolic end products are continuously removed and therefore do not impact reaction kinetics. Accordingly, to better understand how Fe(III) oxide structure and composition shape Fe(III)-reducing microbial communities and pathways, we conducted flow-through column experiments containing natural sediment and the indigenous microbial community. A series of columns were amended with four diverse Fe(III) oxide phases (ferrihydrite, Al-doped ferrihydrite, goethite, and hematite) and run under conditions mimicking a natural groundwater system to allow for the establishment of microbial and geochemical gradients. The dominant fermentation products lactate and acetate were both added to the influent solution to relieve carbon substrate competition between respiratory communities and avoid selecting for a dominant Fe(III) respiration pathway.

3.2. Material and Methods

3.2.1 Mineral synthesis of Fe-coated sands: Two-line ferrihydrite, goethite, and hematite were prepared following the procedure in Schwertmann and Cornell (Schwertmann and Cornell, 2007). In addition, ferrihydrite containing 13 mole % aluminum (Al) was synthesized by the mixing of 0.2 M $FeCl_3$ with 0.2 M $Al(NO_3)_3$ to a final Al concentration of 13 mole %. Both hematite and goethite were washed with hydroxylamine to remove disordered regions. All minerals were washed several times either via dialysis or mixing and centrifugation with deionized water.

Washed minerals slurries were mixed with pure quartz sand and dried at 20°C under convection while being periodically stirred. The dried Fe oxide-coated sands were suspended in water and washed to remove any loose mineral not attached to the sand. Both X-ray diffraction (XRD) (Harvard University) and X-ray absorption spectroscopy (XAS) (Stanford Synchrotron Radiation Lightsource, SSRL – see description below) were used to verify the purity of the Fe (hydr)oxide phases. No changes in mineralogy were noted after sterilization.

3.2.2 Column design and flow conditions: Shallow core samples were collected from Ashumet Pond, Falmouth, MA, USA, in spring of 2012, and placed on ice until transfer back to the anaerobic chamber in the laboratory. The sampling site is enriched in Fe as a result of the installation of a permeable reactive barrier containing zero valent Fe [3% Fe(0) by weight] which was emplaced sub-horizontally on the bottom of the pond (0.6 m deep) to intercept phosphate-laden water that discharged near the shore of Ashumet Pond (McCobb et al., 2009).

Once in the anaerobic chamber, the inner core of the sediments (labeled SediFresh) was mixed and allowed to incubate for ~30 days in pond water in order to consume any excess electron donors and acceptors indigenous to the sediment (labeled SedT). Before inoculation, the sediment was sterilely sieved (1 mm^2) to ensure uniform distribution and remove larger pebbles. The sediment was mixed (1:10) with one of the four Fe oxides (ferrihydrite, goethite, hematite and Al-ferrihydrite) precipitated onto quartz sand or pure quartz sand (no Fe control). Eight columns (1.5 cm X 10 cm) (Hansel et al., 2004) were packed with approximately 40 g of Fe oxide-coated sand resulting in a mass of Fe within the columns of approximately 2400 μmoles. The columns were secured vertically in an anaerobic glovebox and artificial groundwater media was pumped through the bottom and out the top of the column at a velocity

of 0.2 m/d (within normal groundwater flow rates) using a communal peristaltic pump. The artificial groundwater medium contained the following ingredients (in μmoles/L): KCl, 67; NaCl, 82; $MgSO_4$, 200; $MgCl_2 \cdot 6H_2O$, 215; KH_2PO_4, 20; NH_4Cl, 320 and 100 μL/L each of Wolfe's trace element and vitamin stock solutions. Both lactate and acetate were provided as electron donors to provide a final concentrations of 500 μM each. The medium was equilibrated with calcite (~0.4 g/L) and CO2 at 0.02 atm (pH ~7) as described in Hansel et al., 2003.

Ten columns were run in parallel with half terminated after 19 days (T-19) and the other half following 29 days (T-29) of reaction. Effluent solution chemistry was monitored daily while solid-phase and microbiological analysis was conducted upon termination at each time point (see below).

3.2.3 Effluent measurements: Effluent chemistry was monitored daily by collecting the solution coming out of the column (effluent) into a sealed serum vial. In order to avoid the build up of backpressure, the serum vials were exhausted into a secondary vial, which contained a $ZnCl_2$ solution to trap gaseous sulfide. Approximately every 24 hours the effluent solution was weighed and measured for the following: ferrous Fe, total Fe, dissolved sulfide, ammonium, alkalinity, pH, organic acids and major cations and anions. Fe(II) and total Fe (Fe_{TOT}) were measured using a modified Ferrozine method with Fe_{TOT} measured by first reducing Fe(III) to Fe(II) via reaction with hydroxylamine under a flame (Stookey, 1970). Sulfide was monitored in both the effluent solution and Zn trap via the methylene blue method (Cline, 1969). Ammonium was monitored by reaction with phenol in the presence of alkaline hypochlorite and sodium nitroprusside. Major cations, including Al for the Al-ferrihydrite columns, were measured via

inductively coupled plasma optical emission spectroscopy (ICP-OES). Organic acids and major anions (e.g., sulfate) were measured using ion chromatography (IC).

3.2.4 Solids phase measurements: Upon reaction termination, solid samples were carefully extracted from the glass columns to preserve spatial distributions. The column sediments where divided in half according to weight to allow for analyses and comparison of the top and the bottom of the reacted sediments. Solid-phase Fe(II) and total Fe were measured by digesting a weighed amount of solid in anaerobic 6 M HCl within the anaerobic chamber for several hours. Fe^{2+} and Fe_{TOT} were then measured using the Ferrozine method (as described above) with an ammonium acetate buffer where needed. Acid volatile sulfide (AVS) was measured by addition of the solid-phase to anaerobic HCl under flow of N_2. The gas was passed though a Zn hydroxide EDTA solution for approximately 4 hours and measured via methylene blue method (Cline, 1969).

Secondary minerals were characterized via X-ray absorption spectroscopy (XAS) on solid samples that were stored anaerobically and frozen until analysis at the Stanford Synchrotron Radiation Lightsource (SSRL). For Fe analysis, the samples were dried in an anaerobic chamber and mounted onto Teflon holders with Kapton tape. For S, dried samples were mounted onto S-free Lexan. Fe and S XAS spectra were collected under a He-purged sample chamber under a continuous He flow with a Lytle detector at BL 4-3. The identification and quantification of secondary Fe and S phases were determined by fitting either the k^3-weighted EXAFS (Fe) or XANES region (S) of the unknown spectra (samples) with a linear combination of reference compounds using the program SIXPack (Webb, 2005) and described in detail previously (Hansel et al., 2003a). Linear combinations of the empirical model spectra

were optimized where the only adjustable parameters were the fractions of each model compound contributing to the fit. The goodness of fit was established by minimization of the *R*-factor (Newville, 2001).

Model compounds used in the Fe and S XAS linear combination fitting included 2- and 6-line ferrihydrite ($Fe(OH)_3 \bullet nH_2O$), goethite (α-FeOOH), lepidocrocite (γ-FeOOH), hematite (α-Fe_2O_3), magnetite (Fe_3O_4), poorly crystalline iron sulfide (FeS), mackinawite (FeS), pyrite (FeS_2), elemental S, vivianite ($Fe_3[PO_4]_2 \bullet nH_2O$), siderite ($FeCO_3$), three green rust varieties ($[Fe^{II}_{(1-x)}Fe^{III}_x(OH)_2]^{x+} \bullet [(x/n)A^{n-} \bullet (m/n)H_2O]^{x-}$; where A^{n-} = sulfate, carbonate or chloride), hornblende, biotite, and Fe-rich nontronite. Goethite, ferrihydrite, hematite, and lepidocrocite were synthesized following the procedures of Schwertmann and Cornell (Schwertmann and Cornell, 2007). Green rust chloride and sulfate were synthesized per the method of Schwertmann and Fechter (Schwertmann and Fechter, 1994) and green rust carbonate via Benali et al. (Benali et al., 2001). Iron sulfides were produced by the method described in Morse and Arakaki (Morse and Arakaki, 1993). The remainder of the minerals were obtained from the Stanford University Mineral Collection. All standards were verified using X-ray diffraction (XRD).

3.2.5 Microbial Analysis: DNA was extracted from the solid-phase samples and sequenced by Molecular Research LP (www.mrdnalab.com). DNA was extracted using the MoBio powersoil kit per the manufacturer instructions. Upon extraction, 454 sequences (GS FLX Titanium) of the V1- V3 bacterial 16S rRNA region were generated using the primer pair 27F- 519R. The QIIME pipeline was used to deplete the sequences of barcodes and primers. Sequences were removed from the dataset that were short reads (< 200bp), had ambiguous base calls, or were

homopolymer runs exceeding 6bp. The cleaned sequences were further denoised and chimeric sequences removed. After removal of singleton sequences, operational taxonomic units (OTU) were defined by clustering at 3% divergence and classified using BLASTn against a curated GreenGenes database (DeSantis et al., 2006).

3.2.6 Statistical Analysis: First, all samples were normalized by randomly sampling without replacement until the total counts equaled the minimum number of sequences contained within a single sample (609 counts for Al-ferr T-19). Once normalized, phylogenetic counts were arranged into a site by genera matrix and statistical analyses were performed. All alpha-diversity measures were calculated using the statistical programming language R (http://www.R-project.org/, 2012) and associated packages. Specifically, the Vegan package (Hothorn et al., 2008) was used to calculate the Shannon and Simpson index while the EstimateR package was used to obtain Chao1 and ACE measures of richness. Code was further developed to calculate the Gini coefficient (subtraction of the area under a Lorenz curve from a straight line with slope 1).

Beta diversity calculations were also performed in R using the Vegan package. To compare between sample diversity, the Bray-Curtis dissimilarity measure was used. A dissimilarity matrix was made to perform clustering and ordination. Hierarchical clustering analysis was performed using the hclust function of the stats package in R with the agglomeration method being Unweighted Pair Group Method with Arithmetic Mean (UPGMA). Non-metric Multidimentional Scaling (nMDS) was performed using the metaMDS functions in Vegan. Given the nature of the data, typically nonparametric and heteroskedastic, typical comparisons test that rely on the assumption of normality and homogeneity of variance could not

be used. Therefore permutation test were performed for most statistical testing using the coin package in R (Hothorn et al., 2008). In this type of testing, a statistical distribution against which a statistic will be tested is generated by randomly permuting the data (i.e. no previous statistical distribution needed). All samples that underwent multiple comparisons were Bonferroni corrected. Taxa correlation tests were performed on the ranked relative abundance using Spearman's rho.

3.3. Results

Iron(III) reduction by natural microbial communities was investigated as a function of the structure of the Fe oxide substrate provided over space and time. The experiments were conducted in packed mineral beds (columns) amended with the structurally diverse Fe oxides 2-line ferrihydrite (Fh), 12 mole % Al ferrihydrite (Al-Fh), goethite (Gt), and hematite (Hm). An artificial ground water solution amended with both lactate and acetate flowed through the columns to mimic natural groundwater conditions. Duplicate columns were run for each condition, including a no Fe amendment control (natural sediment only), to allow for microbial and solid-phase analysis at two time points (19 and 29 days).

After, 452.4 hours (~19 days) the mean volume of effluent passed through each of the 10 columns was 641 mL, equivalent to approximately 64 pore volumes. At this point half of the columns were broken down and will be hereinafter be referred to as time point T-19. Visual darkening of the columns was observed starting after ~7 days. In all columns, solids in the bottom half the columns (up-gradient) were near black after 19 days (Figure 3.1). For the top half of the columns, however, goethite and hematite showed only minimal darkening, while solids in Al-ferrihydrite and ferrihydrite columns had substantial darkening observed throughout.

Continued reaction to 705 hours (~29 days) resulted in further darkening in all the columns, yet the top of the goethite and hematite columns remained unchanged. Upon termination of each column set, the solids were split into the top and bottom halves to identify the microbial and solid-phase composition associated with these visual differences among and within the columns over time (10 columns, 2 column locations, 2 time points = 40 samples to be discussed below).

At 19 days, during the termination of the first set of columns, flow was suspended in the duplicate set of columns to conduct a stopped-flow event. Under these conditions, the system is closed as in a batch system to allow for relief of kinetic barriers to microbial metabolism and mineral transformations. Flow was initiated after two hours.

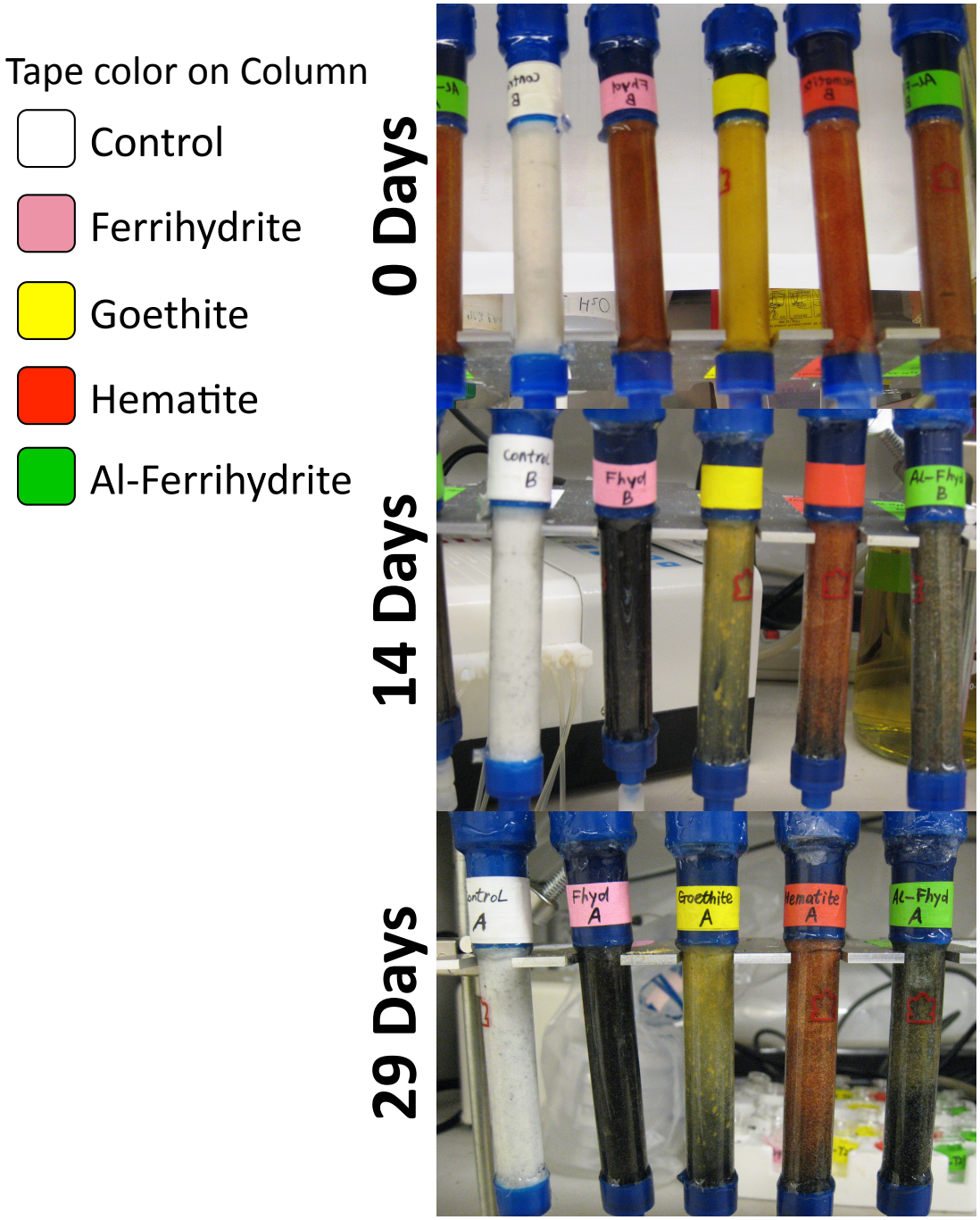

Figure 3.1. Photographs of columns illustrating visual color changes indicative of solid-phase transformations of the Fe phases over time.

3.3.1 Effluent Chemistry: Within the first 48 hours, both lactate and acetate were detected within the effluent of all the columns (Figure 3.2). After 48 hours effluent lactate levels rapidly declined becoming non-detectable within 140 hours in all the columns. Conversely, during this time acetate levels steadily increased reaching a pseudo steady-state between 200 and 400 hours depending on the Fe oxide substrate (Figure 3.2). These steady-state acetate values for Fh, Al-Fh, Gt, Hm were 2500, 2300, 2400, 1000 μM, respectively. Interestingly, acetate values in the effluent of all the columns were 2-5 times greater than the influent concentration suggesting a secondary input of acetate. After the stopped-flow event at 476 hours, acetate values spiked to concentrations 2-4 times greater than the steady-state values. Effluent acetate values declined to new steady state values after ca. 150-200 hours after flow was restarted (ca. 650 hours).

The influent pH fluctuated between 7 and 7.5 as a function of small deviations in the influent media solution (Figure 3.2). Under all conditions, the pH of the effluent solution increased to values averaging approximately 8 consistent with microbial metabolism, including both Fe(III) and sulfate respiration. A short-lived decline in pH in all the columns was observed following the stopped-flow event as observed previously (Hansel et al., 2004) and consistent with loss of protons from mineral surfaces upon dissolution and/or transformation.

Sulfate is observed in the effluent in all columns for the first ca. 160 hours with concentrations at 18 hours already 4-10 times (20-50 μM) lower than the influent sulfate concentration (160 μM) (Figure 3.2). Similar to that observed for lactate, sulfate concentrations continued to steady decline and were typically below detection within 164 hours for all the columns regardless of Fe oxide amendment.

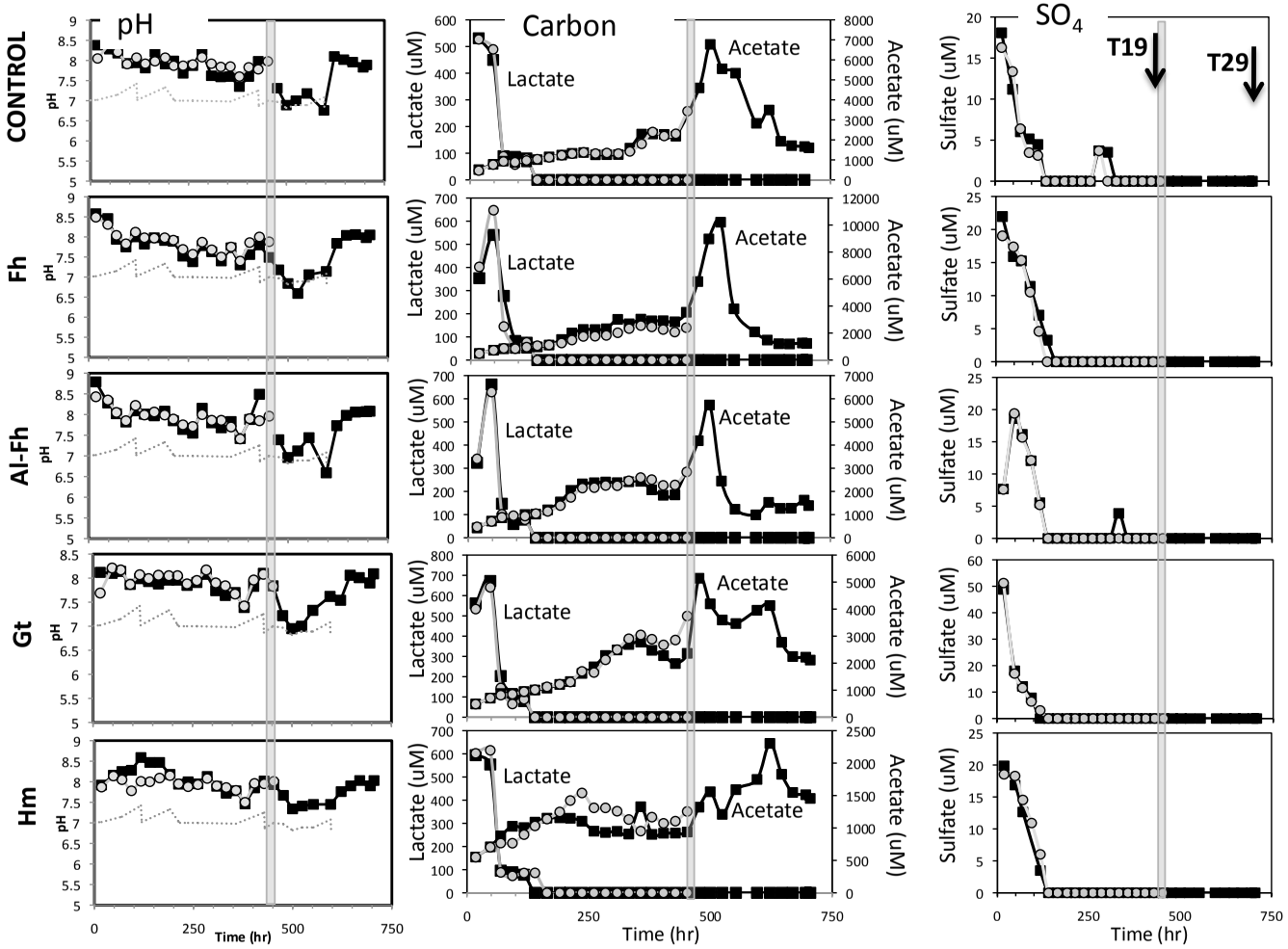

Figure 3.2. Aqueous chemistry of the column effluent, including (left) influent and effluent pH values, (middle) effluent lactate and acetate concentrations, and (right) effluent sulfate concentrations over time. Gray circles are duplicate column set terminated at 19 d and columns represented by black squares were terminated after 29 days (arrows). Vertical gray bar highlights timing of stopped flow event.

Within the control column, sulfide was detected in the effluent at 70 hours and steadly increased reaching a pseudo steady state at ca. 117 hours and a concentration of ~155 μM (Figure 3.3). The effluent sulfide fluctuated hovering around 150 μM until the stopped flow event resulting in a short-lived decline to ~80 μM. In contrast, within the Fe oxide amended columns, a single pulse of effluent sulfide was detected between 93 and 170 hours with the peak concentration varying with Fe oxide type. Peak concentrations for Fh, Al-Fh, Gt, and Hm were 10, 6, 50, 55 μM, respectively. Upon reaching its maximum value, sulfide decreased in all Fe amended columns and was below detection within 200-300 hours. No change in effluent sulfide was detected after the stopped flow event. Of the total sulfur (as sulfate) introduced to the columns, 2-6% (Hm) and 5-8% (Gt) of this total S pool was detected in the effluent as dissolved sulfide (Table 3.1). In contrast, less than 1% of the total sulfur provided was eluted from the column as sulfide in both the Al-Fh and Fh columns.

Effluent dissolved Fe(II) levels showed a short-lived spike ranging from 1 (Gt, Hm) to 4 μM (Fh) within the first 48 hours (Figure 3.3). Between 48 and ca. 160 hours, all Fe amended columns had effluent Fe(II) values below 1.5 μM. Effluent Fe^{2+} values began to increase at 140 hours for the Al-Fh and Fh columns, reaching steady state values of ~45 and ~120 μM, respectively, by 284 hours. For Hm and Gt, effluent Fe^{2+} did not increase until later (190 hours and 305 hours) and steady state values of ~25 and 17 μM were reached at 236 and 356 hours, respectively. The stopped flow event at 452 hours resulted in a large spike in effluent dissolved Fe(II) levels in the all the columns with steady-state values resuming at approximately ~650 hours.

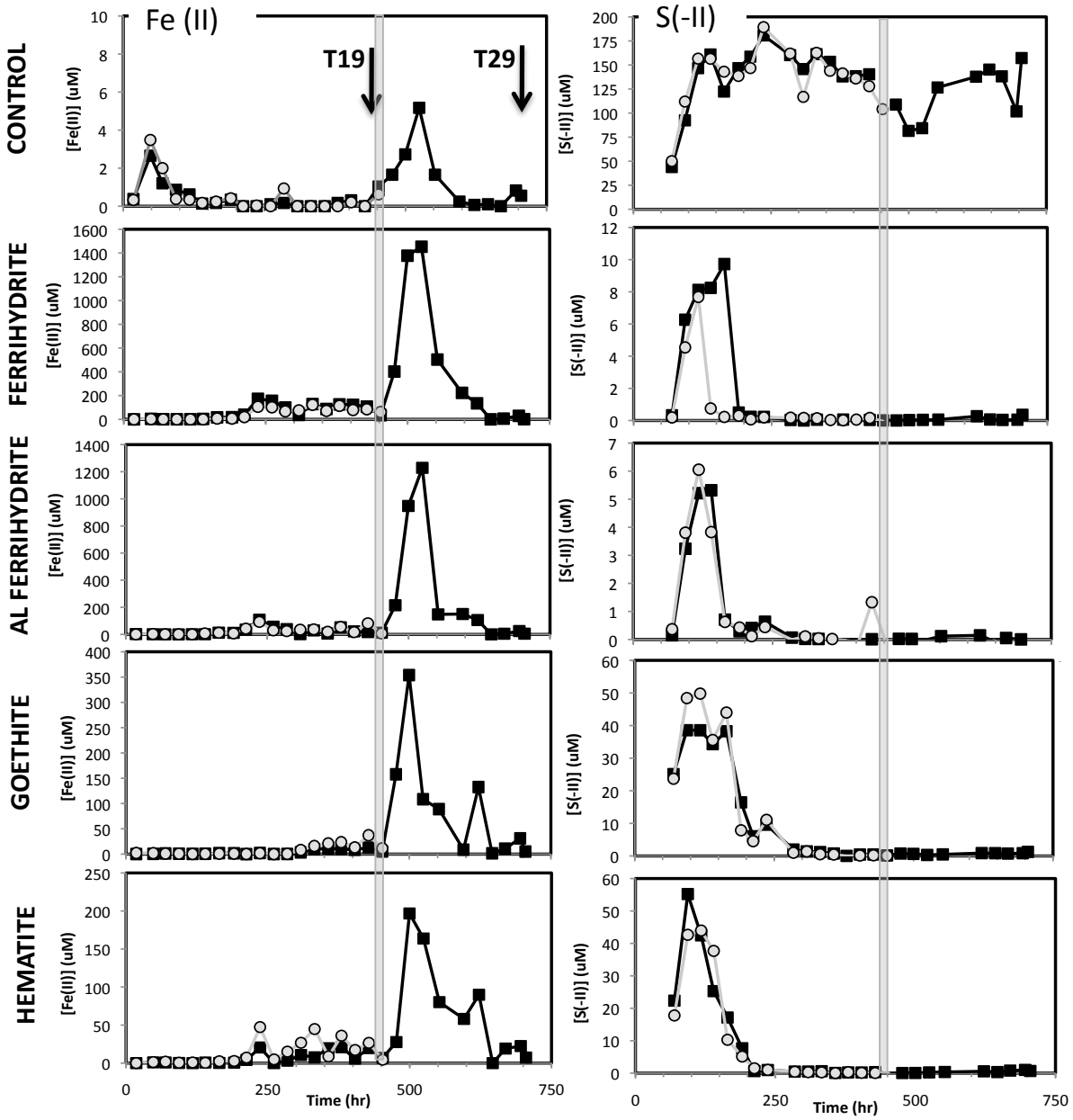

Figure 3.3. Effluent concentrations of (left) Fe(II) and (right) sulfide over time. Gray circles are duplicate column set terminated at 19 d and columns represented by black squares were terminated after 29 days (arrows). Vertical gray bar highlights timing of stopped flow event.

3.3.2 Solid-phase Extractions: After 452 hours, greater than 95% of the total Fe(III) added to the Fe amended columns remained within or associated with the solid-phase fraction (Table 3.1).

The distribution of total Fe within the column was nearly uniform with the percentage of total Fe within the column slightly higher in the top section (49 to 58%) than the bottom (41 to 48%). After 705 hours, the amount of total Fe remaining in the Fe amended column ranged from 85 to 96% of the total Fe provided. The percentage of total Fe within the solid-phase declined within each column, particularly the Fh (85%) and Al-Fh (89%) amended columns. More substantial differences in total Fe distribution relative to the first 452 hours were observed for Al-Fh and hematite but not for Fh and Gt (Table 3.1).

After 452 hours, substantial concentrations of Fe(II) were associated with the solid-phase varying with the Fe(III) oxide substrate provided (Table 3.1). The concentration of Fe(II) associated with the solid-phase decreased in order of Al-Fh (1559 μmoles), Fh (1262 μmoles), Hm (315 μmoles), and Gt (264 μmoles). When normalized to the amount of total Fe within the column at this time, the percentage of Fe within the solid-phase present as Fe(II) is 78, 47, 15, and 13% for Al-Fh, Fh, Gt, and Hm, respectively. For each section individually, the fraction of total Fe that is Fe(II) is more uniform for Fh and Al-Fh but substantially lower in the top (~6%) relative to the bottom sections (~27-20%) of Gt and Hm (Table 3.1). After 705 hours, the total concentration of Fe(II) within the solid-phase for all the Fe amended columns was not substantially higher than the values observed at 452 hours. Similarly, the percentage of Fe(II) to total Fe within the solid-phase was similar to the earlier time point, being 74, 50, 14, 12% for Al-Fh, Fh, Gt, and Hm, respectively.

Table 3.1. Iron and sulfur dynamics as a function of Fe oxide substrate and time

	Control	Fh	Al-Fh	Gt	Hm
Total Fe	t19/t29	t19/t29	t19/t29	t19/t29	t19/t29
Solid Fe loaded in columns (T0) (μmoles)	77/25	2674/2834	2034/2173	1717/1864	2345/2401
Aqueous Fe in effuent (μmoles)	3/6	115/416	71/232	26/89	40/102
Solid Fe in reacted columns (μmoles)	74/19	2559/2418	1963/1941	1690/1775	2305/2298
• in top of column (μmoles)	36/10	1376/1334	986/1120	995/939	1183/1276
• in bottom of column (μmoles)	37/9	1183/1083	977/821	696/836	1122/1022
Aqueous Fe in effuent (%)	4/25	4/15	4/11	2/5	2/4
Solid Fe in reacted columns (%)	96/75	96/85	97/89	98/95	98/96
• in top of column (%)	47/40	51/47	48/51	58/50	50/52
• in bottom of column (%)	49/35	44/38	48/38	41/45	48/43
Fe(II)					
Total Fe(II) produced (μmoles)	15/4	1262/1422	1558/1568	264/288	315/314
Aqueous Fe(II) in effluent (μmoles)	0/1	67/208	29/133	6/38	11/43
Solid Fe(II) in column (μmoles)	15/3	1195/1215	1529/1435	257/249	304/271
• in top of column (μmoles)	9/2	566/563	761/787	68/18	79/50
• in bottom of column (μmoles)	6/1	629/652	768/648	189/231	226/221
Total Fe(II)/ Total Fe initially available (%)	20/18	47/50	77/72	15/15	13/13
Total solid Fe(II)/ Tot solid Fe in columns (%)	20/16	47/50	78/74	15/14	13/12
• in top of column (%)	26/24	41/42	77/70	7/2	7/4
• in bottom of column (%)	15/7	53/60	79/79	27/28	20/22
Aqueous Fe(II) in effluent/ Total Fe(II) generated (%)	0/25	5/15	2/8	2/13	3/14
Solid Fe(II) in column/ Total Fe(II) generated (%)	100/75	95/85	98/92	97/86	97/86
• in top of column (%)	60/50	45/40	49/50	26/6	25/16
• in bottom of column (%)	40/25	50/46	49/41	72/80	72/70
Sulfur					
Total S introduced to column as sulfate (μmoles)	108/205	131/184	109/179	104/176	116/160
Total sulfate in effluent (μmoles)	15/25	23/24	19/22	28/31	41/22
Total sulfide generated (μmoles)	-/158	-/121	-/148	-/146	-/135
Total sulfide in effluent (μmoles)	80/154	1/1	1/1	8/8	7/3
Total solid-phase sulfide (AVS) in column (μmoles)	-/4	-/120	-/146	/138	-/132
• top of column (μmoles)	-/3	-/1	-/2	-/4	-/0
• bottom of column (μmoles)	-/1	-/119	-/145	-/134	-/132
Solid sulfide in column/ Total sulfide generated (%)	-/3	-/100	-/100	-/95	-/98
• in top of column (%)	-/2	-/1	-/1	-/3	-/0
• in bottom of column (%)	-/1	-/98	-/98	-/92	-/98

Solid-phase sulfide was detected in all of the columns (Table 3.1). This phase is operationally defined, and measured via acid volatilization of reduced sulfur species (not including S^0 or FeS_2). While minor levels were measured in the top sections of the Fe amended columns (0-4 μmoles), substantial solid-phase sulfide was observed in the bottom sections ranging from 119 to 145 μmoles.

3.3.3 Spectroscopic Analysis: After 29 days (705 hours), significant secondary mineralization of Fe was observed for all solids excluding the top sections of the Gt and Hm columns (Figure 3.4). The dominant secondary Fe minerals observed were magnetite, mackinawite, amorphous FeS, and green rust, whose spectral features are highlighted by the standard spectra illustrated in

Figure 3.4. Fe LC-EXAFS fitting of the solid-phases within the Fhy column after 29 days indicated the presence of residual ferrihydrite (29-41%) and the secondary phases magnetite (55%) and FeS (4%) in the bottom section and magnetite (56%) and goethite (15%) in the top section (Figure 3.4, Table 3.2). Within the Al-Fhy column, ferrihydrite is no longer detected and instead various phases are observed. Within the bottom section, the Fe exists as green rust (62%), mackinawite (23%), magnetite (7%), and lepidocrocite (7%). Within the top, sulfide phases are not observed but rather green rust (62%), magnetite (19%), lepidocrocite (13%), and goethite (6%).

Within the Gt and Hm columns, the LC-EXAFS did not detect any secondary phases within the solid-phase within the top section and spectra resembled solely the parent mineral. However, within the bottom sections of both the Gt and Hm columns, mackinawite (15% and 10%) and amorphous FeS (10% and 15%) were detected, while magnetite (11%) was also observed for the Gt columns.

S XANES spectroscopy indicated a dominant peak at 2470 eV consistent with an FeS phase, confirming that the majority of the solid sulfur within the column was indeed an FeS mineral (Figure 3.4). For reference, spectra of elemental S and sulfate were included but peaks associated with these compounds were not significant.

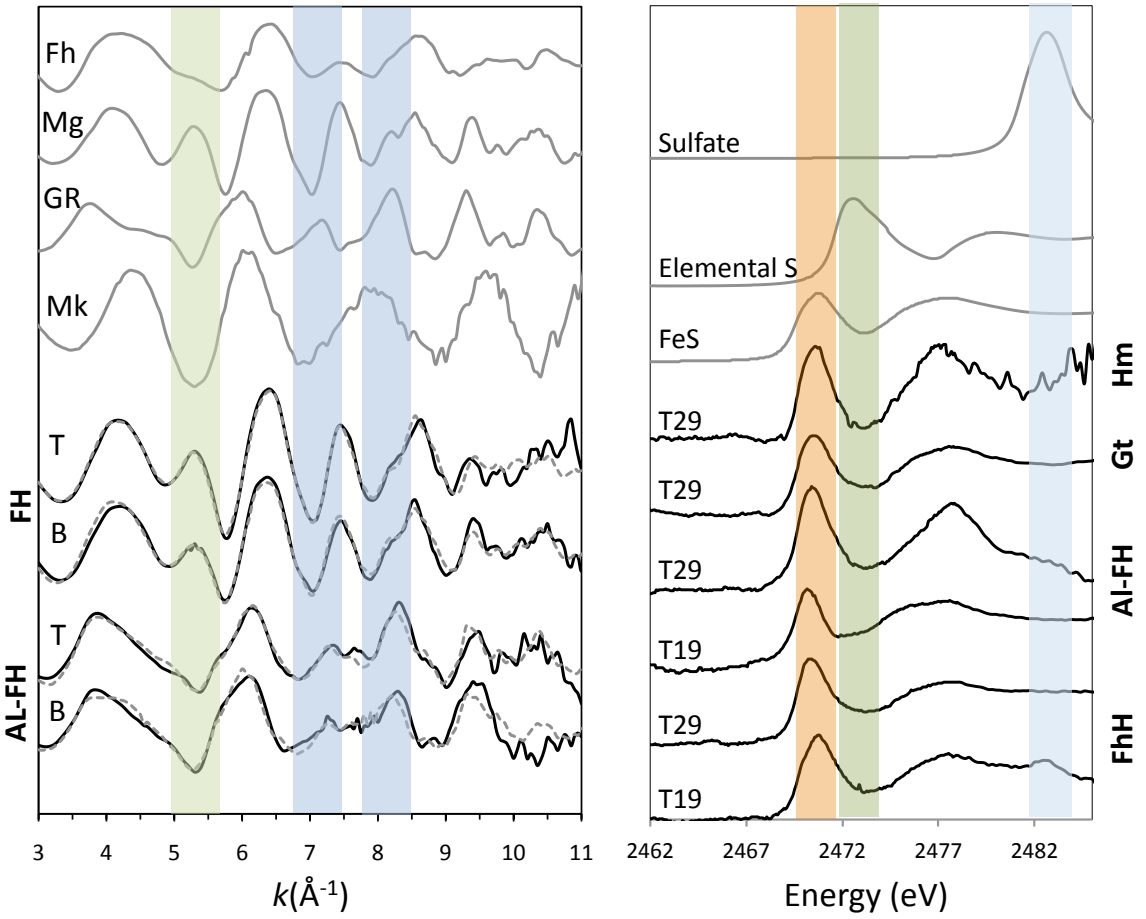

Figure 3.4. (left) k^3-weighted Fe-EXAFS spectra (solid-line) and linear combination fit (dotted line) for the solid-phase products as a function of location after 29 days in the Fh, Al-Fh columns. The green box highlights the region indicative of magnetite as seen by a shoulder at approximately 5.2 $Å^{-1}$. The blue boxed regions highlight two spectral oscillations representative of green-rust phases. (right) Sulfur XANES spectra for the solid-phase products. All spectra represent samples from the bottom half of the column (solid black line). The blue boxed region highlights the edge indicative of sulfate while the green and orange boxed regions represent edges for elemental S and FeS respectively.

Table 3.2. K-edge Fe LC-EXAFS derived relative percentages of phases formed as a function initial Fe(III) substrate and location within the column

		mole % Fe									
Initial substrate	**Section**	**Ferrihydrite**	**Goethite**	**Hematite**	**Lepidocrocite**	**Magnetite**	**Green Rust**	**FeS**	**Mackinawite**	***k* window**	**R value**
Ferrihydrite	top	29	15			56				3-11	0.127
	bottom	41				55		4		3-12	0.14
Al-ferrihydrite	top		6		13	19	62			3-11	0.814
	bottom				7	7	62		23	3-11	0.6
Goethite	top		100							3-10.5	0.04
	bottom		63			11		10	15	3-11	0.09
Hematite	top			93				7		3-10.5	0.086
	bottom			74				15	11	3-10.5	0.069

3.3.4. Fe and S Dynamics: The amount of total Fe(III) reduced (whole column) after 29 days varied both as a function of Fe oxide composition and structure. While substantial solid-phase reduction was observed for both ferrihydrite and Al-ferrihydrite, minimal reduction was observed for goethite and hematite. After 29 days, 72% of the Fe(III) provided was reduced within the Al-doped ferrihydrite columns yet only 50% was reduced within the pure ferrihydrite columns (Table 3.1). The percentage of Fe(III) reduced within the goethite and hematite columns were 15 and 13%, respectively, substantially less than that observed for the more bioavailable ferrihydrite phases.

The proportion of total Fe(II) that is eluted from the columns was minor and similar among the columns. After 29 days, aqueous Fe(II) eluted from the column accounted for 15, 8, 13 and 14% of the total Fe(II) generated within the Fh, Al-Fh, Gt, and Hm columns, respectively. The findings that a large portion of the Fe(II) was retained within the column are consistent with previous research under similar flow conditions for model microbial Fe(III)-reducing communities (Hansel et al., 2003a).

The spatial variability of solid-phase associated Fe(II) within the columns varied by Fe oxide type. After 29 days within the Fh columns, the Fe(II) distribution was nearly equivalent throughout the columns with 46 and 40% of the total Fe(II) generated retained within bottom and top portions of the column, respectively (Table 3.1). Similarly, 41 and 50% of the Fe(II) generated was retained in the solid-phase within the bottom and top portions, respectively, of the Al-Fh columns. In contrast, within the Gt and Hm columns, a substantially higher proportion of the total Fe(II) produced was retained in the bottom of the column relative to the top (Table 3.1), indicative of greater Fe(III) reduction upgradient. For Gt, 80% of the total Fe(II) produced was retained within the solids in the bottom section as compared to 6% in the top. Similarly, Fe(II)

within the hematite columns had 70% of the Fe(II) generated in the bottom portion and 16% in the top.

A small fraction of the sulfate introduced was eluted from the column and sulfate was not detected within the solid-phase (Table 3.1). Thus, the difference between the amount of sulfate introduced to the column and that eluted represents the fraction of sulfate reduction. The majority (82-88%) of the sulfate introduced to the columns was reduced after 29 days, regardless of Fe oxide type. Further, with the exception of the control (no Fe) column, the majority (95-99%) of the sulfide generated was retained within the solid-phase and not eluted from the columns. Of this solid-phase associated sulfide within the column, the majority (91-98%) of the sulfide was retained within the bottom section of the columns.

3.3.5 Microbial Community Analysis

3.3.5.1. Microbial Abundance: Quantitative PCR was used to quantify the number of bacterial 16S rRNA gene copies for all samples (Table 3.3), which is a proxy for bacterial abundance. Conversion of bacterial 16S rRNA gene copy to bacterial colony forming units (CFU) per gram of sediment revealed significant variability in bacterial abundance among the different samples. Fresh sediment collected from Ashumet Pond contained 5.6×10^8 CFU/g. After incubation within the glovebox to deplete electron acceptors within the natural sediment prior to inoculation of the columns, the bacterial abundance had decreased to 2.3×10^6 CFU/g. Within the Fe amended columns, bacterial abundance increased within the bottom sections but decreased in top sections compared to the initial inoculum (Table 3.3). After 19 days, the abundance of bacteria within the top sections was 1-3 orders of magnitude lower than that observed for the bottom sections for all columns (Figure 3.5). Indeed, while the average CFU/g was 2.2×10^8 (Fh and

Al-Fh grouped as labile) and 1.8 x 10^7 (Gt and Hm grouped as recalcitrant) in the bottom sections, an average CFU/g of only 2.4 x 10^5 (labile) and 2.9 x 10^6 (recalcitrant) was observed in the top of the column. Statistical testing showed a significant difference ($p < 0.05$) between both the top sections when compared to the bottom (Figure 3.5).

Table 3.3. Bacterial diversity and abundance via q-PCR(molecular CFU/g) of 20 samples plus sediment.

					Alpha Diversity					
					Estimates of Richness			Eveness	Diversity	
Sample Name	Timepoint	# of original Sequences	Normalized # of Counts	molecular CFU/g	S_{obs} (sequences)	Chao1	ACE	Gini coefficient (lorenz curve)	Shannon (Sequences)	Simpson (1-D)
Cont top	T-19	6347	609	2.06E+07	18	23	24	0.757	1.65	0.66
Cont bot	T-19	6290	609	1.32E+06	27	35	42	0.831	1.59	0.62
Al-f top	T-19	609	609	2.59E+03	31	42	44	0.776	2.14	0.80
Al-f bot	T-19	8760	609	1.92E+07	24	27	30	0.774	1.95	0.79
ferr top	T-19	3298	609	4.19E+05	28	37	37	0.665	2.52	0.89
ferr bot	T-19	8160	609	6.72E+08	20	29	35	0.810	1.58	0.70
Goe top	T-19	9311	609	2.23E+05	17	26	35	0.813	1.40	0.66
Goe bot	T-19	8912	609	5.72E+07	19	33	33	0.824	1.43	0.65
Hem top	T-19	3387	609	1.40E+05	32	43	47	0.809	1.84	0.66
Hem bot	T-19	4172	609	3.27E+06	21	30	42	0.801	1.69	0.72
Cont top	T-29	4918	609	2.14E+06	21	24	24	0.772	1.81	0.75
Cont bot	T-29	6262	609	3.72E+08	22	36	34	0.748	1.96	0.78
Al-f top	T-29	1868	609	5.40E+04	29	47	39	0.707	2.43	0.88
Al-f bot	T-29	3107	609	1.77E+08	27	45	44	0.761	2.14	0.83
ferr top	T-29	6236	609	4.73E+05	21	23	25	0.648	2.29	0.86
ferr bot	T-29	6892	609	2.01E+07	26	31	32	0.734	2.21	0.85
Goe top	T-29	7198	609	1.12E+07	20	28	26	0.734	1.94	0.81
Goe bot	T-29	3031	609	6.98E+06	24	33	39	0.773	1.97	0.80
Hem top	T-29	6103	609	6.20E+04	22	45	53	0.760	1.89	0.76
Hem bot	T-29	6980	609	3.69E+06	19	24	22	0.759	1.78	0.75
SediFresh	T-29	2984	609	5.62E+08	112	167	159	0.646	3.76	0.94
SedT0	T-29	4715	609	2.30E+06	88	121	126	0.736	2.72	0.75

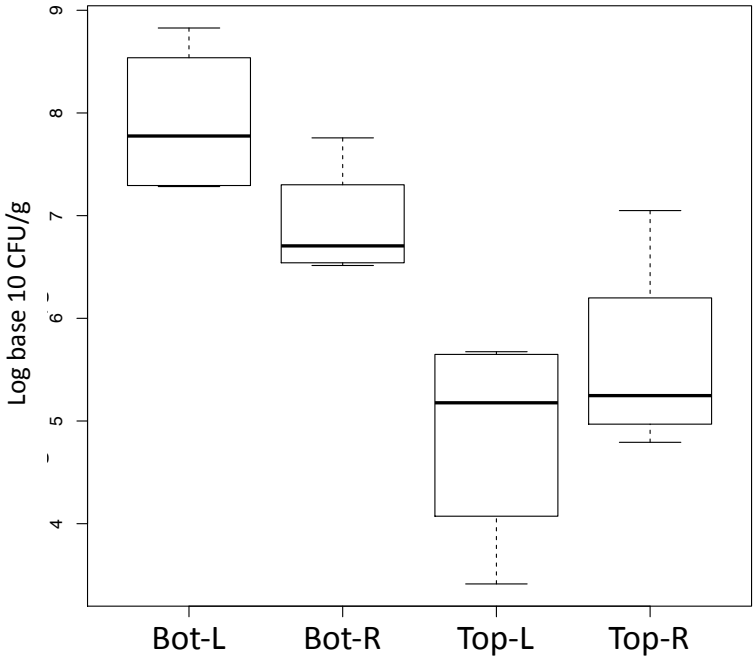

Figure 3.5. Box-plot for quantitative-PCR represented as Log_{10} colony forming units per gram (CFU/g) of sand. X-axis labels correspond to the following: Bot-Bottom half of column, Top-Top half of column, L-Labile phases (ferrihydrite and Al-Ferrihydrite), and R-Recalcitrant phases (Goethite and Hematite).

3.3.5.2 Microbial Composition: After binning of taxa at the genus level, clear trends in the microbial communities were observed. Within the Fe samples (controls and sediment removed) 9744 sequences revealed 76 different taxa at the genus level. Of these sequences, only 12 taxa (*Desulfosporomusa*, *Desulfovibrio*, *Clostridium*, *Streptosporangium*, *Lentzea*, *Sulfurospirillum*, *Acetobacterium*, *Anaerospora*, *Streptomyces*, *Geobacter*, *Atobium*, *Treponema*) accounted for greater then 1% of the total counts. In addition, all but 2 (*Atobium*, *Treponema*) of the 12 taxa accounted for at least 10% of the counts within a single sample (i.e., at least 61 counts in one of the 16 samples).

For 8 taxa (*Desulfosporomusa*, *Desulfovibrio*, *Clostridium*, *Lentzea*, *Sulfurospirillum*, *Acetobacterium*, *Streptomyces*, *Geobacter*), spatial, temporal and Fe oxide variability was

observed (Figure 3.6). These 8 taxa represent different functional guilds, including those involved in sulfate and sulfur reduction (*Desulfosporomusa*, *Desulfovibrio*, *Sulfurospirillum*), Fe(III) respiration (*Geobacter*), and fermentation or carbon oxidation (*Clostridium*, *Lentzea*, *Acetobacterium*, *Streptomyces*). The relative percentages of these 8 taxa vary as function of Fe(III) oxide, location in the column (top versus bottom) and over time (19 versus 29 days).

Within the ferrihydrite columns, all 8 taxa are observed in the top of the columns, with the abundance of *Acetobacterium* and *Sulfospirillum* increasing relative to the other taxa over time (Figure 3.6). Within the bottom half of the ferrihydrite column, however, the community is initially dominated by *Desulfovibrio* and *Desulfosporomusa*, whose relative abundance relative to the other taxa decreases over time. Similar trends are observed for the Al-doped ferrihydrite columns, but with differences in the relative percentages of each taxa.

The goethite and hematite columns appear distinctly different than the two ferrihydrite columns, particularly in the earlier time point (19 d) (Figure 3.6). At 19 days, both the Gt and Hm columns are dominated by *Desulfovibrio* and *Desulfosporomusa* throughout the length of the column. The relative percentages of these two taxa decrease over time, coincident with a substantial increase in *Clostridia* sp. After 29 days, the top and bottom of the Gt and Hm columns still support similar microbial compositions. Of particular interest is the lack of the Fe(III) respiring organism *Geobacter* within either the Gt or Hm column at either point in time or space.

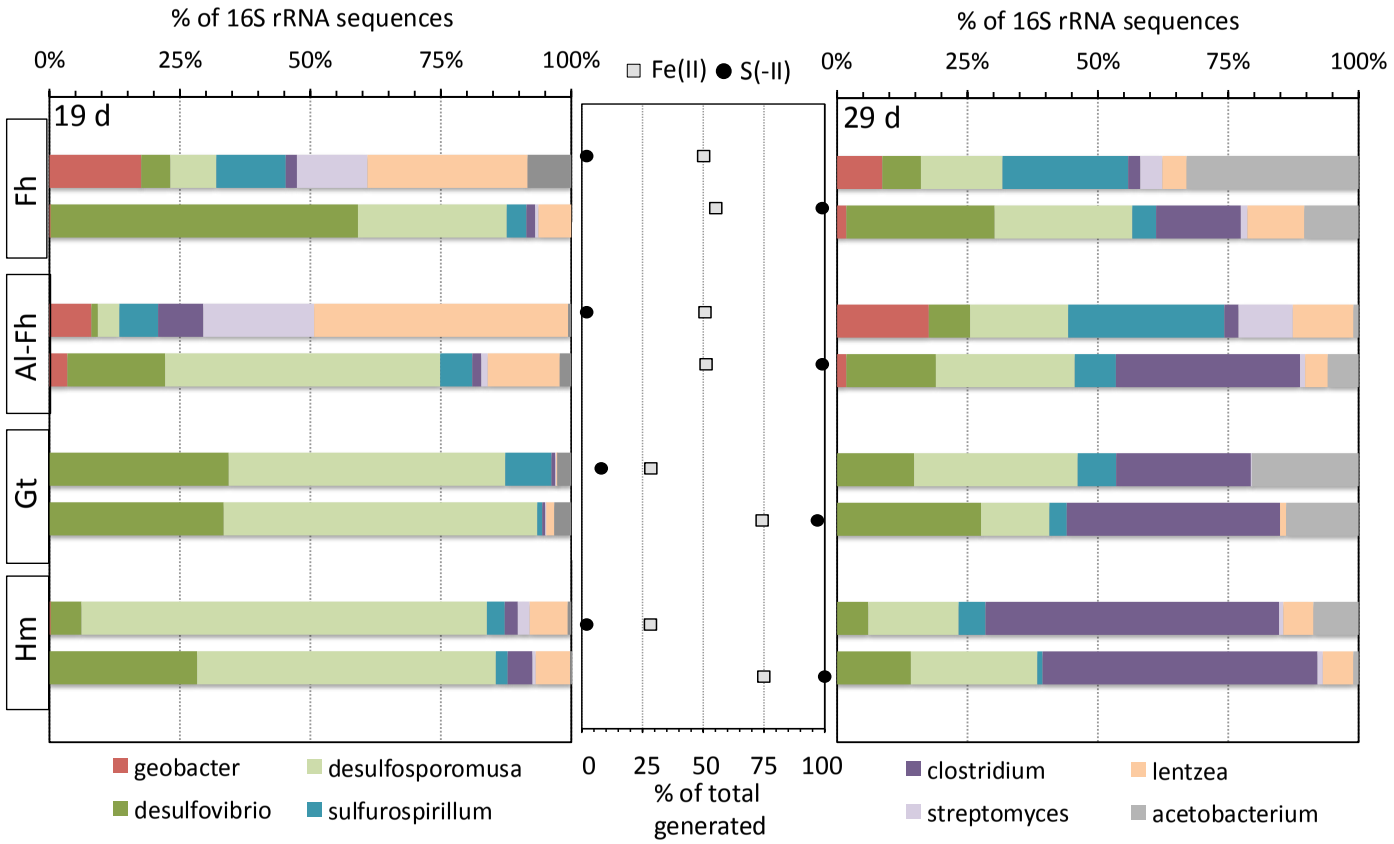

Figure 3.6. Bar graphs depicting the relative abundance of the 8 dominant taxa within the columns after 19 (left) and 29 days of reaction (right). The bars for each mineral are positioned to illustrate the top and bottom of each column. The middle panel shows the percentage of total Fe(II) and sulfide generated that is retained within the top and bottom of the columns.

3.3.5.3 Statistical Variation in Microbial Composition: Given the geochemical results, samples fit into one of four possible patterns based of the availability of the Fe oxide (labile vs. recalcitrant) and spatial distribution in the column (top vs bottom) resulting in 4 factors (labile-top, labile-bottom, recalcitrant-top and recalcitrant-bottom). The more bioavailable Fe oxides, Fh and Al-Fh, are grouped together as labile forms and the less bioavailable forms, Gt and Hm, are grouped together as recalcitrant. To test the influence of these 4 factors on the abundance of taxa, non-parametric (ranked sum) multiple comparison tests were performed. Of the 10 taxa, 4 taxa (*Clostridium, Lentzea, Acetobacterium, Anaerospora*) showed no significant difference ($p < 0.05$) between any of the pairwise comparisons. For the 6 remaining taxa, boxplots of taxa abundance vs. factors were generated to visually compare pairwise difference (Figure 3.7). Both the availability of the Fe oxide and the distribution within the column clearly played a role in selecting for *Geobacter* abundance, therefore, the labile-top samples contained 88% of the *Geobacter* counts and were statistically different from all other factors. In addition, further pairwise comparisons revealed that the *Geobacter* abundance in the labile-bottom samples (12% of the sequences) were statistically different from both the recalcitrant-top (<1 % of the sequences) and the recalcitrant-bottom (0% of the sequences) factors. *Streptomyces* abundance showed similar trends, with labile-top samples (84% of the taxa sequences) being most abundant and statistically different ($p < 0.05$) from the other three factors.

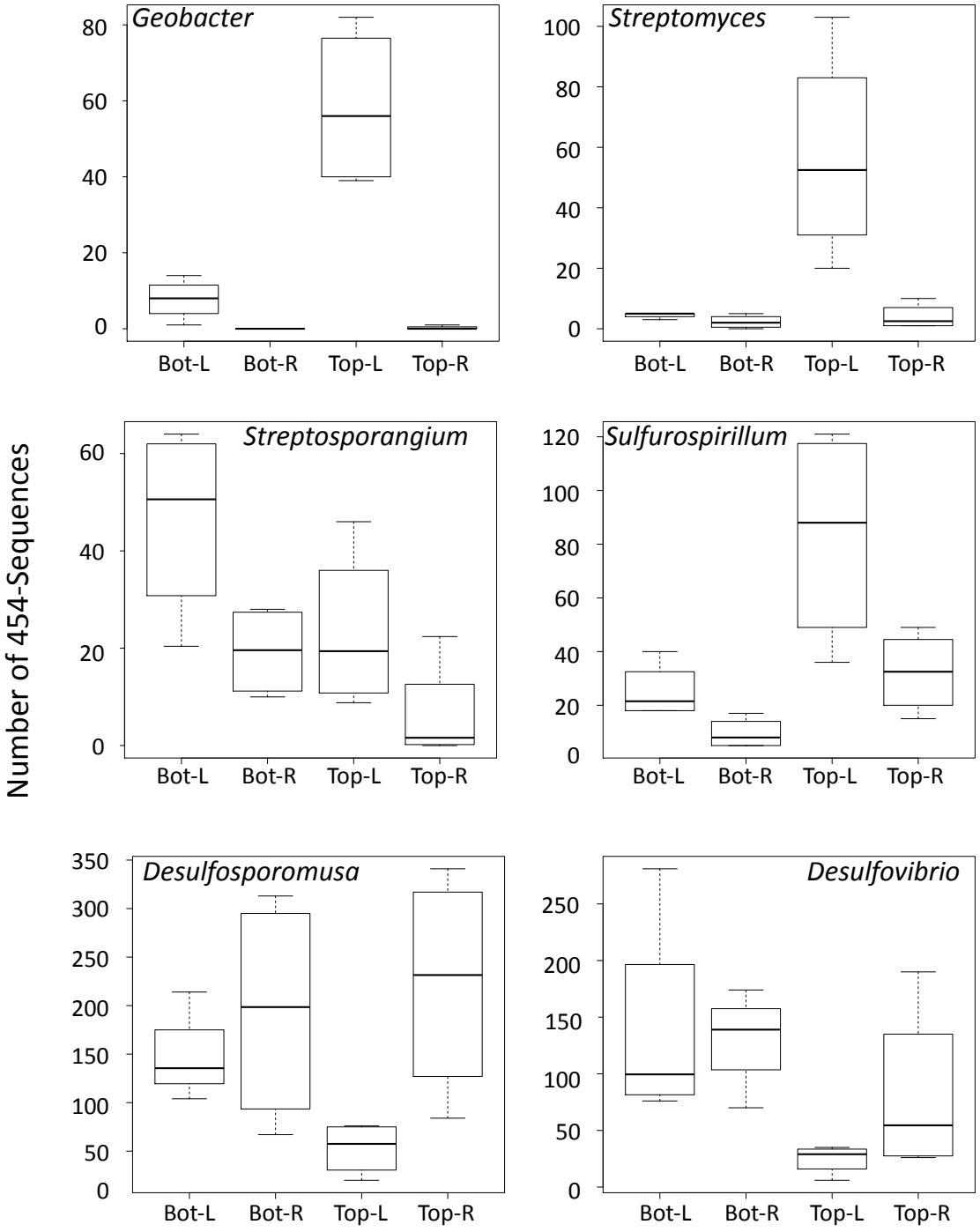

Figure 3.7. Box-plots of the number of 454-sequences for six different taxa as a function of Fe mineralogy and location within the columns. Look to main text for information regarding statistical comparisons of the factors for the different taxa. X-axis labels correspond to the following: Bot-Bottom half of column, Top-Top half of column, L-Labile phases (ferrihydrite and Al-Ferrihydrite), and R-Recalcitrant phases (Goethite and Hematite).

Further, the known elemental sulfur reducer *Sulfurospirillum* showed statistically different abundance between the labile-top samples (55% of sequences) and the bottoms for both the labile (17 % of sequences) and recalcitrant (6% of sequences) Fe phases (Figure 3.7). However, the difference between the top factors (recalcitrant–top 22% of sequences) was not significant, suggesting that the spatial distribution was the most important factor selecting for the abundance of this taxa. *Desulfovibrio* also showed significant differences between the labile-top and both bottom factors, however the differences resulted from the greater abundance in the bottom samples (37% and 35%) as compared to the labile-top (7%). Similarly to *Desulfovibrio*, the abundance of *Desulfosporomusa* showed a significant difference between the labile-top (9% of sequences) vs. labile-bottom samples (24% of sequences).

3.3.5.4. Correlation between most abundant taxa: Correlating the ranked relative abundance of different taxa within samples, especially to model DIRM *Geobacter* and/or SRB *Desulfovibrio* revealed possible similarities in metabolic functionality and/or unknown syntrophy among these diverse taxa. Thus, significant correlations (using Spearman's rho) were discovered in 11 taxa pairs (Figure 3.8). Interestingly, *Geobacter*, showed a significant ($p < 0.05$) positive correlation with 3 taxa (*Streptomyces, Lentzea,* and *Sulfurospirillum*) and a significant ($p < 0.05$) negative correlation with 2 taxa, both of which are known to sulfate reducers (*Desulfovibrio* and *Desulfosporomusa*). The widespread and well-characterized sulfate-reducing bacterium *Desulfovibrio* showed significant ($p < 0.05$) negative correlations with assumed Fe(III)-reducing organisms (*Geobacter, Lentzea, Streptomyces*) while having a positive correlation with a *Firmicutes* genus know to reduce sulfate, *Desulfosporomusa* ($p = 0.07$).

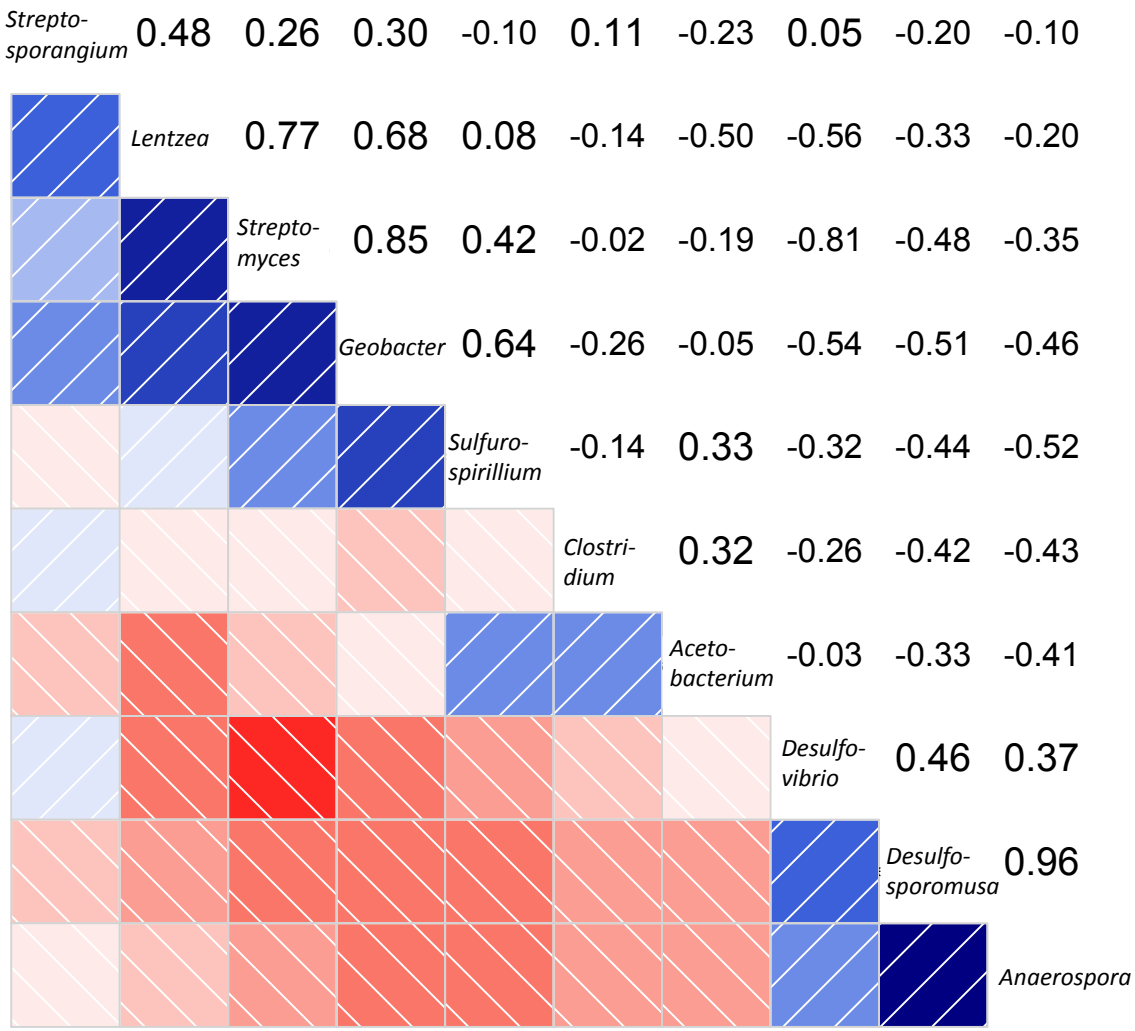

Figure 3.8. Correlogram of the Spearman rank correlation of the ten most abundant taxa. The bottom left half of the figure is a graphical representation of correlation with dark red meaning strong negative correlation and dark blue meaning strong positive correlation. Values in the top right half are Spearman rank correlation values; using test for association, the values were deemed significant ($P < 0.05$) if they were greater than 0.48 and less than -0.48.

3.3.6. Microbial Diversity: In addition to comparing the abundance of known taxa, many important indices are used in the analysis of microbial communities as a whole and result from the concept of bacterial α and β diversity. The α- diversity represents the within sample diversity and is a function of species richness (number of organism) and evenness (whether one organism

dominates) which can be calculated with commonly used indices (Chao1, ACE, Shannon, Gini coefficient). The other measure, β diversity, is often referred to as "between sample diversity" and numerous indices can be used to compare the community composition between samples. The focus of most of this research will be on β diversity, however, α- diversity is quickly addressed and its importance should not be undervalued.

3.3.6.1 Alpha Diversity: The within sample diversity was calculated using a number of different diversity indices that are summarized in Table 3.3. Both Chao1 and ACE indices are used to estimate "true" richness. Using these richness indices revealed no significant differences among the variables except when the original sediment samples were included. As would be expected, the addition of the original environmental sediments to columns containing well-defined media resulted in a loss in overall diversity.

As a measure of evenness within the columns, a Lorenz curve was plotted and the Gini coefficient calculated. When comparing all samples, excluding the original sediment, the Gini coefficient showed a significant difference ($p < 0.05$) when the time points were compared; T19 ($\mu=0.715$ $\sigma=0.085$) versus T-29 ($\mu=0.806$ $\sigma=0.047$). In addition, the diversity indices (Shannon and Simpson), which take into account both richness and evenness, also showed significant differences based on the time sampled. Interestingly, while alpha diversity, wasn't significantly impacted by Fe mineralogy, columns that ran for longer resulted in sediment communities that were more even.

3.3.6.2 Beta Diversity: To measure the between sample diversity of the 16 Fe oxide samples, the Bray-Curtis dissimilarity index was used. Hierarchical clustering using the Unweighted Pair

Group Method with Arithmetic Mean (UPGMA) algorithm revealed a dendrogram with distinct groups that represented the original dissimilarity matrix well (cophenetic correlation coefficient = 0.82) (Figure 3.9). The dendrogram revealed the clustering of two distinct groups below a cophenetic distance (CD) = 0.66. These two groups could be categorized by whether they were sampled from the top portion of the labile Fe phases Fhy and Al-Fhy (CD = 0.50; red grouping) or not (CD = 0.53; blue and grey groupings). Comparisons of the heat map of the 10 most abundant taxa (below the dendrogram) showed that the top sediments from the labile Fh and Al-Fh columns were enriched in *Lentzea* (average 18% of the sequences for samples within this group), *Sulfuospurillum* (average 14%), *Geobacter* (average 10%) and *Steptomyces* (average 9%). This finding is in good agreement with the analysis of taxa abundance, which statistically showed that many of these organisms preferentially grew in this mineralogical niche.

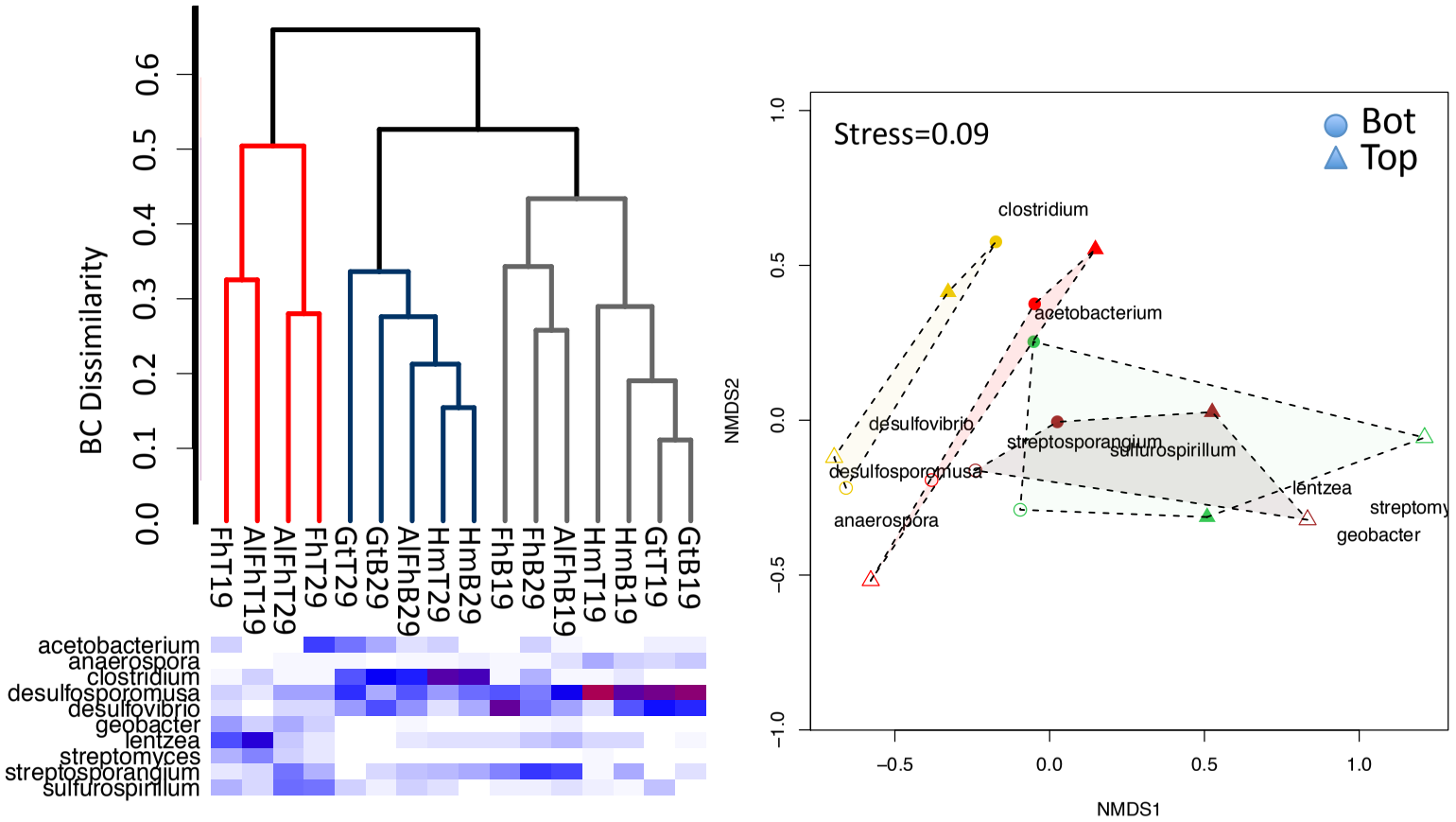

Figure 3.9. (Left) Average agglomerative (UPGMA) clustering based on Bray-Curtis dissimilarity using bacterial 454 sequences. Below clustering is a heatmap showing the relative abundance of of the 10 most abundant taxa in these samples. Name structure is a follows: Fe type (Fh, AlFh, Gt, Hm) followed by T or B (Top or Bottom half of column) and lastly 19 or 29 (sampled at 19 or 29 days). Red cluster on far left represents a group of samples that were located in the top have of a labile Fe columns. The blue cluster is a cluster with mostly representatives from the T29 time point, while the grey cluster represents mostly samples from the T19 sampling point. (Right): Non-Metric Multidimensional Scaling (NMDS) of 16 samples. Sample symbols are Circle = Bottom, Triangle = Top, Empty Symbol = T19, Filled Symbol = T29, Colors = Fe oxide type, Brown= Ferrihydrite, Green = Al-Ferrihydrite, Yellow = Goethite, and Red = Hematite. Convex hulls are drawn around the samples based on Fe oxide type to better display the role that Fe plays in shaping the bacterial communities. The weighted average scores of the 10 most abundant taxa were used to calculate the ordination configuration of taxa of interest.

The larger, 12-sample cluster was further broken down into two clusters (CD = 0.35 blue and CD = 0.44 grey groupings) based on the time point in which the samples were taken (T-19 versus T-29). Relative averages of these taxa within samples reveals that *Desulfosporomusa* (average 39% in grey cluster) and *Desulfovirio* (average 23% in grey cluster) were dominant members of samples within the grey cluster while *Clostridium* sequences averaged 35% in samples within the blue grouping. Further, the grey cluster yields evidence that Fe mineralogy may also play a role in shaping the bottom communities with the poorly crystalline Fe phases Fh and Al-Fh being more similar to each other (CD = 0.34) then they are to the recalcitrant Fe phase (Gt and Hm) cluster (CD = 0.34).

To further elucidate how microbial communities are affected by the complex interactions between Fe oxide type, spatial distribution and time point, non-metric multi-dimensional scaling (nMDS) of the communities at the genus level was performed (Figure 3.9). To more clearly understand the role of Fe oxide in shaping the microbial communities, convex hulls were placed around the samples based on which Fe oxide column they were sampled from. While nMDS is not an eigenvector method, and it therefore is not trying to explain variance (only trying to replicate distance in 2 dimensions), these groupings suggest that the first axis of the nMDS plot is separating out the samples based on Fe oxide type, with no overlap between the hulls of the recalcitrant iron and the labile phases.

Further, statistical testing using permutations of environmental variables revealed a significant difference when samples were grouped in one of the four factors from above (labile-top, labile-bot, recal-top, recal-bot). Trends along the first axis were further confirmed by plotting the first nMDS axis vs. Fe oxide type/top or bottom, confirming that the first axis showed a significant difference in the grouping of the poorly crystalline top phases versus all

other samples (Figure 3.10). Interestingly, Al substitution in ferrihydrite did not have a significant effect on the microbial community, as can be seen in the amount of hull overlap. The large horizontal distribution of the poorly crystalline hulls suggests that the first MDS axis additionally separated the poorly crystalline samples based on location within the columns, bottom vs. top (circles and triangles respectively), with the bottom samples closer in oridination space to the more recalcitrant Fe phases. The second axis in the nMDS plot explains a large amount of the community variation based on time point, with the T-19 (open symbols) being projected below the T-29 (closed symbols) samples. Interestingly, the vertical distribution of the samples is greater for the recalcitrant iron phases suggesting that sampling times might have had a larger impact on these samples.

Scores for the 10 most abundant taxa were then calculated using weighted averages of site scores and added to the nMDS plot (Figure 3.9). This analysis confirmed many of trends discussed above. *Geobacter*, *Streptomyces*, and *Lentzea* plotted close to the labile top phases, while the known sulfate reducers (*Desulfovibrio* and *Desulfosporomusa*) were closest to the bottom half recalcitrant samples.

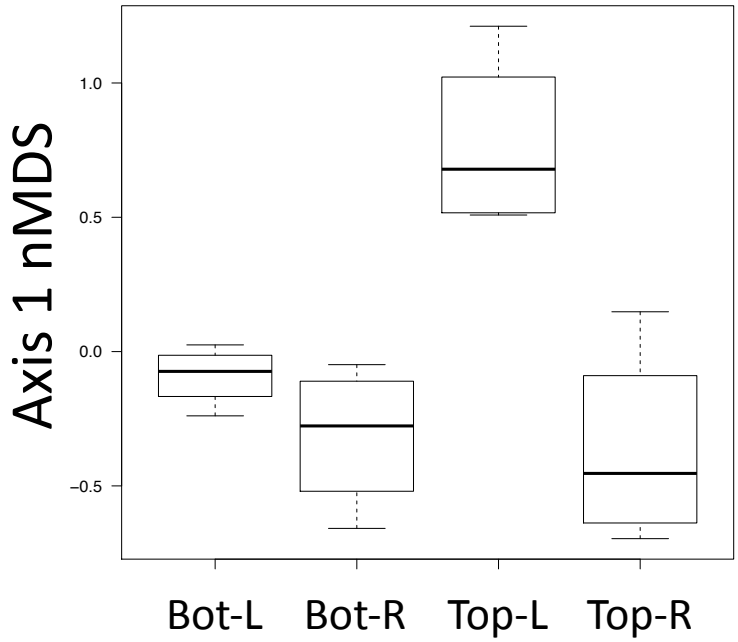

Figure 3.10. Box plot showing the scores of the 1st NMDS axis versus four different factors: Bot - Bottom half of coulumn, Top – Top half of column, L – Labile iron forms (Ferrihydrite and Al-Ferrihydrite), R- Recalcitrant Fe forms (Goethite and Hematite).

3.4. Discussion

The amount and rates of Fe(III) reduction by sediment microbial communities varies widely with the structure and composition of Fe(III) oxides. Here we show that the initial Fe oxide substrate provided is a key variable dictating Fe(III) reduction, the mechanisms of reduction, the subsequent secondary mineral phases, extent of carbon oxidation, and structure of the microbial communities. Fe(III) reduction was also spatially variable within each column reflecting geochemical controls on the establishment of microbial communities and subsequent respiratory processes. These results as discussed below indeed highlight the importance of mineral-based niche differentiation within metal- and sulfate-respiring microbial communities.

Under these conditions, reduction of the more crystalline, hence recalcitrant, phases goethite and hematite is driven by sulfate reduction rather than Fe(III) respiration by sediment microbial populations. In fact, known Fe(III)-respiring microbes (e.g., *Geobacter* sp.) were not detected within the goethite or hematite columns, although they are present within the ferrihydrite columns (Fig 6 and 7). Instead, solid-phase Fe(II) concentrations correlated with the widespread abundance of sulfate-reducing bacteria, *Desulfosporomusa* and *Desulfovibrio*. Previous isolates of both these organisms have demonstrated the ability to directly reduce poorly crystalline Fe(III) phases (Coleman et al., 1993;Sass et al., 2004;Park et al., 2008). However, here the majority of the Fe(II) generated was retained within the bottom half of the columns and correlated with solid-phase sulfide, identified as a poorly crystalline FeS phase. Indeed, the sulfide levels within the bottom of the goethite and hematite columns could account for nearly 60% of the Fe(II) within the solid-phase (Table 3.1), indicating that sulfate reduction was a primary pathway for Fe(III) reduction. The abundance of SRB, even at μM amounts of sulfate within the columns is in good agreement with previous batch experiments in which communities enriched in the presence of more recalcitrant Fe(III) oxides and low sulfate were dominated by *Desulfovibrio* when lactate was the carbon source (Lentini et al., 2012).

Given the lack of lactate and sulfate elution from the columns, we predict that both are consumed by the SRB within the bottom half of the column coinciding with high sulfide concentrations and relative SRB abundance. The increased concentration of solid-associated Fe(II) within the bottom half of the columns is indicative of higher Fe(III) reduction within these sections of the column. Further, lower Fe(II) levels, bacterial abundances, and proportions of SRB upgradient indicate that minimal Fe(III) reduction was supported in the top of the column. If reduction rates were uniform within the column, then flow induced gradients of Fe(II) would

lead to steadily increasing Fe(II) concentrations downgradient as observed previously (Hansel et al., 2003a;Hansel et al., 2004). Thus, even though high levels of acetate are flowing through and out of the column, Fe(III) reduction coupled to acetate oxidation, as in Fe(III) respiration, is not observed. While respiration of poorly crystalline Fe phases such as ferrihydrite has been continually demonstrated, Fe(III)-respiring organisms such as *Geobacter* sp. can only sparingly couple the oxidation of acetate (the most commonly used organic carbon source for this genus) to the reduction of more recalcitrant Fe phases (Hori et al., 2010;Lentini et al., 2012). In fact, thermodynamic predictions suggest that under natural environmental conditions, the free energy gained from acetate oxidation coupled to goethite or hematite reduction is not sufficient to support Fe(III) respiration (Postma and Jakobsen, 1996;Lentini et al., 2012). Consequently, these redox couples are not likely support microbial growth and instead the reduction of more crystalline Fe(III) phases will be a consequence of the activity of organisms that produce exogeneous redox active metabolites capable of reducing Fe(III), such as sulfide.

In fact, model Fe(III)-respiring organisms were exclusively enriched within the pure and Al-substituted ferrihydrite columns as evidenced by greater than 99% of the *Geobacter* counts (n=265) associated with these poorly crystalline Fe phases. Fe(II) profiles were relatively uniform through the ferrihydrite and Al-ferrihydrite columns indicating that Fe(III) reduction occurred throughout the column. The Fe(III)-reducing organism *Geobacter* sp. is often a dominant member of microbial populations hosted within Fe(III)-reducing conditions, particularly when acetate is available as electron donor (Holmes et al., 2007;Hori et al., 2010;Lentini et al., 2012). Thus, the presence of *Geobacter* sp. within the ferrihydrite and Al-ferrihydrite columns points to microbial respiration as an operative Fe(III) reduction pathway.

Furthermore, the ranked relative abundance of *Geobacter* to other abundant taxa within column samples pointed to other potential Fe(III)-reducing organisms. In particular, a statistically relevant correlation between *Geobacter* and two taxa within the *Actinobacteria* phylum (*Streptomyces* and *Lentzea*) was observed. Interestingly, neither of these taxa have previously been isolated as Fe(III)-reducing microorganisms yet members of both genera are known to produce antibiotics and siderophores (Imbert et al., 1995;Barona-Gomez et al., 2006), which have demonstrated roles in Fe cycling (Hernandez et al., 2004). While their role in either carbon oxidation or Fe(III) reduction within these columns is unknown at this time, their strong correlation with *Geobacter* and yet higher relative abundance suggest they are important in either the direct or indirect reduction of the more labile Fe substrate ferrihydrite. Hierarchical clustering and nMDS ordination further confirmed these trends with the microbial communities in the poorly crystalline Fe phases belonging to their own hierarchical cluster and grouping distinctly on the right side of the nMDS plot (green and brown triangles).

Surprisingly, however, sulfate reduction is also a primary pathway for ferrihydrite reduction even in the presence of acetate and a resident Fe(III)-respiring community. Within the bottom half (upgradient) of the ferrihydrite columns, the high concentration of sulfide, presence of FeS and high relative abundance of known sulfate-reducing bacteria (*Desulfovibrio* and *Desulfosporomusa* sp.) point to sulfate reduction happening concurrently or in the absence of Fe(III) reduction. Similar to the goethite and hematite columns, sulfate and lactate appear to be consumed in the lower half of the columns resulting in a large acetate plume that travels upgradient and is eluted from the column. Suppression of SRB activity in the absence of sulfate and lactate at top of column allows for proliferation of Fe(III)-respiring bacteria as discussed above. This geochemical observation was supported by a strong negative correlation between the

known SRB (*Desulfovibrio* and *Desulfosouromusa*) and DIRB (*Geobacter, Lentzea*, and *Streptomyces*), suggesting some sort of competitive interaction between these organisms and subsequent spatial segregation along the flow path.

Typically, when considering competition between sulfate and Fe(III)-reducing bacteria, the free energy yield for the respiration reactions is used to predict the more viable electron acceptor in both pure and mixed communities (Canfield et al., 2005). Based on energy yield alone, the preferential activity of Fe(III)- to sulfate-respiring organisms is expected under most conditions and therefore used to explain the frequent observation of a succession of terminal electron accepting processes (TEAP) within natural systems. However, given the large range in reduction potentials for Fe(III) oxides (Hansel and Lentini, 2011), a partial equilibrium model approach under conditions of carbon substrate competition predict that the preferred electron acceptor will in fact be a function of the Fe oxide present (Postma and Jakobsen, 1996;Jakobsen and Postma, 1999). This model has been employed previously to explain the (co-)occurrence of sulfate reduction in the presence of recalcitrant Fe phases within the environment (Postma and Jakobsen, 1996). Given, however, that the oxidation of acetate coupled to ferrihydrite yields ample energy to support Fe(III) respiration, thermodynamic predictions alone would not predict the flow of electrons to a terminal electron acceptor of lower energy (i.e., sulfate over ferrihydrite) as observed here. Further, we see here in the ferrihydrite columns the enrichment of SRBs within the upgradient portion of the columns seemingly at the expense of DIRMs (which showed significant enrichment downgradient). Further, the presence of both carbon substrates needed for sulfate and Fe(III) respiration preclude the use of a competitive model to explain microbial activity. Thus, within the ferrihydrite other factors are operative to allow for the proliferation of sulfate reduction at the expense of Fe(III) respiration.

We predict that the kinetics of microbial respiration and reaction of secondary metabolites with the ferrihydrite surface are playing a role in establishing the observed Fe-S dynamics. Since carbon (especially acetate) is not lacking within the upgradient section of the column, Fe(III)-respiring organisms are not electron donor limited but may in fact have difficulty in accessing the oxide electron acceptor. It is likely that sulfate reduction is kinetically faster, leading to the production of sulfide, which reacts abiotically with the ferrihdyrite surface producing ferrous Fe. Here we observe the accumulation of iron sulfides within the bottom of the ferrihydrite columns. As observed previously (Kocar et al., 2010), these FeS secondary phases will heterogeneously precipitate on the ferrihydrite surface leading to passivation of the ferrihydrite by Fe(II)-bearing phases that can no longer support the growth of Fe(III)-reducing bacteria. This scenario is similar to that observed for magnetite passivation of ferrihydrite and subsequent cessation of microbial activity under strictly Fe(III)-reducing conditions (Hansel et al., 2004).

While it is clear that SRB played a key role in the reduction of the various Fe(III) phases here, the question still remains as to how much how much Fe(II) could have been generated from sulfide under these lower sulfate (200 μM) conditions? If, all of the sulfate that was converted to sulfide reacted with Fe(III) approximately 258 umoles of Fe(II) could have been generated as a result of sulfide oxidation after 19 days of reaction. While this amount of Fe(II) is in good agreement with the amount of Fe(II) generated within the goethite and hematite columns as discussed above, it would not predict the much higher amount of Fe(II) in the bottom half of the ferrihydrite columns (up to 767 umoles of Fe(II)). In addition, the above assumes that all the available sulfide reacts with an Fe(III), yet given the amount of FeS minerals observed a large portion of the free HS^- was trapped as FeS before reacting with Fe(III). Therefore given the

scarcity of known DIRMs within the bottom half of the columns, either SRBs are directly reducing Fe(III) or that a so-called "cryptic sulfur cycle" accounts for the larger than expected values of Fe(II). For the latter, intermediate sulfur products would be re-oxidized back to sulfate to fuel further sulfate reduction.

A proliferation of organisms within the genus *Sulfurospirillum* (6.2% of all sequences) in all of the Fe oxide columns points to the presence of an oxidative sulfur cycle. This genus is known to couple the oxidation of lactate and/or H_2 to the reduction of elemental S. Interestingly, no isolates from this genus are known to reduce sulfate but instead reduce the intermediate sulfur species elemental S and thiosulfate. Therefore, given that elemental S is predicted to be one of the main oxidation product of HS^- reacting with Fe(III) and the abundance of a known elemental S reducer within these columns, a catalytic sulfur cycle in which a S intermediate drives Fe(III) reduction is likely. In fact, previous research of an isolate from the same genus *Sulfurospirillum deleyianum,* has shown ferrihydrite dependent growth under low S conditions (50 μM thiosulfate) with sulfur being cycled up to 60 times.

The composition and distribution of microbial communities and Fe(III) reduction pathways were similar between the ferrihydrite and Al-bearing ferrihydrite columns (Figure 3.6 and 3.9). While Al substitution has been shown previously to inhibit both microbial reduction and abiotic secondary mineralization of ferrihydrite (Ekstrom et al., 2010;Hansel et al., 2011), here we see substantial reduction and secondary mineralization of Al-bearing ferrihydrite, even more so than pure ferrihydrite. Interestingly, however, the secondary minerals formed upon reduction of Al-bearing ferrihydrite are substantially different than pure ferrihydrite with the proliferation of the highly reactive mixed valence Fe oxide, green rust. Considering that within natural soils and sediments, ferrihydrite contains an abundance of foreign ions and impurities,

including Al, these results suggest that we may be dramatically underestimating the potential for green rust formation within natural systems. As green rust is a highly reactive intermediate, it is likely short-lived due to reaction with many (in)organic oxidants and reductants.

Here we show that under conditions mimicking natural freshwater environments, both Fe oxide mineralogy and flow induced substrate gradients play key roles in shaping functional microbial communities and subsequent Fe(III) reduction pathways. It is well established that the Fe and S cycles are tightly linked within natural systems, yet the importance of S in driving the Fe cycle has typically been limited to high sulfate environments (e.g., estuaries, marine sediments). Here, using geochemical and phylogenetic evidence we show that a S driven Fe cycle is important even under conditions favorable to Fe(III) reduction representing typical freshwater conditions. Further, we show juxtapositioning of sulfate and Fe(III) respiration even in the presence of ferrihydrite. These findings are in contrast to the canonical view of a energy yield based succession of terminal electron accepting processes within natural systems, which predicts that sulfate reduction would not proceed until ferrihydrite was fully consumed. These findings, therefore, have broad implications in predicting microbially mediated electron flow to oxidized substrates which will dictate the pathways and degree of carbon mineralization and subsequent carbon sequestration within within sediments and soils. Further, given the important of Fe(III)-reducing communities and Fe(II) in the sequestration of both inorganic (e.g., hydrocarbons) and organic contaminants (e.g., uranium, chromium), these findings will have direct bearing on contaminant mitigation and remediation.

3.5. References Cited

Afkar, E., Reguera, G., Schiffer, M., and Lovley, D.R. (2005). A novel Geobacteraceae-specific outer membrane protein J (OmpJ) is essential for electron transport to Fe (III) and Mn (IV) oxides in Geobacter sulfurreducens. *Bmc Microbiology* 5**,** 11.

Barona-Gomez, F., Lautru, S., Francou, F.X., Leblond, P., Pernodet, J.L., and Challis, G.L. (2006). Multiple biosynthetic and uptake systems mediate siderophore-dependent iron acquisition in Streptomyces coelicolor A3(2) and Streptomyces ambofaciens ATCC 23877. *Microbiology-Sgm* 152**,** 3355-3366.

Benali, O., Abdelmoula, M., Refait, P., and Genin, J.M.R. (2001). Effect of orthophosphate on the oxidation products of Fe(II)-Fe(III) hydroxycarbonate: The transformation of green rust to ferrihydrite. *Geochimica Et Cosmochimica Acta* 65**,** 1715-1726.

Bonneville, S., Behrends, T., and Van Cappellen, P. (2009). Solubility and dissimilatory reduction kinetics of iron(III) oxyhydroxides: A linear free energy relationship. *Geochimica Et Cosmochimica Acta* 17**,** 5273-5282.

Brown, G.E., and Parks, G.A. (2001). Sorption of trace elements on mineral surfaces: Modern perspectives from spectroscopic studies, and comments on sorption in the marine environment. *International Geology Review* 43**,** 963-1073.

Bucking, C., Popp, F., Kerzenmacher, S., and Gescher, J. Involvement and specificity of Shewanella oneidensis outer membrane cytochromes in the reduction of soluble and solid-phase terminal electron acceptors. *Fems Microbiology Letters* 306**,** 144-151.

Canfield, D.E., Jorgensen, B.B., Fossing, H., Glud, R., Gundersen, J., Ramsing, N.B., Thamdrup, B., Hansen, J.W., Nielsen, L.P., and Hall, P.O.J. (1993). Pathways of Organic-Carbon Oxidation in 3 Continental-Margin Sediments. *Marine Geology* 113**,** 27-40.

Canfield, D.E., Kristensen, E., and Thamdrup, B. (2005). Aquatic geomicrobiology. *Adv Mar Biol* 48**,** 1-599.

Cline, J.D. (1969). SPECTROPHOTOMETRIC DETERMINATION OF HYDROGEN SULFIDE IN NATURAL WATERS. *Limnology and Oceanography* 14**,** 454-&.

Coates, J.D., Ellis, D.J., Blunt-Harris, E.L., Gaw, C.V., Roden, E.E., and Lovley, D.R. (1998). Recovery of humic-reducing bacteria from a diversity of environments. *Applied and Environmental Microbiology* 64**,** 1504-1509.

Coleman, M.L., Hedrick, D.B., Lovley, D.R., White, D.C., and Pye, K. (1993). REDUCTION OF FE(III) IN SEDIMENTS BY SULFATE-REDUCING BACTERIA. *Nature* 361**,** 436-438.

Cummings, D.E., Zimmerman, A.E., Unruh, K.R., and Spring, S. (2010). Influence of Microbially Reducible Fe(III) on the Bacterial Community Structure of Estuarine Surface Sediments. *Geomicrobiology Journal* 27**,** 292-302.

Desantis, T.Z., Hugenholtz, P., Larsen, N., Rojas, M., Brodie, E.L., Keller, K., Huber, T., Dalevi, D., Hu, P., and Andersen, G.L. (2006). Greengenes, a chimera-checked 16S rRNA gene database and workbench compatible with ARB. *Appl Environ Microbiol* 72**,** 5069-5072.

Ekstrom, E.B., Learman, D.R., Madden, A.S., and Hansel, C.M. (2010). Contrasting effects of Al substitution on microbial reduction of Fe(III) (hydr)oxides. *Geochimica Et Cosmochimica Acta* 74**,** 7086-7099.

Fendorf, S.E., and Li, G.C. (1996). Kinetics of chromate reduction by ferrous iron. *Environmental Science & Technology* 30**,** 1614-1617.

Fennessey, C.M., Jones, M.E., Taillefert, M., and Dichristina, T.J. (2010). Siderophores Are Not Involved in Fe(III) Solubilization during Anaerobic Fe(III) Respiration by Shewanella oneidensis MR-1. *Applied and Environmental Microbiology* 76**,** 2425-2432.

Ginder-Vogel, M., Criddle, C.S., and Fendorf, S. (2006). Thermodynamic constraints on the oxidation of biogenic UO2 by Fe(III) (hydr) oxides. *Environmental Science & Technology* 40**,** 3544-3550.

Gorby, Y.A., Yanina, S., Mclean, J.S., Rosso, K.M., Moyles, D., Dohnalkova, A., Beveridge, T.J., Chang, I.S., Kim, B.H., Kim, K.S., Culley, D.E., Reed, S.B., Romine, M.F., Saffarini, D.A., Hill, E.A., Shi, L., Elias, D.A., Kennedy, D.W., Pinchuk, G., Watanabe, K., Ishii, S., Logan, B., Nealson, K.H., and Fredrickson, J.K. (2006). Electrically conductive bacterial nanowires produced by Shewanella oneidensis strain MR-1 and other microorganisms. *Proceedings of the National Academy of Sciences of the United States of America* 103**,** 11358-11363.

Hansel, C.M., Benner, S.G., and Fendorf, S. (2005). Competing Fe(II)-Induced Mineralization Pathways of Ferrihydrite. *Environmental Science & Technology* 39**,** 7147-7153.

Hansel, C.M., Benner, S.G., Neiss, J., Dohnalkova, A., Kukkadapu, R.K., and Fendorf, S. (2003a). Secondary mineralization pathways induced by dissimilatory iron reduction of ferrihydrite under advective flow *Geochemica et Cosmochimica Acta* 67**,** 2992.

Hansel, C.M., Benner, S.G., Nico, P., and Fendorf, S. (2004). Structural constraints of ferric (hydr)oxides on dissimilatory iron reduction and the fate of Fe(II). *Geochemica et Cosmochimica Acta* 68**,** 3217-3229.

Hansel, C.M., Learman, D.R., Lentini, C.J., and Ekstrom, E.B. (2011). Effect of adsorbed and substituted Al on Fe(II)-induced mineralization pathways of ferrihydrite. *Geochimica Et Cosmochimica Acta* 75**,** 4653-4666.

Hansel, C.M., and Lentini, C.J. (2011). "Mineralogical Controls on Microbial Reduction of Fe(III) (Hydr)oxides," in *Microbial Metal and Metalloid Metabolism: Advances and Applications,* eds. J.F. Stolz & R.S. Oremland. (Washington, DC: ASM Press), 93-115.

Hansel, C.M., Wielinga, B.W., and Fendorf, S.R. (2003b). Structural and compositional evolution of Cr/Fe solids after indirect chromate reduction by dissimilatory iron-reducing bacteria. *Geochimica Et Cosmochimica Acta* 67**,** 401-412.

He, Q., and Sanford, R.A. (2003). Characterization of Fe(III) reduction by chlororespiring Anaeromxyobacter dehalogenans. *Applied and Environmental Microbiology* 69**,** 2712-2718.

Hernandez, M.E., Kappler, A., and Newman, D.K. (2004). Phenazines and other redox-active antibiotics promote microbial mineral reduction. *Applied and Environmental Microbiology* 70**,** 921-928.

Holmes, D.E., O'neil, R.A., Vrionis, H.A., N'guessan, L.A., Ortiz-Bernad, I., Larrahondo, M.J., Adams, L.A., Ward, J.A., Nicoll, J.S., Nevin, K.P., Chavan, M.A., Johnson, J.P., Long, P.E., and Lovley, D.R. (2007). Subsurface clade of Geobacteraceae that predominates in a diversity of Fe(III)-reducing subsurface environments. *Isme Journal* 1**,** 663-677.

Hori, T., Muller, A., Igarashi, Y., Conrad, R., and Friedrich, M.W. (2010). Identification of iron-reducing microorganisms in anoxic rice paddy soil by C-13-acetate probing. *Isme Journal* 4**,** 267-278.

Hothorn, T., Hornik, K., Van De Wie, L.M.A., and Zeileis, A. (2008). Implementing a Class of Permutation Tests: The coin Package. *Journal of Statistical Software* 28**,** 1-23.

Http://Www.R-Project.Org/ (2012). *R: A Language and Environment for Statistical Computing* [Online]. Vienna, Austria. Available: http://www.R-project.org/ [Accessed].

Imbert, M., Bechet, M., and Blondeau, R. (1995). COMPARISON OF THE MAIN SIDEROPHORES PRODUCED BY SOME SPECIES OF STREPTOMYCES. *Current Microbiology* 31**,** 129-133.

Islam, F.S., Gault, A.G., Boothman, C., Polya, D.A., Charnock, J.M., Chatterjee, D., and Lloyd, J.R. (2004). Role of metal-reducing bacteria in arsenic release from Bengal delta sediments. *Nature* 430**,** 68-71.

Jakobsen, R., and Postma, D. (1999). Redox zoning, rates of sulfate reduction and interactions with Fe-reduction and methanogenesis in a shallow sandy aquifer, Romo, Denmark. *Geochimica Et Cosmochimica Acta* 63**,** 137-151.

Jones, M.E., Fennessey, C.M., Dichristina, T.J., and Taillefert, M. (2010). Shewanella oneidensis MR-1 mutants selected for their inability to produce soluble organic-Fe(III) complexes are unable to respire Fe(III) as anaerobic electron acceptor. *Environmental Microbiology* 12**,** 938-950.

Kim, C.S., Lentini, C.J., and Waychunas, G.A. (2008). "Associations between Iron Oxyhydroxide Nanoparticle Growth and Metal Adsorption/Structural Incorporation " in *Adsorption of Metals by Geomedia II: Variables, Mechanisms, and Model Applications,* eds. M.O. Barnett & D. Kent. Elsevier Science & Technology Books), 478.

Kocar, B.D., Borch, T., and Fendorf, S. (2010). Arsenic repartitioning during biogenic sulfidization and transformation of ferrihydrite. *Geochimica Et Cosmochimica Acta* 74**,** 980-994.

Lalonde, K., Mucci, A., Ouellet, A., and Gelinas, Y. (2011). Preservation of organic matter in sediments promoted by iron. *Nature* 483**,** 198-200.

Lentini, C.J., Wankel, S.D., and Hansel, C.M. (2012). Enriched Iron(III)-Reducing Bacterial Communities are Shaped by Carbon Substrate and Iron Oxide Mineralogy. *Frontiers in Microbiology* 3**,** 404.

Li, H.J., Peng, J.J., Weber, K.A., and Zhu, Y.G. (2011). Phylogenetic diversity of Fe(III)-reducing microorganisms in rice paddy soil: enrichment cultures with different short-chain fatty acids as electron donors. *Journal of Soils and Sediments* 11**,** 1234-1242.

Liger, E., Charlet, L., and Van Cappellen, P. (1999). Surface catalysis of uranium(VI) reduction by iron(II). *Geochimica Et Cosmochimica Acta* 63**,** 2939-2955.

Lin, B., Braster, M., Roling, W.F.M., and Van Breukelen, B.M. (2007). Iron-reducing microorganisms in a landfill leachate-polluted aquifer: Complementing culture-independent information with enrichments and isolations. *Geomicrobiology Journal* 24**,** 283-294.

Lovley, D.R., Holmes, D.E., and Nevin, K.P. (2004). "Dissimilatory Fe(III) and Mn(IV) reduction," in *Advances in Microbial Physiology, Vol. 49,* ed. R.K. Poole. Academic Press), 219-286.

Lovley, D.R., and Phillips, E.J.P. (1986). AVAILABILITY OF FERRIC IRON FOR MICROBIAL REDUCTION IN BOTTOM SEDIMENTS OF THE FRESH-WATER TIDAL POTOMAC RIVER. *Applied and Environmental Microbiology* 52**,** 751-757.

Lovley, D.R., and Phillips, E.J.P. (1988). Novel Mode of Microbial Energy Metabolism: Organic Carbon Oxidation Coupled to Dissimilatory Reduction of Iron or Manganese *Applied and Environmental Microbiology* 54**,** 1472-1480.

Marsili, E., Baron, D.B., Shikhare, I.D., Coursolle, D., Gralnick, J.A., and Bond, D.R. (2008). Shewanella Secretes flavins that mediate extracellular electron transfer. *Proceedings of the National Academy of Sciences of the United States of America* 105**,** 3968-3973.

Mccobb, T.D., Leblanc, D.R., and Massey, A.J. (2009). Monitoring the Removal of Phosphate from Ground Water Discharging through a Pond-Bottom Permeable Reactive Barrier. *Ground Water Monitoring & Remediation* 29**,** 43-55.

Morse, J.W., and Arakaki, T. (1993). ADSORPTION AND COPRECIPITATION OF DIVALENT METALS WITH MACKINAWITE (FES). *Geochimica Et Cosmochimica Acta* 57**,** 3635-3640.

Nealson, K.H., Belz, A., and Mckee, B. (2002). Breathing metals as a way of life: geobiology in action. *Antonie Van Leeuwenhoek International Journal of General and Molecular Microbiology* 81**,** 215-222.

Nevin, K.P., and Lovley, D.R. (2002). Mechanisms for accessing insoluble Fe(III) oxide during dissimilatory Fe(III) reduction by Geothrix fermentans. *Appl Environ Microbiol* 68**,** 2294-2299.

Newville, M. (2001). IFEFFIT: interactive XAFS analysis and FEFF fitting. *J. Synchrotron Rad.* 8**,** 322-324.

Park, H.S., Lin, S., and Voordouw, G. (2008). Ferric iron reduction by Desulfovibrio vulgaris Hildenborough wild type and energy metabolism mutants. *Antonie Van Leeuwenhoek International Journal of General and Molecular Microbiology* 93**,** 79-85.

Pedersen, H.D., Postma, D., and Jakobsen, R. (2006). Release of arsenic associated with the reduction and transformation of iron oxides. *Geochimica Et Cosmochimica Acta* 70**,** 4116-4129.

Perret, D., Gaillard, J.-F.S., Dominik, J., and Atteia, O. (2000). The Diversity of Natural Hydrous Iron Oxides. *Environmental Science & Technology* 34**,** 3540-3546.

Phillips, E.J.P., Lovley, D.R., and Roden, E.E. (1993). Composition of Non-Microbially Reducible Fe(Iii) in Aquatic Sediments. *Applied and Environmental Microbiology* 59**,** 2727-2729.

Postma, D. (1993). THE REACTIVITY OF IRON-OXIDES IN SEDIMENTS - A KINETIC APPROACH. *Geochimica Et Cosmochimica Acta* 57**,** 5027-5034.

Postma, D., and Jakobsen, R. (1996). Redox zonation: Equilibrium constraints on the Fe(III)/SO4-reduction interface. *Geochimica Et Cosmochimica Acta* 60**,** 3169-3175.

Poulton, S.W. (2003). Sulfide oxidation and iron dissolution kinetics during the reaction of dissolved sulfide with ferrihydrite. *Chemical Geology* 202**,** 79-94.

Poulton, S.W., Krom, M., and Raiswell, R. (2004). A revised scheme for the reactivity of iron (oxyhydr)oxide minerals towards dissolved sulfide. *Geochim. Cosmochim. Acta* 68**,** 3703-3715.

Reguera, G., Mccarthy, K.D., Mehta, T., Nicoll, J.S., Tuominen, M.T., and Lovley, D.R. (2005). Extracellular electron transfer via microbial nanowires. *Nature* 435**,** 1098-1101.

Roden, E.E. (2003). Fe(III) oxide reactivity toward biological versus chemical reduction. *Environmental Science & Technology* 37**,** 1319-1324.

Roden, E.E., and Edmonds, J.W. (1997). Phosphate mobilization in iron-rich anaerobic sediments: Microbial Fe(III) oxide reduction versus iron-sulfide formation. *Archiv Fur Hydrobiologie* 139**,** 347-378.

Roden, E.E., Kappler, A., Bauer, I., Jiang, J., Paul, A., Stoesser, R., Konishi, H., and Xu, H.F. (2010). Extracellular electron transfer through microbial reduction of solid-phase humic substances. *Nature Geoscience* 3**,** 417-421.

Roling, W.F.M., Van Breukelen, B.M., Braster, M., Lin, B., and Van Verseveld, H.W. (2001). Relationships between microbial community structure and hydrochemistry in a landfill leachate-polluted aquifer. *Applied and Environmental Microbiology* 67**,** 4619-4629.

Rozan, T.F., Taillefert, M., Trouwborst, R.E., Glazer, B.T., Ma, S.F., Herszage, J., Valdes, L.M., Price, K.S., and Luther, G.W. (2002). Iron-sulfur-phosphorus cycling in the sediments of a shallow coastal bay: Implications for sediment nutrient release and benthic macroalgal blooms. *Limnology and Oceanography* 47**,** 1346-1354.

Sass, H., Overmann, J., Rutters, H., Babenzien, H.D., and Cypionka, H. (2004). Desulfosporomusa polytropa gen. nov., sp nov., a novel sulfate-reducing bacterium from sediments of an oligotrophic lake. *Archives of Microbiology* 182**,** 204-211.

Schwertmann, U., and Cornell, R.M. (2007). "Iron Oxides in the Laboratory," in *Iron Oxides in the Laboratory*. (Weinheim: Wiley-VCH Verlag GmbH).

Schwertmann, U., and Fechter, H. (1994). THE FORMATION OF GREEN RUST AND ITS TRANSFORMATION TO LEPIDOCROCITE. *Clay Minerals* 29**,** 87-92.

Scott, T.B., Allen, G.C., Heard, P.J., and Randell, M.G. (2005). Reduction of U(VI) to U(IV) on the surface of magnetite. *Geochimica Et Cosmochimica Acta* 69**,** 5639-5646.

Steefel, C.I., and Vancappellen, P. (1990). A NEW KINETIC APPROACH TO MODELING WATER-ROCK INTERACTION - THE ROLE OF NUCLEATION, PRECURSORS, AND OSTWALD RIPENING. *Geochimica Et Cosmochimica Acta* 54**,** 2657-2677.

Stookey, L.L. (1970). Ferrozine---a new spectrophotometric reagent for iron. *Analytical Chemistry* 42**,** 779-781.

Straub, K.L., and Buchholz-Cleven, B.E.E. (2001). Geobacter bremensis sp. nov. and Geobacter pelophilus sp. nov., two dissimilatory ferric-iron-reducing bacteria. *Int J Syst Evol Microbiol* 51**,** 1805-1808.

Thamdrup, B. (2000). "Bacterial manganese and iron reduction in aquatic sediments," in *Advances in Microbial Ecology, Vol 16,* ed. B. Schink. (New York: Kluwer Academic / Plenum Publ), 41-84.

Thompson, A., Chadwick, O.A., Rancourt, D.G., and Chorover, J. (2006). Iron-oxide crystallinity increases during soil redox oscillations. *Geochimica Et Cosmochimica Acta* 70**,** 1710-1727.

Wagai, R., and Mayer, L.M. (2007). Sorptive stabilization of organic matter in soils by hydrous iron oxides. *Geochimica Et Cosmochimica Acta* 71**,** 25-35.

Webb, S.M. (2005). *Sam's Interface for XAS Package (SixPACK)* [Online]. Available: http://www-ssrl.slac.stanford.edu/~swebb/index.htm [Accessed].

Wielinga, B., Mizuba, M.M., Hansel, C.M., and Fendorf, S. (2001). Iron promoted reduction of chromate by dissimilatory iron-deducing bacteria. *Environmental Science & Technology* 35**,** 522-527.

Yao, W.S., and Millero, F.J. (1996). Oxidation of hydrogen sulfide by hydrous Fe(III) oxides in seawater. *Marine Chemistry* 52**,** 1-16.

Zachara, J.M., Fredrickson, J.K., Li, S.M., Kennedy, D.W., Smith, S.C., and Gassman, P.L. (1998). Bacterial reduction of crystalline Fe3+ oxides in single phase suspensions and subsurface materials. *American Mineralogist* 83**,** 1426-1443.

Zachara, J.M., Kukkadapu, R.K., Fredrickson, J.K., Gorby, Y.A., and Smith, S.C. (2002). Biomineralization of Poorly Crystalline Fe(III) Oxides by Dissimilatory Metal Reducing Bacteria (DMRB). *Geomicrobiology Journal* 19**,** 179-207.

Zeng, H., and Giammar, D.E. U(VI) reduction by Fe(II) on hematite nanoparticles. *Journal of Nanoparticle Research* 13**,** 3741-3754.

Zhang, C.L., Stapleton, R.D., Zhou, J.Z., Palumbo, A.V., and Phelps, T.J. (1999). Iron reduction by psychotrophic enrichment cultures. *FEMS Microbiology Ecology* 30**,** 367-371.

CHAPTER 4

BIOGENIC SULFIDIZATION OF FERRIHYDRITE BY DESULFOVIBRIO PUTEALIS LEADS TO NON-STOICHIOMETRIC LEVELS OF FE(II): A POSSIBLE FE DRIVEN SULFUR CYCLE

Abstract

In low-sulfidogenic environments where freshly precipitated forms of Fe oxyhydroxides (i.e. ferrihydrite) exist, it is generally assumed that under anaerobic conditions respiration via Fe(III) reduction is the dominant microbial metabolism. However, recent evidence suggest that sulfate reducing bacteria coexist, are metabolically active, and may outcompete dissimilatory iron reducing microorganisms even under conditions that thermodynamically favors Fe(III) over sulfate respirations. These findings provided the motivation for the present study to investigate how much Fe(II) could be generated in sulfate reducing communities given varying micromolar amounts of sulfate. In these experiments, *Desulfovibrio putealis* was inoculated into 160ml batch serum vials containing 3200 μM Fe and between 0 – 728 μM sulfate. In the five experiments where microbial sulfidogenesis occured, significant amounts of FeS was generated with no/minimal S intermediates being detected. The amount of Fe(II) formed during the sulfate reduction phase (up to 97 hours) range from 197 to 1709 μM dependent on the initial amount of sulfate given (49 – 728 μM) with higher sulfate concentration resulting in higher Fe(II) values. However, the stoichiometric values of Fe(II) generated per mole of sulfate reduced varied between 2.3 to 4.0 moles of Fe(II) per mole sulfate, with lower initial sulfate samples generating more Fe(II) per mole of sulfate. Interestingly, in experiments where lactate was not depleted, the amount of Fe(II) generated continued to increase despite non-detectable levels free sulfide or sulfate. Between 31 to 40% of the total Fe(II) produced during the 257 hour long experiment was generated post sulfate reduction (i.e. after sulfate was non-detectable). The continued generation of Fe(II) appears to biologically driven as acetate levels are directly related (1:1) to the amount of

Fe(II) generated. Within the no sulfate control, there was no evidence of Fe(III) reduction with only 10 μM of the Fe(II) being generated during the length of the experiment. It is therefore being suggested that an Fe driven S cycle contributed to the sustained Fe(II) generation and resulted in the skew from stoichiotmetric values of Fe(II) to sulfate. We show potential mechanisms that could lead to such an Fe-S-C cycle are numerous.

4.1 Introduction

Within anoxic environments, dissimilatory sulfate-reducing bacteria (SRB) are ubiquitous and play a major role in carbon mineralization even in low sulfate environments such as lake sediments (Bak and Pfennig, 1991). These organisms couple the oxidation of organic carbon (or H_2) to the reduction of sulfate producing the metabolite sulfide. The resulting sulfide acts as a potent reductant of oxidized metals such as Fe(III). Chemical reduction of the poorly crystalline Fe(III) mineral ferrihydrite by sulfide (H_2S and HS^- pKa =7.0) happens on fast times scales ($t_{1/2}$ ~ 5 min to 12 hours) (Poulton et al., 2004) and represents an important mechanism for ferrihydrite reductive dissolution. This process of reductive dissolution is important because upon the reduction of ferrihydrite, Fe(II) is released into the surrounding environment along with any potentially sorbed contaminants or nutrients (Roden and Edmonds, 1997;Burton et al., 2010;Kocar et al., 2010). In addition, the Fe(II) produced can: 1) act as a further reductant to oxidized contaminants and thus reduce their solubility (i.e. chromium; (Fendorf and Li, 1996)), 2) precipitate as a solid Fe(II) phase (i.e. FeS, $FeCO_3$), 3) resorb onto the ferrihydrite surface resulting in solid-state transformations (Hansel et al., 2005;Hansel et al., 2011) or 4) oxidize and reprecipitate as a new Fe(III) mineral. Clearly, an understanding of how Fe and S interact under natural conditions is needed to completely understand Fe, S, and C cycling in anoxic systems.

Fortunately, the reaction between dissolved sulfide and Fe(III) minerals has been well documented (see following references). The accepted reaction mechanism, as suggested by Dos Santos Afonso (Afonso and Stumm, 1992) involves 4 steps: 1) formation of $Fe^{III}S^-$ surface complex, 2) electron transfer to Fe^{III}, 3) production and

release of the $S^{\bullet -}$ radical and 4) detachment of Fe(II). The generally assumed oxidation product of sulfide reaction with ferrihydrite is elemental S (Rickard, 1974;Pyzik and Sommer, 1981;Peiffer et al., 1992;Yao and Millero, 1996;Poulton, 2003;Poulton et al., 2004;Hellige et al., 2012), polysulfides (Pyzik and Sommer, 1981;Peiffer et al., 1992), however, thiosulfate (Pyzik and Sommer, 1981;Afonso and Stumm, 1992), and sulfate (Afonso and Stumm, 1992) have also been observed. In addition, it is important to note that the detachment of Fe(II) (step 4), is the rate determining step in the formation of FeS and not sulfide oxidation (Poulton, 2003). Therefore the rate of Fe(II) detachment will ultimately determine the amount of FeS formed and as a result how much Fe(III) is potentially reduced by sulfide (as FeS traps sulfide before it can be oxidized). While the detailed studies above have provided insightful results about the oxidation of sulfide with Fe(III) minerals under abiotic conditions, microorganisms can oxidize and/or reduce intermediate sulfur compounds of various oxidation states formed during the oxidation of sulfide (Thamdrup et al., 1993;Lovley and Phillips, 1994). Therefore in systems that include sulfur-based microbial metabolisms, these intermediate sulfur compounds have the potential to be cycled back to sulfide further reducing Fe(III) and hence changing the rates, products, and extent of Fe(III) oxide sulfidization.

In fact, in anoxic, nitrate-free sediments, it has been shown that radiolabeled H_2S was completely oxidized back to sulfate (Fossing and Jorgensen, 1990;Elsgaard and Jorgensen, 1992). In addition, recent microbial evidence suggests that even under low sulfate conditions, sulfate-reducing bacteria coexist and may outcompete dissimilatory iron reducers (Jakobsen and Postma, 1999). For example, we recently revealed that sulfate-reducing communities dominate at the expense of Fe(III) reducers under low

(~200 μM) sulfate conditions even when ferrihydrite was provided as an Fe electron acceptor (Lentini et al., 2012;Lentini, 2013). Within these experiments members of the genus *Desulfovibrio* were abundant and the amount of Fe(II) generated could not be accounted for based on sulfate concentrations only assuming the following reaction of sulfide with Fe(III):

$$HS^- + 2Fe(OH)_3 + 5H^+ \rightarrow 2Fe^{2+} + S^0 + 6H_2O$$

Therefore, in order to explain these result we suggested that within these systems, a catalytic S cycle in which Fe(III) is continually reduced may account for the greater than expected generated Fe(II) per mole of sulfate and the abundance of *Desulforvibrio* within these enrichments. This type of Fe driven sulfur cycle has been suggested in the past to explain both pure culture experiments (Straub and Schink, 2004) and a potential "cryptic S cycle" in the sulfate methane transition zone within marine sediments (Holmkvist et al., 2011). In addition, previous experiments with *Desulfovibrio* hint that during Fe oxide microbial sulfidogenesis the amount of Fe(II) generated may far exceed that generated during abiotic reduction (Li et al., 2006). These previous experiments and observations have provided the motivation for the present study to test whether micro-molar amounts of sulfate could potentially support elevated levels of Fe(III) reduction in pure cultures of the model sulfate-reducing bacterium *Desulfovibrio putealis*. We seek to identify how sulfidization of ferrihydrite under varying sulfate concentrations impacts Fe-S dynamics, the oxidation of carbon, and the ensuing secondary products.

4.2 Material and Methods

4.2.1 Synthesis of two-line ferrihydrite: Two-line ferrihydrite was synthesized via the rapid hydrolysis at room temperature of ferric chloride solution by bringing the pH close

to neutral (Schwertmann and Cornell, 2007). Once a stable pH was reached over several hours, the mineral was allowed to settle and the overlaying solution was decanted off. The mineral was then washed multiple times via centrifugation until deflocculation was observed. Once washed, ferrihydrite was made anaerobic with vigorous bubbling of N2 through the ferrihydrite slurry for ~ 45 mins. The anaerobic mineral slurry was capped and autoclaved using a quick 15-minute cycle. Sterilization using this method did not result in significant transformation of the mineral as confirmed via X-ray diffraction. All minerals were stored anaerobically at 4° C until use. Detail characterization of the mineral was done previously (Hansel et al., 2003)

4.2.2 Media and Desulfovibrio preparation: A bicarbonate buffered basal media was used to examine the role of sulfate concentrations during microbial sufidogenesis by *Desulfovibrio putealis*. *Desulfovibrio putealis* is a known sulfate reducing bacteria that couples the incomplete oxidation of lactate to acetate. It was also a common species observed during Fe reduction enrichments with low sulfate concentrations (Lentini et al., 2012). Standard practices for sterile and anaerobic media preparation and cultivation were used throughout the experiment. In addition all gases were passed though heated copper fillings to remove any trace oxygen. Anaerobic basal media was prepared by boiling water and cooling under ultra high purity N_2:CO_2 (80:20) gas. The composition of the basal media was 4.41 mM KH_2PO_4, 5.62 mM NH_4Cl, and 29.7 mM $NaHCO_3$ in the final solution. Trace metals (excluding Fe) and vitamins were added with care not to include chemical known to chelate Fe (i.e. NTA). A stock salt solution was sterilely added to the basal media after autoclaving and with a final concentration of 4.2 mM

$MgCl_2$ and .9mM $CaCl_2$. The concentration of $MgSO_4$ in the salt solution was between 0 and 800 μM. In all experiments ferrihydrite was added to the solution as a wet slurry to a final total Fe concentration of 3.2mM. Additionally, lactate was also added at a concentration of 3.2mM. The final pH of media was 7.1. Before inoculation of the experiment, cells were grown on the same media as above but with Fe added back to the trace metals and sulfate and lactate concentration adjusted to 15 mM and 30 mM respectively. Seed cultures were prepared by growing cells in the dark at room temperature to late exponential growth. When ready to be harvested, cells were spun down anaerobically (under N_2:CO_2) at 6000g and 10° C for 10 minutes. This was repeated 3 times with the cells being resuspended in the basal media above without lactate and sulfate. Upon concentrating the cells the third time, the cells were resuspended in basal media and inoculated at 5% (approximately $5x10^6$ cells). Incubations of all experiments took place in the dark with the 160ml serum vials laying on their sides.

4.2.3 Aqueous chemistry and solid phase extraction: Samples were monitored using degassed anaerobic syringes and 22 gauge needles. In order to ensure that the N_2:CO_2 volume did not change during sampling, the volume sampled was replace with equal volume N_2:CO_2 gas. Upon sampling, the needle was removed and the syringe was connected to a stopcock under flowing N_2:CO_2 gas and a positive pressure headspace was created in the syringe. Immediately before transfer to the anaerobic chamber, the stopcocks were turned such that the port leading to the syringe was off. Initial test showed that the stopcocks left in this position were capable of holding a positive pressure for greater than 10 minutes (insinuating that they were air impermeable). In comparison,

it took approximately 20 seconds to turn all stopcocks to this position and transfer the all syringes to the transfer chamber.

***4.2.3.1 Solution chemistry*:** Once inside the anaerobic chamber, approximately half of the sample solution was filtered though a 0.2 μm filter. The filtered solution was measure for Fe(II), sulfide, lactate, acetate, sulfate and thiosulfate. Soluble Fe(II) was measured using the ferrozine assay (50mM HEPES buffered at pH 7) at 562 nm (Stookey, 1970). Filterable sulfide was measured by the Cline assay using:1,4-Benzenediamine, N,N-dimethyl sulfate, sulfuric acid and ferric chloride hexahydrate (Cline, 1969). For both colorimetric assays samples were incubated in the dark for 20 minutes before immediate measurement on the UV-Vis spectrophotometer. Organic acids, sulfate and thiosulfate were obtained by first adding 1ml of sample to 10 μl of 1M zinc chloride (ensured that sulfide was not oxidized by O_2 after sampling). Samples were then frozen (-20° C) until further analysis using ion chromatography.

4.2.3.2 Solid Phase: For total Fe, solid phase extractions were performed by adding 1ml of the sample slurry to 1ml of concentrated acid that was being bubbled with N_2 to expel any sulfide that was generated during the reaction. Once the Fe was extracted, appropriate dilutions were performed and samples were measured using ferrozine. For those samples that were not diluted, the 50mM HEPES buffer could not buffer the strong acid. In that case, an ammonium acetate buffer solution was added to the ferrozine to further help with buffering the acid. Cline extractable sulfide was obtained by adding 1 ml of sample to 10 μl of 1M zinc chloride solution to trap any sulfide as ZnS. Upon

trapping the solutions, the sample slurry were added to the cline reagents. Samples were incubated in the dark for 15 minutes before being centrifuged down (11,000g) for 5 minutes. The non-pelleted solution was then measured on the spectrophotometer (670 nm). Solid phase sulfide was then assumed to be the Cline extractable sulfide minus the concentration of filterable sulfide.

4.2.4 Construction of electrodes: Gold-Hg amalgam electrodes were constructed in PEEK™ tubing using the method of Brendel and Luther (Brendel and Luther, 1995). Quickly, a 100 µm diameter gold wire was connected to a conductive wire and was inserted through PEEK™ tubing. The wiring was fixed in the PEEK™ housing with epoxy with care being taken to not introduce bubbles. Upon setting, the tip of the electrode was sanded and then polished successively using diamond polishing compounds down to ¼ micron. Approximately 12 hours before sampling, the electrodes were plated with Hg by reduction of Hg(II) in an N_2 bubbled (10 minutes) 0.1 N Hg/0.05 N HNO_3 solution and a holding potential of -0.1V (vs. Ag/AgCl) for 240 seconds. Conditioning of the Au/Hg electrode was performed by polarizing (-9V) the electrode in 1 M NaOH for 90 seconds. The electrode was then placed in deionized water until use.

For the reference electrode, a Ag/AgCl electrode was constructed by housing a silver wire in PEEK™ as above, however the wire was aloud to produce ~ 3 cm rather than polishing down the electrode. The protruding Ag wire is then lightly sanded and a AgCl coating was generated by polarizing the electrode at 9V for 60 seconds. The AgCl wire was then place in heat-shrink tubing filled with saturated KCl and a Vycor® frit end.

Finally, a counter electrode was constructed similarly to the reference electrode however the Pt wire was left as is after light sanding to remove epoxy.

4.2.5 Cyclic voltammetry: A three electrode system which consisted of the electrodes mentioned above, Ag/AgCl (sat. KCl) reference electrode, platinum counter electrode, and Au/Hg amalgam working electrode were used for all measurements. Cyclic voltammetry was performed in an anaerobic glove bag using a potentiostat (Analytical Instrument Systems, DLK-60) and computer controller. The range of potentials scanned was between -0.1 and -1.8 V (versus Ag/AgCl) at a scan rate of 1,000 mV s^{-1}. In order to remove any Fe or S deposited on the surface of the electrode between samples, the electrode was placed in blank media and the scans were collected until no peaks were visible. Then immediately before data collection a conditioning step of -0.2V was held for 2 seconds. The current flow that is measured for a given electrochemically active species is proportional to the concentration of that species in solution. To remove the small amount of faradaic noise from the scans a smoothing spline was fit to the data. This smoothing helped to better observe small differences in signals.

4.2.6 Sulfur X-ray Absorption Near Edge Structure Spectroscopy (S-XANES): Sulfur X-ray Absorption Near Edge Structure Spectroscopy (S-XANES) was collected on beamline 4-3 at Stanford Synchrotron Radiation Laboratory (SSRL) using a fully tune beam. X-ray fluorescence was measured using a lylte or vortex detector and the incident light was calibrated using a thiosulfate standard. Early sampling efforts revealed that the FeS compound generated during SO_4^{2-} reduction was extremely sensitive to sample

manipulation and/or oxidation by O_2. Therefore, in order to limit sample manipulation, multiple SO_4^{2-} reduction experiments were staggered and sampled chronologically at the synchrotron directly before analysis. All samples were dried onto sulfur free Kapton® tape and placed in anaerobic boxes before transfer to the beam line. A makeshift anaerobic glove bag (being flushed with He) was placed above the sampling chamber. The anaerobic box containing the sample was transferred into this glove bag before being opened. Once opened, the sample was quickly transferred the sample holder and placed in the sample chamber which is continually flushed with He. The position of the XANES peaks are indicative of the oxidation state of the S in the compound of interest. Sulfur XANES collected on standards revealed that peaks from S compounds of interest are approximately 2469.5 eV for the Fe monosulfide (2-), 2472.0 eV for elemental S, and 2482.0 eV for Na2SO4 (6+).

Once collected, data was processed using the software package SIXPACK (Webb, 2005). Samples were first averaged and then normalized to unity by fitting the pre-edge and post-edge. To understand the contribution of different species to unknown samples, linear combination of known compounds were used to reconstruct unknown spectra.

4.3 Results

4.3.1 Kinetics of Sulfate Reduction, Acetate and Fe(II) production: Figure 4.1 shows the reaction kinetics for five sulfate reduction experiments with ferrihydrite as the oxidant for the sulfide generated. Within the first 50 hours, acetate levels increase concurrently with a decline in sulfate as expected during the incomplete oxidation of lactate coupled to sulfate reduction (reaction 1; Table 4.1). During this time period and up to 257 hours, the

0 μM sulfate control (Fhy0, not shown) showed minimal acetate and Fe(II) generation (10 μM). In the Fhy50, Fhy80, Fhy150, and Fhy360 samples, sulfate concentrations declined and became non-detectable by 73 hours. In the sample with the most initial sulfate, Fhy730, sulfate became non-detectable at 97 hours (indicated by the vertical dotted line in Figure 4.1). Given that sulfate is no longer detectable in all samples by 73 to 97 hours, the following analysis of the aqueous and chemical extraction data is broken down into two parts: 1) to the left of the vertical dashed line, referred to as the sulfate reduction phase and 2) to the right of the vertical dashed line, referred to as post-sulfate reduction.

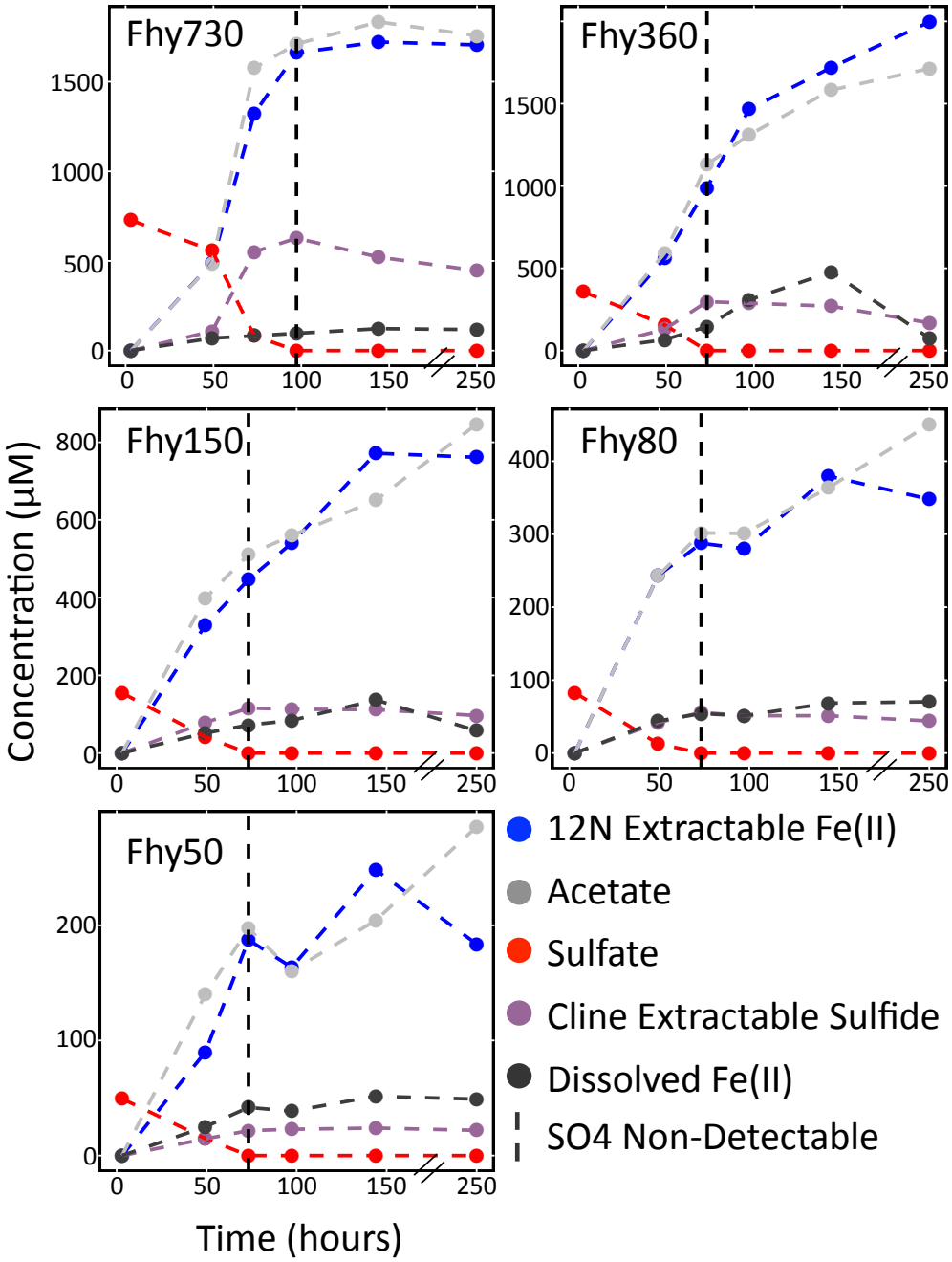

Figure 4.1. Reaction kinetics for the five samples that contained sulfate. To the left of the vertical dashed lines, the incomplete oxidation of lactate is coupled to sulfate reduction as can be seen with the increase in acetate and decrease in sulfate. During this time Fe(II) values increase as a result of sulfide generation. Interestingly, to the right of the vertical dashed line no sulfate is detectable yet Fe(II) and acetate continue to increase in all but the Fhy730 sample (see explanation in text). Note that the zero sulfate control showed minimal Fe(III) reduction and was therefore not shown.

Table 4.1. Potentially relevant reactions to Fe-S-C cycling in this system

Reaction Number	Reactions	Comments
1	$2C_3H_5O_3^- + SO_4^{2-} \rightarrow 2CH_3COO^- + 2HCO_3^- + HS^- + H^+$	
2	$HS^- + 2Fe(OH)_3 + 5H^+ \rightarrow 2Fe^{2+} + S^0 + 6H_2O$	
3	$2C_3H_5O_3^- + SO_4^{2-} + 2Fe(OH)_3 + 4H^+ \rightarrow 2CH_3COO^- + 2HCO_3^- + 2Fe^{2+} + S^0 + 6H_2O$	Sum of 1 and 2
4	$Fe^{2+} + HS^- \rightarrow FeS + H^+$	
5	$6C3H5O3^- + 3S042^- + 2Fe(OH)3 \rightarrow 6CH3COO^- + 6HCO3^- + S0 + 2FeS + 6H2O$	Sum of 1, 2, and 4
6	$2S^0 + C_3H_5O_3^- + 2H_2O \rightarrow 2HS^- + HCO_3^- + C_2H_3O_2^- + 3H^+$	
7	$S^0 + 6Fe(OH)_3 + 10H^+ \rightarrow SO_4^{2-} + 6Fe^{2+} + 14H_20$	ΔG = 54 kj/reaction
8	$S^0 + 6Fe^{3+} + 4H_20 \rightarrow SO_4^{2-} + 6Fe^{2+} + 8H^+$	ΔG = -560 kj/reaction
9	$4S^0 + 4H_20 \rightarrow SO_4^{2-} + 3HS^- + 5H^+$	
10	$2HS^- + 8Fe(OH)_3 + 16H^+ \rightarrow S_2O_3^{2-} + 8Fe^{2+} + 21H_2O$	
11	$HS^- + 6Fe(OH)_3 + 11H^+ \rightarrow SO_3^{2-} + 6Fe^{2+} + 15H_2O$	
12	$HS^- + 8Fe(OH)_3 + 15H^+ \rightarrow SO_4^{2-} + 8Fe^{2+} + 20H_2O$	
13	$3HS^- + 2Fe(OH)_3 + 3H^+ \rightarrow S^0 + 2FeS + 6H_2O$	
14	$3S^0 + 2Fe(OH)3 \rightarrow SO_4^{2-} + 2FeS + 2H^+ + 2H_2O$	
15	$4Fe(OH)_3 + C_3H_5O_3^- + 7H^+ \rightarrow 4Fe^{2+} + C_2H_3O_2^- + 10H_2O + HCO_3^-$	
16	$4Fe^{3+} + C_3H_5O_3^- + 2H2O \rightarrow 4Fe^{2+} + C_2H_3O_2^- + HCO_3^- + 5H+$	

* ΔG values for reaction 6 and 7 (Lovley and Phillips, 1994)

4.3.2 Sulfate Reduction Phase (left of vertical line Figure 4.1): The maximum sulfate reduction rates reached during this period (slope of red line) were 0.7 μM SO_4^{2-} hr^{-1} (Fhy50), 1.5 μM SO_4^{2-} hr^{-1} (Fhy80), 2.4 μM SO_4^{2-} hr^{-1} (Fhy150), 6.4 μM SO_4^{2-} hr^{-1} (Fhy360), and 19.8 μM SO_4^{2-} hr^{-1} (Fhy730) (Table 4.2). Parallel with the loss of sulfate, filterable sulfide (not shown) reached a maximum of 7-8 μM for all samples at 50 hours and was below the limit of detection by 100 hours. Filterable Fe(II) levels steadily increased to a maximum of between 54 - 145 μM for all 5 samples. The amount of filterable Fe(II) generated during this time was directly related to the concentration of the initial sulfate given, with higher initial sulfate values resulting in greater amounts of filterable Fe(II). Total Fe(II) (acid extractable) and acetate values increased concurrently and also showed a strong dependence on initial sulfate concentrations. The maximum

total Fe(II) concentrations during this period were 187 μM (Fhy50), 287 μM (Fhy80), 446 μM (Fhy150), 989 μM (Fhy360), and 1661 μM (Fhy730), while the maximum acetate concentrations were 197 μM (Fhy50), 301 μM (Fhy80), 511 μM (Fhy150), 1130 μM (Fhy360), and 1709 μM (Fhy730) (Table 4.2).

Table 4.2. Concentrations of organic acids and ions produced during experiment

	Sulfate		**Acetate**		**Fe2+**		**Sulfur**	
Sample Name	Initial SO4 (μM)	Max SRR (μM/hr)	No more sulfate measurable (μM)	Maximum Acetate (μM)	No more sulfate measurable (μM)	Maximum Fe(II) (μM)	Cline Extractable Sulfide	% S Recovered
Fhy730	728	19.8	1709	1769	1661	1721	627	86
Fhy360	357	6.4	1130	1713	989	1997	297	83
Fhy150	155	2.4	511	846	446	771	115	74
Fhy80	83	1.5	301	451	287	379	56	67
Fhy50	49	0.7	197	285	187	248	24	49
Fhy0	-	-	-	-	-	10	-	-

According to the stoichiometry of reaction 3 in table 4.1, acetate and Fe(II) production should be twice that of the loss of sulfate. While Fe(II) and acetate concentrations did mirror each other, their stoichiometries when compared to the initial sulfate provided were larger then expected, especially in the low sulfate samples. Therefore, in the lowest sulfate sample (Fhy50), the amount of acetate and Fe(II) generated should not have exceeded 98 μM, yet these values were ~2 times that expected (187 and 197 μM). This trend away from correct stoichiometric levels of acetate and Fe(II) was most skewed for low sulfate samples and approached correct stoichiometric values with increasing sulfate concentrations (Figure 4.2).

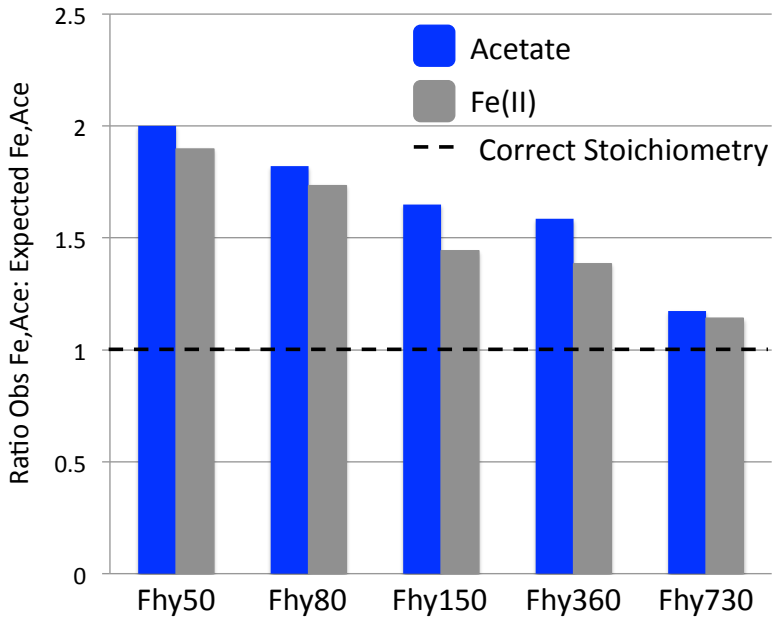

Figure 4.2. The ratio of the observed Fe(II) or acetate stoichiometry to the amount of sulfate reduced as compared to the that expected from reaction 3 in table 4.1 (dotted line). Deviation from correct stoichiometric values is greatest for low concentration samples.

While filterable sulfide levels were low throughout the experiment, solid-phase extractable sulfide via the Cline method (Cline, 1969) increased substantially during the sulfate reduction period (Figure 4.1). By subtracting out the dissolved sulfide concentration, Cline extractable sulfide consisted only of surface bound sulfide or sulfide great than 0.2 µm that can be volatized in a weakly acidic solution. Within all experiments, the Cline extractable sulfide reached a maximum for all samples concurrent with the complete loss of sulfate. The maximum rate at which Cline extractable sulfide was generated was greatest for all samples between the 50-73 hour sampling periods. With the maximum rates of generation being 0.46 µM S^{2-} hr^{-1} (Fhy50), 0.75 µM S^{2-} hr^{-1} (Fhy80), 1.79 µM S^{2-} hr^{-1} (Fhy150), 7.17 µM S^{2-} hr^{-1} (Fhy360), and 18.51 µM S^{2-} hr^{-1} (Fhy730). These rates correspond to 62% (Fhy50), 50% (Fhy80), 73% (Fhy150), 110% (Fhy360) and 93% (Fhy730) of the maximum sulfate reduction rates for the identical

samples. The maximum percent of total sulfur (given as sulfate) recovered as Cline extractable sulfide plus dissolved sulfide, varied based on the initial sulfate concentration with greater than 80% of the total sulfur as Cline extractable plus filterable in the high initial sulfate samples (Fhy360 and Fhy730). However, in lower initial sulfate samples, the percent of S recovered via Cline extractable sulfide decreased to 74% (Fhy150), 67% (Fhy80) and 49% (Fhy50).

4.3.3 Post-Sulfate Reduction Phase (right of vertical line in Figure 4.1): Curiously, while both sulfate and filterable sulfide concentrations were below the limit of detection after 73-97 hours, Fe(II) and acetate levels continually increased (Figure 4.1). The exception being the Fhy730 sample where lactate levels were completely exhausted to the right of the dotted line. During this post sulfate reduction phase, the remaining four samples that still had lactate available showed an increase of Fe(II) equivalent to 61 μM (Fhy50), 92 μM (Fhy80), 325 μM (Fhy150) and 985 μM (Fhy360) (Table 4.2). In addition to Fe(II), acetate concentrations also increased in these samples: 88 μM (Fhy50), 149 μM (Fhy80), 335 μM (Fhy150), and 583 μM (Fhy360). During this post reduction period, the amount of Cline extractable sulfide decreased substantially in the Fhy730 and Fhy360 samples with up to 56% (Fhy360 sample) of the original Cline extractable sulfide no longer extractable; likely representing aging to a more crystalline sulfide phase that is no longer extractable with this method.

4.3.4 Fe and Sulfur Speciation: Aqueous chemistry data suggested that 49% to 86% of the S in these systems was as a Cline extractable sulfide, suggesting that a majority of the

S ends up as a labile FeS phase. In addition, Fe(II) and acetate levels increase while sulfate levels remain non-detectable suggesting the possible generation of short-lived S intermediates. To test for the production of FeS and/or S intermediates, aqueous and solid-phase analysis of Fe and S compounds were monitored using cyclic voltammetry and sulfur X-ray Absorption Near Edge Structure (S-XANES) spectroscopy.

4.3.5 Electrochemistry of Fe and S species: To monitor the aqueous speciation of Fe and S species in these experiments, cyclic voltammetry was employed. Voltammetry has the benefit that it is a non-destructive sampling technique and allows for the simultaneous detection of multiple Fe (Fe(II), Fe(III), and FeS_{aq}) and S (S^0, HS^-, $S_2O_3^{2-}$, S_x^{2-}, FeS) species (Luther III et al., 2008) While the peak potentials (E_p) and half potentials ($E_{1/2}$) are well-defined, these positions are matrix specific and must be calibrated within a specific system. Therefore, standard additions of known compounds to the defined media used in this project were performed to confirm the peak positions of Fe and S compounds. This analysis confirmed that the sulfide and elemental S peak positions showed significant overlap. To test if elemental S could be distinguished from sulfide in solution, an experiment was conducted in which S^{2-} and elemental S were added to the basal media and Zn^{2+} was used to precipitate S^{2-} while leaving elemental S behind (Figure 4.3). Quickly, a solution containing basal media and elemental S dissolved in SDS was first measured electrochemically (Steudel and Holdt, 1988). Aqueous sulfide was then added to the solution increasing the S^{2-}/S^0 peak. With the addition of Zn^{2+} to the solution containing both elemental S and S^{2-} the S^{2-}/S^0 peak returned to a value consistent with the

S^0 pre-sulfide addition. This approach suggested that electrochemically active S^0 should be distinguishable from HS^- upon the addition of Zn^{2+} to solution.

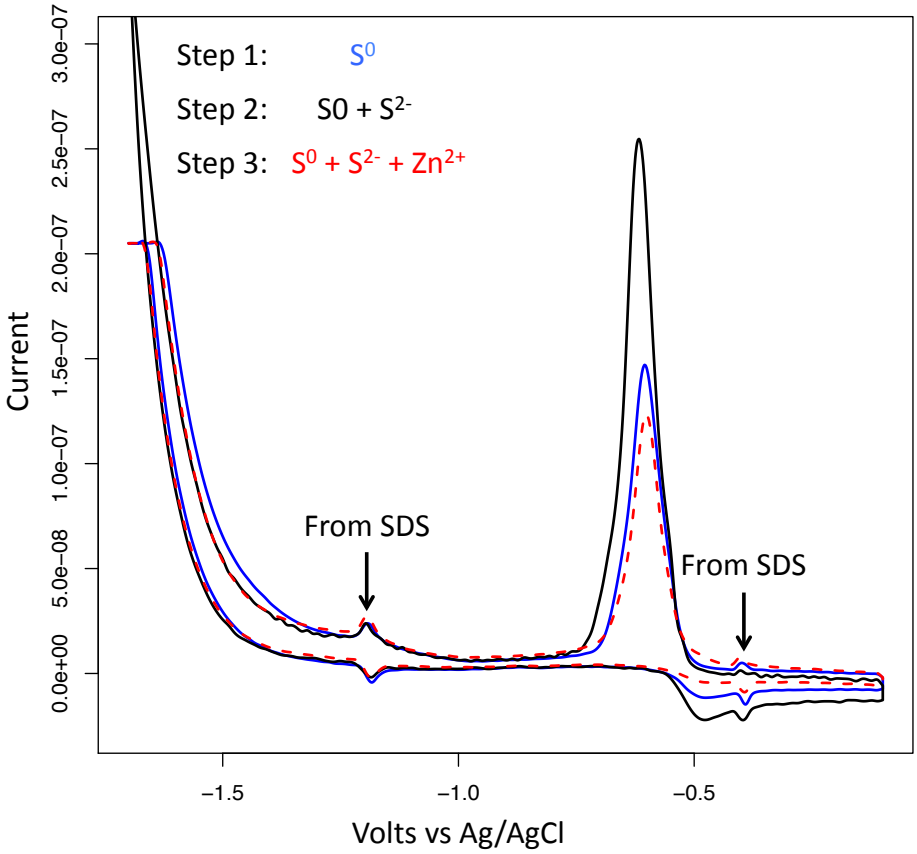

Figure 4.3. Test to see if elemental S could be distinguished from sulfide using electrochemistry despite significant peak overlap. The experiment proceeded as follows: step 1 Elemental S in basal media and SDS (SDS was needed to get elemental S in solution) produced a signal at ~ -0.6V (blue line). Upon the addition of sulfide (step 2) the peak increase as a result of the peak overlap (black line). With the addition of $ZnCl_2$ (Step 3) the peak returns to pre-sulfide addition values suggesting elemental S is left behind (red dashed line). Proving that this method is a potential was to distinguish between sulfide and elemental S.

Figure 4.4 shows the currents generated for Fe and S compounds during cyclic voltammetry measurements as function of time within the sulfate reduction experiments. These measurements indicated a peak at ~ -0.6V consistent with sulfide within 29 hours along with trace amounts of Fe(II) (Figure 4.4). At 50 hours, the sulfide peak reached a

maximum current for all samples with the exception of the Fhy730 sample, which reached a maximum at 76 hours. Addition of Zn^{2+} to multiple samples during the 0 to 76 hour period resulted in the near instantaneous removal of the peak at ~ -0.6V, suggesting the presence of only minimal amounts of electrochemically active elemental S during the period of maximum sulfate reduction/sulfide oxidation. The HS^- levels varied according to initial sulfate concentration with the maximum amount detected being inversely related to the amount of initial sulfate given (pale versus dark red lines, Figure 4.4). This trend was likely a result of the amount of free Fe(II) within the samples.

A peak consistent with aqueous Fe(II) ($E_{1/2}$ ~ -1.45V) was detected and increased with a slight lag behind the current for sulfide. Despite this lag, Fe^{2+} currents reached a maximum during the sulfate reduction phase (50 and 76 hours), similar to HS^-. However, the rate at which the Fe(II) peak decreased was slower than the HS^- peak. The differences in the amount of aqueous Fe(II) generated between the samples was directly related to the initial sulfate concentration with the Fhy50 and Fhy80 (light blue; Figure 4.4) samples showing consistently lower currents, (maximum currents = 69 and 114 nA, respectively), when compared to the higher concentration samples (maximum currents = 204 nA for Fhy150, 170 nA for Fhy360, and 246 nA for Fhy730). A peak consistent with electrochemically active FeS ($E_{1/2}$ ~ -1.1 to -1.2 nA) begins to increase with the detection of sulfide (trace amounts at 29 hours) and reaches a maximum ~24 – 48 hours after the maximum of Fe(II) and sulfide. For the three lowest initial sulfate concentrations, the maximum FeS current was reached at 76 hours (15 nA Fhy50, 36 nA Fhy80, and 62.4 nA Fhy150), while in the Fhy360 and Fhy730 the FeS current reaches a maximum of 105 nA and 121 nA at 95 and 113 hours, respectively. Unexpectedly, another peak consistent

with an aqueous Fe(III) compound was also detected beginning at 50 hours and reached a maximum between 113 and 164 hours. This electrochemical peak has been well documented in the literature (Taillefert et al., 2000;Taillefert et al., 2002), yet under highly reducing conditions was not expected here. It is also worth noting, that an Fe(III) peak was not detected in the no sulfate (Fhy0) incubation (data not shown).

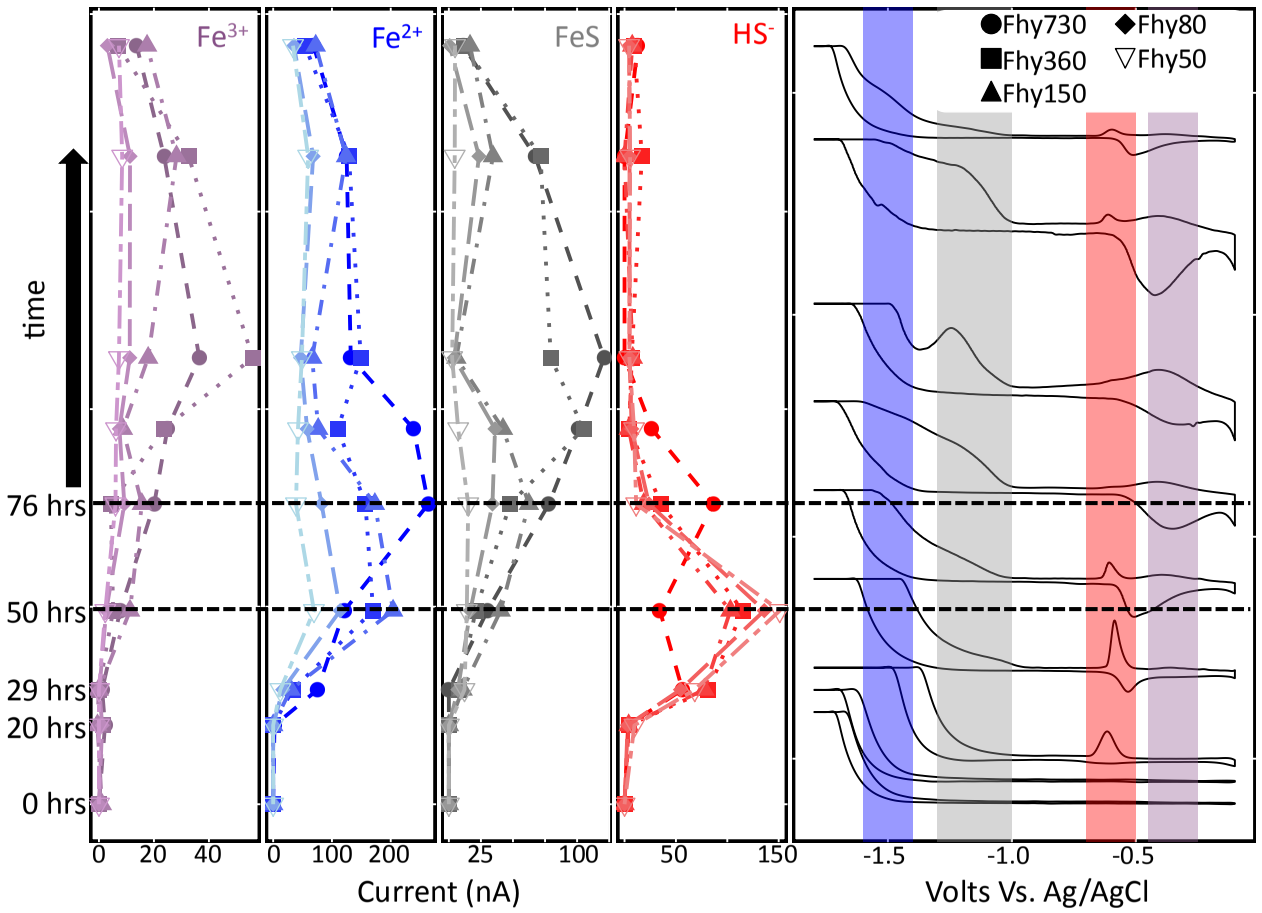

Figure 4.4. Current generation for Fe and S compounds during cyclic voltammetry measurements as function of time within the sulfate reduction experiments. The voltammograms at the right of the figure are from a single representative samples (Fhy360). Similar voltammograms were used to generate the current data. In addition to unique symbols, the colors in the current data go from light to dark dependent on concentration of sulfate (low to

4.3.6 S-XANES spectroscopy: Cyclic voltammetry along with chemical extraction analysis indicated that during the sulfate reduction/sulfide oxidation period (up to 76 hrs), the main product of sulfate reduction in these solutions was FeS. To confirm these analyses and look for potential S intermediates X-ray Absorption Near Edge Structure (XANES) spectroscopy was employed. Linear combination fitting of S-XANES spectra showed consistent trends with the extraction and voltammetry results (Figure 4.5; Table 4.3). For all samples, during the initial sulfate reduction phase (50 hours), S-XANES spectra showed two peaks, one at 2482 eV, which is consistent with the sulfate edge and one at 2469.5 eV consistent with FeS. Linear combination fitting of these spectra suggested that sulfate accounts for 44% to 73% of the signal at 50 hours, while FeS accounts for 38% to 56% of the signal. With time, the loss of sulfate coincided with an increase in the amount of FeS to greater than 90% by 82 hours along with minor amounts of elemental S (2-12%) (Figure 4.5, Table 4.3). It is important to note that in the absence of mixed FeS/Elemental S standards that can exactly mimic the secondary products, fits less than 5-10% should be regarded with caution until further confirmation. Indeed, mathematically generated spectra using linear combinations of FeS and elemental S standards suggest that a peak should be visible at 2472eV when the FeS and elemental S are mixed in a 90:10 ratio (Figure 4.6). This indicative peak is not observed for the 147 hour samples where elemental S seems to increase and thus this value may be an over estimate of the amount of elemental S. Spectra for the lower sulfate samples, Fhy80 and Fhy150, however, show a substantial fraction as elemental S, 11% and 27% respectively. The contribution of this elemental S peak to the S-XANES signal decreased with time to 7-9% (Table 4.3).

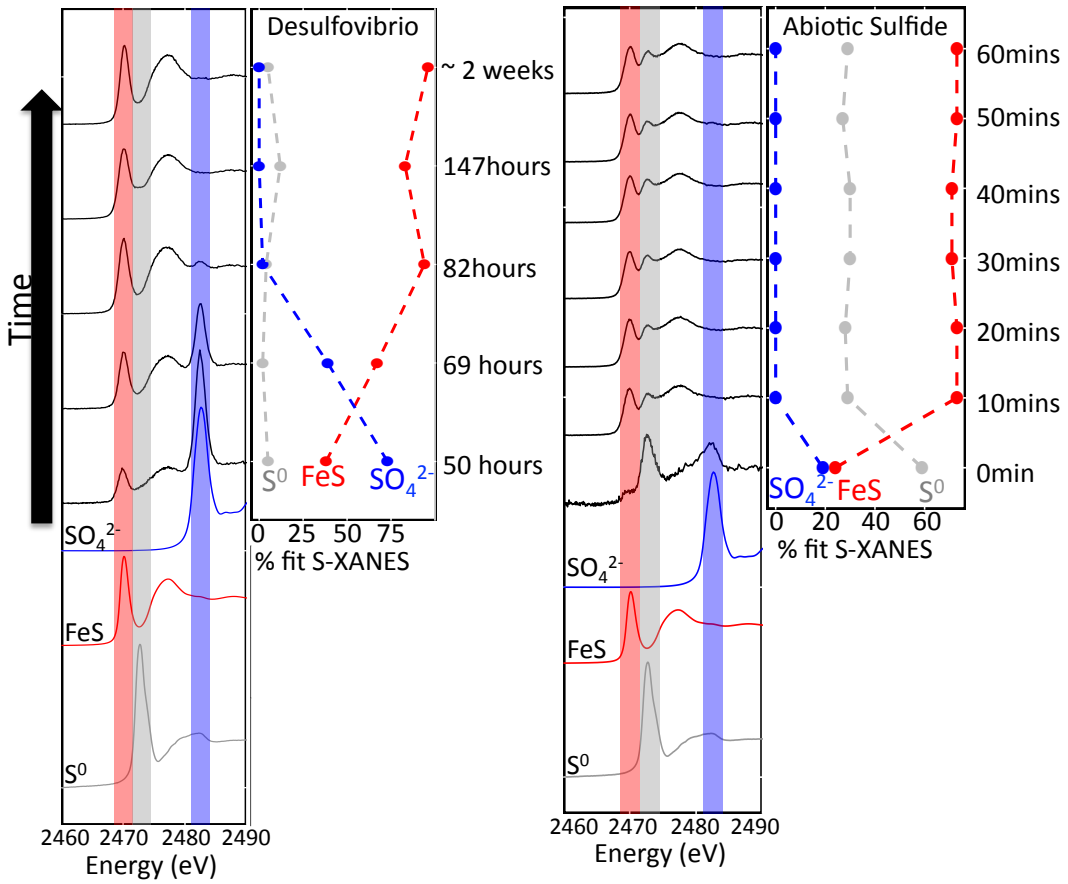

Figure 4.5. Sulfur X-ray Absorption Near Edge Structure (S-XANES) spectroscopy of biological (left) and abiotic (right) sulfidization of ferrihydrite. Linear combination fitting of the S-XANES spectra with known compounds resulted in the percentages seen to the right of the spectra (% fits). Clearly, elemental S is a major product of abiotic sulfide oxidation yet it is not seen in appreciable amounts in the microbial sulfate reduction experiment. See table 4.3 for detail of fit and further samples.

Table 4.3. Fitting results of linear combination fitting of unknown S-XANES spectra.

Fhy730	FeS	S0	Sulfate	R-val
50hrs	38	4	74	0.023
69hrs	67	1	39	0.010
82hrs	94	3	3	0.003
147hrs	88	12	0	0.003
~ 14 days	96	4	0	0.003
oxidized Ferr-800	49	46	6	0.003
Fhy360				
50hrs	40	5	75	0.023
69hrs	79	3	25	0.006
82hrs	95	4	2	0.004
147hrs	90	11	0	0.002
~ 14 days	98	2	0	0.003
Fhy180				
50hrs	56	11	46	0.012
69hrs	87	8	6	0.005
82hrs	95	4	2	0.004
147hrs	90	8	3	0.003
~ 14 days	94	5	2	0.002
Fhy80				
50hrs	55	27	29	0.009
69hrs	76	21	6	0.005
82hrs	91	9	2	0.005
Abiotic-Ferr800				
0 mins	22	59	24	0.009
10 mins	73	28	0	0.003
20 mins	73	28	0	0.003
30 mins	71	30	0	0.003
40 mins	71	30	0	0.003
50 mins	72	27	1	0.003
60 mins	73	29	0	0.003

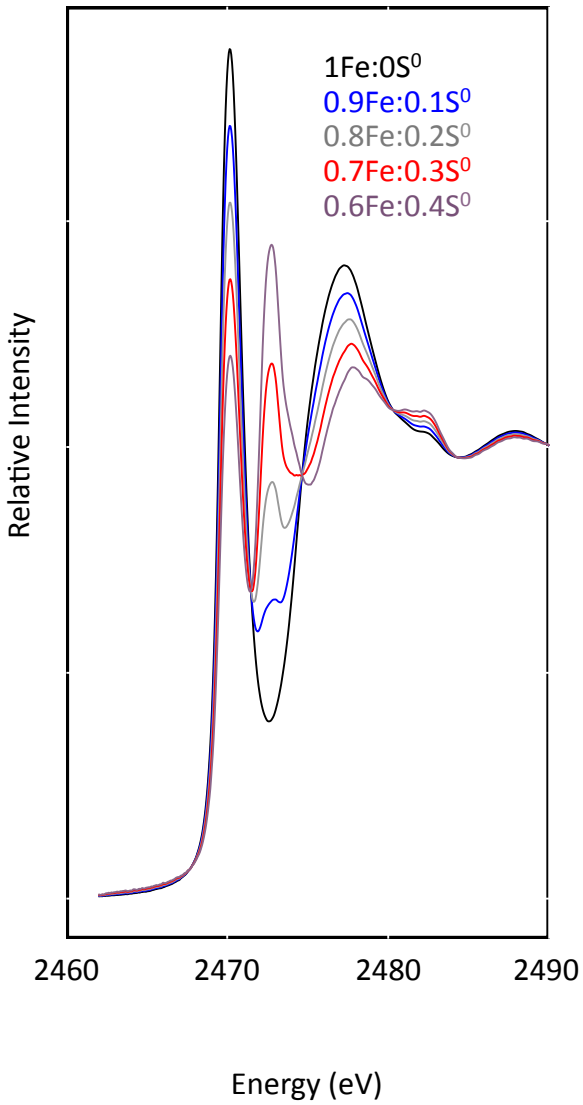

Figure 4.6. Theoretical FeS and elemental S spectra of varying ratios produced by linear combinations of data collected on pure end-members. The data suggest that at a 0.9:0.1 ratio of FeS:elemental S that a indicative elemental S peak should be visible at ~2472eV.

***4.3.7 Comparison of S-XANES to Abiotic S addition*:** The above findings that only minor elemental S was generated during the reaction of sulfide and $Fe(OH)_3$ are in contradiction with what would be expected based on the generally assumed reaction pathway (reaction 2; Table1) and what has been observed in past abiotic experiments (Poulton, 2003;Poulton et al., 2004). Therefore, in order to compare the products of

biogenetically produced sulfide to sulfide added abiotically, sodium sulfide was added to a ferrihydrite sample (no sulfate) to a final concentration of 800 μM S and sampled every 10 minutes. The abiotic oxidation of sulfide revealed that the major product of sulfide reaction with ferrihydrite was initially elemental S (~59% of the S) with smaller amounts of FeS (24%) and sulfate (19%). As the reaction proceeded the contribution of sulfate to the overall signal was no longer distinguishable and the contributions of FeS and elemental S changed to approximately 70% and 30%, respectively (Figure 4.5; Table 4.3). While FeS was still the major HS^- removal pathway, the contribution of elemental S to the S-XANES spectra was significantly higher than in the biotic sulfate reduction experiments. This increase in elemental S can visually be seen as a peak at ~2472 eV (grey shading) in the abiotic S-XANES (Figure 4.5). The 2FeS:1 elemental S ratio is in good agreement with reaction 5 in Table 4.1 where 3 moles of sulfide reacts with 2 moles of ferrihydrite designated as $Fe(OH)_3$ to give 1 mole elemental S and 2 moles of FeS.

4.3.8 Details of Fe-S Analysis

4.3.8.1 Potential for Sample Artifacts: As mentioned in the methods above, early sampling efforts revealed that the FeS compound generated in these experiments was extremely sensitive to sample manipulation and/or oxygen with the end result being an apparent color change back to the parent mineral (Figure 4.7a). These changes were particularly noticeable during short exposure to oxygen or during the drying of the sample even in an anaerobic chamber on a filter membrane. To investigate how sample manipulation and/or oxidation introduced sample artifacts, S-XANES was collected on the FeS product after short exposure (~ 5 minutes) to atmospheric oxygen and by drying

anaerobically on a filter. Oxidation of an Fhy730 sample via oxygen, led to a change in the S products with an increase in elemental S to 40 to 50% (Figure 4.7b; Table 4). Early attempts to collect S-XANES on filter membranes revealed a similar result (Figure 4.7c). In addition, for samples with low S concentrations, this FeS oxidation artifact can result in elemental S being the dominant S signal (Figure 4.7c).

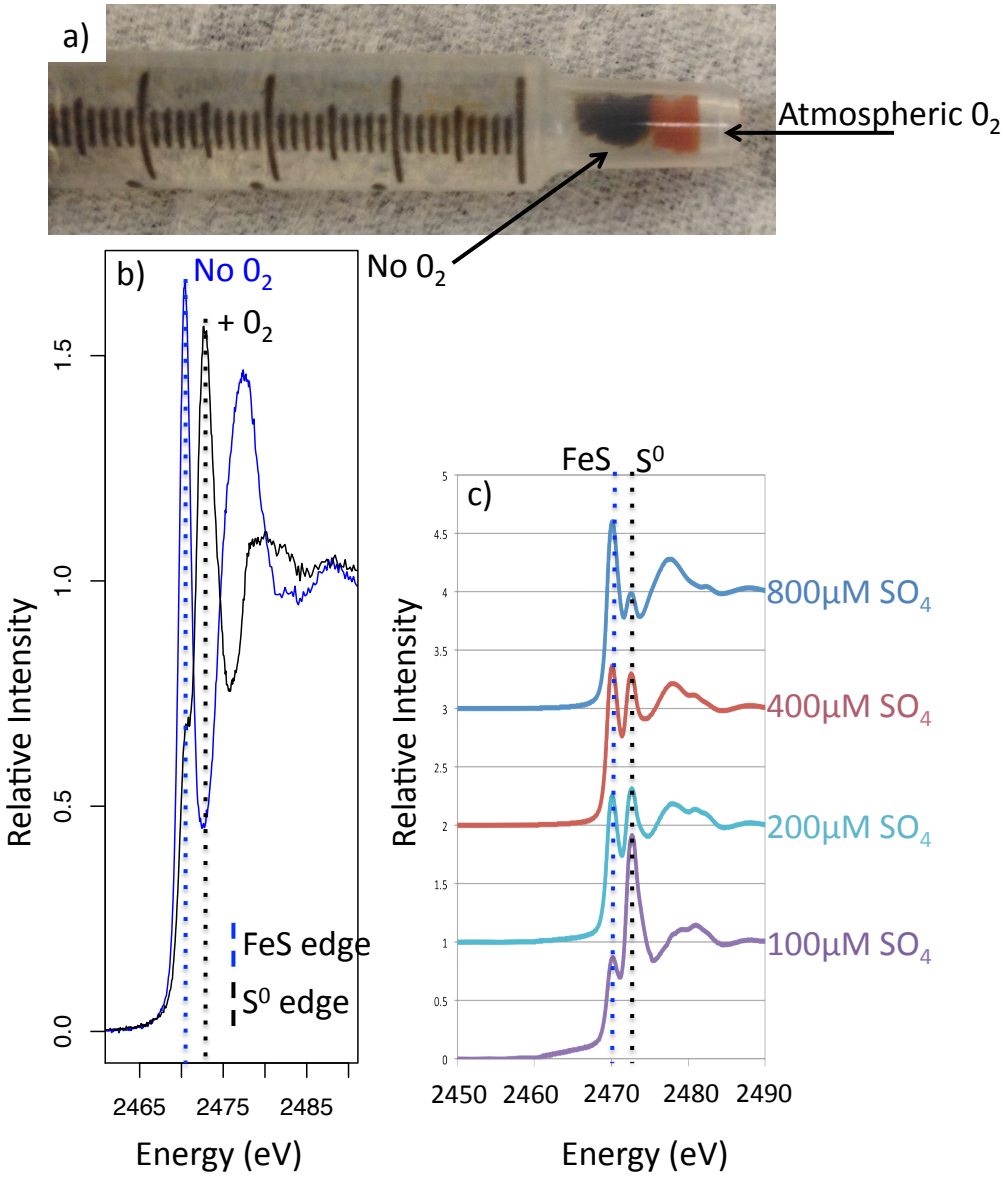

Figure 4.7. a) Visible oxidation gradient of a syringe exposed to O_2 for ~ 10 minutes. The color change from black to brown is indicative of FeS oxidation. b) S-XANES spectra of a sample that was oxidized by O_2 suggesting that FeS oxidizes to elemental S rather quickly. c) Attempts to sample on a filter resulted in oxidation of the FeS product. This oxidized product (elemental S) became the majority of the symbol in the low S samples.

***4.3.8.2 Challenge in Obtaining Representative Sulfur Standards*:** Typically, sample XAS (both XANES and EXAFS) spectra can be adequately fit using linear combinations of standard compounds within a robust spectral library and this technique is used widely

in the literature (Gorbaty et al., 1991;Fleet, 2005;Burton et al., 2009;Prietzel et al., 2011). However in this experiment, using the S-XANES spectra collected for FeS and elemental S resulted in inadequate fits of the unknown data. Figure 4.8 shows S-XANES spectra for different elemental S compounds: ground sublimed elemental S flowers, elemental S flowers dissolved in toluene filtered then re-precipitated, and elemental S obtained through oxidation of FeS. Dampening of the peak in Figure 4.8 suggests significant self-absorption of the signal in the sublimed elemental S spectra. Given that the thicknesses of the samples were all consistent, self-absorption in this case is likely due to differences in particle size and suggests that the elemental S produced upon sulfide oxidation by ferrihydrite is much smaller than the common reference standards.

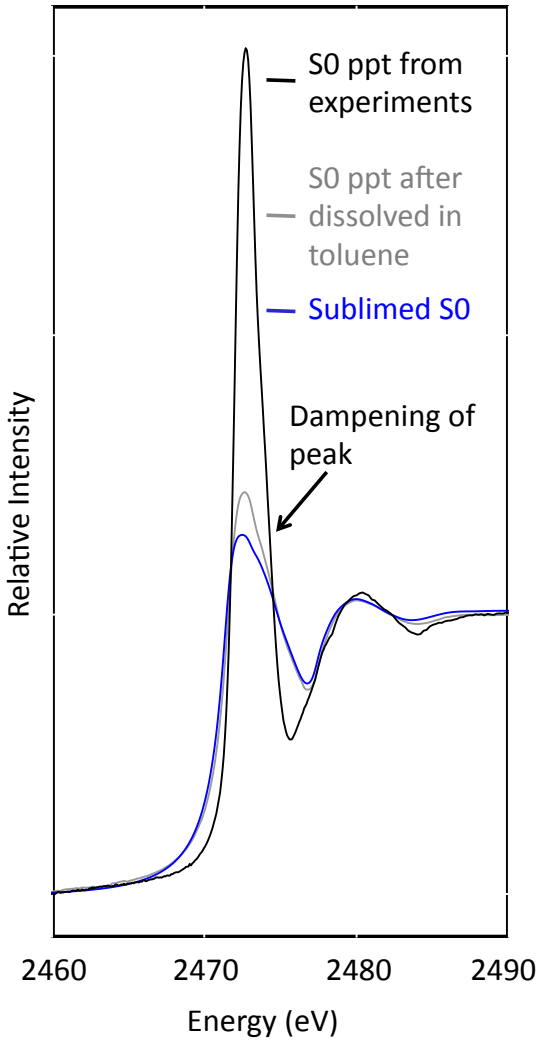

Figure 4.8. Comparison of elemental S S-XANES spectra. Sublimed elemental S flowers (blue line) and elemental S dissolved in toluene and reprecipitated showed significant amounts of self-adsorption (results in peak dampening) when compared to the elemental S produced during the oxidation of sulfide by ferrihydrite. Significant differences between spectra such as these must be accounted for when doing linear combination fitting the data (table 4.3) to obtain accurate fits.

For FeS, attempts to fit the data with both a synthetic poorly crystalline FeS compound and mackinawite also resulted in poor fits. Comparing the K-edge S-XANES spectra for biologically produced FeS and synthetic mackinawite also showed significant differences when compared to each other (Figure 4.9). Mainly, the observed peak energy

for the different FeS phases were 2470.1 eV for biologically produced FeS, 2470.7 eV for freshly precipitated mackinawite, and 2470.9 eV for aged mackinawite. In addition, the broadness of the peak in freshly precipitated mackinawite along with the shoulder in the data at approximately 2470 eV suggest that the freshly precipitated form is transforming to a stable FeS endmember with a more oxidized S value. The first derivative of the S-XANES spectra shows this transition clearly; with the freshly precipitated mackinawite data showing two inflections at the peaks of the two end members, biologically produced FeS and aged mackinawite.

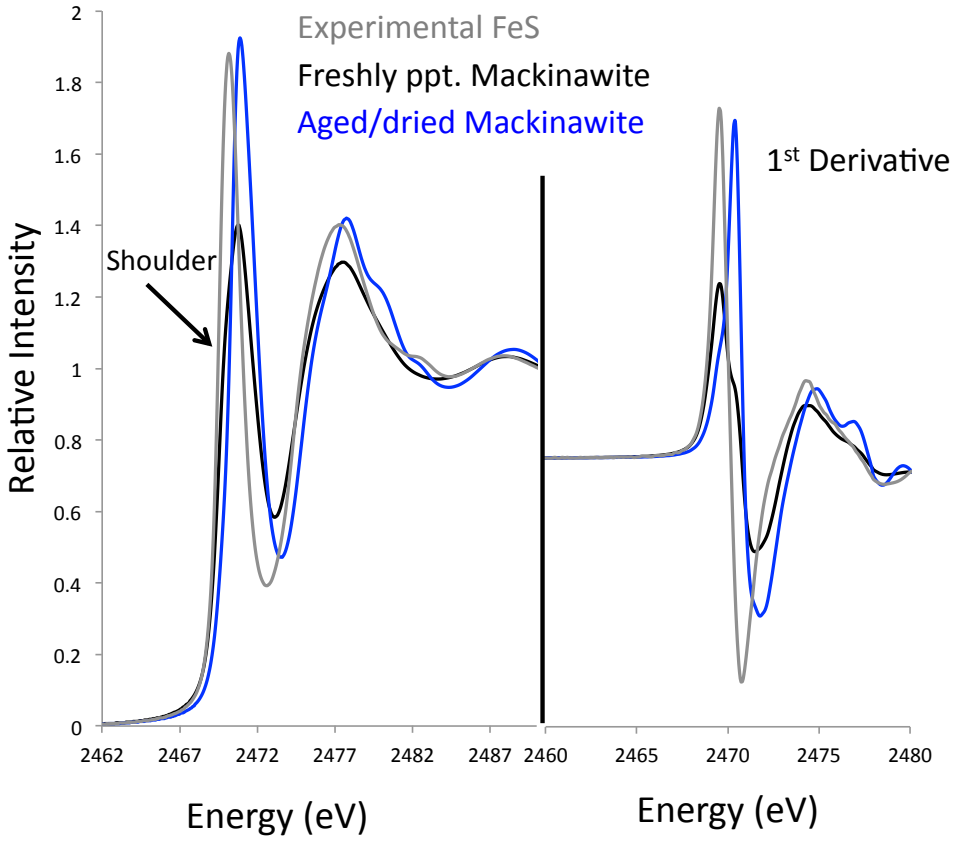

Figure 4.9. Comparison of FeS S-XANES spectra. Significantly different S-XANES spectra are produced for FeS when comparing the FeS produced during sulfate reduction and FeS produced by mixing Fe(II) with sulfide. The observed peak energy for the different FeS phases were 2470.1 eV for biologically produced FeS (grey), 2470.7 eV for freshly precipitated mackinawite(black), and 2470.9 eV for aged mackinawite (blue). The data suggest that aging of the FeS mineral results in S (in FeS) being in a higher oxidation state (blue line; higher energy). Even in freshly precipitated forms of synthetically produced FeS, the S-XANES edge suggest that it is already transitioning to this higher oxidation state FeS when compared to the biogenically produced FeS.

4.4 Discussion

The dissimilatory reduction of sulfate by *Desulfovibrio putealis* resulted in the sulfide-induced reductive dissolution of ferrihydrite and the subsequent formation of both aqueous and solid-phase FeS and minor amounts of elemental sulfur (Figure 4.1 and 4.4,

Table 4.2 and 3). As is common for members of the genus *Desulfovibrio* , the reduction of sulfate was carried out via the incomplete oxidation of lactate to acetate:

$$2C_3H_5O_3^- + SO_4^{2-} \rightarrow 2C_2H_3O_2^- + 2HCO_3^- + HS^- + H^+ \quad \text{(Rxn 1 table 4.1)}$$

When sulfide comes in contact with ferrihydrite, reductive dissolution of the Fe(III) phase coupled to the oxidation of sulfide (with the oxidation product generally assumed to be elemental S) rapidly proceeds as follows:

$$HS^- + 2Fe(OH)_3 + 5H^+ \rightarrow 2Fe^{2+} + S^0 + 6H_2O \quad \text{(Rxn 2 table 4.1)}$$

The fast kinetics of reaction 2 was evident by the lack of substantial accumulation of aqueous sulfide levels (below 8 μM) relative to conditions without Fe(III). While reaction 2 assumes that elemental S is the major product of sulfide oxidation with Fe(III), numerous sulfur compounds of varying oxidation states have been suggested as potential oxidation products, including elemental S (Rickard, 1974;Pyzik and Sommer, 1981;Peiffer et al., 1992;Yao and Millero, 1996;Poulton, 2003;Poulton et al., 2004;Hellige et al., 2012), polysulfides (Pyzik and Sommer, 1981;Peiffer et al., 1992), however, thiosulfate (Pyzik and Sommer, 1981;Afonso and Stumm, 1992), and sulfate (Afonso and Stumm, 1992) have also been observed.. In any case, the oxidation of 1 mole of sulfide results in the formation of between 2-8 moles of Fe(II), depending on the reaction mechanism, which will then react with residual dissolved sulfide to precipitate as FeS:

$$HS^- + Fe^{2+} \rightarrow FeS + H^+ \quad \text{(Rxn 4 table 4.1)}$$

The time-series voltammetric profiles of the sulfate-reducing experiments under all conditions suggest that reactions 1,2, and 4 all occurred (Figure 4.4). Therefore, as reaction 1 proceeded, the first pulse of sulfide (29 hours) was measured concurrently with the formation of small amounts of Fe(II) (via reaction 2). Further production of sulfide

and Fe(II) resulted in FeS becoming a significant fraction of the aqueous S and Fe signal in these experiments (reaction 4). Interestingly, despite the production of copious amounts of Fe(II) via the oxidation of sulfide during this time period, minimal sulfur intermediates were measured via voltammetry (Figure 4.4). However, elemental sulfur was observed via S-XANES spectroscopy (Figure 4.5). The elemental sulfur may, therefore, be solid-bound (e.g., heterogeneously nucleated on ferrihdyrite), thus precluding its measurement via voltammetry. Reaction 1, 2, and 4 proceeded until sulfate became limiting and ultimately non-detectable at 73 or 97 hours.

The amount of total Fe(II) generated during the sulfate reduction phase of the experiment was a function of initial sulfate concentration with the total concentration ranging from 197 to 1709 μM (Figure 4.1). However, the ratio of Fe(II) produced per mole of initial sulfate provided was inversely related to the initial sulfate concentration with 2.3 to 3.8 moles of Fe(II) being produced per mole of initial sulfate (Table 4.2). This range in stoichiometric ratios for Fe(II) to initial sulfate suggests different (bio)geochemical processes occurred. For instance, in high initial sulfate experiments where the stoichiometric ratio is closer to 2 moles of Fe(II) to 1 mole of sulfate (Figure 4.1, Table 4.2), the general assumption that Fe(III) oxidizes sulfide to elemental S could be supported as follows (sum of reaction 1 and 2):

$$2C_3H_5O_3^- + SO_4^{2-} + 2Fe(OH)_3 + 4H^+ \rightarrow 2C_2H_3O_2^- + 2HCO_3^- + 2Fe^{2+} + S^0 + 6H_2O \quad \text{(Rxn 3 table 4.1)}$$

Reaction 3, however, cannot explain the larger Fe(II) to sulfate ratios measured within the lower sulfate incubations (Figure 4.1, Table 4.2). In addition, the assumption that two moles of Fe(II) are generated for each mole of sulfate is likely an overestimate as it assumes that all of the sulfide generated is oxidized by Fe(III). A more likely scenario, as supported by the S-XANES data (Figure 4.5), is abiotic sulfide oxidation by ferrihydrite

lead to 2 moles of Fe(II) generated during the first oxidation of sulfide to elemental S (reaction 2) that subsequently reacts with 2 moles of sulfide generated via sulfate reduction (reaction 1) to form FeS (reaction 4). The formation of FeS thereby inhibits further reductive dissolution of ferrihydrite. Indeed, Cline extractable sulfide measurements suggested that between 49 to 86% of the total S ended up as FeS (Table 4.2). These estimates are likely a lower estimate of the total FeS, since aqueous FeS clusters can become resistant to dissociation and complexation by the Cline assay (Roesler et al., 2007). For the higher sulfate conditions, S-XANES analysis indicated that greater than 90% of the S in all the incubations was present as FeS (Figure 4.5, Table 4), in support of the prediction that FeS values are greater than those estimated by the Cline assay. Consequently, under the conditions here formation of FeS must also be considered with the net reactions being (sum reaction 1, 2 and 4):

$$6\ C_3H_5O_3^- + 3SO_4^{2-} + 2Fe(OH)_3 \rightarrow 6\ C_2H_3O_2^- + 6\ HCO_3^- + S^0 + 2FeS + 6H_2O$$ (Rxn 5 table 4.1)

Fe(II) values during sulfate reduction are then 3.5 to 6 times greater then that expected based on initial sulfate concentrations and this revised reaction (as opposed to reaction 3). While reaction 3 and 5 are both idealized end-members, if elemental S is the main oxidation product, the true stoichiometric ratio is likely to lie somewhere between 0.66 to 2 moles of Fe(II) per mole sulfate. In any case, the deviation from the measured and predicted stoichiometric values of reaction 3 or 5 likely did not result from the direct reduction of Fe(III) by *D. putealis* since Fe(II) generation was not observed during the first 97 hours in the no sulfate control (Fhy0). The fact that the greatest deviation from predicted to measured stoichiometric ratios for Fe(II) to initial sulfate occurred in low sulfate incubations suggests that either (1) under low sulfur conditions, sulfur is more likely to be cycled and therefore increase the amount of Fe(II) generated per mole of

sulfate, or (2) the process controlling this stoichiometric deviation occurred in all samples yet was masked by the larger Fe(II) background in higher sulfate samples.

Based on the reactions outlined above and the fact that *D. putealis* was not able to directly reduce ferrihydrite, it would be expected that Fe(III) reduction would cease upon the depletion of sulfate (with S being trapped as FeS and/or elemental S). Instead, in the post sulfate reduction period where no sulfate or free sulfide was detectable, Fe(II) and acetate values continually increased to as much as 102% more than the value reached during the period of sulfate reduction (Figure 4.1, Table 4.2). The magnitude of this increase was directly related to the initial amount of sulfate provided with the exception of the highest sulfate sample, Fhy730 (see explanation below). Given the strong correlation between Fe(II) and acetate production, it is unlikely that solely abiotic reactions are responsible for the reduction of Fe(III) (Figure 4.10). Instead, this coupling of Fe(II) and acetate suggest a biologically-driven process is operative, with acetate formation a result of incomplete enzymatic oxidation of lactate. Further evidence for biologically-mediated Fe(II) formation is provided by the metabolite profiles observed for the Fhy730 sample. In contrast to the other incubations, lactate was completely consumed during the sulfate reduction phase for unknown reasons in the Fhy730 incubation (Figure 4.1). Consequently, this absence of lactate resulted in only minimal amounts of Fe(II) generated (4%), which contrasts with the other incubations where lactate was still present to fuel microbial respiration. By 257 hours within the other incubations, approximately 184 hours after sulfate was no longer detectable, the amount of Fe(II) generated per mole of initial sulfate increased to 6.8 to 8.4.

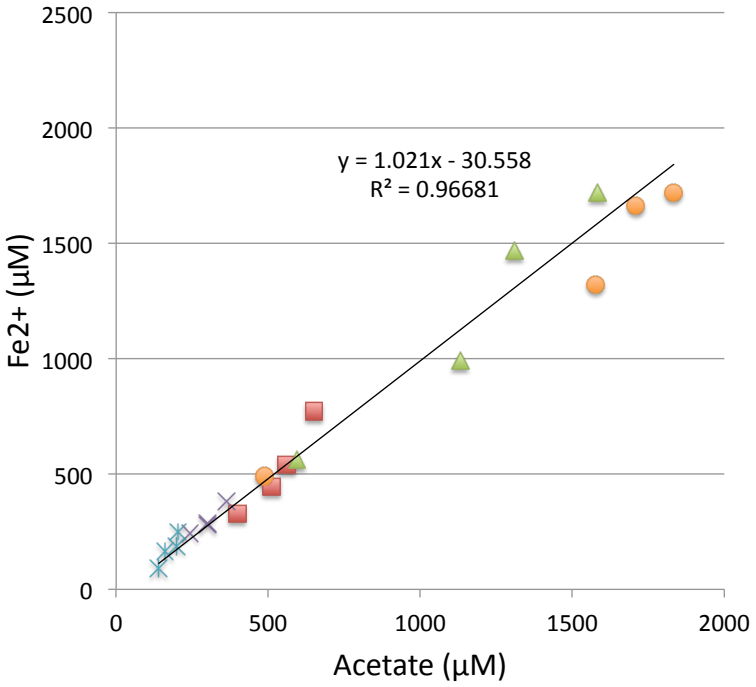

Figure 4.10. Linear relationship between the amount of Fe(II) and the amount of acetate generated during the bacterial reduction experiments. Symbols represent experiments with different sulfate concentrations. The near 1:1 relationship between acetate and Fe(II) suggest that the continued production of Fe(II) is biological and likely connected to the incomplete oxidation of lactate.

Given the continued generation of Fe(II) and acetate and the fact that *D. putealis* could not directly reduce ferrihydrite, a S driven Fe cycle is likely operative. This scenario suggests that sulfide generated during sulfate reduction is oxidized back to an intermediate or fully oxidized sulfur compound capable of being reduced again by *D. putealis*. Based on the detailed metabolism of *D. putealis,* potential sulfur compounds that could be reduced by this organism are sulfate, sulfite, and thiosulfate but not elemental S (Basso et al., 2005). Despite using multiple methods that would have detected sulfite or thiosulfate, neither intermediate was detected in these experiments. Any regeneration of sulfate could theoretically be masked by the initial high sulfate background, and therefore would have only become detectable after sulfate was depleted

(assuming the rate of sulfate generation was greater than the rate of sulfate reduction). Of course, the lack of detection of sulfate or S intermediates does not necessarily preclude their formation, as their presence could have been short-lived and yet of relevance.

Elemental S is the most commonly observed oxidation product of sulfide reacting with Fe(III) compounds (Rickard, 1974;Pyzik and Sommer, 1981;Peiffer et al., 1992;Yao and Millero, 1996;Poulton, 2003;Poulton et al., 2004;Hellige et al., 2012). Similarly, abiotic reaction of sulfide with ferrihydrite here leads to the formation of high concentrations of elemental sulfur (Figure 4.5). While elemental sulfur was detected in only minor amounts in the higher sulfate concentration biotic experiments, considerable elemental sulfur concentrations were observed at lower starting sulfate concentrations (Table 4.3, Figure 4.5). It is therefore likely that elemental sulfur was also present under the higher sulfate conditions but was short-lived. It is important to note however that a direct comparison between the abiotic and biotic experiments is compromised by the fact that sulfide was introduced differently in these two systems. In the biotic experiments, even at the higher sulfate concentrations, sulfide levels gradually and continuously increased, while the abiotic experiments received one pulse of sulfide. It has in fact been shown that under conditions where MnO_2 concentration are much greater than sulfide, thiosulfate and sulfate become important oxidation products, yet when the MnO_2 to sulfide ratio is closer to 1:1 this is not the case (Yao and Millero, 1996). This was not observed for Fe oxides, however. Accordingly, we are currently investigating the impact of the rate of sulfide introduction to the products and rates of abiotic sulfidization of ferrihydrite. Regardless, in the lower sulfate biotic incubations, elemental sulfur is observed and in these systems, the largest deviation from predicted to observed Fe(II)

stoichiometry is observed (Figure 4.2). Thus, while a plethora of theoretical microbially mediated Fe-S cycles could be operative if all sulfur intermediates are considered, we predict that elemental sulfur is the primary sulfur intermediate here and is thus responsible for the observed Fe-S cycling. Three possible reaction networks involving the consumption of elemental sulfur are discussed below.

4.4.1 Scenario 1: The direct reduction of Elemental S: Perhaps the most unassuming explanation would be that *D. putealis* directly reduces elemental S coupled to the incomplete oxidation of lactate as follows:

$$C_3H_5O_3^- + 2S^0 + 2H_2O \rightarrow C_2H_3O_2^- + HCO_3^- + 2HS^- + 3H^+ \text{ (Rxn 6 table 4.1)}$$

Therefore, elemental S produced during the reduction of Fe(III) undergoes reduction back to sulfide. Sulfide produced during this reaction may react with Fe(II) to form FeS via reaction 3 or react with Fe(III) to form 2 moles of elemental S and 4 moles of Fe(II) in a catalytic cycle until Fe(III) or organic carbon was depleted. The ability to reduce elemental sulfur is widespread among *Desulfovibrio* species (Fauque et al., 1980;Qatibi et al., 1991;Ouattara et al., 1999;Magot et al., 2004;Thabet et al., 2007). Previous investigations however indicate that this strain of *Desulfovibrio* is incapable of reducing elemental S. Yet, the crystallinity and source of elemental S used in these studies was not indicated. Here, S-XANES spectroscopy indicated that the elemental S produced via oxidation of sulfide is much smaller in particle size and has lower crystallinity (Figure 4.8) than commercially available elemental sulfur, which is widely used in biological investigations. Further, the rates of elemental S oxidation have been shown previously to vary substantially with composition and purity (Fortuny et al., 2010) and thus it cannot be

ruled out that the elemental sulfur produced under these conditions supported biological respiration resulting in sulfide regeneration.

4.4.2 Scenario 2: S^0 oxidation coupled to Fe(III) reduction: Another possible reaction mechanism could involve the oxidation of elemental S coupled to Fe(III) reduction, either abiotically or biotically. It has previously been shown that *Desulfovibrio* species could couple the reduction of manganese oxides to elemental sulfur oxidation (Lovley and Phillips, 1994). This oxidation process led to the formation of sulfate. Yet, oxidation of elemental S was not coupled to the reduction of ferrihydrite by this species. Indeed, the thermodynamics of this reaction are unfavorable (Rxn 7 table 4.1) and would therefore not occur abiotically or support microbial respiration. However, reaction between elemental S and various soluble Fe(III) complexes is thermodynamically favorable (Rxn 8 table 4.1) . Interestingly, here, we observe a prominent electrochemically active Fe(III)-ligand complex (Figure 4.4) that persists within these incubations. It is unclear at this time how this complex is formed, but is likely due to destabilization of surface atoms on ferrihydrite upon sulfidization. The identification of this complex and its potential role in sulfur oxidation, both biotic and abiotic, is currently under investigation. If this process is operative, sulfate would be continuously regenerated until aqueous Fe(III) was consumed.

4.4.3 Scenario 3: S^0 disproportionation coupled to Fe(III) reduction: Disproportionation of elemental S coupled to the chemical reduction of Fe(III) has been shown to be an important process within marine enrichments (Thamdrup et al., 1993) and

tidal sediments (Canfield and Thamdrup, 1994; 1996). During this process, elemental sulfur is disproportionated to sulfate and sulfide:

$$4S^0 + 4H_2O \rightarrow SO_4^{2-} + 3HS^- + 5H^+ \text{ (Rxn 9 table 4.1)}$$

In a manner similar to elemental S reduction (scenario 1 above), the (re)generated sulfide could then be (re)oxidized to elemental S via Fe(III) or react with free Fe(II) to form FeS. While disproportionation of thiosulfate has been documented in some *Desulfovibrio* species (Bak and Pfennig, 1987;Cypionka et al., 1998), they do not appear to disproportionate elemental sulfur. Thus, it is unclear if this process is possible for this *Desulfovibrio* species. Regardless, this would not explain the close association of acetate and Fe(II) generation observed here which is suggestive of a respiratory process based on carbon oxidation.

While it appears likely that a sulfur intermediate is key to the Fe-S cycling observed here, other possible scenarios cannot be fully ruled out. For instance, while we show that *D. putealis* was not capable of directly reducing Fe(III) as ferrihydrite in the no sulfate control, the reduction of Fe(III)-organic complexes with higher reduction potentials may be possible. There are in fact a number of examples of organisms incapable of reducing solid Fe(III) yet able to reduce chelated forms (Roden and Lovley, 1993;Knight and Blakemore, 1998). In addition, many species in the *Desulfovibrio* genus are known Fe(III) reducers (Coleman et al., 1993;Lovley et al., 1993;Vandieken et al., 2006). As discussed above, an electrochemically active soluble Fe(III) compound was present in these experiments and varied as a function of initial sulfate concentration. However, this scenario would not explain the lack of substantial elemental sulfur observed within the bacterial sulfate reduction experiments. Further, the 4 electrons

transferred to Fe(III) during the partial oxidation of lactate leads to a 4:1 Fe(II) to acetate ratio which far exceeds the 1:1 ratio seen here.

Further, reaction between Fe(III) and sulfide oftentimes results in intermediate sulfur species other than elemental sulfur (Pyzik and Sommer, 1981;Afonso and Stumm, 1992;Peiffer et al., 1992) that could have been short-lived and consequently not detected. For instance, sulfide could be oxidized to thiosulfate, which may be subsequently reduced or disproportionated by *Desulfovibrio*. To allow for the formation of FeS as observed here, a representative reaction could be:

$$2HS^- + 8Fe(OH)_3 + 16H^+ \rightarrow S_2O_3^{2-} + 8Fe^{2+} + 21H_2O \qquad \text{(Rxn 10 table 4.1)}$$

$$4C_3H_5O_3^- + 2SO_4^{2-} + 8Fe(OH)_3 + 14H^+ \rightarrow 4C_2H_3O_2^- + 4HCO_3^- + S_2O_3^{2-} + 8Fe^{2+} + 21H_2O$$

(Sum Rxn 1 and 10)

$$20\ C_3H_5O_3^- + 10SO_4^{2-} + 8Fe(OH)_3 \rightarrow 20\ C_2H_3O_2^- + 20\ HCO_3^- + S_2O_3^{2-} + 8FeS + 2H^+ + 21H_2O$$

(Sum Rxn 1, 4 and 10)

While this reaction may explain the lack of substantial elemental S, the Fe(II) to acetate ratio is 0.4, too low to account for the 1:1 stoichiometry observed here.

In conclusion, here we show that microbially mediated sulfidization of ferrihydrite involves an intricate Fe-S cycle, that is likely centered on a short-lived elemental sulfur intermediate. At this time, the reaction network involved in the (re)cycling of sulfur and whether the consumption of sulfur is biotic or abiotic are unknown. A number of critical questions have arisen based on this research, including (1) what is the composition, reactivity, and mechanism of formation of Fe(III)-complexes formed during ferrihydrite sulfidization, (2) what metabolic processes can be supported by environmentally relevant elemental sulfur, and (3) what is the role of abiotic reactions between short-lived intermediates in Fe-S cycling? In a broader sense, Fe cycling may be

maintained with merely catalytic amounts of sulfate and explain frequent observations of persistent Fe(III)-reducing conditions in the absence of metal respiring communities (Lentini – Chapter 3). Further, a catalytic Fe-based sulfur cycle will have substantial impacts on carbon mineralization within freshwater sediments and soils.

4.5 References Cited

Afonso, M.D., and Stumm, W. (1992). Reductive Dissolution of Iron(III) (Hydr)Oxides by Hydrogen-Sulfide. *Langmuir* 8, 1671-1675.

Bak, F., and Pfennig, N. (1987). CHEMOLITHOTROPHIC GROWTH OF DESULFOVIBRIO-SULFODISMUTANS SP-NOV BY DISPROPORTIONATION OF INORGANIC SULFUR-COMPOUNDS. *Archives of Microbiology* 147, 184-189.

Bak, F., and Pfennig, N. (1991). MICROBIAL SULFATE REDUCTION IN LITTORAL SEDIMENT OF LAKE CONSTANCE. *FEMS Microbiology Ecology* 85, 31-42.

Basso, O., Caumette, P., and Magot, M. (2005). Desulfovibrio putealis sp. nov., a novel sulfate-reducing bacterium isolated from a deep subsurface aquifer. *Int J Syst Evol Microbiol* 55, 101-104.

Brendel, P.J., and Luther, G.W. (1995). DEVELOPMENT OF A GOLD AMALGAM VOLTAMMETRIC MICROELECTRODE FOR THE DETERMINATION OF DISSOLVED FE, MN, O-2, AND S(-II) IN POREWATERS OF MARINE AND FRESH-WATER SEDIMENTS. *Environmental Science & Technology* 29, 751-761.

Burton, E.D., Bush, R.T., Sullivan, L.A., Hocking, R.K., Mitchell, D.R.G., Johnston, S.G., Fitzpatrick, R.W., Raven, M., Mcclure, S., and Jang, L.Y. (2009). Iron-Monosulfide Oxidation in Natural Sediments: Resolving Microbially Mediated S Transformations Using XANES, Electron Microscopy, and Selective Extractions. *Environmental Science & Technology* 43, 3128-3134.

Burton, E.D., Johnston, S.G., and Bush, R.T. (2010). Microbial sulfidogenesis in ferrihydrite-rich environments: Effects on iron mineralogy and arsenic mobility. *Geochimica Et Cosmochimica Acta* 75, 3072-3087.

Canfield, D.E., and Thamdrup, B. (1994). THE PRODUCTION OF S-34-DEPLETED SULFIDE DURING BACTERIAL DISPROPORTIONATION OF ELEMENTAL SULFUR. *Science* 266, 1973-1975.

Canfield, D.E., and Thamdrup, B. (1996). Fate of elemental sulfur in an intertidal sediment. *FEMS Microbiology Ecology* 19, 95-103.

Cline, J.D. (1969). SPECTROPHOTOMETRIC DETERMINATION OF HYDROGEN SULFIDE IN NATURAL WATERS. *Limnology and Oceanography* 14, 454-&.

Coleman, M.L., Hedrick, D.B., Lovley, D.R., White, D.C., and Pye, K. (1993). REDUCTION OF FE(III) IN SEDIMENTS BY SULFATE-REDUCING BACTERIA. *Nature* 361, 436-438.

Cypionka, H., Smock, A.M., and Bottcher, M.E. (1998). A combined pathway of sulfur compound disproportionation in Desulfovivrio desulfuricans. *Fems Microbiology Letters* 166, 181-186.

Elsgaard, L., and Jorgensen, B.B. (1992). Anoxie transformations of radiolabeled hydrogen sulfide in marine and freshwater sediments. *Geochimica Et Cosmochimica Acta* 56, 2425-2435.

Fauque, G.D., Barton, L.L., and Le Gall, J. (1980). "OXIDATIVE PHOSPHORYLATION LINKED TO THE DISSIMILATORY REDUCTION OF ELEMENTAL SULFUR BY DESULFOVIBRIO," in *Elliott, K. And J. Whelan*.), P71-86.

Fendorf, S.E., and Li, G.C. (1996). Kinetics of chromate reduction by ferrous iron. *Environmental Science & Technology* 30, 1614-1617.
Fleet, M.E. (2005). Xanes spectroscopy of sulfur in earth materials. *Canadian Mineralogist* 43, 1811-1838.
Fortuny, M., Guisasola, A., Casas, C., Gamisans, X., Lafuente, J., and Gabriel, D. (2010). Oxidation of biologically produced elemental sulfur under neutrophilic conditions. *Journal of Chemical Technology and Biotechnology* 85, 378-386.
Fossing, H., and Jorgensen, B.B. (1990). OXIDATION AND REDUCTION OF RADIOLABELED INORGANIC SULFUR-COMPOUNDS IN AN ESTUARINE SEDIMENT, KYSING FJORD, DENMARK. *Geochimica Et Cosmochimica Acta* 54, 2731-2742.
Gorbaty, M.L., George, G.N., and Kelemen, S.R. (1991). DIRECT DETERMINATION AND QUANTIFICATION OF SULFUR FORMS IN HEAVY PETROLEUM AND COAL - SULFUR-K EDGE X-RAY ABSORPTION AND X-RAY PHOTOELECTRON SPECTROSCOPIC APPROACHES. *ACS Symposium Series* 461, 127-136.
Hansel, C.M., Benner, S.G., and Fendorf, S. (2005). Competing Fe(II)-Induced Mineralization Pathways of Ferrihydrite. *Environmental Science & Technology* 39, 7147-7153.
Hansel, C.M., Benner, S.G., Neiss, J., Dohnalkova, A., Kukkadapu, R.K., and Fendorf, S. (2003). Secondary mineralization pathways induced by dissimilatory iron reduction of ferrihydrite under advective flow *Geochemica et Cosmochimica Acta* 67, 2992.
Hansel, C.M., Learman, D.R., Lentini, C.J., and Ekstrom, E.B. (2011). Effect of adsorbed and substituted Al on Fe(II)-induced mineralization pathways of ferrihydrite. *Geochimica Et Cosmochimica Acta* 75, 4653-4666.
Hellige, K., Pollok, K., Larese-Casanova, P., Behrends, T., and Peiffer, S. (2012). Pathways of ferrous iron mineral formation upon sulfidation of lepidocrocite surfaces. *Geochimica Et Cosmochimica Acta* 81, 69-81.
Holmkvist, L., Ferdelman, T.G., and Jorgensen, B.B. (2011). A cryptic sulfur cycle driven by iron in the methane zone of marine sediment (Aarhus Bay, Denmark). *Geochimica Et Cosmochimica Acta* 75, 3581-3599.
Jakobsen, R., and Postma, D. (1999). Redox zoning, rates of sulfate reduction and interactions with Fe-reduction and methanogenesis in a shallow sandy aquifer, Romo, Denmark. *Geochimica Et Cosmochimica Acta* 63, 137-151.
Knight, V.V., and Blakemore, R. (1998). Reduction of diverse electron acceptors by aeromonas hydrophila. *Arch Microbiol* 169, 239-248.
Kocar, B.D., Borch, T., and Fendorf, S. (2010). Arsenic repartitioning during biogenic sulfidization and transformation of ferrihydrite. *Geochimica Et Cosmochimica Acta* 74, 980-994.
Lentini, C.J. (2013). *THE ROLE OF FE(III) OXYHYDROXIDES IN SHAPING MICROBIAL COMMUNITIES CAPABLE OF FE(III) REDUCTION*. PhD, Harvaard.
Lentini, C.J., Wankel, S.D., and Hansel, C.M. (2012). Enriched Iron(III)-Reducing Bacterial Communities are Shaped by Carbon Substrate and Iron Oxide Mineralogy. *Frontiers in Microbiology* 3, 404.

Li, Y.L., Vali, H., Yang, J., Phelps, T.J., and Zhang, C.L. (2006). Reduction of iron oxides enhanced by a sulfate-reducing bacterium and biogenic H2S. *Geomicrobiology Journal* 23, 103-117.

Lovley, D.R., and Phillips, E.J.P. (1994). NOVEL PROCESSES FOR ANAEROBIC SULFATE PRODUCTION FROM ELEMENTAL SULFUR BY SULFATE-REDUCING BACTERIA. *Applied and Environmental Microbiology* 60, 2394-2399.

Lovley, D.R., Roden, E.E., Phillips, E.J.P., and Woodward, J.C. (1993). Enzymatic iron and uranium reduction by sulfate-reducing bacteria. *Marine Geology* 113, 41-53.

Luther Iii, G.W., Glazer, B.T., Ma, S., Trouwborst, R.E., Moore, T.S., Metzger, E., Kraiya, C., Waite, T.J., Druschel, G., Sundby, B., Taillefert, M., Nuzzio, D.B., Shank, T.M., Lewis, B.L., and Brendel, P.J. (2008). Use of voltammetric solid-state (micro)electrodes for studying biogeochemical processes: Laboratory measurements to real time measurements with an in situ electrochemical analyzer (ISEA). *Marine Chemistry* 108, 221-235.

Magot, M., Basso, O., Tardy-Jacquenod, C., and Caumette, P. (2004). Desulfovibrio bastinii sp nov and Desulfovibrio gracilis sp nov., moderately halophilic, sulfatereducing bacteria isolated from deep subsurface oilfield water. *International Journal of Systematic and Evolutionary Microbiology* 54, 1693-1697.

Ouattara, A.S., Patel, B.K.C., Cayol, J.L., Cuzin, N., Traore, A.S., and Garcia, J.L. (1999). Isolation and characterization of Desulfovibrio burkinensis sp. nov. from an African ricefield, and phylogeny of Desulfovibrio alcoholivorans. *International Journal of Systematic Bacteriology* 49, 639-643.

Peiffer, S., Afonso, M.D., Wehrli, B., and Gachter, R. (1992). KINETICS AND MECHANISM OF THE REACTION OF H2S WITH LEPIDOCROCITE. *Environmental Science & Technology* 26, 2408-2413.

Poulton, S.W. (2003). Sulfide oxidation and iron dissolution kinetics during the reaction of dissolved sulfide with ferrihydrite. *Chemical Geology* 202, 79-94.

Poulton, S.W., Krom, M., and Raiswell, R. (2004). A revised scheme for the reactivity of iron (oxyhydr)oxide minerals towards dissolved sulfide. *Geochim. Cosmochim. Acta* 68, 3703-3715.

Prietzel, J., Botzaki, A., Tyufekchieva, N., Brettholle, M., Thieme, J., and Klysubun, W. (2011). Sulfur speciation in soil by S K-Edge XANES spectroscopy: comparison of spectral deconvolution and linear combination fitting. *Environ Sci Technol* 45, 2878-2886.

Pyzik, A., and Sommer, S. (1981). Sedimentary iron monosulfides: kinetics and mechanism of formation. *Geochim. Cosmochim. Acta* 45, 687-698.

Qatibi, A.I., Niviere, V., and Garcia, J.L. (1991). DESULFOVIBRIO-ALCOHOLOVORANS SP-NOV, A SULFATE-REDUCING BACTERIUM ABLE TO GROW ON GLYCEROL, 1,2-PROPANEDIOL AND 1,3-PROPANEDIOL. *Archives of Microbiology* 155, 143-148.

Rickard, D.T. (1974). Kinetics and mechanism of the sulfidation of goethite. *American Journal of Science* 274, 941-952.

Roden, E.E., and Edmonds, J.W. (1997). Phosphate mobilization in iron-rich anaerobic sediments: Microbial Fe(III) oxide reduction versus iron-sulfide formation. *Archiv Fur Hydrobiologie* 139, 347-378.
Roden, E.E., and Lovley, D.R. (1993). Dissimilatory Fe(III) Reduction by the Marine Microorganism Desulfuromonas acetoxidans. *Appl Environ Microbiol* 59, 734-742.
Roesler, A., Gammons, C., Druschel, G., Oduro, H., and Poulson, S. (2007). Geochemistry of Flooded Underground Mine Workings Influenced by Bacterial Sulfate Reduction. *Aquatic Geochemistry* 13, 211-235.
Schwertmann, U., and Cornell, R.M. (2007). "Ferrihydrite," in *Iron Oxides in the Laboratory*. Wiley-VCH Verlag GmbH), 103-112.
Steudel, R., and Holdt, G. (1988). Solubilization of Elemental Sulfur in Water by Cationic and Anionic Surfactants. *Angewandte Chemie International Edition in English* 27, 1358-1359.
Stookey, L.L. (1970). Ferrozine---a new spectrophotometric reagent for iron. *Analytical Chemistry* 42, 779-781.
Straub, K.L., and Schink, B. (2004). Ferrihydrite-dependent growth of Sulfurospirillum deleyianum through electron transfer via sulfur cycling. *Applied and Environmental Microbiology* 70, 5744-5749.
Taillefert, M., Bono, A.B., and Luther, G.W. (2000). Reactivity of freshly formed Fe(III) in synthetic solutions and (pore)waters: Voltammetric evidence of an aging process. *Environmental Science & Technology* 34, 2169-2177.
Taillefert, M., Hover, V.C., Rozan, T.F., Theberge, S.M., and Luther, G.W. (2002). The influence of sulfides on soluble organic-Fe(III) in anoxic sediment porewaters. *Estuaries* 25, 1088-1096.
Thabet, O.B.D., Fardeau, M.L., Suarez-Nunez, C., Hamdi, M., Thomas, P., Ollivier, B., and Alazard, D. (2007). Desulfovibrio marinus sp nov., a moderately halophilic sulfate-reducing bacterium isolated from marine sediments in Tunisia. *International Journal of Systematic and Evolutionary Microbiology* 57, 2167-2170.
Thamdrup, B., Finster, K., Hansen, J.W., and Bak, F. (1993). Bacterial disproportionation of elemental sulfur coupled to chemical reduction of iron or manganese. *Appl Environ Microbiol* 59, 101-108.
Vandieken, V., Knoblauch, C., and Jorgensen, B.B. (2006). Desultovibrio frigidus sp nov and Desulfovibrio ferfireducens sp nov., psychrotolerant bacteria isolated from Arctic fiord sediments (Svalbard) with the ability to reduce Fe(III). *International Journal of Systematic and Evolutionary Microbiology* 56, 681-685.
Webb, S.M. (2005). *Sam's Interface for XAS Package (SixPACK)* [Online]. Available: http://www-ssrl.slac.stanford.edu/~swebb/index.htm [Accessed].
Yao, W.S., and Millero, F.J. (1996). Oxidation of hydrogen sulfide by hydrous Fe(III) oxides in seawater. *Marine Chemistry* 52, 1-16.

APPENDIX

Supplementary information for Chapter 2

A.1 Secondary Mineralization

A.1.1. Methods

Secondary Fe phases formed following the reduction of Fe(III) were investigated using X-ray absorption spectroscopy (both X-ray absorption near edge spectroscopy (XANES) and extended X-ray absorption fine structure (EXAFS) spectroscopy) and scanning electron microscopy (SEM). Before analysis, samples were dried anaerobically in a glove bag. For XAS, the samples were then mounted on a Teflon holder and sealed with Kapton polyimide film. Following data collection at beam line 11-2 (Stanford Synchrotron Radiation Lightsource) a set of Fe reference standards were fit to the data (k^3weighted linear combination fitting; k-range 2–14Å) using the program SIXPack (Webb, 2005) (For further details see (Hansel et al., 2003).

For SEM, samples were mounted on SEM stubs with double-sided carbon tap and sputter-coasted with Au prior to imaging. SEM was performed at the Harvard University Center for Nanoscale Systems using a Zeiss FESEM Supra 55VP with a high efficiency in-lens secondary electron detector and equipped with an EDAX Genesis (EDS) system.

A.1.2. Results

The reduction of ferrihydrite and goethite leads to the precipitation of the secondary Fe phase, siderite ($Fe^{II}CO3$) regardless of the carbon source or dilution. For instance, for the goethite enrichments amended with glucose or lactate where substantial Fe(III) reduction is observed (10^{-3} dilution), there is a shift in the XANES spectra to lower energies indicating a higher proportion of Fe(II) to Fe(III) within the solid-phase products (Figure A.1a). The EXAFS spectra are best fit using a linear combination comprised of 61% siderite and 39% goethite for the glucose enrichments and 62% siderite and 33% goethite for the lactate enrichments (Figure

A.1b). These percentages are in good agreement with the percent Fe(II) found via ferrozine (see Figure 1).

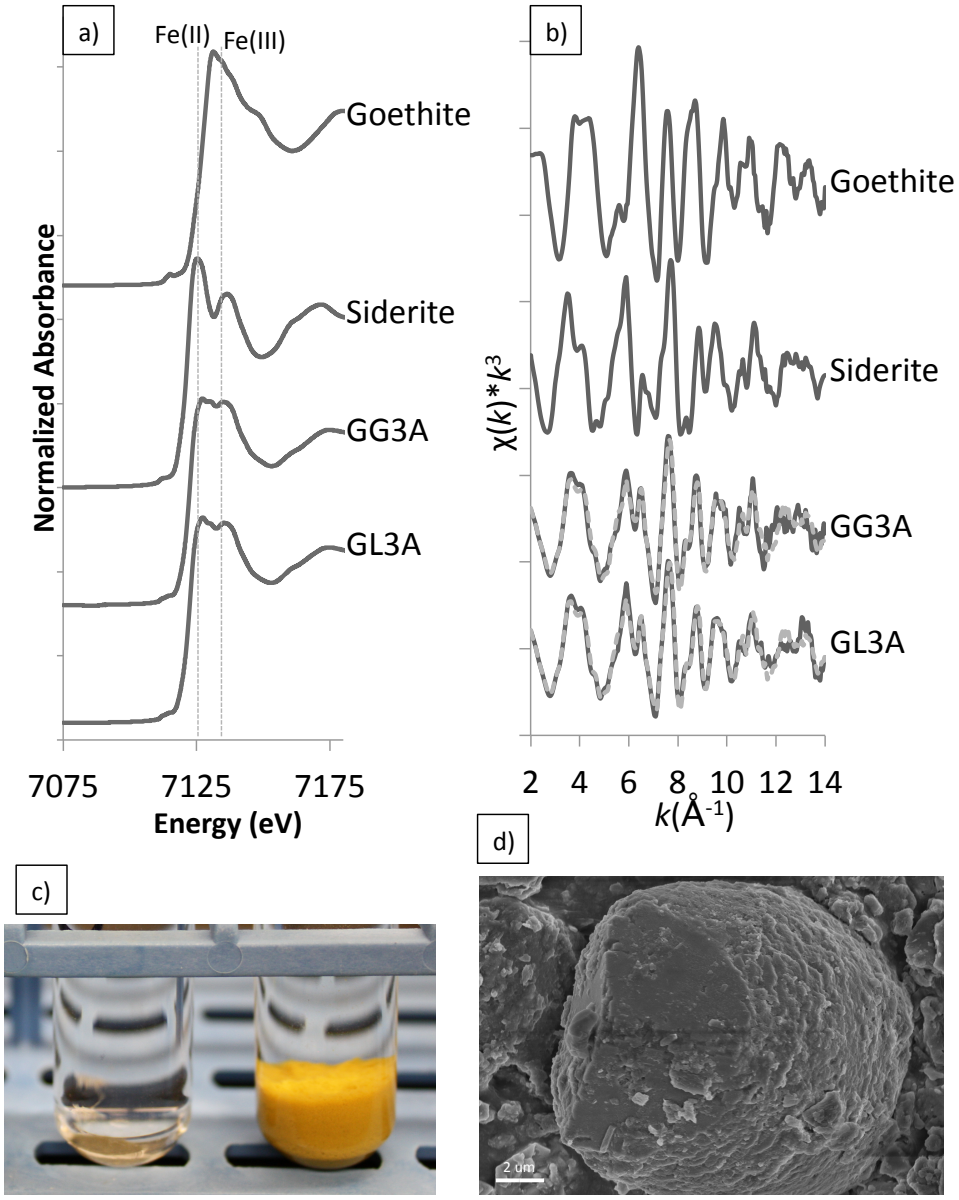

Figure A1 The top images show (A) XANES and (B)EXAFS spectra for secondary minerals formed within goethite enrichments in the presence of glucose or lactate. The reference spectra goethite and siderite are also included to illustrate the relative binding energies of Fe(II) and Fe(III) and line shape for the two mineral phases. The bottom images illustrate (C) the visual disappearance of the goethite mineral after incubation and (D) observation of secondary siderite grains via SEM.

In addition to spectroscopic evidence, visible indications of reduction were also noted as demonstrated by comparing the solid-phase appearance before (Figure S1c – right) and after (Figure S1c - left) incubation. This striking difference was seen over continuous transfers for goethite in the 3rd and 4th dilution of lactate and glucose, providing further confirmation of repeated reduction of goethite in these enrichments. Microscopic analysis reveals that the siderite particles are small (average 10 μm diameter) and have a botryoidal morphology similar to frequently observed biogenic siderite (Figure S1 D). Indeed, EDS indicated that these particles contained only iron and carbon.

A.2 Organic carbon analysis

A.2.1. Methods

Selected organic acids (acetate, butyrate, citrate, formate, fumarate, gluconate, lactate, malate, maleate, malonate, oxalate, propionate, pyruvate, succinate, tartrate) and major ions (SO_4^{-2}, Cl) were analyzed via suppressed anion chromatography with conductivity detection using a Dionex ICS-2000 (AS11 Column) with a KOH eluent generator. An eluent gradient method was employed (flow rate 1.5ml/min): beginning for 6 minutes at 1mM, followed by a linear ramp to 30mM over 8 minutes, another linear ramp to 60mM over 4 minutes, followed by 5 minute re-equilibration at 1mM between samples. Samples were diluted 1:10 in DI water and frozen until analysis. Standard solutions were made gravimetrically and a full size range of standards (1000, 250, 100, 50, and 10 μM) was analyzed approximately every 20 samples (r^2 typically > 0.999) while a single 100uM standard was analyzed every 10 samples to account for any potential instrument drift. Based on repeated analysis of standard solutions, standard errors for the compounds detected and quantified in our enrichments, lactate, acetate, succinate,

propionate, butyrate, formate, and SO_4^{-2} were ± 20, 206, 414, 367, 81, 27, and 29 μM, respectively (Table A1).

Table A.1. Organic acids produced in glucose and lactate enrichments

Mineral	Dilution	Lactate mM (±0.02 mM)	Acetate mM (±0.2 mM)	Succinate mM (±0.4 mM)	Propionate mM (±0.4 mM)	Butryate mM (±0.08 mM)	Formate mM (±0.03 mM)
GLUCOSE AMENDED							
Ferrihydrite	10^{-1}	–	–	–	0.9	–	–
Ferrihydrite	10^{-2}	***	14.2	***	2.6	2.0	***
Ferrihydrite	10^{-3}	–	9.2	***	8.4	***	–
Ferrihydrite	10^{-4}	0.5	9.8	1.8	***	–	2.8
Goethite	10^{-1}	–	19.3	–	5.1	***	***
Goethite	10^{-2}	***	13.5	–	4.4	***	***
Goethite	10^{-3}	***	24.7	1.2	0.4	***	***
Hematite	10^{-3}	–	3.3	***	***	–	***
LACATE AMENDED							
Ferrihydrite	10^{-1}	6.0	3.9	***	***	***	0.3
Ferrihydrite	10^{-2}	–	13.5	–	***	***	***
Ferrihydrite	10^{-3}	2.6	7.3	***	***	–	***
Goethite	10^{-3}	7.8	1.3	–	***	–	***
Hematite	10^{-3}	3.5	4.9	***	0.5	***	0.3

*–, Not detected; ***, trace amount detected, not quantifiable.*
Error estimates are calculated as standard error multiplied by factor for analysis of 10× diluted samples.

A.2.2. Results

All enrichment cultures containing lactate and glucose exhibited varying accumulation of acetate, lactate, succinate, propionate, butyrate and formate, reflecting underlying changes in community metabolism (Table A1). Enrichments grown on lactate showed variability in both the amount of lactate consumed and the amount of acetate accumulated as a product of incomplete lactate oxidation. While some amount of lactate consumption was observed in all enrichments shown in Table A1, initial levels of lactate were drawn down completely in only one enrichment, ferrihydrite (10^{-2}). Further, low levels of succinate, propionate, butyrate and formate were observed (though not quantifiable) across all lactate enrichments, with accumulation of up to 0.3 mM formate in ferrihydrite (10^{-1}) and hematite (10^{-3}) and 0.5 mM propionate in hematite (10^{-3}).

Enrichments on glucose also demonstrated considerable variability in production and accumulation of organic acids. In general more acetate was produced in the goethite enrichments (9.7 to 24.7 mM) followed by ferrihydrite (0 to 14.2 mM) and then hematite (3.3 mM). No acetate formation was observed in the ferrihydrite 10^{-1} dilution. Variable accumulation of succinate, propionate, butyrate and formate was observed across all mineral enrichments. Quantifiable amounts of succinate (1.2 to 2.8 mM) were only observed in higher dilutions of ferrihydrite (10^{-4}) and goethite (10^{-3}) with only trace amounts of observed in hematite enrichments. Accumulation of propionate was observed across all Fe minerals, although considerably higher levels were seen in the ferrihydrite (up to 8.4 mM) and goethite (5.1 mM) enrichments as compared with hematite (trace to 0.5 mM). Up to 2.0 mM butyrate accumulated in the ferrihydrite 10^{-2} dilution with only trace amounts of butyrate detected in the goethite enrichments and none detected with hematite. Finally, as with succinate, quantifiable levels of formate (2.8 mM) were only observed in the higher dilutions of ferrihydrite (10^{-4}), with trace amounts detected in all other dilutions of hematite, goethite and ferrihydrite (except 10^{-1} and 10^{-3}). Organic acid products were not detected in any of the acetate enrichments.

While it is difficult to link these results directly with the activities of the enriched phylotypes, the observed variability in the accumulation of fermentation and other metabolic products indicates distinct shifts in community metabolism that is undoubtedly related to both the iron mineralogy and initial dilution of the inoculum – these differences are currently under investigation.

A.3. References Cited

Hansel, C.M., Benner, S.G., Neiss, J., Dohnalkova, A., Kukkadapu, R.K., and Fendorf, S. (2003). Secondary mineralization pathways induced by dissimilatory iron reduction of ferrihydrite under advective flow Geochemica et Cosmochimica Acta 67**,** 2992.

Webb, S.M. (2005). Sam's Interface for XAS Package (SixPACK) [Online]. Available: http://www-ssrl.slac.stanford.edu/~swebb/index.htm [Accessed].